Assessment of a High Temperature Refractory-lined Suspension Flow Solar Particle Receiver

Muhammad Mujahid Rafique

School of Mechanical Engineering

The University of Adelaide

South Australia 5005

Australia

A Thesis Submitted in Fulfilment of the Requirements for the Degree of Doctor of Philosophy

February 2023

This page is intentionally left blank

Executive summary

The use of ceramic particles, alone or in suspension within an air stream, as a heat transfer medium is one of the current focussed areas for the development of high temperature receiver-based concentrated solar thermal technologies. These solid particle receiver systems have the potential to achieve operating temperatures of >1000∘C, which is typically required for high temperature industrial processes. This requires the use of either expensive high temperature metals or linings of refractory, which is both brittle and has high thermal inertia. While the refractory is a proven material used in high temperature furnaces, limited information is available on the use of refractory linings in solar receivers while accounting for transient thermal input. Hence there is a need to better understand the thermal behaviour of these high temperature refractory-lined particle receivers considering their response to solar transients during start-up, turn down and shutdown periods. Also, the use of air as the heat transfer fluid for retrofit applications in industry arises the need to understand the system-level performance of these receivers, when operating in combination with sensible thermal storage, while accounting for the true variations in the returned thermal inputs from the process. To meet these needs, this thesis reports on the thermal performance and optimization of a refractory-lined suspension-flow windowless vortex receiver for a solar thermal particle technology used to generate high temperature air. These assessments are made with a transient mathematical model developed to calculate the heat and mass transfer within the cavity of a Solar Expanding Vortex Receiver (SEVR) together with the thermal losses to the surroundings, incorporating the influence of solar transients during start-up, turn down and shutdown periods. New insights are provided of the influences of the variables of refractory configuration and of the potential operating controller parameters to manage the influence of solar variability. Further to this,

new understandings are provided on the system level performance of a refractory-lined SEVR operating in combination with a packed bed sensible thermal storage, and other components of a complete concentrated solar thermal plant. Overall, the results show that it is possible to size a refractory lining appropriately to allow reliable operation under the transient and cyclical conditions of a solar receiver. This offers advantages in terms of cost and efficiency. The results also provide insights of a strong dependence of the overall system performance on the interaction between the individual sub-systems, indicating the importance of carefully sizing the sub-systems in combination rather than in isolation for retrofit industrial applications. The findings also show how to optimize refractory lining for such conditions which makes it relevant to other types of high temperature receivers, to integrate and simulate different system types, and to assist in identifying which type of system is best suited to which application, when accounting for start-up, turndown and shutdown losses.

Declaration

I certify that this work contains no material which has been accepted for the award of any other degree or diploma in my name in any university or other tertiary institution and, to the best of my knowledge and belief, contains no material previously published or written by another person, except text from my work published as a part of this thesis and where due reference has been made in the text for other's work. In addition, I certify that no part of this work will, in the future, be used in a submission in my name for any other degree or diploma in any university or other tertiary institution without the prior approval of the University of Adelaide and where applicable, any partner institution responsible for the joint award of this degree.

The author acknowledges that the copyright of published works contained within this thesis resides with the copyright holder(s) of those works.

I give permission for the digital version of my thesis to be made available on the web, via the University's digital research repository, the Library Search and also through web search engines, unless permission has been granted by the University to restrict access for a period of time.

I acknowledge the support I have received for my research through the provision of an Australian Government Research Training Program (RTP) Scholarship.

15/01/2023

Muhammad Mujahid Rafique   **Date**

This page is intentionally left blank

Acknowledgment

First of all, I would like to thank ALLAH almighty, the Most Beneficent and the Most Merciful, for this beautiful life and all the blessings to accomplish another milestone, my PhD degree.

I would like to express my most sincere gratitude to those who have helped me in my journey toward completing this thesis. I would like to thank my supervisors Prof. Graham 'Gus' Nathan and Dr. Woei Saw for helping me significantly in many different ways. I thank Prof. Nathan and Dr. Saw and for sharing their extensive knowledge in the field of concentrated solar thermal technology, and for their enthusiasm and motivation, all of which have helped me tremendously throughout my PhD research. I also acknowledge the assistance of Dr. Leok Lee and Dr. Philip Ingenhoven for providing the system modelling support.

I would like to thank my parents, for their continued support and encouragement. Without them, I would not be where I am today. Their unconditional trust, timely encouragement, and endless patience have helped me to achieve this goal. My parents, brothers and sisters have always been generous with their love and encouragement.

Finally, special thanks with love to my beautiful and caring wife Nayab, and my lovely children Nawal and Aalyan. Throughout my PhD journey they loved, supported, encouraged, entertained, and helped me to get through this challenging period in the most positive way.

This page is intentionally left blank

Table of contents

This page is intentionally left blank

CHAPTER 1

INTRODUCTION

1.1.   Background

The challenge of decarbonizing high temperature industrial processes requires further advancements to enable the deployment of renewable-based technologies into energy-intensive heavy industrial processes requiring continuous high temperature heat, above $1000^{o}C$, such as the production of steel, aluminium and cement. These processes are contributing ~15% of global CO_2 emissions [1, 2]. Only in Australia, the industrial processes contribute ~42% of CO_2 emissions and ~220 PJ/year is consumed by alumina refineries only, of which 67% is supplied using natural gas [3, 4]. Also, these processes are hard to abate as they are making a huge contribution to the economy. Australia generated US$ 8 billion from the alumina industry in the year 2018 [4]. The progressive increase of these greenhouse gas emissions is causing an environmental imbalance such as extreme weather conditions around the world. Meanwhile, the prices of diminishing fossil fuels are increasing rapidly and are projected to further rise in the next 20 years. Furthermore, the gap between energy supply and demand is also expected to widen due to this rapid increase in global energy demand [5-7]. The issues associated with the excessive use of fossil fuels for different commercial and industrial applications require the development and implementation of new technologies that are environmental friendly.

Solar energy stands out among the other alternative energy sources which have the potential to replace fossil fuels. This source of renewable energy is sustainable and inexhaustible, unlike finite fossil fuels. It has been predicted that the amount of solar energy falling onto the surface of the earth in just one hour could fulfil the global energy needs for one year, but this requires the right technologies to capture and utilize this renewable source of energy effectively [8]. The intermittent nature of solar resource creates a big challenge for solar energy utilization especially for large-scale applications, which require a

continuous supply of energy [9]. In this regard, concentrated solar thermal, CST, technologies are gaining importance [10-13]. They are considered a potentially suitable alternative to primary fossil fuels due to their ability to meet the load demands of both high and low temperature process heat applications [14, 15]. Furthermore, thermal energy storage can be integrated into a CST plant to overcome the intermittency issues related to solar energy and increase the operational reliability of the system.

New CST technologies are required to achieve operating temperatures of or above $1000^{o}C$, which is typically required for high temperature industrial processes [16]. This is because the current commercially available CST technologies, which use molten salts, have temperature limitations of heat transfer media. The most commonly used molten salts, such as molten nitrate solar salt (60% $NaNO_3$ and 40% KNO_3), have a safe working range of 220 to $565^{o}C$ and causes corrosion to metallic pipes [17, 18]. They freeze below $220^{o}C$ and become chemically unstable above $565^{o}C$, requiring trace heating and limiting the operation of CST technology to below $600^{o}C$ [19]. The molten salts-based technologies are well suited to provide stored heat for steam turbines. However, their temperature limitation restricts the integration of CST into heavy industrial processes requiring high temperatures (~$1000^{o}C$), as shown in Table 1.1 [16, 20-24]. Therefore, further technical assessments of new or existing CST technologies with the ability to achieve higher operating temperatures, than commercially available, are required.

To overcome the limitations of the operating temperature of present CST systems, high temperature particle receiver systems are being pursued for next-generation CST plants with operational temperatures of >1000°C [17]. These receivers are being developed to achieve temperatures in the order of $1000^{o}C$ for advanced power cycles and solar thermochemical processes [25]. The use of particles, as primary HTF or in suspension within an air stream to enhance the heat transfer to the gas phase, has the potential to achieve

6

temperatures in the range of 1000°C [26]. The use of solid particles in suspension within an air stream also has the potential to minimize the limitations of using air as the heat transfer medium (e.g., low heat capacitance, pumping losses, etc.), by increasing the effectiveness of the heat transfer mechanisms within the receiver cavity. Also, the wide range of operating temperatures makes these receivers an enabling technology for scalability [26, 27]. There are different promising concepts of particle-laden receivers including falling particle receivers led by Sandia Laboratory and CSIRO [28-30], centrifugal receiver led by DLR [31-34], tubular fluidized beds led by CNRS [35], Solar Vortex Receiver (SVR) led by ETH Zurich [36-39], Solar Expanding Vortex Receiver (SEVR) led by The University of Adelaide [40-44]. While these various configurations of high temperature central receivers have been studied to achieve high temperatures, there is also a lack of available data of a system configured to provide hot air from these systems at temperatures of >1000°C required for retrofit applications in industry, considering the influence of the time-constants of these various components in response to a long time-series of solar resource variability.

Table 1.1. Typical values of operating temperatures required for a representative range of high temperature industrial processes.

Process	Required Reactor Temperature (°C)
Alumina Calciner	~950
Blast furnace	1200 - 1600
Cement Kiln	~1450
Cement Calciner	~850
Lime kiln	~850
Glass furnace	1100 - 1600

One class of suspension flow solar particle receiver technologies that have received significant attention employs direct irradiation to heat a vortex of air and particles in a

7

cylindrical cavity, termed the Solar Expanding Vortex Receiver (SEVR) [40-44]. This configuration of the receiver offered the potential to act as an air heater, with suspended particles, to reheat returned air from the integrated storage which is already at an elevated temperature (>300°C). Figure 1.1 presents a basic schematic diagram of a receiver system in combination with thermal storage and an optional backup burner, required to deliver reheated air for retrofit industrial applications. In the combined CST system, the hot air from the receiver sub-system is used to charge one of the thermal energy storage (TES) devices with the lowest state of charge. Once a TES device is fully charged, it is discharged to the process while hot air from the receiver is used to charge another device. To keep the charging and discharging cycles separate, the warm air from the thermal storage is used to preheat the ambient air in a heat exchanger, rather than being returned to the receiver. This allows the operation of the windowless receiver at atmospheric pressure, to mitigate particle egress through the open aperture. It also allows the system to operate with only low-temperature fans. The need to direct the hot air to the storage system, rather than directly to the plant, is driven by the need to avoid sending carry-over particles from the receiver to the industrial process since sending it through the packed bed storage system also serves as the second stage of the particle filter, along with energy storage. A detailed description of the process and different elements is provided in following chapters.

Although high temperature particle-laden receiver technology has the potential to achieve operating temperatures of over 1000°C and is suited for this configuration, the performance of these receivers also needs to be assessed based on their transient operation using real-time solar irradiance data. Also, the operating temperatures in the order of 1000°C require the use of refractory linings, similar to non-solar rotary kilns, or expensive high temperature metals. Note that, a detailed description, and properties, of different refractory materials is presented in Chapter 2, whereas Chapter 3 provides a comparative

analysis for different refractory materials. The use of refractories allows the operating temperature to exceed 1000°C but it has low thermal expansion coefficient and high thermal mass. This makes the transient response of a refractory-lined directly irradiated receiver more challenging than tubular receivers, with thin conducting tubes. This needs the understanding of the influence of long-term solar transients on the thermal performance of these particle-laden receivers.
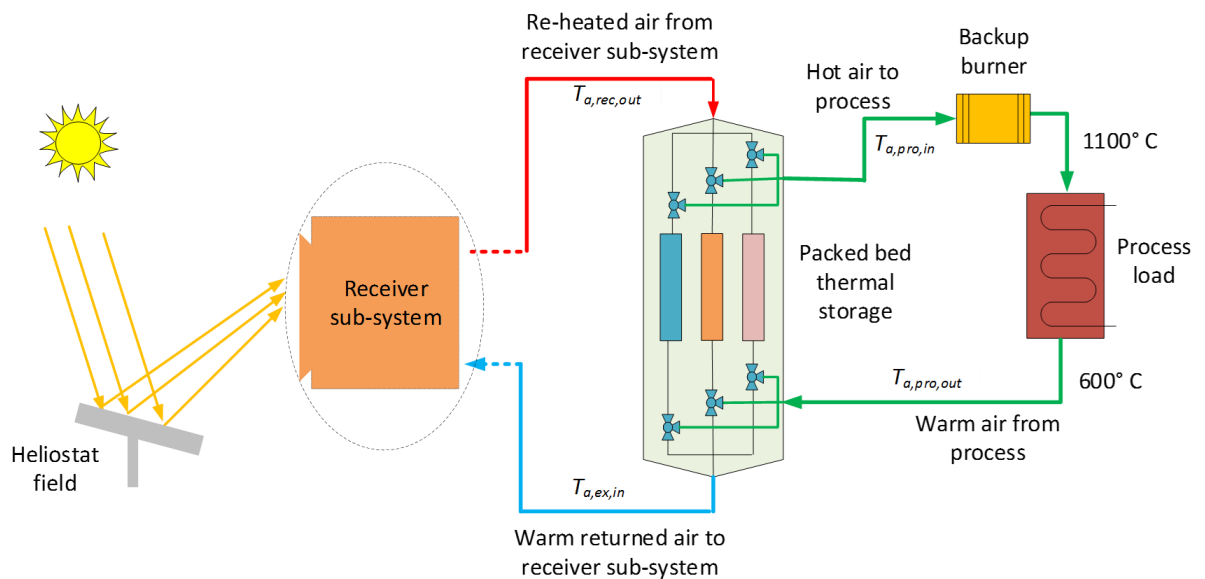

Figure 1.1. A basic schematic diagram of the receiver sub-system in combination with thermal storage and other components to deliver hot air to a high temperature process. (Adapted from the under-preparation journal paper presented in Chapter 6).

The practical implementation of refractory-lined solar receivers requires greater insight into the potential approaches to manage the transient heat inputs. This is because refractories are brittle and have strict requirements for heating rates. Also, the high thermal inertia of the refractory lining can potentially result in a significant fraction of the solar resource being needed to heat the cavity to the required operating temperature. While refractory-lined solar receivers are expected to have longer start-up time, little attention has been provided to the options with which this time might be reduced when considering

long-term solar resource variability [45]. Hence, there is a need to better understand the start-up behavior of these receivers, and the potential options with which the start-up time might be reduced, considering the influence of transients in the incoming concentrated solar radiations [46-48]. Insufficient information is available to guide the selection of refractory type, thickness or operating strategy in response to these challenges, provides further motivation for the present research work.

The integration of high temperature solar central receiver systems has been reported in the literature, but only for the generation of electricity using steam (Rankine) and gas turbine (Brayton) cycles [49-55]. There are limited studies on the integrated systems to produce high temperature heat, above 1000°C, for heavy industrial applications such as alumina or lime calcination. Also, the integration of new technologies and concepts, such as refractory-lined suspension flow systems, is more challenging to customize and requires physical models of the sub-systems which can assess the impact of solar intermittency. This arises the need of system analysis by integrating the physical sub-models with heat and mass transfer equations for each component to understand their combined performance, considering site-specific solar variability. Further to this, the combined effects of key design parameters on the thermo-economic performance of these high temperature CST systems considering transient losses through a year of operation at a potential plant site are still unclear. Hence, there is a need of an assessment that provides a new understanding of the system-level performance of these CST systems along with an assessment of the levelized cost of its solar component of the energy. This thesis also aims to fill these gaps.

To summarize, new insights are required about potential opportunities to enhance the thermal performance of high temperature CST technologies when operating under transient inputs, such as by the use of refractory linings in central receivers and the introduction of particle-laden flow into a receiver cavity. Furthermore, there is a need to understand the

performance of a refractory-lined solar vortex receiver operating in combination with thermal storage and other components of a CST system to supply high temperature heat to a downstream process. Therefore, this project aims to fulfill these needs firstly by modelling and understanding the thermal response of a high temperature refractory-lined particle-laden solar receiver sub-system. Then, providing an understanding of the trade-off between the receiver and thermal storage sub-systems by integrating the developed receiver model with a thermal storage system and other components, to be solved for real-time solar irradiance data over a longer period.

1.2. Research objectives

To meet the above-mentioned needs, this project is divided into following objectives:

- To develop a validated transient mathematical model for a multilayered refractory-lined solar receiver, employing the governing mathematical equations for the mass and energy, to calculate the time-dependent temperature fields in response to solar resource variability.

- To provide new insights and knowledge for the optimization of refractory-lined solar receivers, by understanding the trade-off between the solar DNI input, thermal losses from the receiver, and allowable temperatures of refractory, employing the developed transient mathematical model solved for any given time history of the variable solar resource.

- To increase the understanding of how to manage the transient responses of refractory-lined solar receivers to solar variability during start-up, turn down, and shutdown periods. More specifically, this aims to report the influence of a series of initial temperatures of the cavity internal wall, of covering the aperture and of

delaying the inlet flow, on the transient response of a refractory lined particle-laden receiver.

- To provide data and information on the potential opportunities for the improvement of thermal response and annual useful thermal gain of a particle-laden solar receiver, in response to solar resource variability, by estimating the influence and sensitivity of each major parameter for a particular case study.

- To guide the further development of the technology by establishing baseline for a technically plausible system. This aims to provide an understanding of the system-level performance of a windowless vortex-based high-temperature refractory-lined suspension flow solar particle receiver operating in combination with sensible thermal storage, and other components of a complete CST plant, configured to supply reheated air to thermochemical processes at temperatures of >1000°C.

1.3. Publications resulting from this work

This thesis has produced 4 journal papers (3 published and 1 in preparation), 4 peer-reviewed conference papers and 2 poster presentations. To date, this work has also resulted in 7 other collaborative publications, including 1 journal submission, 3 peer-reviewed conference proceedings and 4 peer-reviewed poster presentations. Furthermore, the developed transient approach has been used to develop a generalized integrated system model, which is flexible to assess different receiver and thermal storage types, according to a specific application, with an option of up-scaling (single or multi-towered) and the potential of assessing the use new heat transfer fluids.

1.3.1. List of journal papers

I. **Rafique, M.M**, Nathan G, Saw W (2021). A mathematical model to assess the influence of transients on a refractory-lined solar receiver. Renewable Energy, 167, 217-235.

II. **Rafique, M.M**, Nathan G, Saw W (2022). Thermal response of multilayered refractory-lined solar receivers to transient operation. Solar Energy, 243, 70-80.

III. **Rafique, M.M**, Nathan G, Saw W (2022). Modelled annual thermal performance of a 50MW$_{th}$ refractory-lined particle-laden solar receiver operating above 1000°C. Renewable Energy, 197, 1081-1093.

IV. **Rafique, M.M.**, Saw W., Lee L., Ingenhoven P., Nathan G (2022). Performance assessment of a system to provide steady high temperature air via solar thermal particle technology with storage and combustion back-up. Prepared in manuscript form.

1.3.2. List of conference papers and poster presentations

I. **Rafique, M.M**, Saw W, Nathan G. Influence of geometric scale on the thermal response of a refractory-lined solar receiver. Asia-Pacific Solar Research Conference, December 16 – 17, 2021, Sydney, Australia.

II. **Rafique, M.M**, Saw W, Nathan G. Impacts of covering the aperture of a refractory-lined solar receiver during the shutdown. SolarPACES2021, September 27 - October 01, 2021.

III. **Rafique, M.M**, Nathan G, Saw W. Assessing the role of refractory lining to overcome the solar intermittency challenge in particle receivers. Proceedings of Asia-Pacific Solar Research Conference, Nov 30 – Dec 03, 2020, Melbourne, Australia.

IV. **Rafique, M.M**, Nathan G, Saw W. Uncertainty in predicting the start-up time and losses for a high temperature particle receiver due to solar resource variability. In Energy Sustainability (Vol. 83631, p. V001T02A007). American Society of Mechanical Engineers.

V. **Rafique, M.M.**, Nathan G, Saw W. Mathematical modelling to assess the influence of transients on refractory-lined solar receivers. CET 2020 Research day, Nov 12, 2020, Adelaide, Australia.

VI. **Rafique, M.M.**, Nathan G, Saw W. Transient modelling of a high temperature refractory-lined particle-laden receiver operating in a CST System. CET 2022 Research day, April 11, 2022, Adelaide, Australia.

1.3.3. Other collaborative work

This work has also contributed to the following publications/poster presentations:

I. Ingenhoven P., Lee L., Saw W., **Rafique, M.M.**, Potter D., Nathan G (2022). Techno-economic assessment from a transient simulation of a concentrated solar thermal plant for delivering high temperature industrial process heat. Renewable and Sustainable Energy Reviews, under review.

II. Potter D, Ingenhoven P, Tian Z, **Rafique M.M**, Salazar D, Saw W, and Beath A. Optimisation of 'beam-up' configurations for the Solar Expanding-Vortex Receiver. Asia-Pacific Solar Research Conference, December 16 – 17, 2021, Sydney, Australia.

III. Ingenhoven P, Saw, **Rafique M.M**, Chinnici A, Potter D, and Nathan G. Energetic assessment of a high temperature packed bed storage system in combination with a solar expanding vortex particle receiver. Solar World Congress, October 25 – 29, 2021.

IV. Ingenhoven P, Saw W, Jafarian M, Seyfaee A, **Rafique M.M**, Potter D, Chinnici A and

Nathan G. Storage system design for solar expanding vortex receiver for process heat integration. Asia-Pacific Solar Research Conference, December 16 – 17, 2021, Sydney, Australia.

V.   Lee L., Ingenhoven P., Saw W., **Rafique, M.M.**, Nathan G (2022). High temperature transmission system and its economic system integration. CET Research day, April 11, 2022, Adelaide, Australia.

VI.   Lee L., Ingenhoven P., Saw W., **Rafique, M.M.**, Nathan G (2022). System modelling for renewable energy to thermal energy in heavy industrial processes. CET Research day, April 11, 2022, Adelaide, Australia.

VII.   Lee L., Ingenhoven P., Saw W., **Rafique, M.M.**, Nathan G (2022). System modelling and technical economic analysis of solar to thermal energy for high temperature heavy industrial processes. HiTeMP Forum: High Temperature Minerals Processing, HiTeMP-3 2022, September 26 – 28, 2022, Adelaide, Australia.

1.4.   Thesis outlines

This thesis comprises a portfolio of publications that are either published, under review, or prepared in manuscript form. This thesis consists of seven chapters as outlined in the following:

- Chapter 1 introduces the research topic and presents the background of CST technology especially focussing on high temperature particle-laden receivers.

- Chapter 2 presents the background literature of the focussed research topic and highlights the knowledge gaps. Particularly, this chapter provides an overview of CST receiver technology and high temperature receivers. It highlights the challenges with current CST state-of-the-art technologies and introduces refractory-lined solar

receivers. This chapter also highlights the need of transient-based assessments of high temperature receivers for CST systems.

- Chapter 3 consists of the first published paper titled: "A mathematical model to assess the influence of transients on a refractory-lined solar receiver". In this paper, an approach to analyse and optimize the thermal performance of a refractory-lined particle receiver in response to solar resource variability has been demonstrated. Further assessment of the time-dependent temperature fields within the receiver cavity has been conducted.

- Chapter 4 consists of the second published paper titled: "Thermal response of multilayered refractory-lined solar receivers to transient operation". In this paper, the thermal response of a multilayered refractory-lined solar receiver during start-up, turn down, and shut down has been reported for cold and hot starts.

- Chapter 5 consists of the third published paper titled: "Modelled annual thermal performance of a 50MW$_{th}$ refractory-lined particle-laden solar receiver operating above 1000°C". This paper assesses the annual thermal performance of an innovative CST technology, employing Solar Expanding Vortex Receiver. It provides new insights of the influences of the refractory use in particle-laden receivers, of the potential operating controllers to manage the influence of solar variability, of particle loadings and temperatures of heat transfer mediums on the annual thermal performance of the system.

- Chapter 6 consists of the fourth paper titled: "Performance assessment of a system to provide steady high temperature air via solar thermal particle technology with storage and combustion back-up". This paper demonstrates an approach to analyse and optimize a high-temperature CST plant based on a particle-laden receiver and

sensible thermal storage. A Simulink environment has been created using the transient mathematical models of the receiver and thermal storage considering solar resource variability, to estimate useful annual thermal gain, thermal efficiency, solar share, and the first-order economic feasibility, for a range of operating parameters.

- Finally, Chapter 7 presents the conclusions of the work presented and recommendations for future research.

CHAPTER 2

LITERATURE REVIEW

2.1. Introduction

The rapid carbon dioxide (CO_2) emissions are increasing at a rapid rate due to rising energy demands from the industrial, transport and domestic sectors. These emissions are a major contributor to global warming and climatic changes. Global CO_2 emissions related to the energy sector in 2021 increased to the highest value of 36.3 Gt as shown in Fig. 2.1 [6, 56]. About 90% of the total CO_2 emissions are generated from the burning of fossil fuels for power generation, process heat and the transport sector [5, 6]. This requires further technological advancements to gradually lower the share of high carbon emitting fossil fuels. In this regard, concentrated solar thermal (CST) technologies are gaining importance as an alternative, clean and renewable energy source both for low and high temperature applications, particularly in the regions with higher solar irradiance [10-12, 14]. The growth of solar thermal installed capacity has shown an encouraging trend over the last few years as depicted in Fig. 2.2 [57, 58], with top share by Spain, the US, China, South Africa, and Morocco [59]. Despite some of the positive indicators, more work is required to increase the share of this vast renewable energy technology especially for high temperature process heat applications.

Concentrated solar thermal, CST, technologies are considered a potentially suitable alternative to primary fossil fuels. CST can be integrated with a high thermal energy storage system, which can be used during the night or on cloudy days, to supply the required input energy and to overcome the solar intermittency issues. Presently, CST technologies are commercially available for power production in the lower temperature range, less than 600°C [60]. There is a driver to develop high temperature solar thermal technologies, above 1000°C, for high temperature calcination processes [16]. In this regard, solar particle-laden (suspension flow) receivers have the potential to achieve temperature above 1000°C [31, 32, 61, 62]. This receiver technology employs sand-like ceramic particles as heat transfer

media, standalone or in suspension within an air stream, which are stable at such high temperatures [31, 32, 61, 63].

High temperature particle-laden receiver technology has the potential to achieve operating temperatures of over 1000°C. However, the variable nature of solar energy resource and higher thermal mass associated with these receivers require their performance to be assessed based on their transient operation using real-time solar irradiance data. The transient analysis is also critical for the assessment of the potential of these receivers for high temperature processes (e.g. calcination) which require continuous supply of process heat. Considering this, the importance and need of transient based thermal analysis of high temperature particle-laden receivers have been highlighted in this review chapter. Note that, the detailed explanation of all gaps with relevant literature, for specific aims and objectives, are provided in individual papers (Chapters 3 to 6).
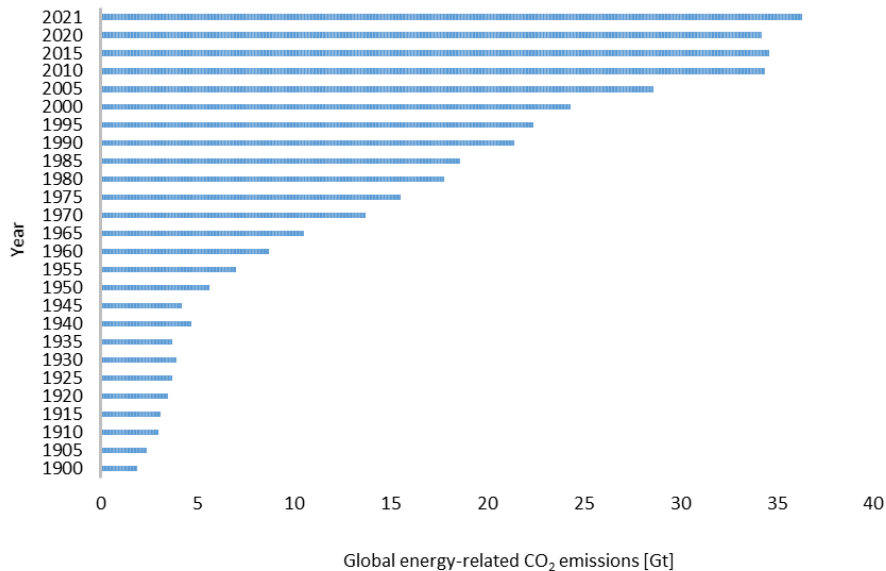

Figure 2.1. The global trend of energy-related CO_2 emissions: 1990 – 2021. Data taken from [5, 56, 64].
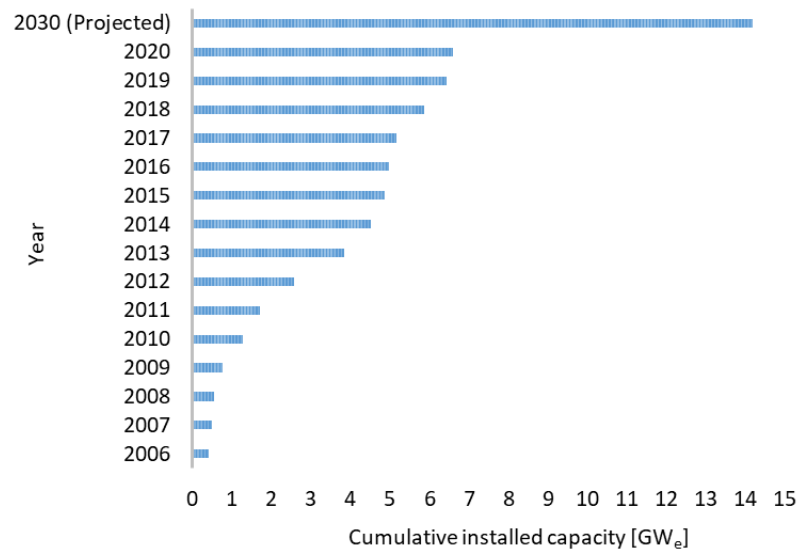
Figure 2.2. The growth of global cumulative installed solar thermal power [57, 58].

2.2. Central receiver technology

The four most common types of CST technologies include linear Fresnel reflector, parabolic trough, central receiver, and parabolic dish, as illustrated in Fig. 2.3 [65]. Among these technologies parabolic trough is the most mature technology which has a share of 80% of total operational solar thermal plants worldwide, as shown in Fig. 2.4 [55]. According to the ITP report on CST technologies [66], the operating temperature ranges of linear (Fresnel reflector and parabolic trough) and point focused (parabolic dish and central receiver) systems are $100 - 450^{\circ}C$ and $300 - 2000^{\circ}C$, respectively. The higher operating temperature of the parabolic dish and central receiver technology in comparison with other CST technologies is due to the possibility of higher solar concentration ratio (>1000). The solar concentration ratio for linear Fresnel reflector and parabolic trough is reported to be less than 90 and 170, respectively [67]. Parabolic dish is only suited to small receivers, owing to the need to mount a receiver onto the dish. This makes central receiver assisted systems potentially suitable for upscaling, to meet the heat demands of high temperature heavy industrial processes. Different types of central receiver technologies have been investigated

21

depending on the type of heat transfer media used, including liquid, gas, and solid-based

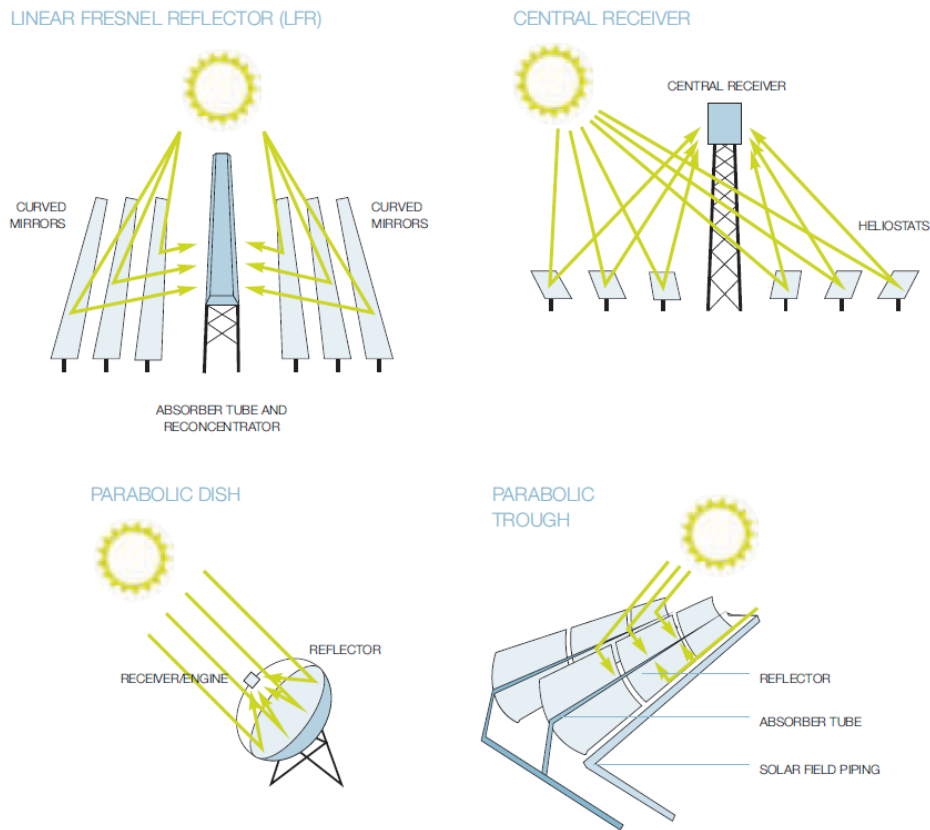receivers [62]. These are discussed below.

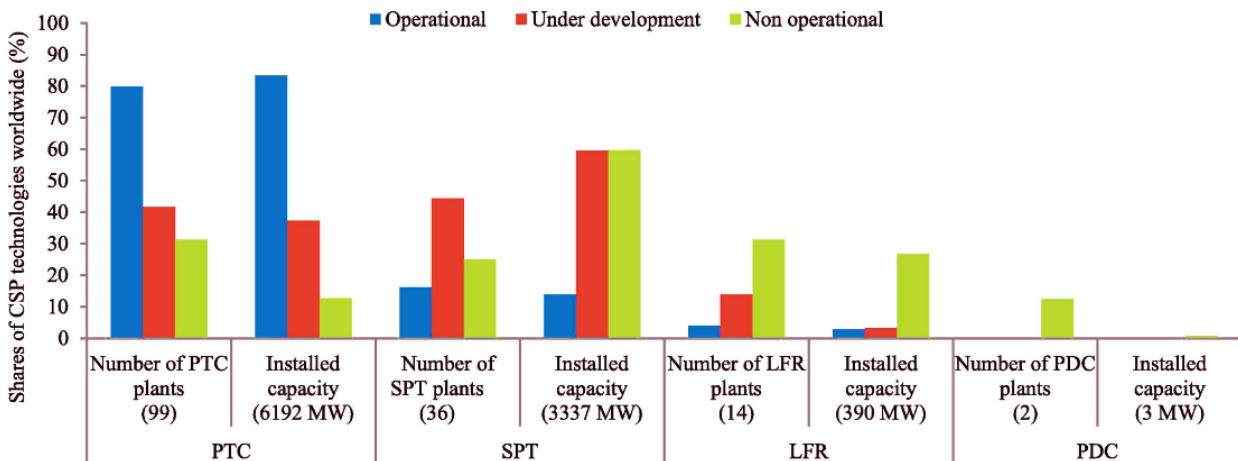Figure 2.3. An illustration of commonly used CST technologies [65].

Figure 2.4. An illustration of the worldwide share of different CSP technologies, including

Parabolic trough collector (PTC), Solar power tower (SPT), Linear Fresnel reflector (LFR),

and Parabolic dish collector (PDC) [55, 59]. The data presented is for year 2020.

2.2.1. Molten salt receivers

Presently, the central receiver technology mostly uses molten nitrate salts as heat transfer fluid but due to the chemical instability of these salts, their operation is limited to below 600°C [68], which is not suitable for high temperature process heat applications (>900°C). Table 2.1 provides a summary of the commonly used molten salts and their stable temperature range [69-71]. These salts become chemically unstable above 600°C resulting in the production of corrosive oxide ions and can cause excessive loss of heat transfer fluid [68, 72]. This limitation of operating temperature is not in line with the motivation of CST technology development for high temperature applications. The chemical instability at higher temperatures limits the use of CST technology for different industrial processes such as the calcination process, which requires an operating temperature of ~1000°C.

Table 2.1. A summary of the commonly used molten salts and their stable working temperature range [69-71].

Molten Salt	Stable temperature range (°C)
$NaNO_3$ - KNO_3	222 – 588
$NaNO_2$ - $NaNO_3$ - KNO_3	142 – 630
$Ca(NO_3)_2$ - $NaNO_3$ - KNO_3	131 – 554
$Li NO_3$ - $NaNO_3$ - KNO_3	130 – 600

2.2.2. Gas receivers

The use of gases, such as air, helium and CO_2, in central receivers is also a promising concept. The gas as a heat transfer fluid is either used inside the tubes (tubular receiver, Fig. 2.5a) or through a structure of honeycomb channels (volumetric receiver, Fig. 2.5b). In both tubular and volumetric receivers, air is heated to a higher temperature which is then used

for a process or heat is stored to a secondary storage media for later use [62]. The literature identified that volumetric air receivers have the potential to achieve temperatures of above 700°C [15, 73]. The German Aerospace Center (DLR) assembled an innovative 200kW high temperature volumetric air receiver, which has hexagonal shaped modular ceramic absorbers, and reached a maximum outlet air temperature of 980°C with a thermal efficiency of 68% [74]. Buck et al. [75] tested a windowed volumetric air receiver with a secondary concentrator for a hybrid gas turbine unit and reported a thermal efficiency of 70% at peak operating temperature of 815°C. Recently, Patil et al. [15] experimentally tested a 5kW volumetric air receiver containing a reticulated porous ceramic structure and reported a nominal thermal efficiency of 69% at output air temperature of 1133°C. Similarly, Pritzkow [76] reported a maximum output air temperature and thermal efficiency of 1050°C and 71%, respectively. Furthermore, the numerical model of a volumetric receiver employed by Stadler et al. [77] showed that these receivers have the potential to achieve peak efficiencies of 70.9% with an output air temperature of 650°C. Some details of these high temperature volumetric air receivers are provided in Table 2.2, whereas a comprehensive summary of volumetric receivers has been provided previously by Ho and Iverson [78], and Ávila-Marín [79]. Most of these cavity air receivers employ an aperture window, which is a critical component, to lower the heat losses. However, window is more prone to failure and increases the maintenance costs [80], in a scale-up design of the receiver operating beyond 1000°C.

Although these air receivers have been widely reported previously in pursuit of high temperatures [15, 73, 78, 79], inferior heat transfer properties are a challenge for their upscaling. In this regard, the use of solid particles in suspension within an air stream has the potential to increase the effectiveness of the heat transfer mechanisms within the receiver cavity, due to their high surface area per unit mass and capacity for direct absorption of

concentrated solar radiation [36]. However, further investigation is required about the quantitative benefits offered by the addition of particles into the air stream.
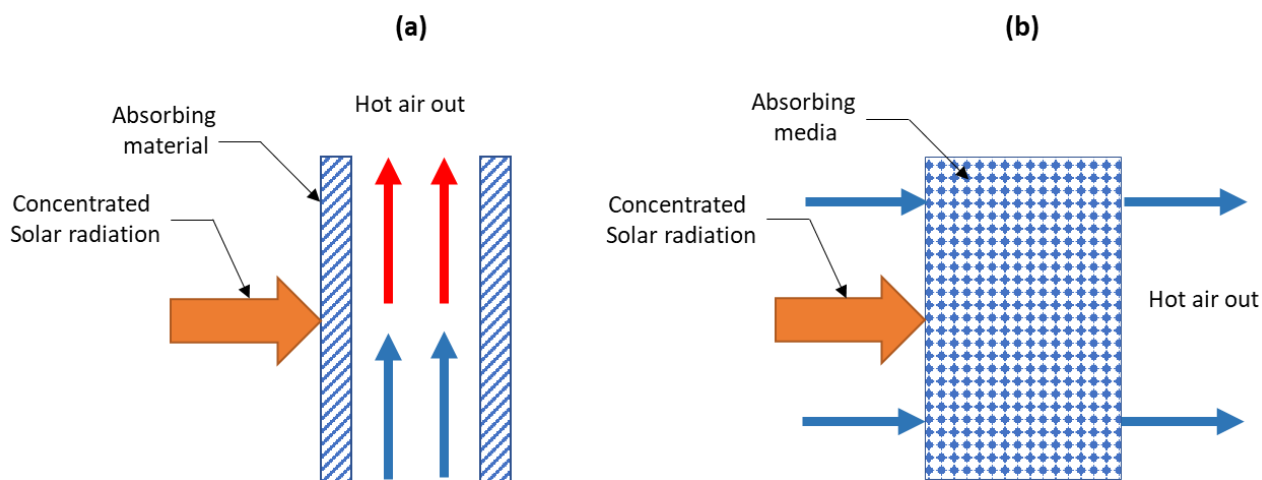
(a)   **(b)**

Figure 2.5. A schematic diagram of (a) tubular receiver and (b) volumetric receiver.

Table 2.2. An overview of volumetric receivers from the point of view of operating temperature and pressure, absorber material, and thermal efficiency.

Reference	Operating temperature	Operating pressure	Thermal efficiency	Thermal Scale	Type of study	Absorber type
Patil et al. [15]	1133˚C	atm	0.69	5 kW	Experimental	reticulated porous ceramic
Hoffschmidt et al. [74]	980˚C	-	0.68	200 kW	Experimental	modular ceramic
Buck et al. [75]	815˚C	5.2 bar	0.70	410 kW	Experimental	heat resistant wires
Pritzkow [76]	1050˚C	5.2 bar	0.71	5 kW	Experimental	ceramic foam absorber (Si_3Ni_4)
Stadler et al. [77]	650˚C	atm	0.71	-	Numerical	ceramic honeycomb
Karni et al. [81]	800˚C	25	-	10 kW	Experimental	-
Chavez and Chaza [82]	550°C	-	0.65	800 kW/m^2	Experimental	porous ceramic absorber
	730°C		0.54			

2.2.3. High temperature particle receivers

One advancement towards achieving the CST development goal for high temperature process heat applications, for a better trade-off between operating temperature and thermal losses, is the use of solid particle-based solar receivers in which ceramic particles,

alone or within a vortex of air, are used as the heat transfer medium [83]. These receivers have the potential to achieve a temperature above 1000°C as particles come in direct contact with the solar radiation as opposed to heat conduction through a wall for indirectly irradiated receiver [84, 85]. Furthermore, the particles used for these receivers are more stable and are less expensive relative to molten salts [86]. Several studies on particle-based receivers have been reported in the literature including the design of receiver, mathematical modelling, and testing of pilot plants [31, 32, 61]. Table 2.3 summaries different particles used for high temperature applications.

Table 2.3. Optical properties of different ceramic particles, from reference [87].

Material Name	Type	Solar weighted absorptivity [-]	Thermal emissivity [-]
CarboProp 40/70	Sintered Bauxite	0.929	0.803
CarboProp 30/60	Sintered Bauxite	0.894	0.752
Accucast ID50K	Sintered Bauxite	0.906	0.754
Accucast ID70K	Sintered Bauxite	0.909	0.789
Fracking Sand	Silica	0.55	0.715

Ho et al. [88] suggested that particle based receiver technology has the potential of scaling to capacity of 10 to 100 MWe at temperatures above 700°C [28, 29, 89-94]. The potential advantages offered by solid particles used in central receiver technology are summarized as:

- Most of the ceramic particles are inert and stable at temperatures of around 1000°C. Also, these particles have no freezing issue which eliminates the trace heating requirements.

- Sensible energy can be storage in a wide temperature range due to the high melting temperature of particles.

- Most of the particles are low-cost in comparison with the commonly used molten salts.

- They can help to reduce the cost of storage as heat is directly stored in the sand like ceramic particles.

- The inert nature of these particles offers the flexibility, based on the process side requirement, to be used as a standalone heat transfer medium or in suspension within gas stream to enhance the heat transfer mechanism.

There are also disadvantages associated with these particle receivers. Some of the disadvantages, which requires further attention, include particle handling and transportation, particle attrition, particle erosion, risk of damage to windows, and egress from open apertures.

The high temperature particle receiver technologies have the potential to achieve operating temperatures of over 1000°C, which is far higher than that of commercial molten salts [35]. However, limited information is available on the transient response of directly irradiated high temperature particle-based receivers, considering transient losses through a year of operation. Also, there is a lack of available data of their industrial level system performance with suitability to heat air to temperatures of around 1000°C for retrofit applications. This arises the need to address the behaviour of high temperature particle receivers during start-up, turn down, and shutdown periods, under unsteady conditions, and how the thermal performance of these receivers is affected under transient operation considering the real-time variability of solar resource.

2.3. Directly irradiated high temperature particle receivers

A directly-irradiated particle-laden receiver utilizes a cavity enclosure to contain concentrated solar radiation and to reduce the thermal losses [13]. The concept of cavity receiver is to direct the reflected solar radiations from the heliostat field to the heat transfer medium through the aperture of the cavity, as shown in Fig. 2.6.

Different types of particle-based receiver designs have been investigated to improve the receiver efficiency by reducing thermal losses and achieving higher operating temperatures [33, 95-97]. Figure 2.7 summarizes the configurations of particle-laden receiver technologies available in literature. The most widely investigated designs include free-falling including obstructed flow [98-100], centrifugal [31-33, 101], and tubular receivers (fluidized) [102-104]. The basic designs of these widely used particle receivers are shown in Fig. 2.8. Using the primary concept of these designs, researchers have considered different other configurations to be used for the particles in central receiver technologies. These secondary designs include a V-shaped mesh [105], porous structure [106], inclined plate [107], and spiral tubes [108] inside a receiver cavity to increase the residence time of particles for higher absorption efficiency. The main characteristics of these configurations are described in Table 2.4. The thermal performance of these receivers when operating alone has been reported to be in the range of 75 to 80% when operating at temperatures of 750 to 900°C. However, their performance when integrated into complete systems has only been reported for the generation of electricity using steam and gas turbine cycles [49-55]. Limited information is available of their performance when integrated into systems that produce high temperature heat, above 1000°C, for heavy industrial applications such as the production of alumina. There is also a lack of available data of their performance when used to reheat warm air that has been returned from a process or thermal storage system, at temperatures >300°C.
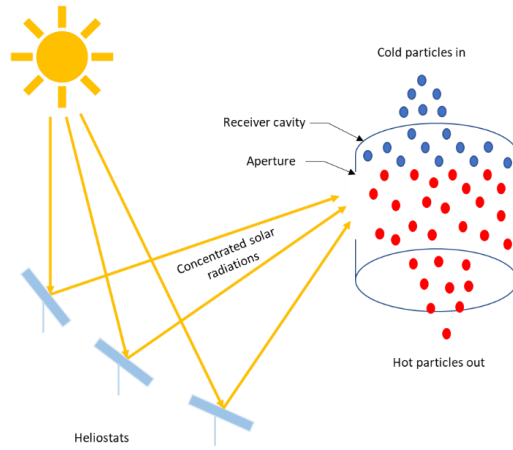
Figure 2.6. A schematic diagram illustrating the basic design of a cavity receiver.
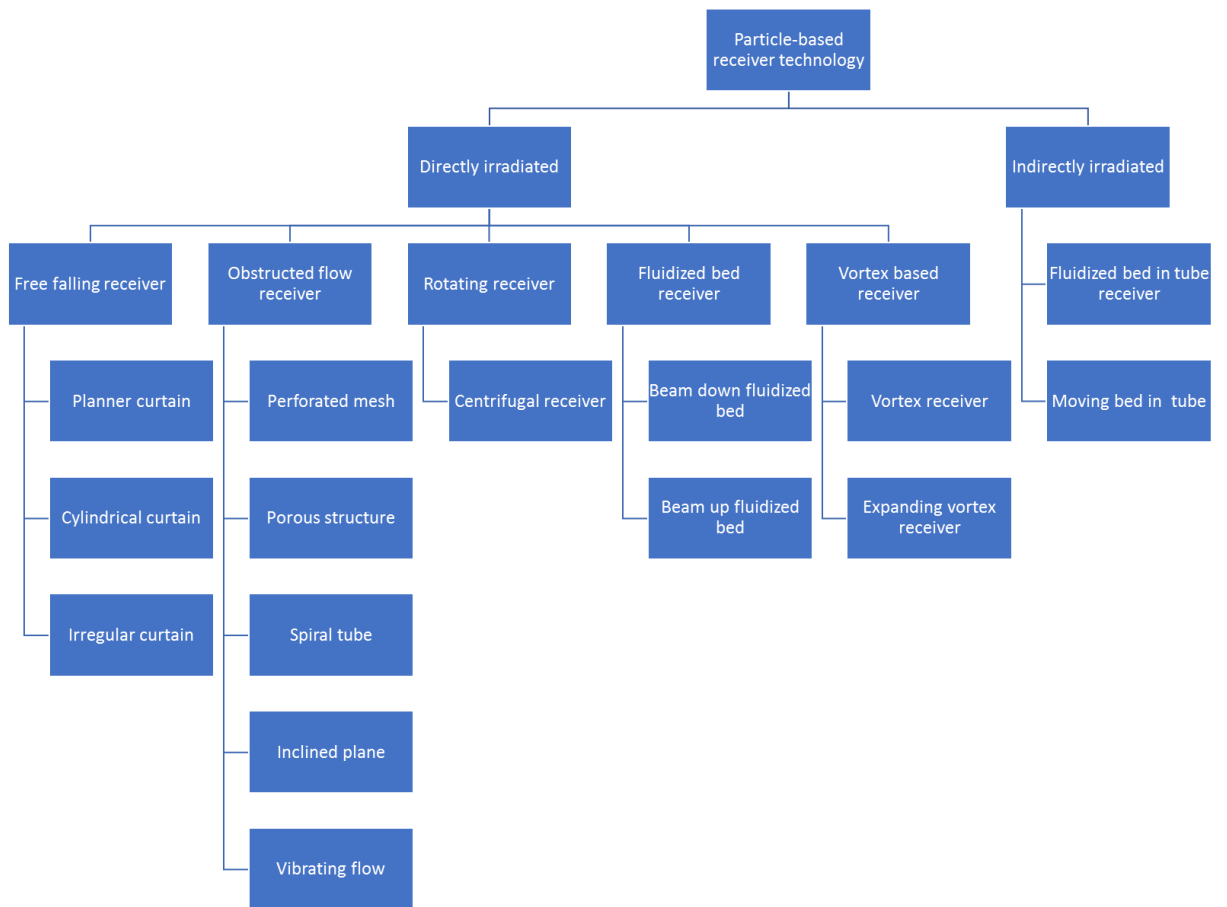

Figure. 2.7. A summary of the classification of particle-based receiver technologies, studied in the literature.
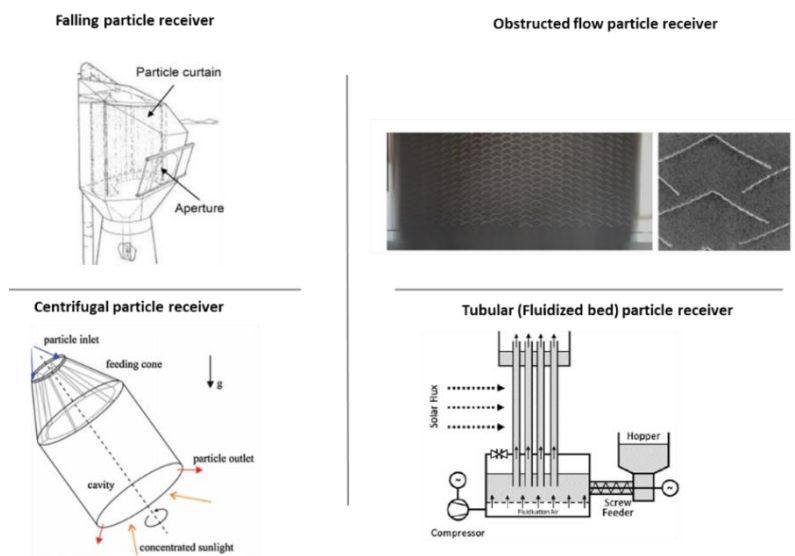
Figure 2.8. The basic designs of particle receiver technology [87, 104].

Table 2.4. The secondary configurations of particle receivers studied using primary designs

listed in Fig. 2.8.

Design	Potential benefits	Challenges	Schematic diagram	Reference
V-shaped mesh	The V-shaped structure inside a receiver cavity helps to increase the residence time and achieve uniform distribution of particles, for higher temperatures and better efficiency.	The structural complexity and required maintenance increase the overall system cost.		Al-Ansary et al. [105]
Porous structure	The porous structure inside a receiver provides an obstruction and increase the particle residence time. It also helps to achieve a stable particle flow.	The porous material selection based on particle size is challenging.		Lee et al. [106]
Inclined plate	The inclined plate inside a receiver increases the particle residence time and reduces the particle circulation loss, relative to falling particle receiver.	The angle of plate for uniform flow of particles is challenging, as particle accumulation on the plate can easily block the flow. This will require an additional flow of air.		Xie et al. [107]
Spiral tubes	The spiral tubes increase the particle residence time and provide better control of the particle flow inside the tubes, relative to falling particle receiver.	The indirect heat transfer to the particles increases the extra resistance to heat exchange. Furthermore, a blockage can easily occur inside the tubes.		Xiao et al. [108]

2.3.1. Solar vortex receivers

One type of cavity receiver which gained particular attention in recent years is solar vortex receiver (SVR) [109]. Concentrated solar radiation is directed to an aperture to directly heat a vortex of particles and gas (i.e., air), inside a cylindrical cavity. The basic configuration of SVR, as shown in Fig. 2.9 [36], consists of an aperture covered by a quartz window placed normal to the cavity axis through which concentrated solar radiations fall onto the particles injected tangentially along with a gas to form a vortex. The heated particles and gas exit from the rear along the axis of the cavity [39, 110]. Although these vortex based receivers give high conversion efficiency, but they have two major drawbacks, which are as follows [111]:

I.   The residence time is independent of the particle size which may result in overheating of smaller particles and underheating of larger ones. This will cause a decrease in the overall thermal performance of an upscaled receiver.

II.   Higher particle deposition on the aperture window lowers the receiver's thermal performance and can also generate a risk of window failure, resulting in higher operating costs. Noting that the overall cost of quartz glass window for high temperature receivers is too high [112], due to the need for high transmittance and large area when upscaled.
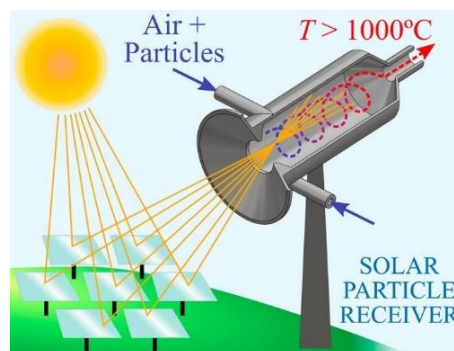

Fig. 2.9. The basic configuration of a SVR, adapted from [36].

31

2.3.2. Solar expanding vortex receiver

To overcome the drawbacks associated with the SVR, Chinnici et al. [40-42] presented a new configuration of cylindrical cavity receiver called as Solar Expanding Vortex Receiver (SEVR), which is shown in Fig. 2.10. This novel configuration has a modified geometry, with the introduction of a conical section. The particles and air exit in the direction which is radial to the axis of the receiver cavity. The residence time is dependent on the particle size in this new configuration, which helps to achieve a uniform outlet temperature. This configuration is also helpful to avoid the particle egress through the aperture. The authors evaluated the effect of receiver geometry on the particle trajectories and residence times using a CFD model [40]. Furthermore, particle's deposition onto the aperture window was also assessed, both experimentally and numerically [41]. It was found that for a fixed aperture size, an increase in the cone angle is favourable as it generates a larger vortex at the aperture plane. That is why a larger cone angle is favourable for smaller size particles, as it will lower the particle flowing towards the aperture. The optimum value of the cone angle was predicted to be 40° for the studied conditions. Chinnici et al. [41, 42] further confirmed that a well-established vortex flow inside the cavity is generated by SEVR compared with SVR. It was also found that a reversed flow is formed in the vortex core region, whereas at the inlet and outlet regions of the cavity, a processing vortex core (PVC) structure is observed, as shown in Fig. 2.10 [42].

The vortex receiver was chosen for the present assessments because it has the potential to achieve temperatures of >1000°C [37-39], and can be configured either as an air or particle heater. This makes SEVR potentially suitable to be used with other components as an air heater, for retrofit industrial applications. Also, the modified version of vortex receiver, SEVR, offer the possibility to operate the receiver windowless.
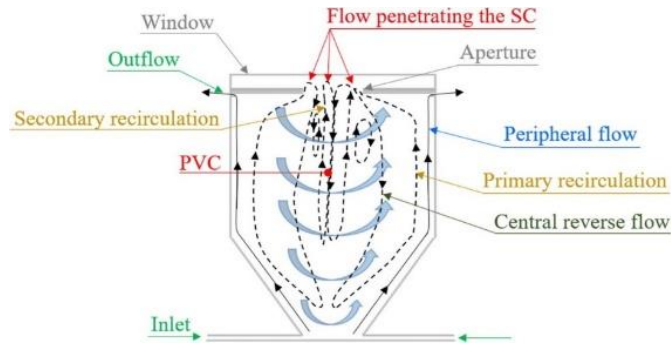
Figure 2.10. An illustration of flow patterns within a SEVR, adapted from [42].

2.4. Need to account for solar intermittency and variability

Although directly irradiated particle-laden receivers have the potential to achieve temperatures of order of 1000°C, there is a lack of knowledge of the influence of the time-constants of particle receivers on dynamic operation caused by solar resource variability. Theoretical and experimental studies have been carried out for cylindrical cavity receivers and most of them have indicated their advantage of achieving better heat transfer to particle-laden flow [16, 113]. The output temperature in the order of 1000°C can be achieved using these receivers and they have the flexibility to be configured in different alternative ways [16]. Numerous studies for high temperature cavity receivers have used a rather computationally expensive, complex and time-consuming computational fluid dynamics (CFD) method to study the effect of different geometric parameters and operating conditions on their performance [99, 111, 114-117]. These CFD studies have contributed significantly to investigating the flow features inside a cavity receiver, the influence of solar transients on the long-term thermal performance of these receivers, considering start-up, turn down and shutdown periods, is still unknown. Some analytical models have also been developed for high temperature particle-laden receivers [36, 118, 119] but those also have not considered the transient effect on the annual thermal performance of these receivers.

While the above-mentioned studies have analysed the thermal performance of high temperature particle-laden receivers and indicated their potential advantages, these have not considered the transient effect on the receiver thermal performance. The solar flux changes significantly from one location to another which means the actual performance of the receiver can only be assessed based on the real-time climatic conditions of each location, considering transient losses. The distribution of minutely, hourly, daily and monthly DNI for a specific location varies significantly [9]. Saw et al. [9] concluded that the performance estimation of solar technologies based on average monthly or daily data can have an uncertainty of $20 - 30\%$. That is why hourly or minutely performance evaluation is recommended to get a reasonably good estimation of system performance. Therefore, the transient performance of the high temperature particle-laden receivers needs to be assessed based on the actual solar DNI data for a specific site. This requires the development of analytical transient models of these receivers to be solved for hourly or minutely solar irradiation data over a longer period.

2.5. Use of refractory lining in high temperature cavity receivers

Directly irradiated particle-laden receivers either require the use more expensive high temperature metals, adding to cost, or a refractory lining, which is both brittle and has high thermal inertia. The selection of refractory material and its behaviour under transient operating conditions will largely influence the thermal performance of a high temperature receiver. The properties and quality of the refractory will also determine the extent of heat losses from a receiver cavity when a variable solar DNI is received at the aperture. Furthermore, the operation of a receiver with particles involves abrasion, so to avoid refractory failures and unplanned shutdowns, a multi-layer refractory is typically employed. While such challenges are likely to be even greater for high temperature particle-laden

receivers, to supply process heat at temperatures of >1000°C, limited information is available with which to assess how the design of refractory lining should be optimised employing real-time solar variability. Furthermore, while refractory-lined solar receivers are expected to have longer start-up time, little attention has been provided to the options with which this time might be reduced when considering long-term solar resource variability [45], such as by reducing the overnight heat losses by implementing some shutdown strategies during shutdown period. Hence there is a need to better understand the start-up behavior of these receivers, and the potential options with which this time might be reduced, considering the influence of solar intermittency. Hence there is a need for a more detailed assessment of how to optimize the performance of the refractory-lined solar receivers under transient operating conditions.

2.5.1. Refractory materials

The lightweight fibre refractories having lower thermal conductivities provide good insulation and lower the heat losses from a refractory-lined receiver to the surroundings. However, these fibre refractories cannot be used as the hot inside lining which comes in direct contact with the particles and high temperature environment, as they offer less resistance to mechanical and thermal stresses. Dense refractory materials having good strength to mechanical abrasion and thermal shock are required on the inside of a receiver cavity. The insulating layer of refractory over the hot face lining can be made of a less dense material having lower thermal conductivity [120]. That is why, most of the non-solar devices such as rotary kilns employ a multilayered cavity under extreme operating conditions, even though they mostly operate under steady-state conditions [121, 122]. This is incompatible with the operation of a directly irradiated solar receiver, which need to accommodate the solar transients during its operation [123]. Therefore, the lack of evaluations of the potential

of refractories to be configured to operate with high changes in flux arise the need of further assessments, which can account for solar intermittency and variability.

The most common materials used for the manufacturing of refractories are oxides of aluminium (alumina), silicon (silica) and magnesium (magnesia):

- Alumina (Al_2O_3) refractories are composed of ≥ 50% of alumina and these are sensitive to thermal shock requiring slow warm-up [121, 124]. Furthermore, higher creep rates of alumina limit its use to below 1,500°C [125]. Alumina refractory bricks are largely employed in cement and metallurgy kilns.

- Silica refractories are composed of >93% silicon oxide (SiO_2). These can withstand high thermal and mechanical shocks [126]. An important property of silica brick is its ability to maintain hardness under high loads to its melting point of ~1700°C [127]. At a temperature of around 593°C, silica bricks are nearly volume stable and virtually free from thermal spalling, while at temperatures below 593°C, silica bricks are highly susceptible to thermal spalling. That is why slow heating of silica refractories during start-up increase their life [127]. Silica refractory bricks are typically used in iron and steel industries.

- Magnesite refractories are composed of ≥85% magnesium oxide (MgO) [128]. These have good thermal shock and excellent slag-corrosion resistance at elevated temperature (around 1500°C) [129], but MgO bricks are not capable of resisting sudden changes of temperature and show a tendency to spall under such conditions. The cost of magnesite refractories is higher than that of silica-based refractories. Typically, magnesite refractories are used in the construction of those parts of a furnace that are required to withstand the corrosive action of basic slags.

- Fireclay refractories such as super duty firebricks with <50% Al_2O_3 is another type of refractory used for high temperature applications [130]. Fireclay refractory bricks have good spalling resistance [131]. It has a lower thermal expansion coefficient relative to alumina [124, 131-133]. Fireclay refractory bricks are cheaper in comparison with alumina, silica and magnesia refractories. The fireclay refractories are used for the linings of blast and heat treatment furnaces.

While some previous investigations of refractory-lined solar cavities have provided information on the heating rates they employed, no systematic investigation is available with which to assess how the design of refractory lining should be optimised for transient operation employing real-time solar variability. The numerical model of a lab scale multilayered cavity reactor employed by Abanades et al. [46] and Charvin et al. [134] showed that, 15 minutes of heating time is required for the reactor to achieve a temperature of 2500K, when alumina refractory lining is used. Similarly, the heating period of a simulated industrial-scale reactor was estimated to be 40–60 minutes with a constant input DNI of 1000 W/m^2, by Charvin et al. [134]. This gives an average heating rate of ~60 K/minute for the first 30 minutes of the reactor operation which is at the upper end of allowable heating rates for alumina refractory to avoid damage from thermal shock [121, 124]. This highlights the need to investigate the influence of refractory thickness with regard to the trade-off between heating time and allowable cavity heating rate for a smooth operation based on the intermittent nature of input solar resource. The optimized design of refractory lining can help in upscaling the concept of these receivers to a higher power level under real-time operating conditions.

2.6. Need of system-level analysis for process heat

Recent technology innovation in the fields of concentrating solar thermal is opening new potential markets to be considered for viability. In particular, high-temperature particle-laden receivers are being developed to achieve temperatures in the order of 1000°C for advance power cycles and solar thermochemical processes [25, 49-54]. The integration of these solar central receiver systems has widely been reported in the literature, but only for low temperature applications or for the generation of electricity using steam and gas turbine cycles. There are limited studies on the integrated systems to produce high temperature heat, above 1000°C, for heavy industrial applications such as for the production of alumina and hydrogen. This requires further information on the system level performance of high-temperature concentrated solar thermal plant, based on suspension flow solar particle receiver integrated with a sensible thermal storage, to supply high temperature heat to a downstream thermochemical process under transient operating conditions. This require further information of the system level performance of a complete CST plant with relative trade-offs between these components, considering the real-time interaction between receiver and thermal storage to understand the performance of refractory-lined particle-laden receivers in combination with a thermal storage and other components of a CST system.

Simulation tools such as SAM [135] and GREENIUS [136] are commonly used for system simulation, and perform well for conventional CST systems such as molten salt tubular receivers. However, the integration of new technologies and concepts, such as refractory-lined suspension flow systems, is more challenging to customize using these available tools. This further arises the need of system analysis by integrating the physical sub-models with heat and mass transfer equations for each component to understand their combined performance considering site-specific solar variability.

2.7. Summary and research gaps

The use of particles, alone or in suspension within an air flow, inside a directly irradiated SEVR, is a promising class of technology for operating at temperatures well above 1000°C and is one of the potential pathways for the next-generation CST plants [4, 5]. However, little is known on the system-level performance of these receivers operating in combination with a sensible thermal storage system to provide steady high temperature air, above 1000°C, for retrofit industrial applications. Also, the design temperature of these receivers above 1000°C, for process heat applications, increases the requirement of a refractory lining which is both brittle and has high thermal inertia [137]. While significant challenges arise from the transient operation of high temperature particle-laden receivers with a lining of refractory material owing to their higher thermal inertia, no equivalent assessment of their transient response during start-up, turn down and shutdown is available. This arises the need to address how refractory-lined high temperature receivers will behave under unsteady conditions and how thermal performance of these receivers will be affected under transient operation considering the variable nature of the solar resource.

Furthermore, there is a lack of investigations on the heat loss overnight for refractory-lined cavity receivers under different geometric parameters and operating conditions. Also, there are limited understandings about receiver shutdown strategy, along with what combination of thicknesses of insulation and inner refractory are needed for better thermal gains to balance different conditions of relevance to practical receivers. That is why the thermal behaviour of the refractory-lined receivers need further investigation to understand the trade-off between operating temperature, temperature drop overnight and start-up time based on the extended time-series of solar input data. Further to this, there is a need of an assessment that provides a new understanding of the system level performance of these CST systems, based on these refractory-lined suspension flow solar particle receivers

integrated with sensible thermal storage, considering solar resource variability and real-time interaction between sub-systems.

The above-mentioned challenges require the development of analytical transient models for particle-laden receivers to be solved for real-time solar irradiation data for prediction of thermal outputs, while also providing the opportunity to integrate into a complete CST system model. This will help to better understand the transient thermal response of a refractory-lined particle-laden receiver system during start-up, turn down, and shutdown with long time-series of variable solar input to guide the design optimization of a CST system. Therefore, this project aims to fulfill these needs firstly by modelling and understanding the thermal response of a high temperature refractory-lined particle-laden receiver sub-system. Then, providing an understanding of the trade-off between the receiver and thermal storage sub-systems with transient mathematical models of the receiver and packed bed thermal storage sub-systems considering solar resource variability, written in a Simulink environment, to be solved for real-time solar irradiance data over a longer period. The detailed objectives, with a comprehensive background, and research outcomes are listed in Chapter 1.

2.8. References

[1]   J. Pedraza, A. Zimmermann, J. Tobon, R. Schomäcker, and N. Rojas, "On the road to net zero-emission cement: Integrated assessment of mineral carbonation of cement kiln dust," *Chemical Engineering Journal,* vol. 408, pp. 127346, 2021/03/15/, 2021.

[2]   P. Wang, M. Ryberg, Y. Yang, K. Feng, S. Kara, M. Hauschild, and W.-Q. Chen, "Efficiency stagnation in global steel production urges joint supply- and demand-side mitigation efforts," *Nature Communications,* vol. 12, no. 1, pp. 2066, 2021/04/06, 2021.

[3]   C. Council, *Australia's Rising Greenhouse Gases Emission, Climate Council of Australia Ltd. ,* 2018.

[4]   W. L. Saw, A. Naufal, A. B. Sandoval, A. Beath, K. Lovegrove, P. v. Eyk, R. McNaughton, R. Bader, and G. Nathan, "Technical feasibility of integrating concentrating solar thermal energy in the Bayer alumina process," *AIP Conference Proceedings,* vol. 2303, no. 1, pp. 140005, 2020.

[5]   IEA. "International Energy Agency, http://www.iea.org," March 15, 2020.

[6]   IEA. "World Energy Outlook, www.worldenergyoutlook.org " March 15, 2020.

[7]   D. Hayes, "Asian renewables: South East Asia regional overview," *Refocus,* vol. 5, no. 3, pp. 48, 2004.

[8]   N. Lewis, and D. Nocera, "Powering the planet: chemical challenges in solar energy utilization," *Proceedings of the National Academy of Sciences,* vol. 103, no. 43, pp. 15729-15735, 2006.

[9]   W. L. Saw, P. Guo, P. J. van Eyk, and G. J. Nathan, "Approaches to accommodate resource variability in the modelling of solar driven gasification processes for liquid fuels synthesis," *Solar Energy,* vol. 156, pp. 101-112, 2017/11/01/, 2017.

[10]   H. L. Zhang, J. Baeyens, J. Degrève, and G. Cacères, "Concentrated solar power plants: Review and design methodology," *Renewable & Sustainable Energy Reviews,* vol. 22, pp. 466-481, 2013.

[11]   O. Behar, A. Khellaf, and K. Mohammedi, "A review of studies on central receiver solar thermal power plants," *Renewable & Sustainable Energy Reviews,* vol. 23, pp. 12-39, 2013.

[12]   T. M. Pavlović, I. S. Radonjić, D. D. Milosavljević, and L. S. Pantić, "A review of concentrating solar power plants in the world and their potential use in Serbia," *Renewable & Sustainable Energy Reviews,* vol. 16, no. 6, pp. 3891-3902, 2012.

[13]   A. Steinfeld, "Solar thermochemical production of hydrogen—a review," *Solar Energy,* vol. 78, no. 5, pp. 603-615, 2005/05/01/, 2005.

[14]   V. Quaschning, "Technical and economical system comparison of photovoltaic and concentrating solar thermal power systems depending on annual global irradiation," *Solar Energy,* vol. 77, no. 2, pp. 171-178, 2004/01/01/, 2004.

[15]   V. R. Patil, F. Kiener, A. Grylka, and A. Steinfeld, "Experimental testing of a solar air cavity-receiver with reticulated porous ceramic absorbers for thermal processing at above 1000 °C," *Solar Energy,* vol. 214, pp. 72-85, 2021/01/15/, 2021.

[16]   D. Davis, F. Müller, W. L. Saw, A. Steinfeld, and G. J. Nathan, "Solar-driven alumina calcination for CO2 mitigation and improved product quality," *Green Chemistry,* vol. 19, no. 13, pp. 2992-3005, 2017.

[17]   C. K. Ho, K. J. Albrecht, L. Yue, B. Mills, J. Sment, J. Christian, and M. Carlson, "Overview and design basis for the Gen 3 Particle Pilot Plant (G3P3)," *AIP Conference Proceedings,* vol. 2303, no. 1, pp. 030020, 2020.

[18]   M. Romero, and J. González-Aguilar, "7 - Next generation of liquid metal and other high-performance receiver designs for concentrating solar thermal (CST) central tower systems," *Advances in Concentrating Solar Thermal Research and Technology*, M. J. Blanco and L. R. Santigosa, eds., pp. 129-154: Woodhead Publishing, 2017.

[19]   R. W. Bradshaw, J. G. Cordaro, and N. P. Siegel, "Molten Nitrate Salt Development for Thermal Energy Storage in Parabolic Trough Solar Power Systems." pp. 615-624.

[20]   S. Gupta, D. French, R. Sakurovs, M. Grigore, H. Sun, T. Cham, T. Hilding, M. Hallin, B. Lindblom, and V. Sahajwalla, "Minerals and iron-making reactions in blast furnaces," *Progress in Energy and Combustion Science,* vol. 34, no. 2, pp. 155-197, 2008/04/01/, 2008.

[21]   A. Sagastume Gutiérrez, J. Van Caneghem, J. B. Cogollos Martínez, and C. Vandecasteele, "Evaluation of the environmental performance of lime production in Cuba," *Journal of Cleaner Production,* vol. 31, pp. 126-136, 2012/08/01/, 2012.

[22]   S. Lang, T. Haimi, and M. Köpf, "Circored Fine Ore Direct Reduction Plus DRI Smelting: Proven Technologies for the Transition Towards Green Steel." pp. 61-71.

[23]   D. Davis, F. Müller, W. L. Saw, A. Steinfeld, and G. J. Nathan, "Solar-driven alumina calcination for CO 2 mitigation and improved product quality," *Green Chemistry,* vol. 19, no. 13, pp. 2992-3005, 2017.

[24]   V. I. Pak, S. S. Kirov, A. Y. Nalivaiko, D. Y. Ozherelkov, and A. A. Gromov, "Obtaining Alumina from Kaolin Clay via Aluminum Chloride," *Materials,* vol. 12, no. 23, pp. 3938, 2019.

[25]   B. H. Mills, C. K. Ho, N. R. Schroeder, R. Shaeffer, H. F. Laubscher, and K. J. Albrecht, "Design Evaluation of a Next-Generation High-Temperature Particle Receiver for Concentrating Solar Thermal Applications," *Energies,* vol. 15, no. 5, pp. 1657, 2022.

[26]   J. Christian, and C. Ho, "System Design of a 1 MW North-facing, Solid Particle Receiver," *Energy Procedia,* vol. 69, pp. 340-349, 2015/05/01/, 2015.

[27]   G. J. Kolb, R. B. Diver, and N. Siegel, "Central-Station Solar Hydrogen Power Plant," *Journal of Solar Energy Engineering,* vol. 129, no. 2, pp. 179-183, 2006.

[28]   N. P. Siegel, C. K. Ho, S. S. Khalsa, and G. J. Kolb, "Development and Evaluation of a Prototype Solid Particle Receiver: On-Sun Testing and Model Validation," *Journal of Solar Energy Engineering,* vol. 132, no. 2, 2010.

[29]   M. Röger, L. Amsbeck, B. Gobereit, and R. Buck, "Face-Down Solid Particle Receiver Using Recirculation," *Journal of Solar Energy Engineering,* vol. 133, no. 3, 2011.

[30]   T. Tan, Y. Chen, Z. Chen, N. Siegel, and G. J. Kolb, "Wind effect on the performance of solid particle solar receivers with and without the protection of an aerowindow," *Solar Energy,* vol. 83, no. 10, pp. 1815-1827, 2009/10/01/, 2009.

[31]   W. Wu, R. Uhlig, R. Buck, and R. Pitz-Paal, "Numerical Simulation of a Centrifugal Particle Receiver for High-Temperature Concentrating Solar Applications," *Numerical Heat Transfer, Part A: Applications,* vol. 68, no. 2, pp. 133-149, 2015/07/18, 2015.

[32]   W. Wu, D. Trebing, L. Amsbeck, R. Buck, and R. Pitz-Paal, "Prototype Testing of a Centrifugal Particle Receiver for High-Temperature Concentrating Solar Applications," *Journal of Solar Energy Engineering,* vol. 137, no. 4, 2015.

[33]   W. Wu, L. Amsbeck, R. Buck, R. Uhlig, and R. Ritz-Paal, "Proof of Concept Test of a Centrifugal Particle Receiver," *Energy Procedia,* vol. 49, pp. 560-568, 2014/01/01/, 2014.

[34]   W. Wu, L. Amsbeck, R. Buck, N. Waibel, P. Langner, and R. Pitz-Paal, "On the influence of rotation on thermal convection in a rotating cavity for solar receiver applications," *Applied Thermal Engineering,* vol. 70, no. 1, pp. 694-704, 2014/09/05/, 2014.

[35]   G. Flamant, D. Gauthier, H. Benoit, J.-L. Sans, R. Garcia, B. Boissière, R. Ansart, and M. Hemati, "Dense suspension of solid particles as a new heat transfer fluid for concentrated solar thermal plants: On-sun proof of concept," *Chemical Engineering Science,* vol. 102, pp. 567-576, 2013/10/11/, 2013.

[36]   D. Davis, M. Jafarian, A. Chinnici, W. L. Saw, and G. J. Nathan, "Thermal performance of vortex-based solar particle receivers for sensible heating," *Solar Energy,* vol. 177, pp. 163-177, 2019/01/01/, 2019.

[37]   A. Z'Graggen, P. Haueter, G. Maag, M. Romero, and A. Steinfeld, "Hydrogen production by steam-gasification of carbonaceous materials using concentrated solar energy—IV. Reactor experimentation with vacuum residue," *International Journal of Hydrogen Energy,* vol. 33, no. 2, pp. 679-684, 2008/01/01/, 2008.

[38]   A. Z'Graggen, P. Haueter, G. Maag, A. Vidal, M. Romero, and A. Steinfeld, "Hydrogen production by steam-gasification of petroleum coke using concentrated solar power—III.

Reactor experimentation with slurry feeding," *International Journal of Hydrogen Energy,* vol. 32, no. 8, pp. 992-996, 2007/06/01/, 2007.

[39]   A. Z'Graggen, P. Haueter, D. Trommer, M. Romero, J. C. de Jesus, and A. Steinfeld, "Hydrogen production by steam-gasification of petroleum coke using concentrated solar power—II Reactor design, testing, and modeling," *International Journal of Hydrogen Energy,* vol. 31, no. 6, pp. 797-811, 2006/05/01/, 2006.

[40]   A. Chinnici, M. Arjomandi, Z. F. Tian, Z. Lu, and G. J. Nathan, "A Novel Solar Expanding-Vortex Particle Reactor: Influence of Vortex Structure on Particle Residence Times and Trajectories," *Solar Energy,* vol. 122, pp. 58-75, 2015/12/01/, 2015.

[41]   A. Chinnici, M. Arjomandi, Z. F. Tian, and G. J. Nathan, "A Novel Solar Expanding-Vortex Particle Reactor: Experimental and Numerical Investigation of the Iso-thermal Flow Field and Particle Deposition," *Solar Energy,* vol. 133, pp. 451-464, 2016/08/01/, 2016.

[42]   A. Chinnici, Y. Xue, T. C. W. Lau, M. Arjomandi, and G. J. Nathan, "Experimental and numerical investigation of the flow characteristics within a Solar Expanding-Vortex Particle Receiver-Reactor," *Solar Energy,* vol. 141, pp. 25-37, 2017/01/01/, 2017.

[43]   A. Chinnici, D. Davis, T. C. W. Lau, D. Ang, M. Troiano, W. L. Saw, Z. F. Tian, R. Solimene, P. Salatino, and G. J. Nathan, "Measured global thermal performance of a directly irradiated suspension-flow solar particle receiver with an open aperture," *Solar Energy,* vol. 231, pp. 185-193, 2022/01/01/, 2022.

[44]   CET.   "https://www.adelaide.edu.au/cet/technologies/solar-expanding-vortex-particle-receiver-reactor-sevr," April 01, 2020.

[45]   O. A. Ortiz, G. I. Suárez, and A. Nelson, "Dynamic simulation of a pilot rotary kiln for charcoal activation," *Computers & Chemical Engineering,* vol. 29, no. 8, pp. 1837-1848, 2005/07/15/, 2005.

[46]   S. Abanades, P. Charvin, and G. Flamant, "Design and simulation of a solar chemical reactor for the thermal reduction of metal oxides: Case study of zinc oxide dissociation," *Chemical Engineering Science,* vol. 62, no. 22, pp. 6323-6333, 2007/11/01/, 2007.

[47]   Y. C. Soo Too, J. García, R. V. Padilla, J.-S. Kim, and M. Sanjuan, "A transient optical-thermal model with dynamic matrix controller for solar central receivers," *Applied Thermal Engineering,* vol. 154, pp. 686-698, 2019/05/25/, 2019.

[48]   M. M. Rafique, et al., "A mathematical model to assess the influence of transients on a refractory-lined solar receiver," *[UPDATE]*, July 2020, 2020.

[49]   F. Rovense, M. Á. Reyes-Belmonte, M. Romero, and J. González-Aguilar, "Thermo-economic analysis of a particle-based multi-tower solar power plant using unfired combined cycle for evening peak power generation," *Energy,* vol. 240, pp. 122798, 2022/02/01/, 2022.

[50]   O. Behar, B. Grange, and G. Flamant, "Design and performance of a modular combined cycle solar power plant using the fluidized particle solar receiver technology," *Energy Conversion and Management,* vol. 220, pp. 113108, 2020/09/15/, 2020.

[51]   M. A. Reyes-Belmonte, A. Sebastián, J. Spelling, M. Romero, and J. González-Aguilar, "Annual performance of subcritical Rankine cycle coupled to an innovative particle receiver solar power plant," *Renewable Energy,* vol. 130, pp. 786-795, 2019/01/01/, 2019.

[52]   L. F. González-Portillo, K. Albrecht, and C. K. Ho, "Techno-Economic Optimization of CSP Plants with Free-Falling Particle Receivers," *Entropy,* vol. 23, no. 1, pp. 76, 2021.

[53]   K. J. Albrecht, M. L. Bauer, and C. K. Ho, "Parametric Analysis of Particle CSP System Performance and Cost to Intrinsic Particle Properties and Operating Conditions."

[54]   R. Buck, and S. Giuliano, "Impact of Solar Tower Design Parameters on xCO2-based Solar Tower Plants," 2018.

[55]   R. P. Merchán, M. J. Santos, A. Medina, and A. Calvo Hernández, "High temperature central tower plants for concentrated solar power: 2021 overview," *Renewable and Sustainable Energy Reviews,* vol. 155, pp. 111828, 2022/03/01/, 2022.

[56]   IEA. "Global Energy Review: CO2 Emissions in 2021."

[57]   Y.-L. He, Y. Qiu, K. Wang, F. Yuan, W.-Q. Wang, M.-J. Li, and J.-Q. Guo, "Perspective of concentrating solar power," *Energy,* vol. 198, pp. 117373, 2020/05/01/, 2020.

[58] GlobalData. "https://www.globaldata.com/."

[59] O. Achkari, and A. El Fadar, "Latest developments on TES and CSP technologies – Energy and environmental issues, applications and research trends," *Applied Thermal Engineering,* vol. 167, pp. 114806, 2020/02/25/, 2020.

[60] G. J. Nathan, M. Jafarian, B. B. Dally, W. L. Saw, P. J. Ashman, E. Hu, and A. Steinfeld, "Solar thermal hybrids for combustion power plant: A growing opportunity," *Progress in Energy and Combustion Science,* vol. 64, pp. 4-28, 2018/01/01/, 2018.

[61] T. Tan, and Y. Chen, "Review of study on solid particle solar receivers," *Renewable and Sustainable Energy Reviews,* vol. 14, no. 1, pp. 265-276, 2010/01/01/, 2010.

[62] C. K. Ho, "Advances in central receivers for concentrating solar applications," *Solar Energy,* vol. 152, pp. 38-56, 2017/08/01/, 2017.

[63] M. T. Islam, N. Huda, A. B. Abdullah, and R. Saidur, "A comprehensive review of state-of-the-art concentrating solar power (CSP) technologies: Current status and research trends," *Renewable and Sustainable Energy Reviews,* vol. 91, pp. 987-1018, 2018/08/01/, 2018.

[64] IEA. "CO2 emissions from energy combustion and industrial processes, 1900-2021, IEA, Paris https://www.iea.org/data-and-statistics/charts/co2-emissions-from-energy-combustion-and-industrial-processes-1900-2021."

[65] Greenpeace International. "https://energypedia.info/wiki/Greenpeace_International_Concentrating_Solar_Power_Global_Outlook," March 30, 2020.

[66] ITP, *CONCENTRATING SOLAR THERMAL TECHNOLOGY STATUS, https://arena.gov.au/assets/2019/01/cst-roadmap-appendix-1-itp-cst-technology.pdf,* 2018.

[67] X. Xu, K. Vignarooban, B. Xu, K. Hsu, and A. M. Kannan, "Prospects and problems of concentrating solar power technologies for power generation in the desert regions," *Renewable and Sustainable Energy Reviews,* vol. 53, pp. 1106-1131, 2016/01/01/, 2016.

[68] R. W. Bradshaw, and R. W. Carling, *A review of the chemical and physical properties of molten alkali nitrate salts and their effect on materials used for solar central receivers*, United States, 1987.

[69] R. G. Reddy, *Novel Molten Salts Thermal Energy Storage for Concentrating Solar Power Generation*, United States, 2013.

[70] A. G. Fernández, H. Galleguillos, E. Fuentealba, and F. J. Pérez, "Thermal characterization of HITEC molten salt for energy storage in solar linear concentrated technology," *Journal of Thermal Analysis and Calorimetry,* vol. 122, no. 1, pp. 3-9, 2015/10/01, 2015.

[71] S. Benammar, "A review study on the modeling and simulation of solar tower power plants," *J. Sol. Energy Res,* vol. 7, pp. 100-121, 2020.

[72] E. S. Freeman, "The Kinetics of the Thermal Decomposition of Sodium Nitrate and of the Reaction between Sodium Nitrite and Oxygen," *The Journal of Physical Chemistry,* vol. 60, no. 11, pp. 1487-1493, 1956/11/01, 1956.

[73] S. Luque, G. Menéndez, M. Roccabruna, J. González-Aguilar, L. Crema, and M. Romero, "Exploiting volumetric effects in novel additively manufactured open solar receivers," *Solar Energy,* vol. 174, pp. 342-351, 2018/11/01/, 2018.

[74] B. Hoffschmidt, R. Pitz-Paal, M. Bohmer, T. Fend, and P. Rietbrock, "200 kW{sub th} open volumetric air receiver (HiTRec) of DLR reached 1000 deg C average outlet temperature at PSA," *Journal de Physique. 4*, pp. Medium: X; Size: page(s) 551-556, 1999.

[75] R. Buck, T. Bra¨uning, T. Denk, M. Pfa¨nder, P. Schwarzbo¨zl, and F. Tellez, "Solar-Hybrid Gas Turbine-based Power Tower Systems (REFOS)*," *Journal of Solar Energy Engineering,* vol. 124, no. 1, pp. 2-9, 2001.

[76] W. E. C. Pritzkow, "Pressure loaded volumetric ceramic receiver," *Solar Energy Materials,* vol. 24, no. 1, pp. 498-507, 1991/12/02/, 1991.

[77] H. Stadler, D. Maldonado, M. Offergeld, P. Schwarzbözl, and J. Trautner, "CFD model for the performance estimation of open volumetric receivers and comparison with experimental data," *Solar Energy,* vol. 177, pp. 634-641, 2019/01/01/, 2019.

[78] C. K. Ho, and B. D. Iverson, "Review of high-temperature central receiver designs for concentrating solar power," *Renewable and Sustainable Energy Reviews,* vol. 29, pp. 835-846, 2014/01/01/, 2014.

[79] A. L. Ávila-Marín, "Volumetric receivers in Solar Thermal Power Plants with Central Receiver System technology: A review," *Solar Energy,* vol. 85, no. 5, pp. 891-910, 2011/05/01/, 2011.

[80] S. Long, T. C. W. Lau, A. Chinnici, and G. J. Nathan, "The flow-field within a vortex-based solar cavity receiver with an open aperture," *Experimental Thermal and Fluid Science,* vol. 123, pp. 110314, 2021/05/01/, 2021.

[81] J. Karni, A. Kribus, B. Ostraich, and E. Kochavi, "A High-Pressure Window for Volumetric Solar Receivers," *Journal of Solar Energy Engineering,* vol. 120, no. 2, pp. 101-107, 1998.

[82] J. M. Chavez, and C. Chaza, "Testing of a porous ceramic absorber for a volumetric air receiver," *Solar Energy Materials,* vol. 24, no. 1, pp. 172-181, 1991/12/02/, 1991.

[83] M. Romero, and J. González-Aguilar, "Solar thermal CSP technology," *Wiley Interdisciplinary Reviews: Energy and Environment,* vol. 3, no. 1, pp. 42-59, 2014.

[84] C. K. Ho, J. Christian, J. Yellowhair, S. Jeter, M. Golob, C. Nguyen, K. Repole, S. Abdel-Khalik, N. Siegel, H. Al-Ansary, A. El-Leathy, and B. Gobereit, "Highlights of the high-temperature falling particle receiver project: 2012 - 2016," *AIP Conference Proceedings,* vol. 1850, no. 1, pp. 030027, 2017.

[85] G. Zanganeh, A. Pedretti, S. Zavattoni, M. Barbato, and A. Steinfeld, "Packed-bed thermal storage for concentrated solar power – Pilot-scale demonstration and industrial-scale design," *Solar Energy,* vol. 86, no. 10, pp. 3084-3098, 2012/10/01/, 2012.

[86] Z. Ma, G. C. Glatzmaier, and M. Mehos, "Development of Solid Particle Thermal Energy Storage for Concentrating Solar Power Plants that Use Fluidized Bed Technology," *Energy Procedia,* vol. 49, pp. 898-907, 2014/01/01/, 2014.

[87] C. K. Ho, "A review of high-temperature particle receivers for concentrating solar power," *Applied Thermal Engineering,* vol. 109, pp. 958-969, 2016/10/25/, 2016.

[88] C. Ho, J. Christian, D. Gill, A. Moya, S. Jeter, S. Abdel-Khalik, D. Sadowski, N. Siegel, H. Al-Ansary, L. Amsbeck, B. Gobereit, and R. Buck, "Technology Advancements for Next Generation Falling Particle Receivers," *Energy Procedia,* vol. 49, pp. 398-407, 2014/01/01/, 2014.

[89] J. Christian, and C. Ho, "Alternative Designs of a High Efficiency, North-facing, Solid Particle Receiver," *Energy Procedia,* vol. 49, pp. 314-323, 2014/01/01/, 2014.

[90] P. K. Falcone, J. E. Noring, and J. M. Hruby, *Assessment of a solid particle receiver for a high temperature solar central receiver system,* SAND-85-8208; Other: ON: DE85008028 United States Other: ON: DE85008028 NTIS, PC A05/MF A01. SNL English, ; Sandia National Labs., Livermore, CA (USA), 1985.

[91] J. M. Hruby, and B. R. Steele, "A solid particle central receiver for solar energy," 1986-02-01, 1986.

[92] K. Kim, S. F. Moujaes, and G. J. Kolb, "Experimental and simulation study on wind affecting particle flow in a solar receiver," *Solar Energy,* vol. 84, no. 2, pp. 263-270, 2010/02/01/, 2010.

[93] J. Spelling, A. Gallo, M. Romero, and J. González-Aguilar, "A High-efficiency Solar Thermal Power Plant using a Dense Particle Suspension as the Heat Transfer Fluid," *Energy Procedia,* vol. 69, pp. 1160-1170, 2015/05/01/, 2015.

[94] J. I. Ortega, J. I. Burgaleta, and F. M. Téllez, "Central Receiver System Solar Power Plant Using Molten Salt as Heat Transfer Fluid," *Journal of Solar Energy Engineering,* vol. 130, no. 2, 2008.

[95] C. K. Ho, "6 - A new generation of solid particle and other high-performance receiver designs for concentrating solar thermal (CST) central tower systems," *Advances in Concentrating Solar Thermal Research and Technology*, M. J. Blanco and L. R. Santigosa, eds., pp. 107-128: Woodhead Publishing, 2017.

[96] R. Bertocchi, J. Karni, and A. Kribus, "Experimental evaluation of a non-isothermal high temperature solar particle receiver," *Energy,* vol. 29, no. 5, pp. 687-700, 2004/04/01/, 2004.

[97] I. Perez Lopez, H. Benoit, D. Gauthier, J. L. Sans, E. Guillot, G. Mazza, and G. Flamant, "On-sun operation of a 150kWth pilot solar receiver using dense particle suspension as heat transfer fluid," *Solar Energy,* vol. 137, pp. 463-476, 2016/11/01/, 2016.

[98] C. K. Ho, J. M. Christian, J. Yellowhair, K. Armijo, W. J. Kolb, S. Jeter, M. Golob, and C. Nguyen, "Performance Evaluation of a High-Temperature Falling Particle Receiver."

[99] A. Meier, "A predictive CFD model for a falling particle receiver/reactor exposed to concentrated sunlight," *Chemical Engineering Science,* vol. 54, no. 13, pp. 2899-2905, 1999/07/01/, 1999.

[100] J. M. Hruby, *Technical feasibility study of a solid particle solar central receiver for high temperature applications*, United States, 1986.

[101] M. Ebert, L. Amsbeck, J. Rheinländer, B. Schlögl-Knothe, S. Schmitz, M. Sibum, R. Uhlig, and R. Buck, "Operational experience of a centrifugal particle receiver prototype," *AIP Conference Proceedings,* vol. 2126, no. 1, pp. 030018, 2019.

[102] G. Flamant, D. Gauthier, H. Benoit, J. L. Sans, B. Boissière, R. Ansart, and M. Hemati, "A New Heat Transfer Fluid for Concentrating Solar Systems: Particle Flow in Tubes," *Energy Procedia,* vol. 49, pp. 617-626, 2014/01/01/, 2014.

[103] J. Martinek, and Z. Ma, "Granular Flow and Heat-Transfer Study in a Near-Blackbody Enclosed Particle Receiver," *Journal of Solar Energy Engineering,* vol. 137, no. 5, 2015.

[104] A. Gallo, J. Spelling, M. Romero, and J. González-Aguilar, "Preliminary Design and Performance Analysis of a Multi-megawatt Scale Dense Particle Suspension Receiver," *Energy Procedia,* vol. 69, pp. 388-397, 2015/05/01/, 2015.

[105] H. Al-Ansary, A. El-Leathy, S. Jeter, E. Djajadiwinata, S. Alaqel, M. Golob, C. Nguyen, R. Saad, T. Shafiq, S. Danish, S. Abdel-Khalik, Z. Al-Suhaibani, N. Abu-Shikhah, M. I. Haq, A. Al-Balawi, and F. Al-Harthi, "On-sun experiments on a particle heating receiver with red sand as the working medium."

[106] T. Lee, S. Lim, S. Shin, D. L. Sadowski, S. I. Abdel-Khalik, S. M. Jeter, and H. Al-Ansary, "Numerical simulation of particulate flow in interconnected porous media for central particle-heating receiver applications," *Solar Energy,* vol. 113, pp. 14-24, 2015/03/01/, 2015.

[107] X. Xie, G. Xiao, M. Ni, J. Yan, H. Dong, and K. Cen, "Optical and thermal performance of a novel solar particle receiver," *AIP Conference Proceedings,* vol. 2126, no. 1, pp. 030065, 2019.

[108] G. Xiao, K. Guo, M. Ni, Z. Luo, and K. Cen, "Optical and thermal performance of a high-temperature spiral solar particle receiver," *Solar Energy,* vol. 109, pp. 200-213, 2014/11/01/, 2014.

[109] D. Hirsch, and A. Steinfeld, "Solar hydrogen production by thermal decomposition of natural gas using a vortex-flow reactor," *International Journal of Hydrogen Energy,* vol. 29, no. 1, pp. 47-55, 2004/01/01/, 2004.

[110] F. Müller, P. Poživil, P. J. van Eyk, A. Villarrazo, P. Haueter, C. Wieckert, G. J. Nathan, and A. Steinfeld, "A pressurized high-flux solar reactor for the efficient thermochemical gasification of carbonaceous feedstock," *Fuel,* vol. 193, pp. 432-443, 2017/04/01/, 2017.

[111] N. Ozalp, M.-H. Chien, and G. Morrison, "Computational Fluid Dynamics and Particle Image Velocimetry Characterization of a Solar Cyclone Reactor," *Journal of Solar Energy Engineering,* vol. 135, no. 3, 2013.

[112] K. Jiang, X. Du, Y. Kong, C. Xu, and X. Ju, "A comprehensive review on solid particle receivers of concentrated solar power," *Renewable and Sustainable Energy Reviews,* vol. 116, pp. 109463, 2019/12/01/, 2019.

[113] A. Steinfeld, A. Imhof, and D. Mischler, "Experimental Investigation of an Atmospheric-Open Cyclone Solar Reactor for Solid-Gas Thermochemical Reactions," *Journal of Solar Energy Engineering,* vol. 114, no. 3, pp. 171-174, 1992.

[114] G. Xiao, K. Guo, Z. Luo, M. Ni, Y. Zhang, and C. Wang, "Simulation and experimental study on a spiral solid particle solar receiver," *Applied Energy,* vol. 113, pp. 178-188, 2014/01/01/, 2014.

[115] N. Ozalp, and D. JayaKrishna, "CFD analysis on the influence of helical carving in a vortex flow solar reactor," *International Journal of Hydrogen Energy,* vol. 35, no. 12, pp. 6248-6260, 2010/06/01/, 2010.

[116] N. Ozalp, and A. Kanjirakat, "A CFD study on the effect of carbon particle seeding for the improvement of solar reactor performance." pp. 143-152.

[117] S. Dai, Z. Chang, C. Chang, J. S. Akhatov, and X. Li, "Numerical study on the directly-irradiated vortex reactor for solar CO2 coal gasification," *Solar Energy,* vol. 188, pp. 573-585, 2019/08/01/, 2019.

[118] F. J. Miller, and R. W. Koenigsdorff, "Thermal Modeling of a Small-Particle Solar Central Receiver," *Journal of Solar Energy Engineering,* vol. 122, no. 1, pp. 23-29, 2000.

[119] A. S. Oles, "Modeling of Falling-Particle Solar Receivers for Hydrogen Production and Thermochemical Energy Storage," University of Maryland, College Park, 2014.

[120] R. J. Nandy, RK., "Selection of Proper Refractory Materials for Energy Saving in Aluminium Melting and Holding Furnaces," *International Journal of Metallurgical Engineering,* vol. 1, no. 6, pp. 117-121, 2012.

[121] H. Weitz, W. Roos, D. Fourie, P. Strydom, and J. Zietsman, "Improving Furnace Start-ups with Computational Modelling: The Key to Refractory Lining Integrity," in The Eleventh International Heavy Minerals Conference, The Southern African Institute of Mining and Metallurgy, Western Cape, 5–6 August 2019, 2019.

[122] J. Jenkins, "Important considerations for refractory dryouts, startups and shutdowns, September 13-16, 2011," in Sulfur Recovery Symposium, Vail, CO., 2011.

[123] S. O. Alexopoulos, J. Dersch, M. Roeb, and R. Pitz-Paal, "Simulation model for the transient process behaviour of solar aluminium recycling in a rotary kiln," *Applied Thermal Engineering,* vol. 78, pp. 387-396, 2015/03/05/, 2015.

[124] Technical Information Alumina Products. "https://www.advaluetech.com/technical-alumina-products," April 01, 2020.

[125] H. R. Doremus, "Alumina," *Ceramic and Glass Materials: Structure, Properties and Processing*, J. F. Shackelford and R. H. Doremus, eds., pp. 1-26, Boston, MA: Springer US, 2008.

[126] Silica refractories. "https://www.termorefractories.com/products/refractory-bricks-blocks/silica-refractories.html," April 02, 2020.

[127] Silica refractories. "https://www.ispatguru.com/silica-refractories/," April 02, 2020.

[128] Magnesite refractories. April 02, 2020.

[129] E. R. Benavidez, E. Brandaleze, Y. S. Lagorio, S. E. Gass, and A. G. T. Martinez, "Thermal and mechanical properties of commercial MgO-C bricks," *Matéria (Rio de Janeiro),* vol. 20, pp. 571-579, 2015.

[130] M. P. Groover, *Fundamentals of modern manufacturing: materials processes, and systems*: John Wiley & Sons, 2007.

[131] K. Dana, S. Sinhamahapatra, H. S. Tripathi, and A. Ghosh, "Refractories of Alumina-Silica System," *Transactions of the Indian Ceramic Society,* vol. 73, no. 1, pp. 1-13, 2014/01/02, 2014.

[132] A. Yurkov, "The Properties of Refractory and Heat Insulation Materials," *Refractories for Aluminium: Electrolysis and the Cast House*, pp. 1-63, Cham: Springer International Publishing, 2015.

[133] W. D. Kingery, *Introduction to ceramics*, 1976.

[134] P. Charvin, S. Abanades, P. Neveu, F. Lemont, and G. Flamant, "Dynamic modeling of a volumetric solar reactor for volatile metal oxide reduction," *Chemical Engineering Research and Design,* vol. 86, no. 11, pp. 1216-1222, 2008/11/01/, 2008.

[135] System Advisor Model. "https://sam.nrel.gov/."

[136] Greenius. "Greenius - The Green Energy System Analysis Tool."

[137] J. J. Gangler, "High-Temperature Testing Techniques for Brittle Refractory Materials," *Journal of the American Ceramic Society,* vol. 37, no. 9, pp. 439-444, 1954.

CHAPTER 3

A MATHEMATICAL MODEL TO ASSESS THE INFLUENCE OF TRANSIENTS ON A REFRACTORY-LINED SOLAR RECEIVER

Statement of Authorship

Title of Paper	A mathematical model to assess the influence of transients on a refractory-lined solar receiver
Publication Status	☑ Published ☐ Accepted for Publication ☐ Submitted for Publication ☐ Unpublished and Unsubmitted work written in manuscript style
Publication Details	Rafique MM, Nathan G, Saw W (2021). A mathematical model to assess the influence of transients on a refractory-lined solar receiver, Renewable Energy, 167, 217-235. DOI: 10.1016/j.renene.2020.11.077

Principal Author

| Name of Principal Author (Candidate)	Muhammad Mujahid RAFIQUE
Contribution to the Paper	Performed the literature review and identified the potential gaps. Jointly defined the scope and aims of the paper. Jointly worked on different approaches to mathematical modelling and its validation. Jointly developed model, performed analysis, interpreted data, wrote the manuscript, and acted as corresponding author. Took primary responsibility for responding to the reviewer's comments.
Overall percentage (%)	60%
Certification:	This paper reports on original research I conducted during the period of my Higher Degree by Research candidature and is not subject to any obligations or contractual agreements with a third party that would constrain its inclusion in this thesis. I am the primary author of this paper.
Signature		Date	23/08/2021

Co-Author Contributions

By signing the Statement of Authorship, each author certifies that:

i. the candidate's stated contribution to the publication is accurate (as detailed above);

ii. permission is granted for the candidate in include the publication in the thesis; and

iii. the sum of all co-author contributions is equal to 100% less the candidate's stated contribution.

Name of Co-Author	Prof. Graham Nathan
Contribution to the Paper	Supervised the work. Jointly defined the scope and aims of the paper. Jointly worked on different approaches to mathematical modelling and its validation. Jointly developed model performed analysis and interpreted data. Critically reviewed the manuscript. Helped to improve the language, structure, and content of the manuscript. Checked and approved the final version of the manuscript.
Signature		Date	09/09/2021

Name of Co-Author	Dr. Woei Saw
Contribution to the Paper	Supervised the work. Jointly defined the scope and aims of the paper. Jointly worked on different approaches to mathematical modelling and its validation. Helped in climatic data acquisition. Jointly performed analysis and interpreted data. Critically reviewed the manuscript. Checked and approved the final version of the manuscript.
Signature		Date	31/8/2021
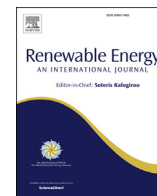
A mathematical model to assess the influence of transients on a refractory-lined solar receiver

Muhammad M. Rafique [a, b, *], Graham Nathan [a, b], Woei Saw [a, c]

[a] Centre for Energy Technology, The University of Adelaide, SA, 5005, Australia
[b] School of Mechanical Engineering, The University of Adelaide, SA, 5005, Australia
[c] School of Chemical Engineering and Advanced Materials, The University of Adelaide, SA, 5005, Australia

ARTICLE INFO

ABSTRACT

An approach to analyze and optimize the thermal performance of a refractory-lined particle receiver in response to solar resource variability has been demonstrated. A transient mathematical model has been developed, incorporating variable direct normal irradiance (DNI) and heat losses associated with a directly irradiated particle receiver. The model is employed to assess the time-dependent temperature fields of the receiver cavity walls, the particles and gas from the initial state to another equilibrium. The influence of the receiver's geometric parameters on the transient thermal response of the receiver has been assessed using real-time solar irradiance data based on the temperature changes for each phase. This can be used to support optimization of the refractory lining and insulation, to trade-off between the solar DNI input, thermal losses from the receiver, and allowable temperatures and heating rates of refractory and outer steel shell, via an energy balance. New insight is provided on the role of the material and thickness of the refractory lining on the system output when accounting for the allowable heating rate of refractory material to avoid failure due to thermal shock.

© 2020 Elsevier Ltd. All rights reserved.

1. Introduction

Presently, concentrating solar thermal (CST) technologies are commercially available for power production in the lower temperature range, up to 580 °C [1,2] but there is a push to develop technologies to higher temperatures to integrate them into processes requiring higher temperatures such as alumina Bayer process which operates at a temperature of about 1000 °C [3,4]. In this regard, solar particle receivers are a promising class of technology for operating at temperatures in this range [5—8]. Solar particle receiver technologies employ sand-like ceramic particles as both a heat transfer and energy storage medium [5—7]. Particles can be stable at temperatures of order 1000 °C, which is far higher than the 580 °C as of commercial molten salts [9—11]. However, there is a lack of knowledge of the influence of the time-constants of particle receivers on dynamic operation caused by solar resource variability. Transient analytical models with low computational resource requirements are needed to allow these influences to be assessed with long time-series of variable solar input and enable design optimization of high temperature particle receivers. The development and application of such a model is undertaken in this paper.

The transient response of directly irradiated receivers with a refractory lining is fundamentally different from that of tubular receivers, which typically employ thin conducting ductile materials. Nevertheless, even with those cases significant challenges arise from transient operation, such as increased stresses relative to steady-state operation [12,13]. Furthermore, the numerical model of an indirectly irradiated molten salt-based receiver employed by Xu et al. [14] showed that a transient, rather than a steady-state, model is needed to accurately predict a receiver's performance. Similarly, Samanes et al. [15] concluded that thermal efficiency of, and thermal losses from, a molten salt receiver varies significantly with transient DNI fluctuations. Furthermore, the relative significance of radiant and convective heat losses differs with temperature due to the fourth power dependence of radiation on temperature. However, while such challenges are likely to be even greater for high temperature particle receivers with a lining of refractory material owing to their higher thermal inertia than metal tubes, no equivalent assessment of these effects is available.

* Corresponding author. Centre for Energy Technology, The University of Adelaide, SA, 5005, Australia.
E-mail addresses: muhammad.rafique@adelaide.edu.au, rana.uet.08@gmail.com (M.M. Rafique).

Most refractory-lined vessels, such as reactors and rotary kilns, employ a multilayered lining that comprises a combination of different materials [16—18] and are typically employed where the temperature approaches or exceeds 1000 °C [19]. While several previous investigations of refractory-lined solar cavities have provided information on the heating rates they employed, no systematic investigation is available with which to assess how the design of refractory lining should be optimised for transient operation employing real-time solar variability. The numerical model of a lab scale multilayered cavity reactor employed by Abanades et al. [20] and Charvin et al. [16] showed that, 15 min of heating time is required for the reactor to achieve a temperature of 2500 K, when alumina refractory lining of constant thickness is used. Similarly, the heating period of a simulated industrial-scale reactor, with a fixed lining thickness of, was estimated to be 40—60 min with a constant input DNI of 1000 W/m^2, by Charvin et al. [16]. This gives an average heating rate of ~60 K/min for the first 30 min of the reactor operation which is at the upper end of allowable heating rates for alumina refractory to avoid damage from thermal shock [21,22]. Their result highlights the need to investigate the influence of refractory thickness with regard to the trade-off between heating time and allowable cavity heating rate for a smooth operation based on the intermittent nature of input solar resource. Hence there is a need to know how to optimize the design of refractory lining for upscaling these emerging receivers to a higher power level under real-time operating conditions.

The receiver geometry, including the aperture diameter and receiver length relative to cavity diameter and the thickness of refractory lining, controls the optimised design of the receiver. The aperture diameter controls both the input energy to the receiver and the thermal losses to the surroundings, whereas the cavity heating rate is limited by the thickness of refractory lining and the flux of solar energy entering the aperture. The maximum heating rate of refractory materials, which are brittle [23], is set by a value that should not be exceeded to avoid damage [24]. This is not difficult to manage for most industrial scaled non-solar devices employing refractory lining, since they operate mostly at steady-state conditions and only operate in transient conditions at the start and end of a maintenance shut-down. This allows the duration of this start-up period to extend over many hours to avoid inducing high differential stresses, which can cause cracking and spalling [22,25]. This is obviously incompatible with the operation of a solar receiver, which must start up and shut down every day and also needs to accommodate the alternating insolation due to the passage of clouds [26]. There is a need for a more detailed assessment of how to optimize the performance of refractory-lined solar receivers under transient operating conditions. Therefore, analytical transient models are required for particle receivers to be solved for real-time solar irradiation data over a longer span of time for quick and accurate prediction of receivers' transient thermal behavior and to optimize the design of these refractory-lined solar receivers.

To meet the above-mentioned needs, the overall objective of the present paper is to develop and implement a transient mathematical model to support the optimization of refractory-lined receivers, considering the trade-off between the thermal performance, allowable temperatures and heating rates, for any given time history of variable solar resource. To achieve this, the first aim is to develop a transient model employing the governing mathematical equations for the mass and energy flows through the receiver cavity, which calculates the time-dependent temperature fields of the receiver, particles, and gas from the initial state to another equilibrium. The second aim is to compare the suitability of various alterative refractory materials to guide in their selection for various performance criteria. The third aim is to assess the influence of refractory lining thickness, insulation thickness, and particles mass flow rate on the transient temperature distributions of inner cavity wall, outer steel shell, particles, and gas for a series of scenarios. The conditions that allow acceptable cavity heating rates under the transient operation of the receiver employing these geometric parameters are also investigated.

2. Methodology

2.1. Receiver description

The receiver chosen for this study is a cylindrical cavity, which is similar to many other cylindrical cavities (e.g. the DLR centrifugal receiver [27]), but has the specific details of the Solar Expanding Vortex Receiver patented by the University of Adelaide [28,29] and ETH Zurich [30]. A schematic diagram of the receiver is shown in Fig. 1. This receiver heats particles transported in a suspension flow and provides some control of the particle residence time as a function of its size [29]. Furthermore, the configuration achieves a low flow of particles through the aperture to offer the potential for operation without a window [29].

The particle receiver has an aperture of diameter D_{ap}, an inner cavity diameter D_1, and cone angle Ψ. The horizontal length of the receiver cavity is denoted by L. The receiver cavity is considered to be made of three different layers with an inner refractory layer, a central insulating layer and an outer mild steel layer. The thickness of layers 1, 2, and 3 are denoted as Δr_1, Δr_2, and Δr_3, respectively. A cross-sectional view of the receiver cavity from the side and aperture front is shown in Fig. 2. The properties of materials commonly employed for refractory lining are listed in Table 1. A sensitivity assessment will be performed to select a suitable material for refractory lining of the particle receivers.

2.2. Transient mathematical model

The transient model employs the governing mathematical equations for mass and energy flows through the receiver cavity, considering the particle and gas phases, thermal losses, and conductive, convective and radiative heat transfer. The following assumptions were employed in the model:

- The solar flux is considered to be uniformly distributed inside the receiver cavity. Although this represents a significant simplification, it has some justification because a cavity enclosure tends to homogenize the temperature of the receiver walls [16].
- The particle and gas phase are uniformly distributed within the receiver cavity.
- The particles and gas move as a plug flow through the receiver, so that the flow rate controls the residence time and the influence of any recirculation is small [40].
- The particles are monodispersed in size, spherical in shape, and follow the gas streamlines inside the receiver.
- Any particle deposition on the inside of the cavity walls is negligible.
- The gas phase is transparent, so that the solar radiation is absorbed either by receiver cavity walls or the particle phase.

Fig. 3 illustrates the heat transfer mechanisms within the refractory-lined solar cavity receiver. An energy balance was performed for each phase and for the walls by solving a set of simultaneous equations iteratively for each time step to calculate each of their temperatures.

2.2.1. Energy conservation for receiver cavity walls

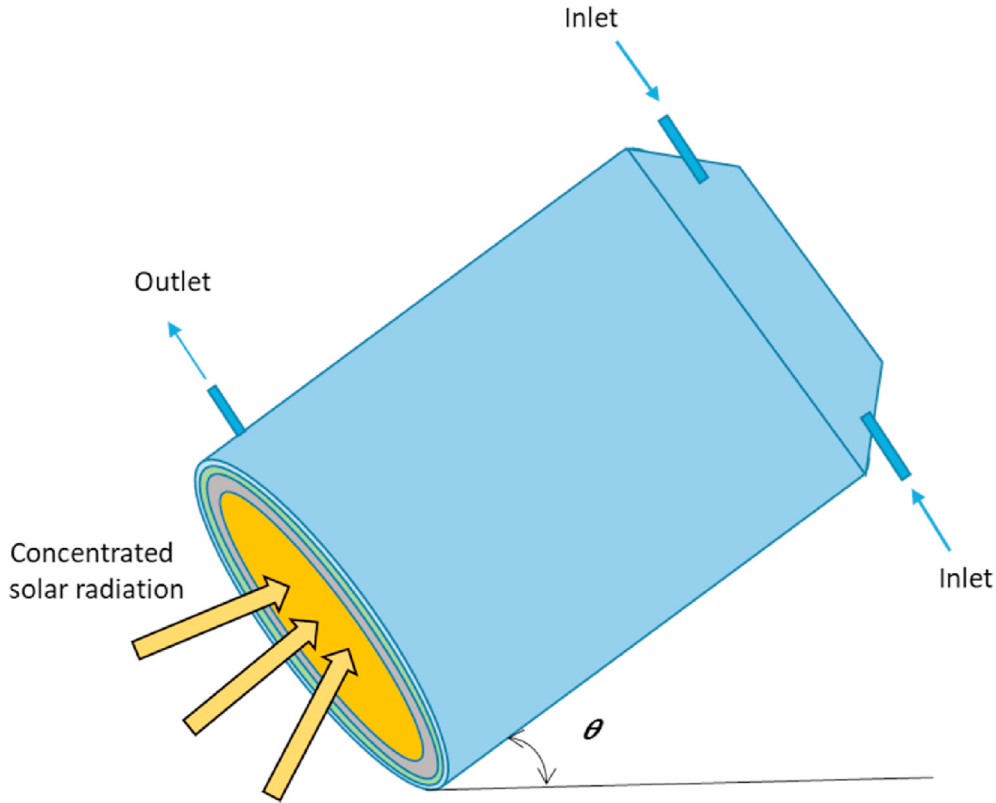The concentrated solar energy from the heliostat field passes

Fig. 1. Schematic diagram of the solar cavity receiver modelled here, termed the Solar Expanding Vortex Particle Receiver.

through the aperture and heats the cavity to a temperature determined by the energy balance that accounts for conduction, convection, and re-radiations losses. That is, the total energy absorbed by the receiver during a time interval ∂t is equal to the change in the thermal mass of the cavity's inner lining plus thermal losses to the surroundings. The energy balance for receiver cavity enclosure is given by the following equation:

$$\dot{Q}_{sol,\,ap-w} = \dot{Q}_{thermal} + \dot{Q}_{rad,\,w-p} + \dot{Q}_{conv,\,w-a} + \dot{Q}_{cond,\,w-s}$$
$$+ \dot{Q}_{conv,\,w-s} + \dot{Q}_{re-rad,\,w-s} \tag{1}$$

Where:

- $\dot{Q}_{sol,\,ap-w}$ is the radiation heat transfer passing through the aperture to the inside surface of the cavity walls
- $\dot{Q}_{thermal}$ is the change in the thermal mass of receiver cavity walls
- $\dot{Q}_{rad,\,w-p}$ is the radiative heat exchange between cavity walls and particle phase
- $\dot{Q}_{conv,\,w-a}$ is the convective heat exchange between cavity walls and air
- $\dot{Q}_{cond,\,w-s}$ is the conduction heat loss to the surroundings through receiver cavity walls
- $\dot{Q}_{conv,\,w-s}$ is the convection heat loss to the surroundings through aperture opening
- $\dot{Q}_{re-rad,\,w-s}$ is the re-radiation heat loss to the surroundings through aperture opening

The change in the thermal mass of the receiver cavity's inside lining during time interval ∂t is given as:

$$\dot{Q}_{thermal} = \rho_w \times c_{pw} \times V_w \times \frac{\partial T_{w,i}}{\partial t}, \tag{2}$$

where ∂t is the time step for each iteration. ρ_w, V_w, and C_{pw} are the density, volume, and specific heat capacity of the inside refractory lining of the cavity wall, respectively.

The total solar energy reaching the aperture of the receiver from the heliostat field can be determined by Equation (3), where η_{helio} is the heliostat instantaneous efficiency, CR is the concentration ratio, A_{ap} is the area of the receiver aperture, and DNI is the direct normal irradiance. The value of DNI is variable and dependent on time.

$$\dot{Q}_{solar} = \eta_{helio} \times CR \times A_{ap} \times DNI \tag{3}$$

The radiative heat transfer from aperture to the inside surface of the cavity walls is given as:

$$\dot{Q}_{sol,\,ap-w} = \alpha_w \times F_{ap-w} \times \dot{Q}_{solar}, \tag{4}$$

where α_w is the absorptivity of the inside refractory lining and F_{ap-w} is the radiative shape factor from the aperture to the receiver inside surface [41].

2.2.1.1. Radiative heat exchange between cavity walls and particles.
The radiative heat exchange between cavity walls and particles is given as:

$$\dot{Q}_{rad,\,w-p} = \pi \times N_{p,i} \times d_p^2 \times h_{w-p,i} \times (T_{w,i} - T_{p,i}), \tag{5}$$

where, $h_{w-p,i}$ is the radiative heat transfer coefficient between the inside surface of the cavity and particles, $N_{p,i}$ is the total number of particles within cavity enclosure at the time i, d_p is the particle

(a)

(b)

Layer 1: Refractory lining
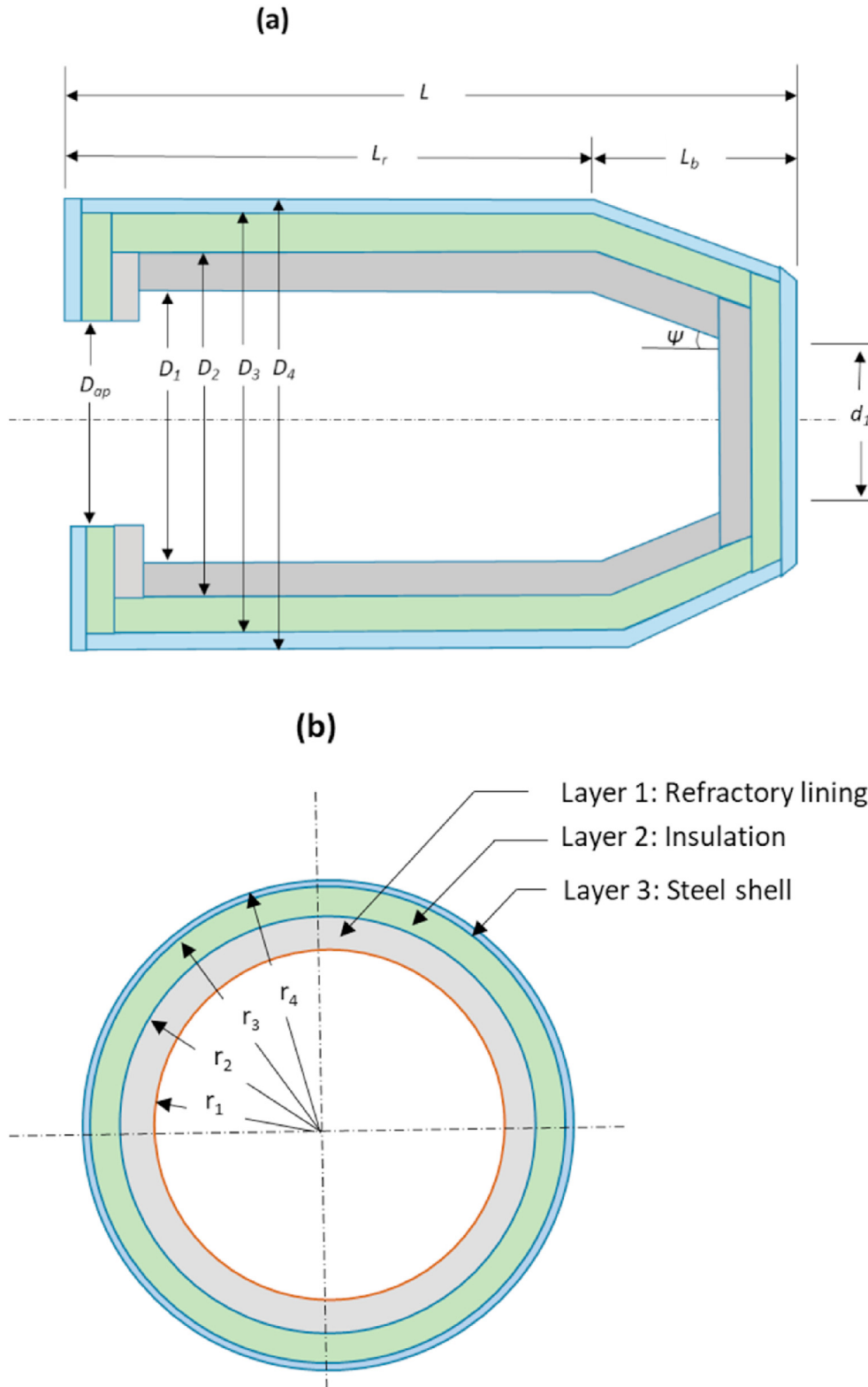Layer 2: Insulation
Layer 3: Steel shell

Fig. 2. Notation used to describe the multi-layered receiver cavity (a) side view (b) front view.

diameter, T_w is the temperature of the inside surface of cavity enclosure, and T_p is the temperature of the particle phase.

Assuming that the total surface of the particles acts as an emissive body, the radiative heat transfer coefficient between wall element and particle phase can be written as [42]:

$$h_{w-p,i} = \sigma \times \varepsilon_p \times \left(T_{w,i}^2 + T_{p,i}^2\right) \times (T_{w,i} + T_{p,i}), \tag{6}$$

where σ is Stefan Boltzmann constant and ε_p is the emissivity of the

Table 1
Thermophysical properties of selected refractory materials.

	Fireclay brick	Alumina	Magnesia
Thermal conductivity (W/m.K) at 300 K	6.5 [31,32]	35 [21]	45 [33]
Specific heat (kJ/kg.K)	1.050 [32]	0.88 [21]	0.95 [33]
Bulk density (kg/m³)	3150 [31]	3800 [21]	3650 [34]
Thermal linear coefficient of expansion (1/K) (°C⁻¹)	4.5×10^{-6} [31]	8.4×10^{-6} [21,35]	8.6×10^{-6} [36]
Absorptivity (−)	0.92 [37]	0.90 [38]	0.70 [39]
Relative cost (−)	Magnesite > Alumina > Fireclay brick		
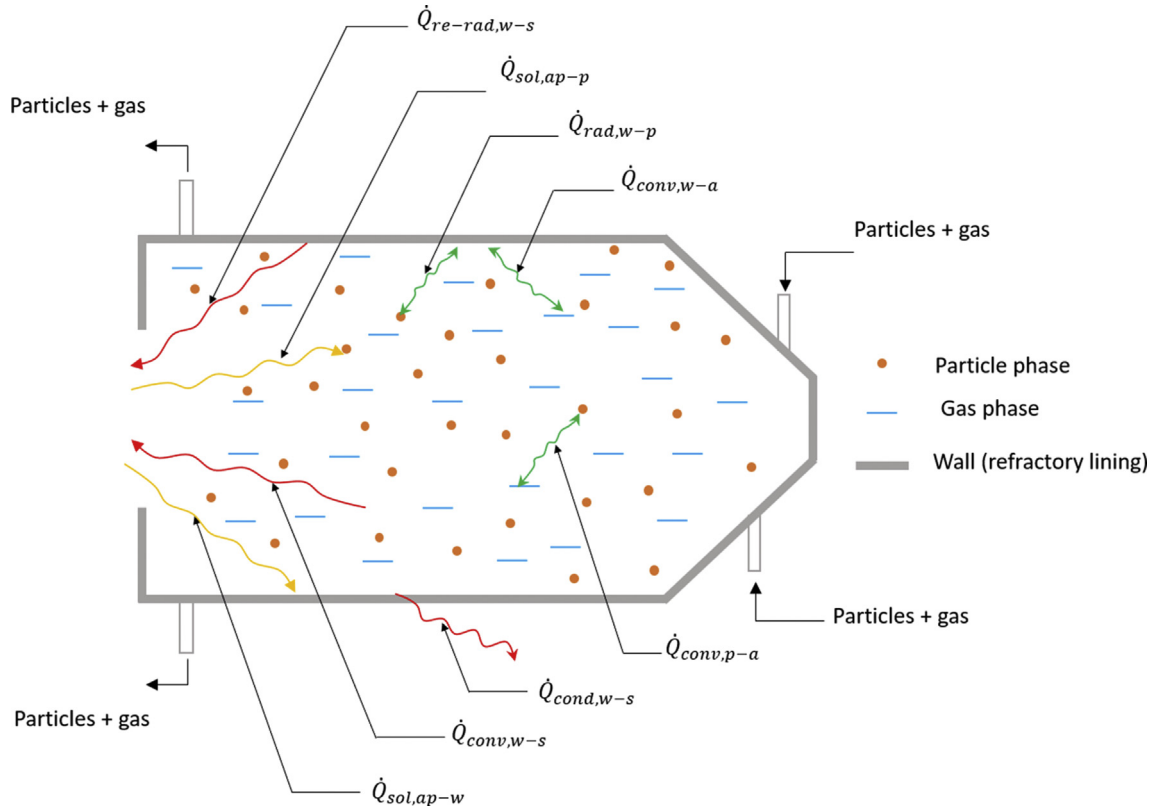
Fig. 3. An illustration of all of the heat transfer terms considered in the model (refer to equations (1) and (22) for a description of the symbols).

particles.

2.2.1.2. Convective heat exchange between cavity walls and air.
The convective transfer of heat from the cavity walls to the gas phase by forced convection is given as:

$$\dot{Q}_{conv,\, w-a} = \pi \times D_1 \times L_e \times h_{w-a,i} \times (T_{w,i} - T_{a,i}) \qquad (7)$$

$$h_{w-a,i} = \frac{Nu_{D_{e,i}} \times k_{a,i}}{D_{e,i}}, \qquad (8)$$

where L_e is the effective internal length of the cavity, T_a is the air temperature, k_a is the thermal conductivity of air, D_e is the effective inside diameter of the cavity.

The heat transferred from the cavity walls to the vortex of air due to forced convection is estimated from a previous correlation for cyclones particle filters [43,44], as follows:

$$Nu_{D_{e,i}} = 0.042 \times Re_{D_{e,i}}^{0.8} \qquad (9)$$

where $Re_{D_{e,i}}$ is instantaneous Reynolds number dependent on the

inlet velocity (u_a), dynamic viscosity (μ_a) and density (ρ_a) of air, calculated at the corresponding temperature of air for each time step.

2.2.1.3. Conduction heat loss through the cavity walls. The conduction heat loss for each iteration were determined using an electrical circuit analogy developed for the three-layered composite walls of the receiver cavity, as shown in Fig. 4. There are four parallel circuits and combined heat conduction through these circuits is:

$$\dot{Q}_{cond,\, w-s} = (T_{w,i} - T_{o,i}) \left[\frac{1}{R_{eq,1}} + \frac{1}{R_{eq,2}} + \frac{1}{R_{eq,3}} + \frac{1}{R_{eq,4}} \right]. \qquad (10)$$

$T_{o,i}$ is the temperature of the outer steel shell. $R_{eq,1}, R_{eq,2}, R_{eq,3},$ and $R_{eq,4}$ are the equivalent resistances to heat flow through the multilayer cavity walls, corresponding to axial direction on aperture side, the central cavity, conical back lip, and on the back end, respectively (Fig. 4).

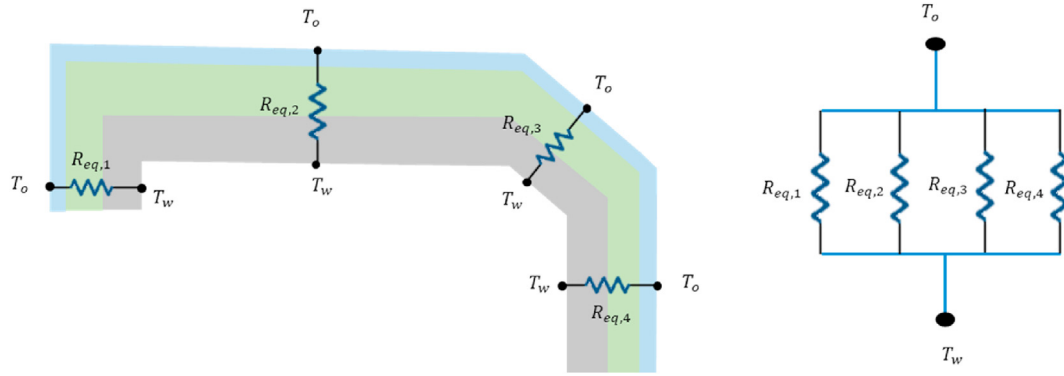Fig. 4. Electric circuit analogy for three-layered cavity walls.

$$R_{eq,1} = \frac{4}{\pi \left(D_1^2 - D_{ap}^2\right)} \times \left[\frac{\varDelta r_1}{k_1} + \frac{\varDelta r_2}{k_2} + \frac{\varDelta r_3}{k_3}\right] \quad (11)$$

$$R_{eq,2} = \frac{1}{2\pi(L_r - \varDelta r_1 - \varDelta r_2 - \varDelta r_3)} \times \left[\frac{\ln\left[\frac{D_2}{D_1}\right]}{k_1} + \frac{\ln\left[\frac{D_3}{D_2}\right]}{k_2} + \frac{\ln\left[\frac{D_4}{D_3}\right]}{k_3}\right]$$
$$(12)$$

$$R_{eq,3} = \frac{cos\varPsi}{2\pi(L_b - \varDelta r_1 - \varDelta r_2 - \varDelta r_3)}$$
$$\times \left[\frac{\ln\left[\frac{d_2+D_2}{d_1+D_1}\right]}{k_1} + \frac{\ln\left[\frac{d_3+D_3}{d_2+D_2}\right]}{k_2} + \frac{\ln\left[\frac{d_4+D_4}{d_3+D_3}\right]}{k_3}\right] \quad (13)$$

$$R_{eq,4} = \frac{4}{\pi d_1^2} \times \left[\frac{\varDelta r_1}{k_1} + \frac{\varDelta r_2}{k_2} + \frac{\varDelta r_3}{k_3}\right], \quad (14)$$

where k_1, k_2, and k_3 are the thermal conductivities corresponding to the material of layers 1, 2, and 3, respectively. The thickness of each layer is assumed to be constant for all walls of the cavity and the values of thermal conductivities are determined at the logarithmic mean temperature of each layer.

2.2.1.4. Convection heat loss through the aperture. The convective losses through the receiver aperture were modelled accounting for cavity temperature, effective length, inner diameter, aperture diameter, and inclination [45,46], as follows:

$$\dot{Q}_{conv, w-s} = \pi D_0 L_e \times h_{ap,i} \times \left(T_{w,i} - T_{amb}\right) \quad (15)$$

$$h_{ap,i} = \frac{Nu_{ap,i} \times k_{a,i}}{L_e} \quad (16)$$

$$Nu_{ap,i} = 0.88 \times Gr^{0.33} \times cos^{2.47}\theta \times \left(\frac{D_{ap}}{L_e}\right)^a \times \left(\frac{T_{w,i}}{T_{amb}}\right)^{0.18} \quad (17)$$

$$a = -0.982 \times \frac{D_{ap}}{L_e} + 1.12 \quad 0° \le \theta \le 90° \quad (18)$$

Here θ is the cavity inclination angle, Gr is the Grashoff number, and g is the gravitational acceleration, while β_a and v_a are the coefficients of volumetric thermal expansion and kinematic viscosity

of the air, respectively.

2.2.1.5. Re-radiation heat loss through the aperture. The re-radiation heat loss from the receiver cavity was calculated to address the following two main terms: (i) emittance due to large temperature difference between inside of the cavity and the surroundings ($\dot{Q}_{re-rad, emit}$) and (ii) reflection of the solar irradiance, which is not absorbed by the cavity's inner surface ($\dot{Q}_{re-rad,ref}$).

$$\dot{Q}_{re-rad, w-s} = \dot{Q}_{re-rad, emit} + \dot{Q}_{re-rad,ref} \quad (19)$$

The re-radiation heat loss from the receiver cavity to the surroundings through the aperture opening due to the temperature difference between the cavity and the surroundings is given by:

$$\dot{Q}_{re-rad, emit} = \frac{\pi D_{ap}^2}{4} \times \varepsilon_w \times \sigma \times F_{w-ap} \times \left(T_{w,i}^4 - T_{amb}^4\right) \quad (20)$$

The re-radiation losses due to reflection from the receiver walls to the surroundings through the aperture were calculated by subtraction of the absorptance by the cavity lining following earlier work [47,48], as follows:

$$\dot{Q}_{re-rad,ref} = (1 - \alpha_w) \times F_{w-ap} \times \dot{Q}_{sol, ap-w} \quad (21)$$

The radiation shape factor from the inside of the receiver wall to aperture opening was calculated following earlier work [41,49].

2.2.2. Energy conservation for the particle phase
The energy conservation equations for the particle phase were formulated by accounting for the enthalpy change of particles transported during each time step, *i*, as follows:

$$\Delta H_{p,i} = \dot{Q}_{sol, ap-p} + \dot{Q}_{conv, p-a} + \dot{Q}_{rad,w-p} \quad (22)$$

Where:

- $\dot{Q}_{sol, ap-p}$ is the radiative heat transfer from aperture to the particle phase
- $\dot{Q}_{conv, p-a}$ is the convective heat exchange between the particles and air

The enthalpy change ($\varDelta H_{p,i}$) of the particle phase was calculated as follows:

$$\Delta H_{p,i} = H_{p,i} - H_{p,i-1} = \dot{m}_p \times \left(c_{pp,i} \times T_{p,i} - c_{pp,i-1} \times T_{p,i-1}\right), \quad (23)$$

where c_{pp} is the specific heat capacity of the particle at the

corresponding particle phase temperature.

2.2.2.1. Radiative heat transfer from aperture to the particles. The radiation heat transfer from the aperture to particle phase was determined as follows:

$$\dot{Q}_{sol,\ ap-p} = N_{p,i} \times \alpha_p \times F_{ap-p} \times \dot{Q}_{solar} \tag{24}$$

The radiation shape factor from the aperture to the particle is based on the characteristic length of the cylindrical cavity.

2.2.2.2. Convective heat exchange between the particles and air. The convective heat exchange between particles and air was calculated based on the flow of air over a sphere [42], as follows:

$$\dot{Q}_{conv,\ p-a} = \pi \times N_{p,i} \times d_p^2 \times h_{p-a,i} \times (T_{a,i} - T_{p,i}) \tag{25}$$

$$h_{p-a,i} = \frac{Nu_{d_p} \times k_a}{d_p}. \tag{26}$$

Here h_{p-a} is the convective heat transfer coefficient between particles and air. The Nusselt number for the no-slip condition is [50]:

$$Nu_{d_p} = 2 \tag{27}$$

2.2.3. Energy conservation for air phase

The energy conservation equations for the air phase was formulated by accounting for the enthalpy change of air transported during a time interval *i*.

$$\Delta H_{a,i} = \dot{Q}_{conv,\ p-a} + \dot{Q}_{rad,w-a} \tag{28}$$

The enthalpy change ($\Delta H_{a,i}$) of the air phase was calculated as follows:

$$\Delta H_{a,i} = H_{a,i} - H_{a,i-1} = \dot{m}_a \times (c_{pa,i} \times T_{a,i} - c_{pa,i-1} \times T_{a,i-1}), \tag{29}$$

where c_{pa} is the specific heat capacity of the air at corresponding air

temperature.

2.3. Thermo-physical properties of the particle and air

The particles were assumed to be high temperature CARBO-HSP ceramic which has density and emissivity of 2000 kg/m³ and 0.93, respectively [51]. These particles have a sphericity of 0.9 parts per unit [52]. The temperature-dependent relationship for the specific heat capacity and thermal conductivity of the CARBO-HSP particle for temperature of up to 1700 K are calculated using equations (30) and (31) [53], whereas, the temperature dependent properties of air are calculated using equation (32)–(37) [54,55].

$$c_{pp,i}\left[\frac{J}{kg.K}\right] = 1.0446 + 0.0001742T_{p,i} - \frac{27960}{T_{p,i}^2} \tag{30}$$

$$k_{p,i}\left[\frac{W}{m.K}\right] = 5.5 + 34.5e^{[-0.0033(T_{p,i}-273)]} \tag{31}$$

$$C_{pa,i}\left[\frac{J}{kg.K}\right] = 1031 - 2.010 \times 10^{-2}T_{a,i} + 3.985 \times 10^{-4}T_{a,i}^2 - 3.080 \times 10^{-10}T_{a,i}^3 \tag{32}$$

$$k_{a,i}\left[\frac{W}{m.K}\right] = 3.180 \times 10^{-3} + 8.616 \times 10^{-5}T_{a,i} - 3.203 \times 10^{-8}T_{a,i}^2 + 6.214 \times 10^{-12}T_{a,i}^3 \tag{33}$$

$$v_{a,i}\left[\frac{m^2}{s}\right] = -7.287 \times 10^{-6} + 5.204 \times 10^{-8}T_{a,i} + 8.281 \times 10^{-11}T_{a,i}^2 - 9.647 \times 10^{-15}T_{a,i}^3 \tag{34}$$

$$Pr_{a,i}[-] = 0.8004 - 0.00031T_{a,i} \tag{35}$$

$$\rho_{a,i}\left[\frac{kg}{m^3}\right] = 352.91 \Big/ T_{a,i} \tag{36}$$

$$\varOmega_{a,i}\left[\frac{m^2}{s}\right] = \frac{k_{a,i}}{\rho_{a,i} \times C_{pa,i}} \tag{37}$$

The temperature of particle and air is used in kelvin (K) for the calculation of thermo-physical properties using the above polynomial relationships.

2.4. Input conditions

A range of parameters including the thickness of the refractory lining and insulating layers, together with the mass flow rate of particles was used to analyze their impact on the receiver's thermal outputs. Table 2 present the reference values and sensitivity variations of geometric and operating parameters. The properties of the middle insulating layer, which was assumed to be made of high temperature insulating material, and of the outer steel ring are listed in Table 3, whereas a sensitivity analysis was carried out to

select a suitable material for the refractory lining from the three different materials listed in Table 1. The performance of the receiver was studied for real-time meteorological conditions with the direct normal irradiation and zenith angle recorded by the Bureau of Meteorology [56] in Alice Spring, Australia every 60s. Two different representative days, one clear sky and other cloudy, were chosen to assess the short-term influence of the intermittent nature of the solar resource on the transient behavior of the refractory-lined receiver.

Fig. 5 presents the distribution of recorded DNI and calculated cosine loss for the sunshine duration of clear sky (December 10, 2018) and cloudy day (December 5, 2018) in Alice Springs. It can be seen that the DNI values on the clear sky have a smooth distribution with a peak of 1022 W/m^2 at solar noon whereas sharp fluctuations can be observed in recorded DNI on the day with the intermittent cloud. The cosine losses vary with the position of the sun during the day so was calculated for each DNI time-step using correlations [47].

2.5. Allowable temperature and heating rate limits

Maintaining the temperatures and heating rates of the inner refractory lining and outer steel shell below critical limits is important to avoid premature failure or reduced cycle life of the receiver. For prolonged life, plain carbon steels are usually limited to a maximum operating temperature of 500 °C [60]. To be conservative and following the standard mechanical design practice [61], a maximum temperature of 475 °C at the outer steel shell was chosen as the allowable limit here. Similarly, the maximum operating temperature of inner refractory linings was set to be 2050 °C [31]. Furthermore, rapid heating during start-up of refractory-lined

Table 2
Geometric and operational input parameters.

Input parameter	Unit	Reference value	Sensitivity variations
Geometric			
D_{ap}/D_1	–	0.55	–
D_1	m	12.0	–
L/D_1	–	1.6	–
θ	degree	45	–
Δr_1	m	0.1	0.02–0.16
Δr_2	m	0.75	0.20–1.60
Δr_3	m	0.01	–
C	–	1000	–
Operational			
$\dot{m}_p$	kg/s	25	10–80
$\dot{m}_a/\dot{m}_p$	–	0.5	–
d_p	µm	100	–
$T_{p,1}$	K	300	–
$T_{a,1}$	K	300	–
$T_{w,1}$	K	300	–
T_{amb}	K	300	–

Table 3
Thermophysical properties of selected materials for the multilayer cavity receiver.

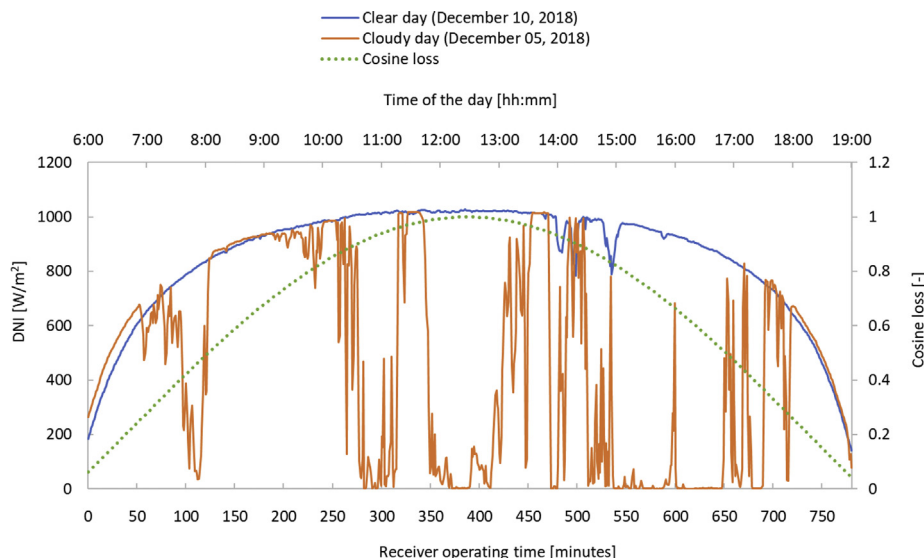|	Superwool [57]	Carbon Steel [58,59]
Thermal conductivity (W/m.K) at 300 K	0.05	45
Specific heat (kJ/kg.K)	1.22	0.47
Bulk density (kg/m^3)	128	7850
Thermal coefficient of linear expansion (1/K)	1×10^{-6}	12×10^{-6}

Fig. 5. Distribution of recorded direct normal irradiance and calculated cosine loss for two summer days, one with clear sky and other with intermittent cloud in Alice Springs, Australia [56].
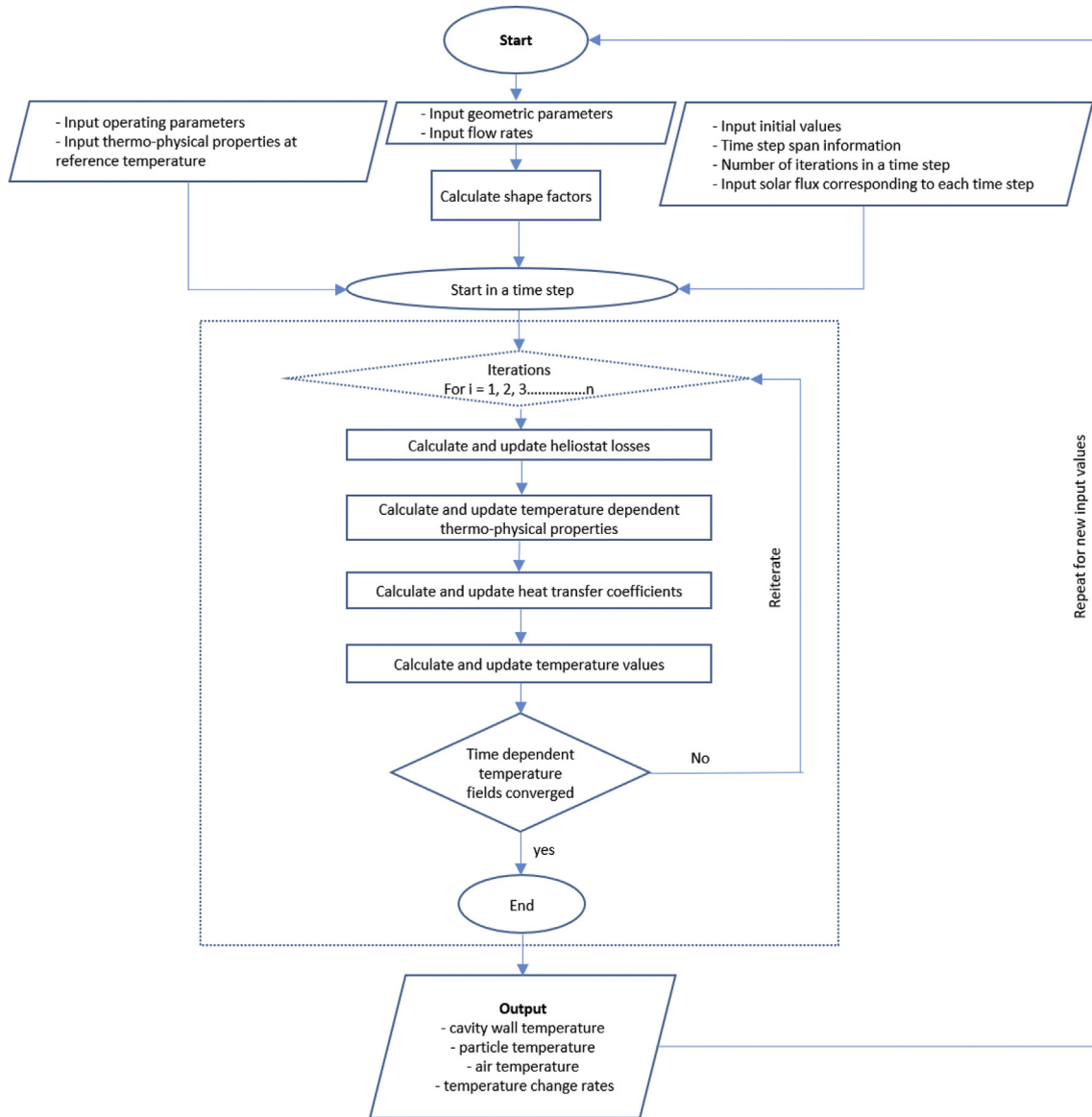
Fig. 6. The iterative procedure used to solve the heat transfer equations at each time step.

devices causes undue stresses in the inner lining which may result in microcracking, thus leading to mechanical spalling and unreliable receiver operation. Heating rates of up to 240 °C/h or lower are usually recommended for refractory linings during the preheating period of 1—2 h to avoid thermal stresses [24]. Although a higher heating rate is not likely to cause immediate damage to the refractory lining, it will reduce its service life [62]. Hence, the calculated values of the temperature and cavity heating rates reported below are compared with these allowable limits.

3. Solution technique

Fig. 6 presents a flow-chart for the solution methodology of the coupled heat transfer equations, which were solved iteratively for each time step. A time step of 60s was chosen since this is significantly shorter than the time constants of the refractory and captures the solar resource variability. The input solar heat flux, local heat transfer coefficients, thermo-physical properties, and cavity

wall temperature were all determined as a function of temperature for each time step. The energy into the receiver, thermal mass change of the receiver cavity, heat losses to the surroundings and energy exchange between three phases at each time step are used to calculate the new temperature fields (T_w, T_p, and T_a).

It should be noted that this control strategy does not seek to limit the solar flux by de-focusing the heliostat field [63], which would be possible to avoid exceeding an allowable heating rate. This approach has been chosen for several reasons. Firstly, this approach is desirable from an efficiency perspective, since de-focusing the solar field constitutes a waste of the energy that could otherwise be captured. It is preferable to seek to capture all of the energy. Secondly, this approach simplifies the control strategy and reduces the risk of damage due to the potential failure of a control strategy. Thirdly, assessing the natural response is most instructive and any additional control could readily be added as an additional measure as needed.

Table 4
Geometric and operational input parameters used by Abanades et al. [20] which are employed for the 6 validation cases.

Input parameter	Unit	Value
Geometric		
D_{ap}	m	0.012
D_1	m	0.02–0.03
L	m	0.04
A_w	m^2	2.71×10^{-4}
Physical properties of ceramic walls		
ρ_w	kg/m^3	3900
$C_{p,w}$	kJ/kg.K	1.274 (1500 K)
ε_w	–	0.8
K_1	W/m.K	$35.245 - 0.0353T + 1.314 \times 10^{-5}T^2 - 1.73 \times 10^{-9}T^3$
Physical properties of insulation		
K_2	W/m.K	0.5
Physical properties of particle		
ρ_p	kg/m^3	5600
$C_{p,p}$	kJ/kg.K	750 (at 2000 K)
k_p	W/m.K	2 (at 2000 K)
Operational		
q_s	kW	1.0
$\dot{m}_p$	kg/s	$1 \times 10^{-6} - 5 \times 10^{-7}$
d_p	μm	0.5–10
$T_{p,in}$	K	300

Table 5
Comparison of the present predictions with the previous simulations of Abanades et al. [20].

Cavity inside diameter (mm)	Particle mass flow rate (kg/s)	Particle diameter (μm)	Cavity wall temperature (K)		Particle temperature (K)	
			Abanades et al. [20]	Present model	Abanades et al. [20]	Present model
20	1×10^{-6}	0.5	2204	2288	2088	2199
20	1×10^{-6}	1	2394	2391	2201	2386
20	1×10^{-6}	5	2390	2386	2269	2334
20	1×10^{-6}	10	2390	2391	2270	2290
20	5×10^{-7}	1	2187	2191	2069	2151
30	1×10^{-6}	1	1805	2071	1627	2065

Table 6
Three different cases used by Charvin et al. [16], which were employed in the present model for model validation.

	Aperture diameter (m)	Direct normal irradiance (W/m^2)	Concentration ratio (−)
Case 1	7.2	1000	1000
Case 2	5.0	1000	2500
Case 3	3.5	1000	5000

4. Model validation

The accuracy of the model was verified by comparison with the numerical results of a refractory lined directly-irradiated solar reactor presented by Abanades et al. [20] and Charvin et al. [16]. Their reactor also comprises a cylindrical cavity enclosure directly heated by concentrated solar energy through the aperture with a ceramic lining of alumina surrounded by an insulation layer to reduce the conduction heat losses. The influence of geometric and operating conditions on the cavity wall and particle temperature were compared for six different cases listed in Table 4.

Table 5 compares the calculated results of the present model with that of Abanades et al. [20], taken for six different validation cases. It can be observed that the cavity wall temperature predicted with the present model agrees with theirs to within 3.8% for five of the six cases and to within 12% for the last one. However, the present predictions of particle temperature are higher. This is consistent with the difference in calculation methods, since the

present model accounts for the radiation absorbed by the particle phase while the previous model [20] does not. Furthermore, the predicted particle temperature rise with decrease in particle diameter is consistent with the previous work for all six cases [20].

The model was also verified by comparing its predictions with those obtained for the dynamic simulations of a 50 MW industrial-scale refractory-lined solar receiver by Charvin et al. [16]. This receiver has a cylindrical cavity diameter and length of 8 m with an inner layer of alumina refractory, a middle layer composed of high-temperature insulating material ($k = 0.5$ W/(m.K)), and outer layer of medium temperature insulating material ($k = 0.05$ W/(m.K)). The geometry and operating conditions in the present model were matched to their conditions shown in Table 6 and the evolution of cavity wall temperature were compared.

Fig. 7 compares the calculated results of the receiver temperature obtained from the present model and that of ref [16] for three different cases. It can be seen that the present model agrees with the previous model to within 3% during the first 30 min when
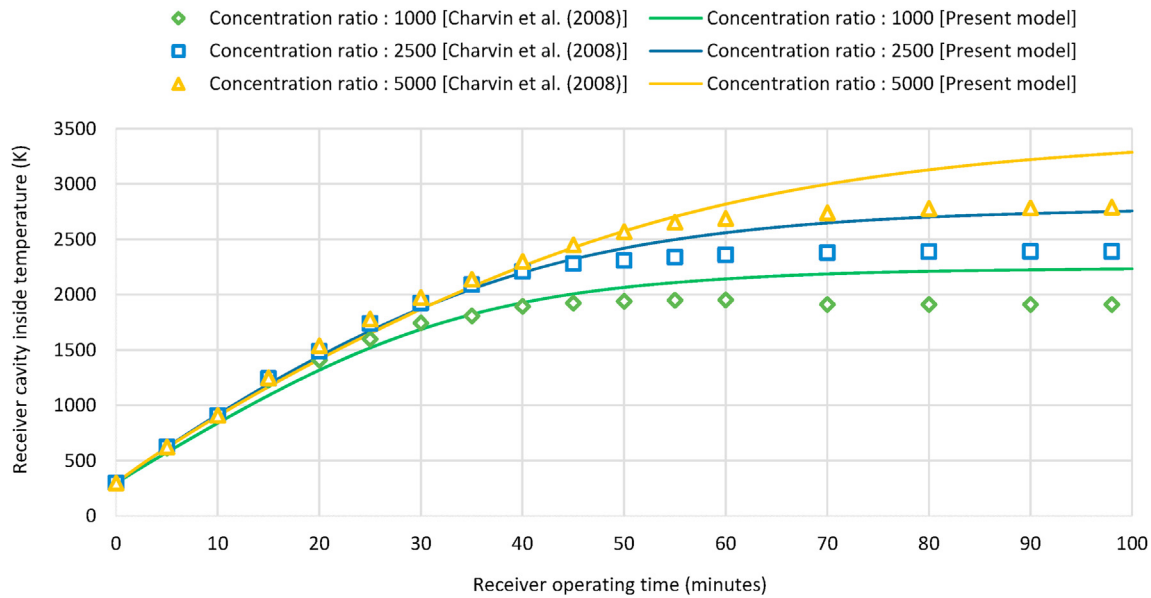
Fig. 7. Comparison of the present model with the simulations of Charvin et al. [16] for an industrial-scale cavity receiver.
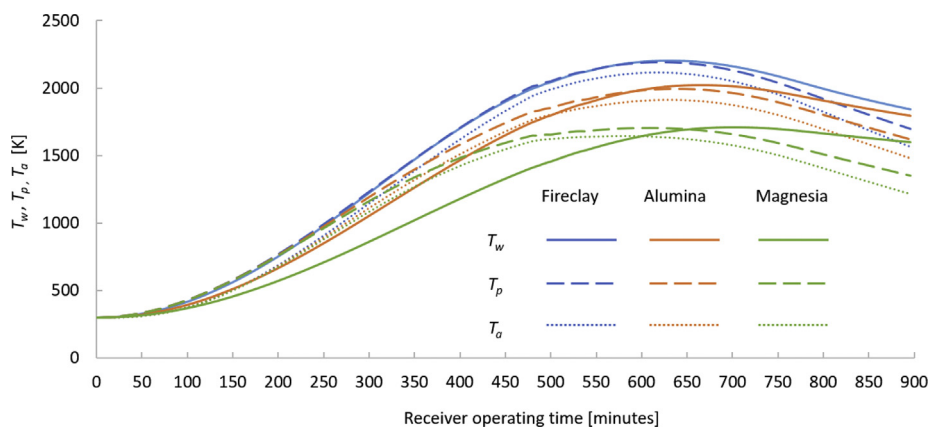

Fig. 8. Calculated transient temperature distributions of the receiver wall (T_w), the particle phase (T_p), and the air phase (T_a), employing 3 different refractory materials for lining of a constant thickness (100 mm), for a variable solar input on a clear summer day in Alice Springs, Australia – December 10th, 2018 ($D_1 = 12$ m, $D_{ap}/D_1 = 0.55$, $L/D_1 = 1.6$, $\theta = 45°$, $\Delta r_1 = 0.10$ m, $\Delta r_2 = 0.75$ m, C = 1000, $d_p = 100$ μm, $\dot{m}_p = 25$ kg/s, $\dot{m}_a/\dot{m}_p = 0.5$, and $T_{in} = 300$ K).

transients dominate. The final predicted temperature is some 320–400 K higher for the present model than for the previous model. Although perfect agreement of these two models cannot be expected, the agreement is good during the period when gradients are most significant (i.e. first 30 min), this suggests that the present model is sufficiently reliable for the purpose of assessing the influence of transients on the refractory-lined solar receivers.

5. Results and discussion

5.1. Sensitivity to the refractory lining material

Fig. 8 presents the calculated transient temperature distributions of the receiver cavity wall, the particle phase and the air phase, employing 3 different refractory materials: alumina, magnesia, and fireclay bricks. The variable DNI on the clear sky summer day (Fig. 5) was employed as the input heat source to the receiver.

It can be observed that, for all cases, the temperature of the particles and cavity wall are relatively close to each other for a given type of refractory. Hence, any limitations in the heating of the walls will also apply to the particles. In addition, the heating rate of the receiver cavity, particle phase, and air phase is better for fireclay refractory than alumina and magnesia. Fireclay has a higher absorptivity than alumina or magnesia, leading to lower radiation losses through the aperture and hence higher temperatures. The fireclay also has a faster response time, which can be explained by a 5.5% reduction in the product of mass and specific heat. Furthermore, fireclay refractory bricks have good spalling resistance, maintain shape when exposed to high temperatures and have a lower coefficient of thermal expansion than alumina and magnesia. Although, bricks can fall out and may have higher maintenance costs, they are comparatively cheaper. For these reasons, fireclay bricks were chosen for the inner lining in the subsequent analysis.

5.2. Influence of refractory lining thickness

Figs. 9 and 10 present the influence of the thickness of the refractory lining on the thermal performance of the receiver during the clear sky and cloudy day, respectively. Fig. 9a presents the
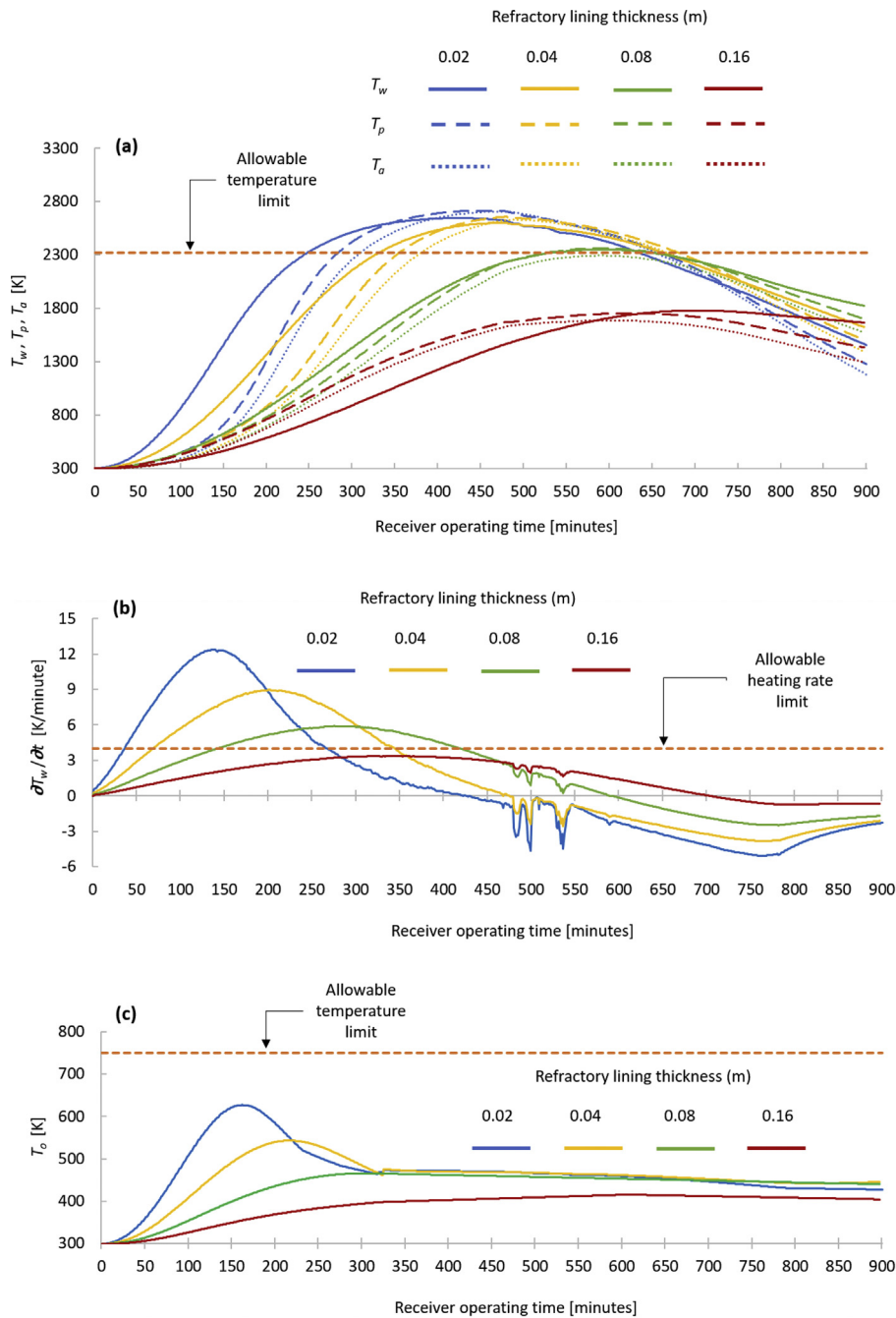
Fig. 9. Influence of refractory lining thickness on (a) the transient temperature distributions of the receiver wall (T_w), the particle phase (T_p), and the air phase (T_a); (b) the cavity heating rate ($\partial T_w/\partial t$); and (c) temperature of the outer steel shell (T_o), for a variable solar input on a clear summer day in Alice Springs, Australia − December 10th, 2018 ($D_1 = 12$, $D_{ap}/D_1 = 0.55$, $L/D_1 = 1.6$, $\theta = 45°$, $\varDelta r_2 = 0.75$ m, C = 1000, $d_p = 100$ μm, $\dot{m}_p = 25$ kg/s, $\dot{m}_a/\dot{m}_p = 0.5$, and $T_{in} = 300$ K).

results of the cavity wall, particles, and air phase temperature distribution for a variable DNI input on the clear sky summer day (Fig. 5) for a range of inner lining thickness from 20 to 160 mm. As expected, the rate of increase in temperatures of the refractory lining, particles, and the air increases with a reduction in the lining thickness. The receiver with a lining thickness of 20 mm takes 4.2 h to approach thermal equilibrium, but this is increased to 5.8, 7.5, and 8.3 h when the thickness of refractory lining is increased to 40, 80, and 160 mm, respectively. The lining thickness of 20 mm gives a maximum operating temperature of 2625 K which is above the allowable limit of refractory material. Similarly, the maximum operating temperature of receiver with a lining thickness of 40 mm

is higher than the allowable limit by a margin of 11%. For a fixed mass flow rate of particles, $\dot{m}_p = 25$ kg/s, the receiver was calculated to operate within the allowable temperature range with a lining thickness of above 80 mm.

A range of observations can be made about the particle temperatures. Firstly, increasing the refractory thickness decreases the output temperature of the particles, which is undesirable. For example, the peak temperature drops from 2695 to 1740 K as the refractory thickness is increased from 20 to 160 mm. Secondly, the particle temperature is not constant with time, but rather varies throughout the day with the input flux. This means that a control strategy would be needed to maintain a constant output
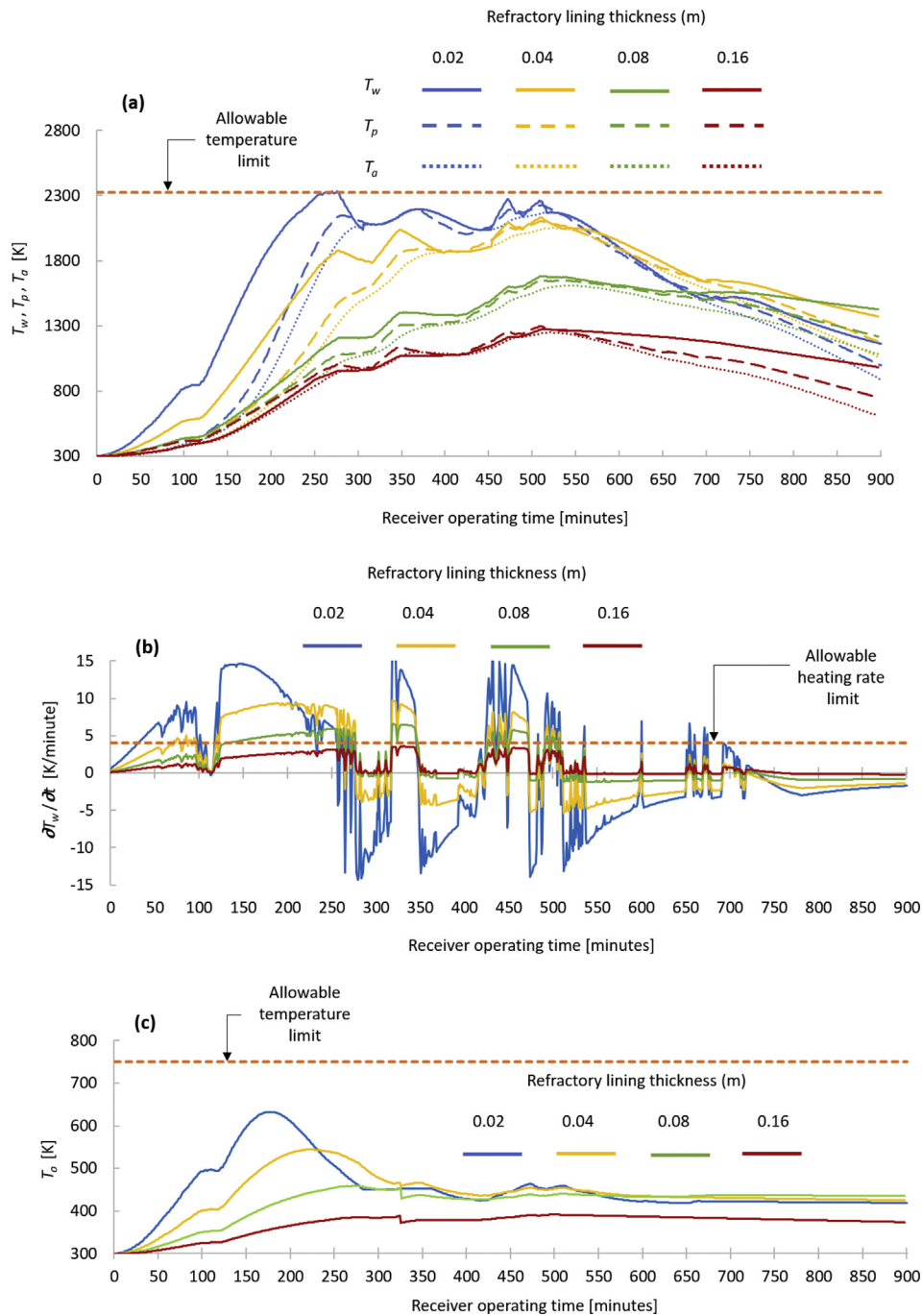
Fig. 10. Influence of refractory lining thickness on (a) the transient temperature distributions of the receiver wall (T_w), the particle phase (T_p), and the air phase (T_a); (b) the cavity heating rate ($\partial T_w/\partial t$); and (c) temperature of the outer steel shell (T_o), for a variable solar input on a cloudy summer day in Alice Springs, Australia − December 5th, 2018 ($D_1 = 12$, $D_{ap}/D_1 = 0.55$, $L/D_1 = 1.6$, $\theta = 45°$, $\Delta r_2 = 0.75$ m, C = 1000, $d_p = 100$ μm, $\dot{m}_p = 25$ kg/s, $\dot{m}_a/\dot{m}_p = 0.5$, and $T_{in} = 300$ K).

temperature, such as by varying the mass flow rate. This point is addressed in more detail below.

Fig. 9b presents the cavity heating rate as a function of refractory lining thickness. It can be observed that the cavity heating rate is increased by reducing the thickness of the lining. The cavity with 20 mm lining is heated at a maximum rate of 12 K/minute during the warm-up period of initial 2 h of receiver operation. Although the cavity heating rate drops rapidly after 1.5 h of operating time, it exceeds the allowable heating rate of 4 K/minute. Similarly, the heating rates for lining thickness of 40 mm during the warm-up period also exceeds the allowable limit by a difference of 2.2 K/

minute. On the other hand, the receiver with a refractory lining thickness of 80 and 160 mm maintains the cavity heating rate within the allowable limit of 4 K/minute during 2 h of initial operation.

The calculated results for the temperature of the outer steel shell are illustrated in Fig. 9c. This shows that the rate of increase in temperature of the outer steel shell increases with a reduction in the lining thickness. This is due to increased conductive losses through the cavity walls as the lining thickness decreases with a fixed thickness of the insulating layer. The maximum outer steel temperatures of 635, 550, 465, and 403 K are observed for receivers
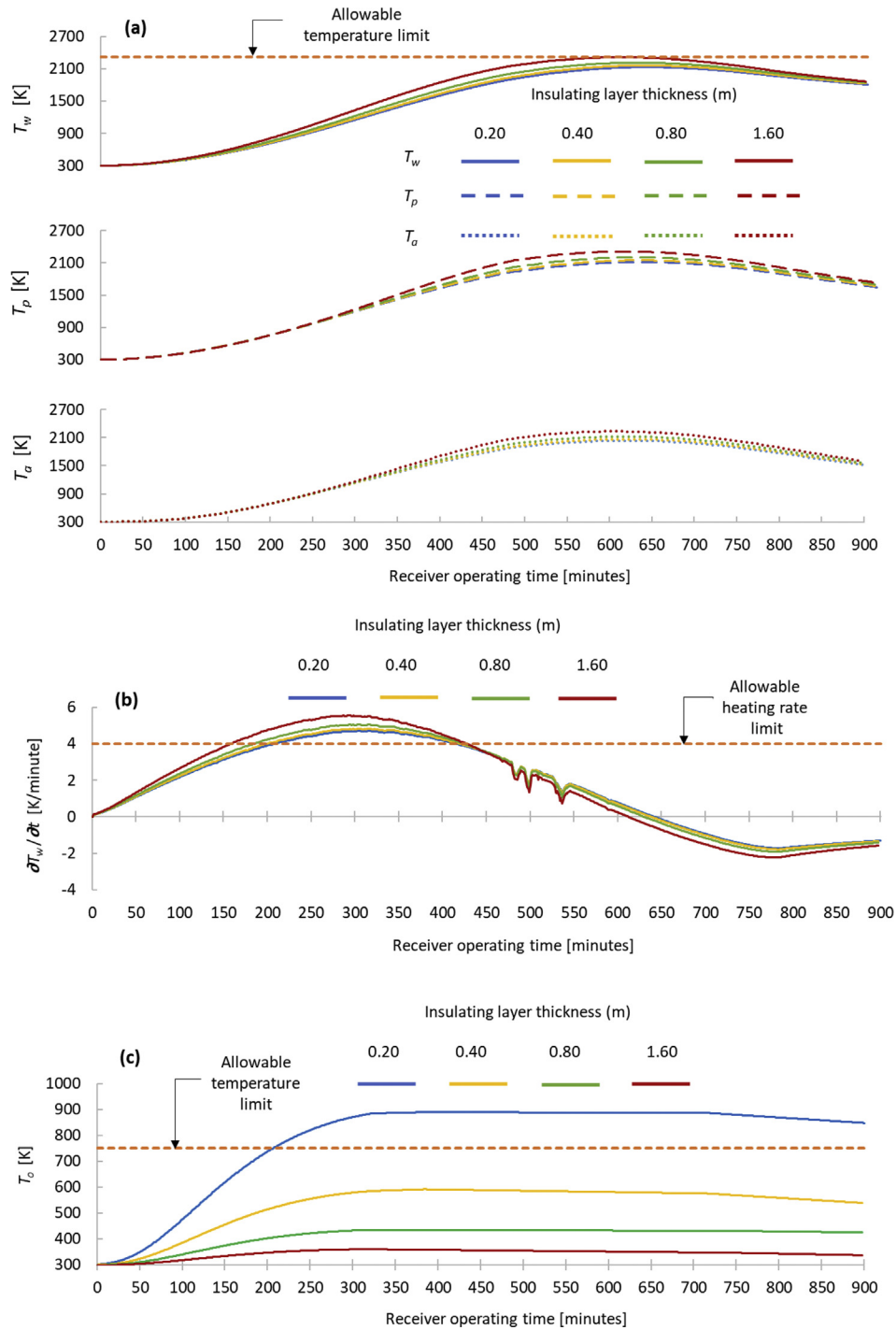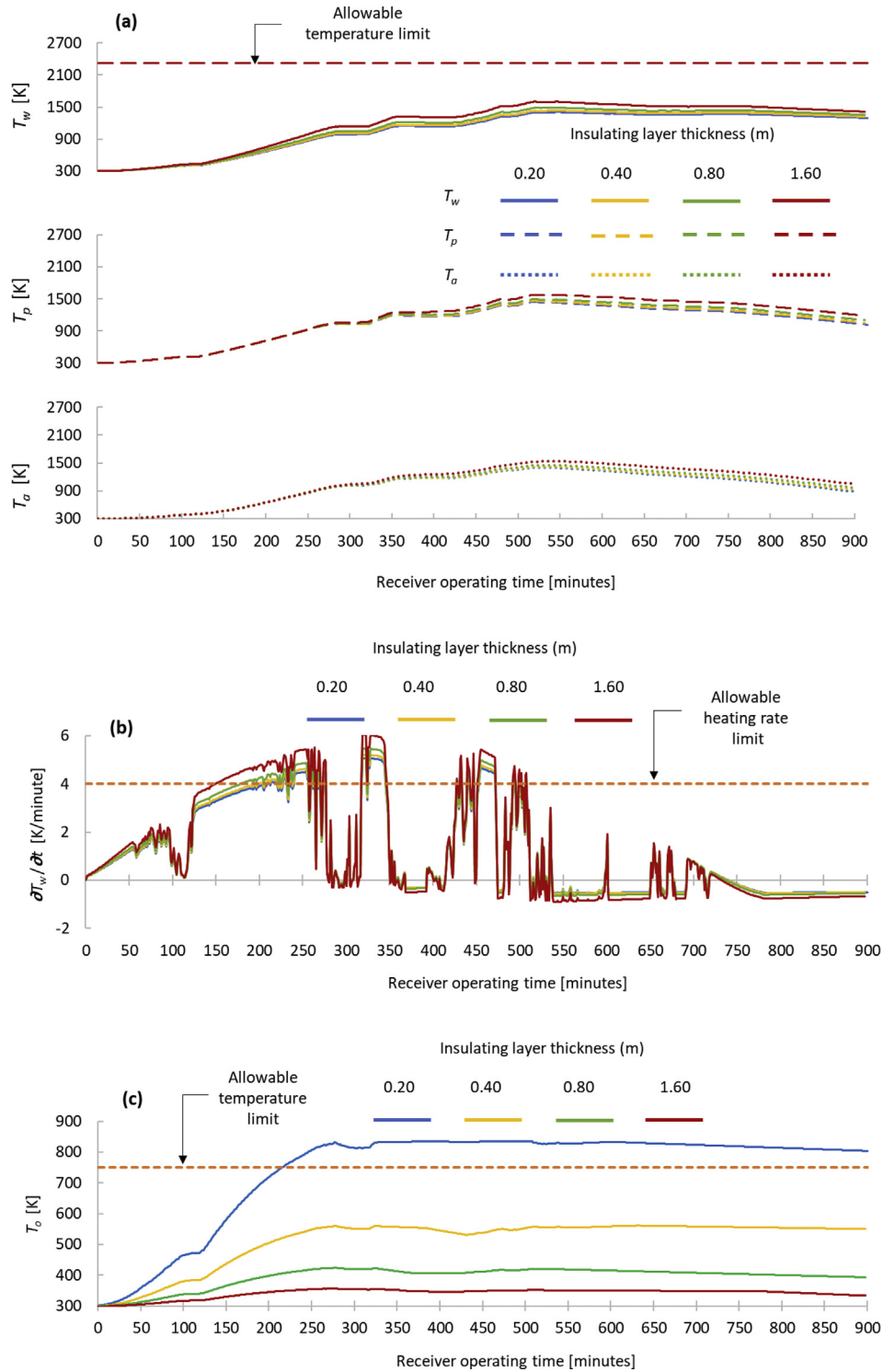
Fig. 11. Influence of insulting layer thickness on (a) the transient temperature distributions of the receiver wall (T_w), the particle phase (T_p), and the air phase (T_a); (b) the cavity heating rate ($\partial T_w/\partial t$); and (c) temperature of the outer steel shell (T_o), for a variable solar input on a clear summer day in Alice Springs, Australia − December 10th, 2018 ($D_1 = 12$, $D_{ap}/D_1 = 0.55$, $L/D_1 = 1.6$, $\theta = 45°$, $\Delta r_1 = 0.10$ m, C = 1000, $d_p = 100$ μm, $\dot{m}_p = 25$ kg/s, $\dot{m}_a/\dot{m}_p = 0.5$, and $T_{in} = 300$ K).

with lining thickness of 20, 40, 80, and 160 mm, respectively which are all well below the allowable limit for carbon steel.

The results indicate that the optimization of lining thickness is a tradeoff between the time to achieve thermal equilibrium, the allowable limits of temperatures, and the cavity heating rate. It is desirable to reach peak temperature quickly to operate at thermal equilibrium for most of the daily run time, while also considering impacts on the outer temperature of the steel shell and the maximum cavity heating rate.

Fig. 10 presents the results of the receiver's thermal behavior for the variable DNI input from the cloudy summer day (Fig. 5) for the same range of lining thickness from 20 to 160 mm. It can be observed that, even for the case of the thin refractory lining (20 mm), the refractory greatly damps the fluctuations in particle temperature. For example, the particle temperature following the total slump in solar power to almost zero at t = 280 and 390 min (Fig. 5), only drops by 30 and 120 K, respectively. This is quite significant given that the mass flow rate of particles is held constant

in these assessments, while it could be reduced in practice. Furthermore, a further increase in the thickness of the refractory lining can greatly damp these fluctuations to result in a relative stable and robust receiver operation despite the large fluctuations in the solar input. For the 80 mm thick refractory, the particle temperature drops by less than 15 K, following the periods of total slump in solar power to zero, whereas the receiver with a lining thickness of 160 mm is observed to maintain a stable operation without any significant drop in temperature of the particles. These results highlight the compensating advantage of a refractory in

Fig. 12. Influence of insulting layer thickness on (a) the transient temperature distributions of the receiver wall (T_w), the particle phase (T_p), and the air phase (T_a); (b) the cavity heating rate ($\partial T_w/\partial t$); and (c) temperature of the outer steel shell (T_o), for a variable solar input on a cloudy summer day in Alice Springs, Australia − December 5th, 2018 ($D_1 = 12$, $D_{ap}/D_1 = 0.55$, $L/D_1 = 1.6$, $\theta = 45°$, $\Delta r_1 = 0.10$ m, C = 1000, $d_p = 100$ μm, $\dot{m}_p = 25$ kg/s, $\dot{m}_a/\dot{m}_p = 0.5$, and $T_{in} = 300$ K).

damping the fluctuations, even though the temperature attained is lower, and shows the value of optimizing this parameter for all considerations.

5.3. Influence of insulting layer thickness

Fig. 11a presents the results of the cavity wall, particle, and air phase temperature distribution for the variable DNI input (Fig. 5) for a range of insulating layer thicknesses from 0.20 to 1.60 m. It can be seen that these changes in thickness have only a small influence on the resulting temperatures, with the temperatures of the receiver cavity, particles, and air increasing only slightly with these increases in the thickness of the insulating layer. This slight increase is due to the lower conductive losses through the cavity wall as the thickness of insulation is increased. The increase also slightly shortens the time to reach equilibrium from 9.2 to 8.3 h.

Fig. 11b and c presents the calculated results for the cavity heating rate and temperature of the outer steel shell, respectively as a function of insulation thickness on a clear sky summer day. It can be observed that the refractory heating rate is only slightly higher for the thicker insulating layer, whereas the temperature of the outer steel shell decreases strongly with an increase in the insulation thickness. The insulation lining thickness of 0.20 m gives a maximum outer steel shell temperature of 960 K which is above the allowable limit of 750 K. This temperature drops to 610, 430, and 359 K for the insulation thickness of 0.40, 0.80, and 1.60 m,

respectively which are within allowable limit of carbon steel. In summary, the insulation thickness has a strong influence on the temperature of the outer shell, but little influence on the temperature or heating rates of the refractory.

Fig. 12 presents the results of receiver's thermal behavior for the variable DNI input from the cloudy summer day for a range of insulation thicknesses. Similar to the results for clear sky day, it can be seen that the insulation thickness has small influence on the resulting temperatures and cavity heating rate but has strong influence on the temperature of the outer steel shell for the variable input on this cloudy day. The insulation thickness of 0.20 m is calculated to give a peak particle phase temperature of 1484 K which increases to 1580 K as the insulation thickness is increased to 1.60 m. The insulation thickness of 0.20 m gives a maximum outer steel shell temperature of 826 K which is above the allowable limit by a margin of 9%. This temperature drops to 554, 418, and 354 K for the insulation thickness of 0.40, 0.80, and 1.60 m, respectively.

5.4. Influence of particle mass flow rate

Fig. 13a presents the dependence of the temperature of the cavity wall, particles, and air phase on the mass flow rate of particles for a variable DNI input on the clear sky day. It can be seen that a decrease in the mass flow rate has the effect of increasing the maximum particle temperature, which is consistent with expectation because decreasing mass flow rate with the same energy
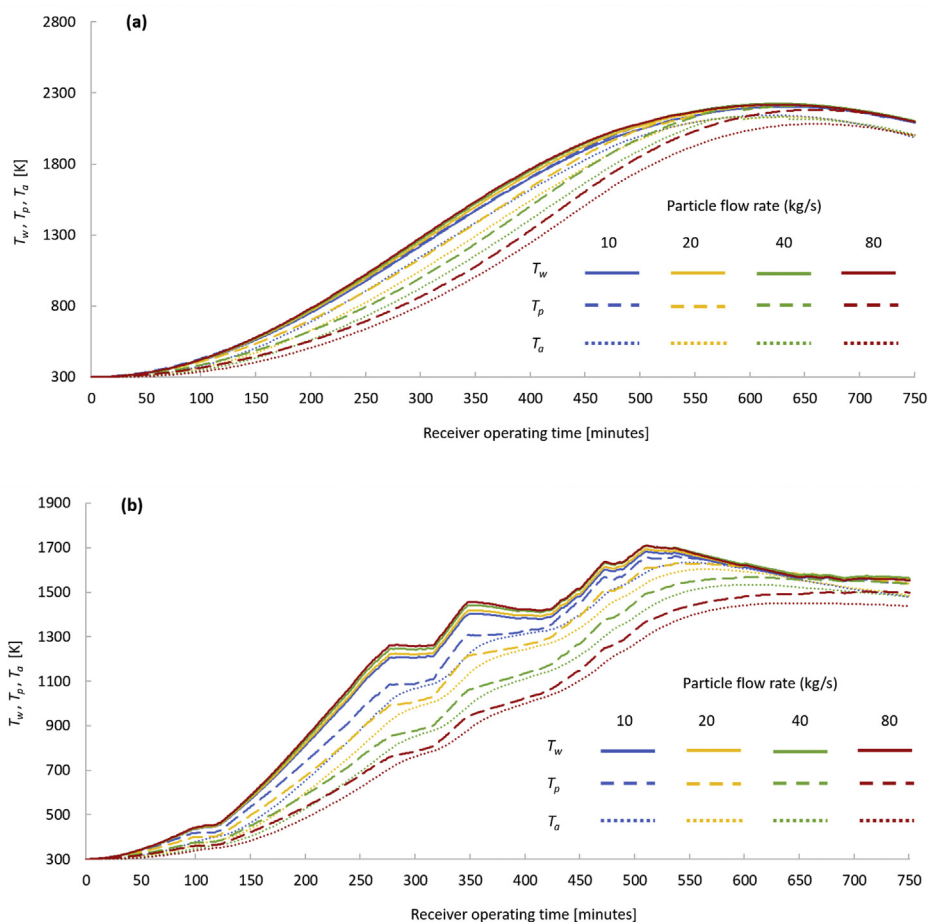

Fig. 13. Influence of the mass flow rate of particles on the transient temperature distributions of the receiver wall (T_w), the particle phase (T_p), and the air phase (T_a), for a variable solar input on (a) clear sky day (December 10th, 2018) and (b) cloudy day (December 5th, 2018) in Alice Springs, Australia ($D_1 = 12$, $\Delta r_2 = 0.75$ m, $L/D_1 = 1.6$, $D_{ap}/D_1 = 0.55$, $\theta = 45°$, C = 1000, $d_p = 100$ μm, $\dot{m}_a/\dot{m}_p = 0.5$, and $T_{in} = 300$ K).

input will increase the temperature rise of the two-phase flow by an energy balance. The decrease in particle mass flow rate also shortens the time to reach thermal equilibrium. For example, with the lowest value of mass flow rate, $\dot{m}_p = 10$ kg/s, 6.7 h are required to approach thermal equilibrium, whereas this time increases to 9.8 h for $\dot{m}_p = 80$ kg/s. Furthermore, it can be observed that the temperature of the air phase also increases with a decrease in particle mass flow rate. This is an indication that the performance of the receiver is strongly correlated with the total heat capacity of the particle and air phases.

Fig. 13b shows the variations of the cavity wall, particles, and air phase temperature with the mass flow rate of particles for the fluctuating DNI input on a cloudy day. It can be seen that the lower mass flow rate of particles is beneficial on a day with low and fluctuating solar input. The receiver is calculated to operate with a peak particle phase temperature of 1650 K with a lowest mass flow rate of particles, $\dot{m}_p = 10$ kg/s, whereas this temperature drops to 1460 K with a highest mass flow rate, $\dot{m}_p = 80$ kg/s. The particle phase can still reach a higher temperature when solar DNI fluctuates and the mass flow rate of particles is decreased. For example, following the total slump in solar power to nearly zero at t = 390 (Fig. 5), receiver can still operate with a particle outlet temperature of 1310 K with a low mass flow rate ($\dot{m}_p = 10$ kg/s). However, the particle temperature is reduced to 980 K when a higher flow rate of particles ($\dot{m}_p = 80$ kg/s) is employed.

To summarize, varying the particle mass flow-rate provides a measure of control of the particle temperature. Reducing the mass flow-rate can shorten the time needed to reach operating temperature by several hours and increase the maximum temperature by several hundred degrees. For example, the flow rate can be reduced during the start-up or turn down periods and increased as the cavity warms up or input DNI increases. This offers a strategy to assist in achieving the desired particle temperature with minimum impact on thermal efficiency by varying the production rate.

6. Conclusions

The main findings of the present analysis are as follows:

- Fireclay refractory linings achieve a higher operating temperature than alumina and magnesia for the same input conditions due to their higher absorptivity. Furthermore, fireclay refractories also have good thermal and mechanical shock resistance and are relatively cheap.
- The thickness of the refractory has a strong influence on the thermal inertia of the receiver, on its maximum internal temperature and on the maximum heating rate, but little influence on the temperature of the outer steel shell. In contrast, thickness of the insulating layer has a strong influence on the temperature of the outer steel shell, but little influence on the refractory temperature or heating rate.
- The thickness of the refractory must be optimised for a range of competing influences. On the one hand increasing the thickness has the beneficial impacts of reducing the peak heating rate and the temperature of the outer shell, while on the other hand it also reduces the outlet temperature of the particles and increasing the heat-up time, both which are undesirable. For example, receiver with a lining thickness of 20 mm achieves a peak operating temperature of 2625 K in 4.2 h, whereas this temperature is reduced to only 1750 K and is achieved in 8.3 h when the thickness of refractory increases to 160 mm.
- Even the thinnest refractory of 20 mm also has a significant compensating advantage of damping out the fluctuations in particle temperature due to intermittent cloud. For example, the particle temperature following the total slump in solar power to

nearly zero at t = 280 and 390 min, only drops by 30 and 120 K, respectively. Further increase in refractory thickness can dampen these responses further.
- A useful control strategy is to vary the particle flow into the receiver. Reducing the particle flow rate can significantly reduce the time to reach operating temperature and also help to further dampen the fluctuations in particle temperature. For example, with the lowest value of mass flow rate, $\dot{m}_p = 10$ kg/s, 6.7 h are required to reach thermal equilibrium, whereas this time increases to 9.8 h for $\dot{m}_p = 80$ kg/s.

For the conditions assessed here, the results highlight the role of refractory and particle mass flow rate in damping the solar fluctuations and show that careful choice of these parameters can be strongly beneficial to receiver operation and its practical implementation.

CRediT authorship contribution statement

Muhammad M. Rafique: conceived the idea, developed the mathematical model, performed analysis, interpreted data, Writing - original draft, and acted as a corresponding author, wrote the initial version of the manuscript and carried out required revisions. **Graham Nathan:** supervised the work and helped in the interpretation and evaluation of data, Also helped to improve the language, structure, and content of the manuscript. **Woei Saw:** supervised the work and helped in the interpretation and evaluation of data, Also helped to improve the language, structure, and content of the manuscript.

Declaration of competing interest

The authors declare that there is no conflict of interest regarding the publication of this article.

Acknowledgments

Nomenclatures

A	area (m^2)
CR	concentration ration ($-$)
c_p	specific heat capacity (kJ/kg.K)
DNI	direct normal irradiance (kW/m^2)
D	cavity diameter (m)
d_p	particle diameter (m)
$\dot{Q}$	energy flow rate (kW)
F	radiation shape factor ($-$)
g	gravitational acceleration (m/s^2)
Gr	Grashoff number ($-$)
h	heat transfer coefficient (kW/m^2.K)
i	number of iterations (1, 2, 3 …. n)
k	thermal conductivity (W/m.K)
L	length (m)
$\dot{m}$	mass flow rate (kg/s)
m_1	mass of a single particle (kg)
N_p	number of particles ($-$)
Nu	Nusselt number ($-$)

Re	Reynolds number (−)
R	resistance to heat flow (K/kW)
r	radius (m)
T	temperature (K)
u	velocity (m/s)
V	volume (m^3)

Greek letters

α	absorptivity (−)
ε	emissivity (−)
∂t	time step for one iteration (s)
Ω	thermal diffusivity (m^2/s)
μ	dynamic viscosity (kg/m.s)
v	kinematic viscosity of the air (m^2/s)
ρ	density (kg/m^3)
η	efficiency (%)
$\tau_{r,p}$	particle residence time (s)
β	thermal expansion coefficient (1/K)
θ	cavity inclination angle (degrees)
Ψ	cone angle (degrees)
σ	Stefan-Boltzmann constant (W/m^2.K^4)

Subscripts

1, 2, 3	cavity layer 1, 2, and 3
a	air
ap	aperture
at	attenuation
amb	ambient
b	blocking
c	cavity
cond	conduction
conv	convection
cos	cosine
e	effective
eq	equivalent
helio	heliostat field
o	outer
p	particle
ref	reference condition
rad	radiation
re-rad	re-radiation
r	reflection
s	surroundings
sol	solar
sh	shading
w	cavity wall lining

Appendix A. Supplementary data

Supplementary data to this article can be found online at https://doi.org/10.1016/j.renene.2020.11.077.

References

[1] G.J. Nathan, M. Jafarian, B.B. Dally, W.L. Saw, P.J. Ashman, E. Hu, A. Steinfeld, Solar thermal hybrids for combustion power plant: a growing opportunity, Prog. Energy Combust. Sci. 64 (2018) 4–28.

[2] Y. Jin, J. Fang, J. Wei, M.A. Qaisrani, X. Wang, Thermal performance evaluation of a cavity receiver based on particle's radiation properties during the day time, Renew. Energy 143 (2019) 622–636.

[3] D. Davis, F. Müller, W.L. Saw, A. Steinfeld, G.J. Nathan, Solar-driven alumina calcination for CO2 mitigation and improved product quality, Green Chem. 19 (13) (2017) 2992–3005.

[4] Rafique, M. M., Nathan, G., and Saw, W., "Uncertainty in predicting the start-up time and losses for a high temperature particle receiver due to solar resource variability," Proc. ASME 2020 14th International Conference on Energy SustainabilityV001T02A007.

[5] T. Tan, Y. Chen, Review of study on solid particle solar receivers, Renew.

[6] W. Wu, D. Trebing, L. Amsbeck, R. Buck, R. Pitz-Paal, Prototype testing of a centrifugal particle receiver for high-temperature concentrating solar applications, J. Sol. Energy Eng. 137 (4) (2015).

[7] W. Wu, R. Uhlig, R. Buck, R. Pitz-Paal, Numerical simulation of a centrifugal particle receiver for high-temperature concentrating solar applications, Numer. Heat Tran., Part A: Applications 68 (2) (2015) 133–149.

[8] C.K. Ho, Advances in central receivers for concentrating solar applications, Sol. Energy 152 (2017) 38–56.

[9] H. Zhang, H. Benoit, I. Perez-Lopèz, G. Flamant, T. Tan, J. Baeyens, High-efficiency solar power towers using particle suspensions as heat carrier in the receiver and in the thermal energy storage, Renew. Energy 111 (2017) 438–446.

[10] J. Baeyens, H. Zhang, W. Kong, P. Dumont, G. Flamant, Solar thermal treatment of non-metallic minerals: the potential application of the SOLPART technology, AIP Conference Proceedings 2126 (1) (2019) 180002.

[11] G. Flamant, H. Benoit, M. Jenke, A.F. Santos, S. Tescari, G. Moumin, A. Rodriguez, A. Azapagic, L. Stamford, J. Baeyens, Y. Boes, F. Pron, M. Prouteau, P. Dumont, N. Abdenouri, H. Mazouz, Solar processing of reactive particles up to 900°C, the SOLPART project, AIP Conference Proceedings 2033 (1) (2018), 020004.

[12] W.R. Logie, J.D. Pye, J. Coventry, Thermoelastic stress in concentrating solar receiver tubes: a retrospect on stress analysis methodology, and comparison of salt and sodium, Sol. Energy 160 (2018) 368–379.

[13] Z. Liao, X. Li, C. Xu, C. Chang, Z. Wang, Allowable flux density on a solar central receiver, Renew. Energy 62 (2014) 747–753.

[14] L. Xu, W. Stein, J.-S. Kim, Y.C.S. Too, M. Guo, Z. Wang, Transient numerical model for the thermal performance of the solar receiver, Appl. Therm. Eng. 141 (2018) 1035–1047.

[15] J. Samanes, J. Garcia-Barberena, A model for the transient performance simulation of solar cavity receivers, Sol. Energy 110 (2014) 789–806.

[16] P. Charvin, S. Abanades, P. Neveu, F. Lemont, G. Flamant, Dynamic modeling of a volumetric solar reactor for volatile metal oxide reduction, Chem. Eng. Res. Des. 86 (11) (2008) 1216–1222.

[17] O.A. Ortiz, G.I. Suárez, A. Nelson, Dynamic simulation of a pilot rotary kiln for charcoal activation, Comput. Chem. Eng. 29 (8) (2005) 1837–1848.

[18] M. Neber, H. Lee, Design of a high temperature cavity receiver for residential scale concentrated solar power, Energy 47 (1) (2012) 481–487.

[19] ASTM Volume 15.01, "Refractories, activated carbon; advanced ceramics.".

[20] S. Abanades, P. Charvin, G. Flamant, Design and simulation of a solar chemical reactor for the thermal reduction of metal oxides: case study of zinc oxide dissociation, Chem. Eng. Sci. 62 (22) (2007) 6323–6333.

[21] Technical Information Alumina Products. https://www.advaluetech.com/technical-alumina-products.

[22] H. Weitz, W. Roos, D. Fourie, P. Strydom, J. Zietsman, Improving furnace start-ups with computational modelling: the key to refractory lining integrity, in: The Eleventh International Heavy Minerals Conference, The Southern African Institute of Mining and MetallurgyWestern Cape, 2019, 5–6 August 2019.

[23] J.J. Gangler, High-temperature testing techniques for brittle refractory materials, J. Am. Ceram. Soc. 37 (9) (1954) 439–444.

[24] A.V. Zabolotsky, Thermal crack growth modeling in refractory linings of metallurgical installations, International Journal of Mathematical Models and Methods in Applied Sciences 5 (3) (2011) 542–548.

[25] J. Jenkins, Important Considerations for Refractory Dryouts, Startups and Shutdowns, Sulfur Recovery SymposiumVail, CO, 2011. September 13-16, 2011.

[26] S.O. Alexopoulos, J. Dersch, M. Roeb, R. Pitz-Paal, Simulation model for the transient process behaviour of solar aluminium recycling in a rotary kiln, Appl. Therm. Eng. 78 (2015) 387–396.

[27] M. Ebert, L. Amsbeck, J. Rheinländer, B. Schlögl-Knothe, S. Schmitz, M. Sibum, R. Uhlig, R. Buck, Operational experience of a centrifugal particle receiver prototype, AIP Conference Proceedings 2126 (1) (2019), 030018.

[28] CET. https://www.adelaide.edu.au/cet/technologies/solar-expanding-vortex-particle-receiver-reactor-sevr.

[29] A. Chinnici, M. Arjomandi, Z.F. Tian, Z. Lu, G.J. Nathan, A novel solar expanding-vortex particle reactor: influence of vortex structure on particle residence times and trajectories, Sol. Energy 122 (2015) 58–75.

[30] A. Steinfeld, Solar thermochemical production of hydrogen––a review, Sol. Energy 78 (5) (2005) 603–615.

[31] K. Dana, S. Sinhamahapatra, H.S. Tripathi, A. Ghosh, Refractories of alumina-silica system, Trans. Indian Ceram. Soc. 73 (1) (2014) 1–13.

[32] J.D. Smith, W.G. Fahrenholtz, in: J.F. Shackelford, R.H. Doremus (Eds.), Refractory Oxides," Ceramic and Glass Materials: Structure, Properties and Processing, Springer US, Boston, MA, 2008, pp. 87–110.

[33] M.-M.O.M.P. Applications. https://www.azom.com/properties.aspx?ArticleID=54.

[34] M.A.L. Braulio, M. Rigaud, A. Buhr, C. Parr, V.C. Pandolfelli, Spinel-containing alumina-based refractory castables, Ceram. Int. 37 (6) (2011) 1705–1724.

[35] A. Yurkov, "The Properties of Refractory and Heat Insulation Materials," Refractories for Aluminium: Electrolysis and the Cast House, Springer International Publishing, Cham, 2015, pp. 1–63.

[36] E.R. Benavidez, E. Brandaleze, Y.S. Lagorio, S.E. Gass, A.G.T. Martinez, Thermal and Mechanical Properties of Commercial MgO-C Bricks, vol. 20, Matéria, Rio de Janeiro, 2015, pp. 571–579.

[37] A.C. Yunus, M.C. John, H.T. Robert, Fundamentals of Thermal-Fluid Sciences,

McGraw Hill Higher Education, London, United States, 2012.

[38] Thermo-optical properties. http://webserver.dmt.upm.es/~isidoro/dat1/Thermooptical.pdf.

[39] Emissivity coefficients materials. https://www.engineeringtoolbox.com/emissivity-coefficients-d_447.html.

[40] A. Chinnici, Y. Xue, T.C.W. Lau, M. Arjomandi, G.J. Nathan, Experimental and numerical investigation of the flow characteristics within a solar expanding-vortex particle receiver-reactor, Sol. Energy 141 (2017) 25—37.

[41] H. Leuenberger, R.A. Person, Compilation of Radiation Shape Factors for Cylindrical Assemblies, American Society of Mechanical Engineers, 1956.

[42] D. Davis, M. Jafarian, A. Chinnici, W.L. Saw, G.J. Nathan, Thermal performance of vortex-based solar particle receivers for sensible heating, Sol. Energy 177 (2019) 163—177.

[43] J. Szekely, R. Carr, Heat transfer in a cyclone, Chem. Eng. Sci. 21 (12) (1966) 1119—1132.

[44] D. Hirsch, A. Steinfeld, Solar hydrogen production by thermal decomposition of natural gas using a vortex-flow reactor, Int. J. Hydrogen Energy 29 (1) (2004) 47—55.

[45] J.A. Harris, T.G. Lenz, Thermal performance of solar concentrator/cavity receiver systems, Sol. Energy 34 (2) (1985) 135—142.

[46] W.B. Stine, Cavity receiver convection heat loss, in: Proc. Of the International Solar Energy Society, Solar World Congress, 1989, p. 1318.

[47] J.A.a. Duffie, Solar Engineering of Thermal Processes, Wiley, 2013.

[48] C. Zou, Y. Zhang, Q. Falcoz, P. Neveu, C. Zhang, W. Shu, S. Huang, Design and optimization of a high-temperature cavity receiver for a solar energy cascade utilization system, Renew. Energy 103 (2017) 478—489.

[49] M.K. Gupta, K.J. Bumtariya, H.A. Shukla, P. Patel, Z. Khan, Methods for evaluation of radiation view factor: a review, Mater. Today: Proceedings 4 (2) (2017) 1236—1243. Part A.

[50] M. Jafarian, M. Arjomandi, G.J. Nathan, The influence of high intensity solar radiation on the temperature and reduction of an oxygen carrier particle in hybrid chemical looping combustion, Chem. Eng. Sci. 95 (2013) 331—342.

[51] N. Siegel, M. Gross, C. Ho, T. Phan, J. Yuan, Physical properties of solid particle thermal energy storage media for concentrating solar power applications, Energy Procedia 49 (2014) 1015—1023.

[52] A. Calderón, C. Barreneche, A. Palacios, M. Segarra, C. Prieto, A. Rodriguez-Sanchez, A.I. Fernández, Review of solid particle materials for heat transfer fluid and thermal energy storage in solar thermal power plants, Energy Storage 1 (4) (2019) e63.

[53] P. Auerkari, Mechanical and Physical Properties of Engineering Alumina Ceramics, Technical Research Centre of Finland Espoo, 1996.

[54] W.M. Haynes, CRC Handbook of Chemistry and Physics, CRC press, 2014.

[55] J. Hilsenrath, Tables of Thermal Properties of Gases: Comprising Tables of Thermodynamic and Transport Properties of Air, Argon, Carbon Dioxide, Carbon Monoxide, Hydrogen, Nitrogen, Oxygen, and Steam, US Department of Commerce, National Bureau of Standards, 1955.

[56] Bureau of Meteorology. http://www.bom.gov.au/climate/glossary/seasons.shtml.

[57] Superwool, High temperature insulation products. http://www.goodfellow.com/corporate/news/2011/Superwool-607-HT-Goodfellow-UK-Sept-2011.pdf.

[58] Materials thermal properties database. https://thermtest.com/materials-database.

[59] German Association of Refractory, Refractory Engineering: Materials-Design-Construction, Vulkan-Verlag GmbH, 2004.

[60] Metallic materials. https://www.allsealsinc.com/teadit/TypicalMetalProperties.pdf.

[61] M. Stewart, O.T. Lewis, 4 - mechanical design of pressure vessels, in: M. Stewart, O.T. Lewis (Eds.), Pressure Vessels Field Manual, Gulf Professional Publishing, 2013, pp. 133—216.

[62] R. Sadeghbeigi, Fluid Catalytic Cracking Handbook: an Expert Guide to the Practical Operation, Design, and Optimization of FCC Units, Butterworth-Heinemann, 2020.

[63] J. Servert, A. González, J. Gil, D. López, J.F. Funes, A. Jurado, Sensitivity analysis of heliostat aiming strategies and receiver size on annual thermal production of a molten salt external receiver, AIP Conference Proceedings 1850 (1) (2017), 030047.

CHAPTER 4

THERMAL RESPONSE OF MULTILAYERED
REFRACTORY-LINED SOLAR RECEIVERS TO
TRANSIENT OPERATION

Statement of Authorship

Title of Paper	Thermal response of multi-layered refractory-lined solar receivers to transient operation
Publication Status	☑ Published ☐ Accepted for Publication ☐ Submitted for Publication ☐ Unpublished and Unsubmitted work written in manuscript style
Publication Details	Thermal response of multilayered refractory-lined solar receivers to transient operation. Solar Energy. 243:70-80. https://doi.org/10.1016/j.solener.2022.07.037

Principal Author

Name of Principal Author (Candidate)	Muhammad Mujahid RAFIQUE
Contribution to the Paper	Performed the literature review and identified the potential gaps. Jointly defined the scope and aims of the paper. Jointly performed analysis, interpreted data, wrote the manuscript, and acted as corresponding author.
Overall percentage (%)	60%
Certification:	This paper reports on original research I conducted during the period of my Higher Degree by Research candidature and is not subject to any obligations or contractual agreements with a third party that would constrain its inclusion in this thesis. I am the primary author of this paper.
Signature		Date	25/08/2022

Co-Author Contributions

By signing the Statement of Authorship, each author certifies that:

i.   the candidate's stated contribution to the publication is accurate (as detailed above);

ii.   permission is granted for the candidate in include the publication in the thesis; and

iii. the sum of all co-author contributions is equal to 100% less the candidate's stated contribution.

Name of Co-Author	Prof. Graham Nathan
Contribution to the Paper	Supervised the work. Jointly defined the scope and aims of the paper. Jointly performed analysis and interpreted data. Critically reviewed the manuscript. Helped to improve the language, structure, and content of the manuscript.
Signature		Date	15/9/2022

Name of Co-Author	Dr. Woei Saw
Contribution to the Paper	Supervised the work. Jointly defined the scope and aims of the paper. Jointly performed analysis and interpreted data. Critically reviewed the manuscript. Helped to improve the language, structure, and content of the manuscript.
Signature		Date	15/09/2022

Check for updates

Thermal response of multilayered refractory-lined solar receivers to transient operation

Muhammad M. Rafique [a,b,*], Graham Nathan [a,b], Woei Saw [a,c]

[a] *Centre for Energy Technology, The University of Adelaide, SA 5005, Australia*
[b] *School of Mechanical Engineering, The University of Adelaide, SA 5005, Australia*
[c] *School of Chemical Engineering and Advanced Materials, The University of Adelaide, SA 5005, Australia*

ARTICLE INFO

ABSTRACT

The thermal response of a multilayered refractory-lined particle-laden solar receiver during start-up, turn down, and shut down has been assessed with a transient model and long time-series of variable solar resource data. The influence of operating conditions and geometric parameters on the temperature of the particles and cavity wall, together with thermal stress distribution, are reported for cold and hot starts from 27 to 800 °C. Both the influence of covering the aperture during shutdown periods of sufficiently low solar resource, and geometric scale on thermal performance are also reported. The results provide insights into optimisation of the refractory-lining and insulation thickness of industrial-scale particle-laden receiver with regard to balancing the trade-off between thermal stability, temperature drop overnight, warm-up time, useful daily solar hours and allowable thermal stresses.

1. Introduction

Solar particle receivers are a promising class of technology for operating at temperatures of about 1000 °C, due to their high surface area per unit mass and capacity for direct irradiation, together with the possibility of a low-cost storage medium (Tan and Chen, 2010; Ho, 2016). High temperature particle receivers employ sand-like ceramic particles which are stable at temperatures of >1000 °C, which is far higher than the 580 °C of commercial molten salts. The particle-driven solar receivers including rotary furnace (Wu et al., 2014), falling particles (Ho et al., 2014), obstructed flow (Ho et al., 2016), particles flow in tubes (Flamant, 1982), and vortex receivers (Davis et al., 2019) have indicated their potential to achieve exit temperatures of above 1000 °C. A summary of these high temperature receivers has been provided previously (Merchán et al., 2022; Ho, 2016, Ho and Iverson, 2014). The design temperature of these receivers is above the melting temperature of mild steel, they must either use more expensive high temperature metals or a refractory lining. While the transient response of these directly irradiated receivers with a refractory lining is more challenging to manage owing to their higher thermal inertia, no equivalent assessment of these effects is available. Hence there is a need to know how to optimize the design of refractory lining for upscaling these emerging

receivers to a higher power level under real-time operating conditions. This paper aims to meet this need.

Greater insight is needed of the influence of the thickness, type and operational strategies for a refractory lining on the thermal performance of the high temperature solar receivers that are under development for solar thermal energy systems, as a potential approach to managing both thermal stresses and the transient heat inputs from the heliostat-field. This is because high thermal inertia of the refractory lining can potentially result in a significant fraction of the solar resource being needed to heat the cavity to the required operating temperature. While previous investigations of refractory-lined solar receivers have provided information on the start-up time required to heat the cavity, little attention has been provided to the options with which this time might be reduced when considering long term solar resource variability. The previous modelling study of an industrial-scale multilayered cavity receiver by Rafique et al. (2021) showed that a substantial portion of the solar day is needed to heat a receiver from ambient temperature. Similarly, Ortiz et al. (2005) also concluded from the dynamic simulation of a laboratory scaled rotary kiln with a refractory lining of ~150 mm that 3 h of heating time was required to achieve a nominal operating temperature for their system. Hence there is a need to better understand the options with which the start-up time might be reduced. This must be achieved in
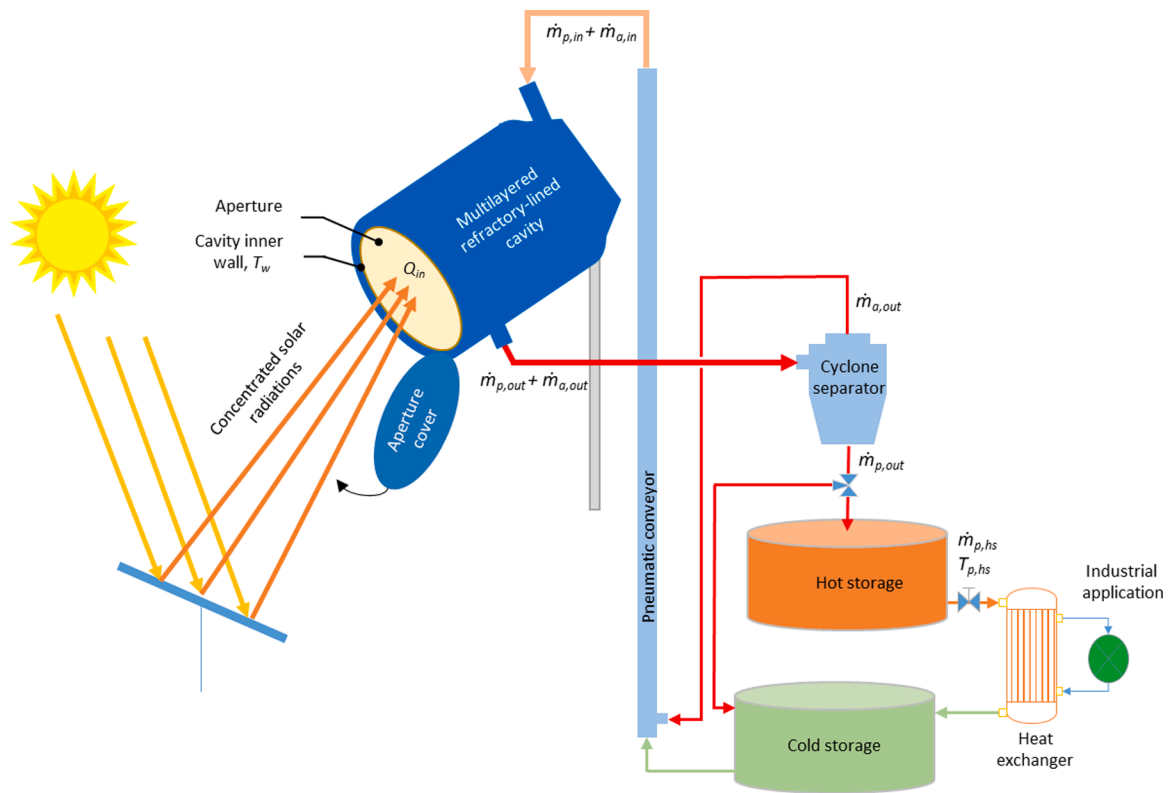

Fig. 1. Schematic diagram of the geometric arrangement assessed here, showing key terminologies used for the refractory-lined Solar Expanding Vortex Particle Receiver, thermal storage system and heat exchanger.

a way that avoids exceeding the maximum allowable heating rate of the ceramic refractory lining, to avoid failure from exceeding the maximum allowable thermal stresses (Abanades et al., 2007; Soo Too et al., 2019; Rafique et al., 2021). Therefore, the influence of transients in the incoming concentrated solar radiation must be considered (Soo Too et al., 2019). Insufficient information is available with which to guide the selection of refractory type, thickness or management strategy in response to these challenges, which provides the motivation for the present investigation.

Two of the main parameters that can be varied in seeking to minimize start-up time are introducing a time delay between the onset of the solar resource and the introduction of particles to the receiver, and turning-down the flow-rate of particles below the nominal design value. However, while it has been shown that a reduction in the particle flow rate can reduce the time to reach a desired particle outlet temperature, or thermal equilibrium (Rafique et al., 2021), it has yet to be shown how a minimum operating temperature can be achieved in a reasonable time. While many control strategies have been developed to achieve a set-point temperature in conventional refractory lined devices, such as rotary kilns (Ortiz et al., 2005), these are yet to be reported for solar receivers with a transient input. The influence of covering the receiver aperture during shutdown periods to minimize thermal losses, is also yet to be reported. Furthermore, it is desirable to determine whether there is a minimum size of the receiver before the overnight heat losses become too great, to guide the design of practical high-temperature refractory-lined solar receivers. Hence, a further objective of the present investigation is to meet the need for better understanding of the influence of these parameters, considering overnight temperature drop, useful daily solar hours, allowable temperature and thermal stress limits.

Keeping the highlighted gaps in mind, the overall objective of this research is to increase understanding of how to manage the transient responses to solar variability of temperature and thermal stress distributions of refractory-lined solar particle-laden receivers during start-up, turn down, and shut down. In particular, the influence of a four-day time

series of variable solar input on these parameters is of interest to guide the design optimization of particle receivers. More specifically, the study aims to report the influence on the transient response of a refractory lined particle-laden receiver of the initial temperature of the cavity internal wall, of covering the aperture, of delaying the particle feed and of geometric scale.

2. Material and methods

The assessments were performed for a cylindrical solar cavity receiver based on the Solar Expanding Vortex Receiver (SEVR) (CET; Chinnici et al., 2015), shown in (Fig. 1), although the trends are expected to be relevant to other configurations such as the cylindrical centrifugal receiver (Ebert et al., 2019; Wu et al., 2014) and the falling particle curtain receiver (Gobereit et al., 2015; Ho et al., 2014). In the SEVR, a vortex of particles is formed inside the cylindrical cavity using a carrier gas, which is considered to be air in the present investigation (Chinnici et al., 2015). This receiver can be configured either as a particle or an air receiver. Here it is treated as a particle receiver considering air as the secondary heat transfer medium. A secondary thermocline storage can be used to recover the thermal gain of the air phase, which is not reported here. The heated particles from the cyclone separator are here proposed to be transported either to the hot storage or cold storage tank based on whether or not they reach a minimum acceptable outlet set-point temperature for the particles ($T_{p,out,\mathrm{min}}$). The desired flow-rate of energy transferred from the hot storage tank to a process can be managed by varying the mass flow rate of particles ($\dot{m}_{p,hs}$) to compensate for some variation in the particle temperature ($T_{p,hs}$), also providing the potential to allow a range in this parameter.

The transient mathematical model of Rafique et al. (2021) was extended to assess the thermal response of the receiver during start-up, turn-up, and shut down with a long time-series of variable solar direct normal irradiance (DNI) data to enable design optimization of particle receivers. The transient model employs the governing mathematical
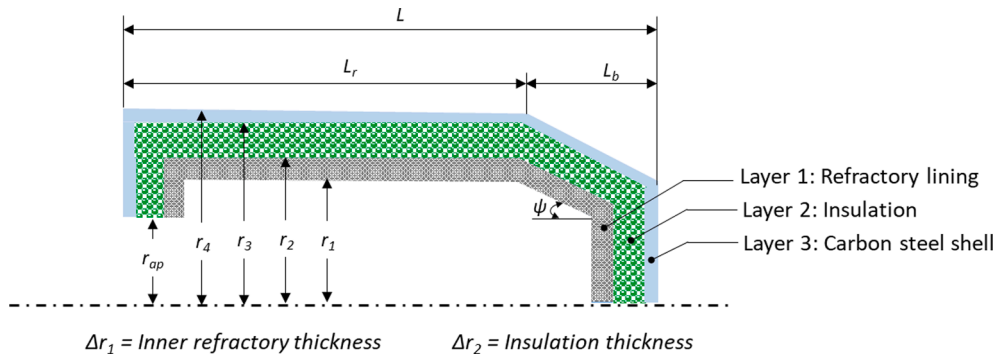
Fig. 2. An axisymmetric cross-sectional view of the SEVR, with the notations used to describe the multi-layered refractory-lined cavity receiver.

Table 1
The main materials employed in the multilayer cavity receiver and their thermophysical properties.

Cavity Layer	Material (–)	Thermal conductivity (W/m.°C)	Specific heat (kJ/kg. °C)	Bulk density (kg/m³)	Young's modulus of elasticity (GPa)	Thermal coefficient of linear expansion (1/°C)	References
1	Fireclay bricks	3.4	1.06	3150	145	3.0×10^{-6}	Callister and Rethwisch, 2018; Dana et al., 2014; Heindl and Pendergast, 1937; Liu and Liu, 2003;
2	High temperature insulation	0.28	1.14	128	80	1.0×10^{-6}	Rafique et al., 2021; Refractory ceramic fibre, 2022
3	Carbon steel	54	0.47	7850	–	1.2×10^{-5}	Charde, 2013

equations for mass and energy flows through the receiver cavity, considering the particle and gas phases, thermal losses, and conductive, convective and radiative heat transfer. The energy balance for each phase and the walls can be written as follows:

$$Q_{thermal} = Q_{sol,ap-w} - Q_{rad,w-p} - Q_{conv,w-a} - Q_{cond,w-s} - Q_{conv,w-s} - Q_{re-rad,w-s} - Q_{rad,ap-p} \tag{1}$$

$$\Delta H_{p,i} = H_{p,i} - H_{p,inlet} = Q_{rad,w-p} - Q_{conv,p-a} + Q_{rad,ap-p} \tag{2}$$

$$\Delta H_{a,i} = H_{a,i} - H_{a,inlet} = Q_{conv,p-a} + Q_{rad,w-a} \tag{3}$$

Here $Q_{sol,ap-w}$ is the radiation heat transfer passing through the aperture to the inside surface of the cavity walls, $Q_{thermal}$ is the change in the thermal mass of receiver cavity walls, $Q_{rad,w-p}$ is the radiative heat exchange between cavity walls and particle phase, $Q_{conv,w-a}$ is the convective heat exchange between cavity walls and air, $Q_{cond,w-s}$ is the conduction heat loss to the surroundings through receiver cavity walls, $Q_{conv,w-s}$ is the convection heat loss to the surroundings through aperture opening, $Q_{re-rad,w-s}$ is the re-radiation heat loss to the surroundings through aperture opening, $Q_{sol,ap-p}$ is the radiative heat transfer from aperture to the particle phase, and $Q_{conv,p-a}$ is the convective heat exchange between the particles and air. ΔH_p and ΔH_a are the enthalpy changes of the particle and air phases.

The detailed formulation of each heat flow mechanism is presented previously (Rafique et al., 2021). This model has been previously verified to show that the dynamic response of the system to various time-series is consistent with available data and expectations (Rafique et al., 2021). The receiver cavity considered here is made of three different layers comprising an inner refractory lining, a middle insulating layer and an outer metal layer as illustrated in Fig. 2. Table 1 presents the details of the materials and the thermophysical properties employed here for mean temperature of >1000°C.

2.1. Solution methodology and input conditions

The iterative solution presented by Rafique et al. (2021) was

Table 2
Geometric and operational input parameters.

Parameter	Unit	Reference value	Sensitivity variations
r_{ap}/r_1	–	0.5	–
r_1	m	4.0	2–4
L/D_1	–	1.5	–
Δr_1	mm	100	50–200
Δr_2	mm	100	50–200
Δr_3	mm	10	–
$\dot{m}_p$	Kg/s	30	0–30
$\dot{m}_p/\dot{m}_a$	–	0.5	–
T_{amb}	°C	27	–
$T_{w,0}$	°C	27	27–800
$T_{p,in}$	°C	500	–
$T_{a,in}$	°C	500	–
$T_{w,start}$	°C	925	–
$T_{p,out,min}$	°C	800	–

employed to solve the coupled heat and mass transfer equations. The energy flows are balanced for each successive temporal input value of solar heat flux addressing the coupled local heat transfer coefficients, thermo-physical properties, and local wall temperature as temperature-dependent variables for each time step. The equations that account for convection, re-radiation and conduction, were solved iteratively using varying solar resource data for the values of parameters listed in Table 2. Here the thermal stresses, created by any change in temperature of a material (Sundén and Fu, 2016), were calculated as a function of the coefficient of thermal expansion, modulus of elasticity and temperature differential of cavity wall for each time step (Zabolotsky, 2011). The solution methodology was extended for various series of conditions to span start-up, turn down, and shut down periods. Each run represents a full day of receiver operation including the cavity cooling down period, overnight. The cavity wall temperature at the end of run 1 served as the input for run 2 in a given time-series, and so on.

A four-day time series of solar direct normal irradiance (DNI) with real time variability was selected from the Bureau of Meteorology (Bureau of Meteorology) at Learmonth, Australia to include both the lowest and highest vulnerability to the unscheduled reduction in input DNI.
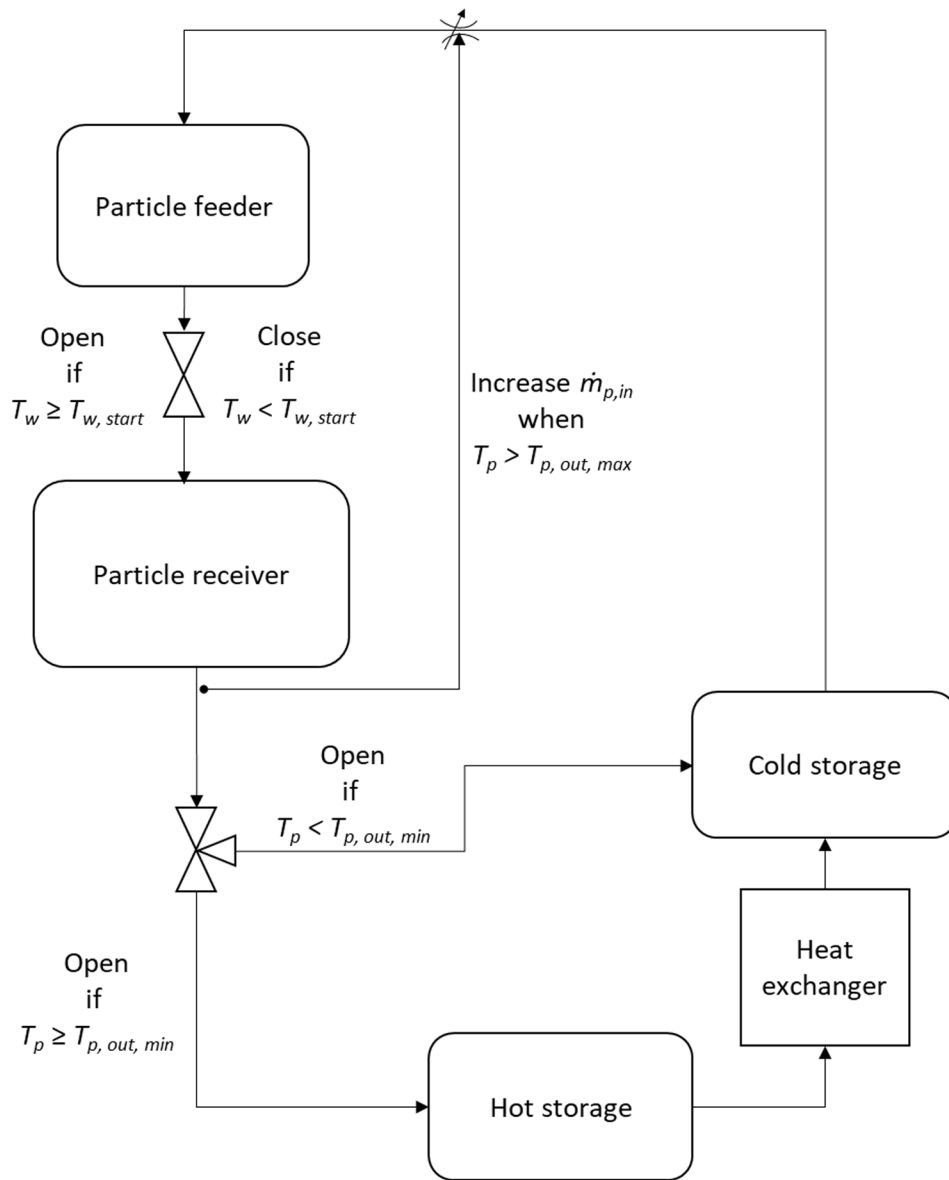
Fig. 3. Block diagram to demonstrate the control of particle feed.

This time-series includes solar DNI data with both smooth distribution (clear summer day) reaching a peak value of 1040 W/m² and with sharp fluctuations (cloudy day), which will help to better understand the thermal response of the refractory-lined solar receiver to transient

operation during different operating periods. Here a typical solar day begins at 06:00 h which corresponds to the start of the receiver operation. The solar flux (Q_{in}) at the receiver was calculated from the DNI, heliostat instantaneous efficiency and concentration ratio. The
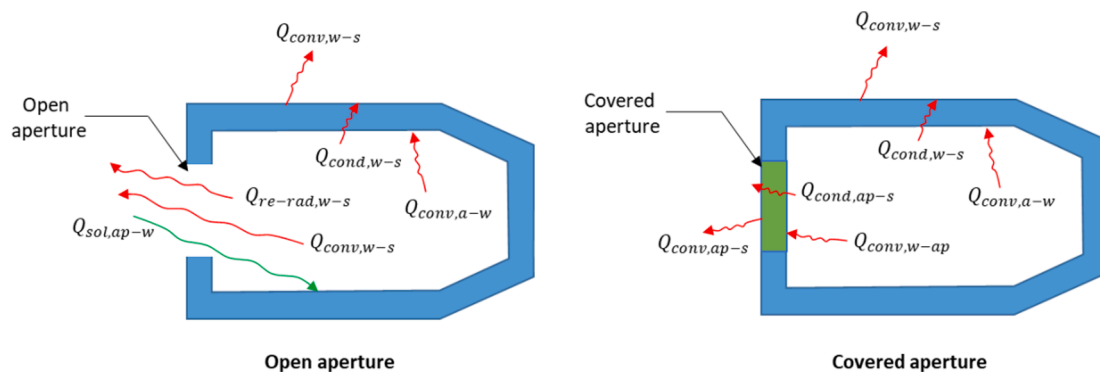
Fig. 4. A diagram of the main heat loss terms for the cavity receiver with an open and covered aperture. Subscripts: *sol* = solar, *conv* = convection, *cond* = conduction, *re-rad* = re-radiation, *ap-w* = aperture to wall, *w-s* = wall to surroundings, *w-ap* = wall to aperture, *a-w* = air to wall, *ap-s* = aperture to surroundings.
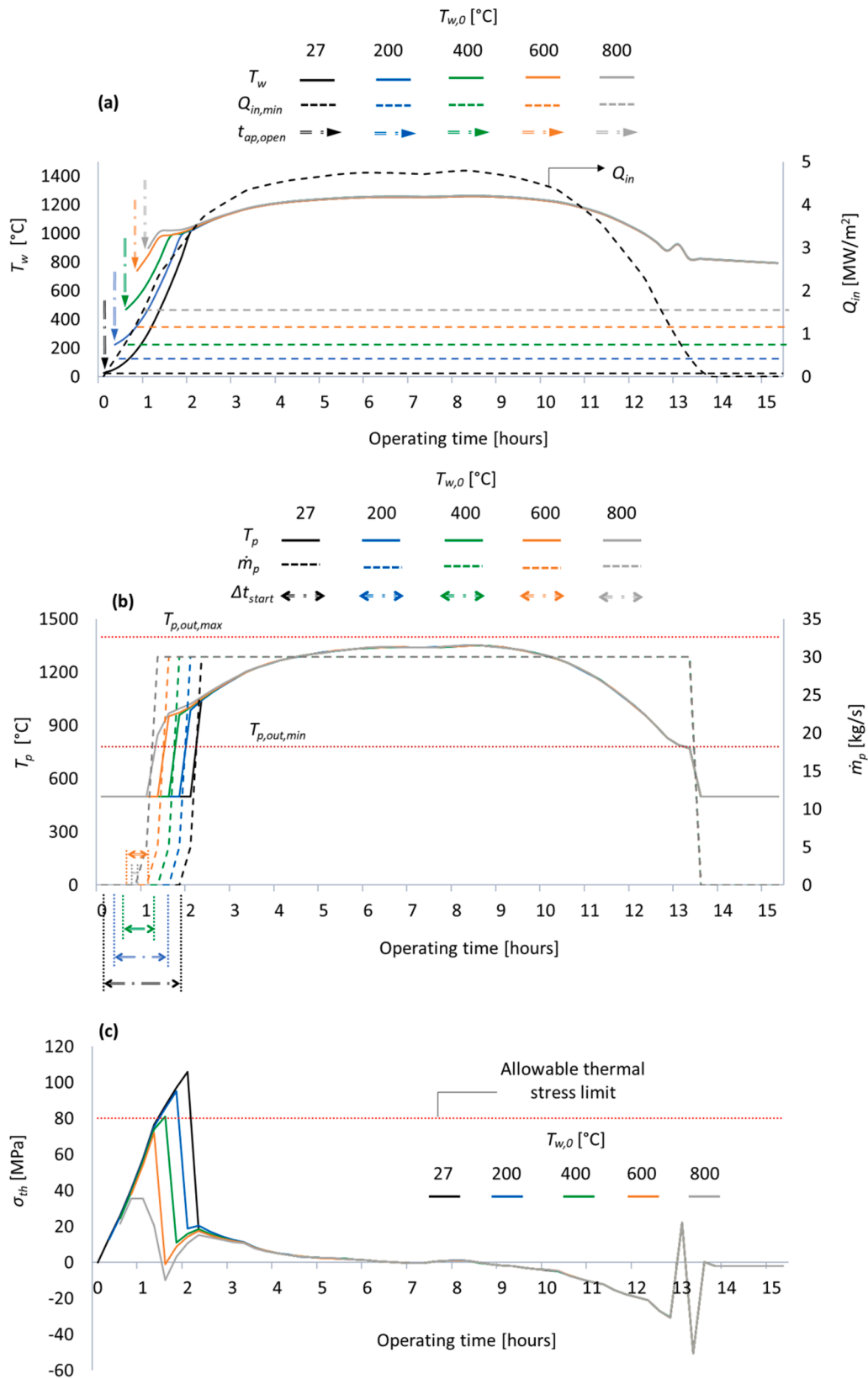
Fig. 5. The effect of the initial temperature on the calculated transient responses of (a) the internal temperature of cavity wall, T_w, (b) the outlet temperature of the particles, T_p, and (c) thermal stress of the wall, σ_{th}, for the variable solar input. See Table 2 for other reference conditions.
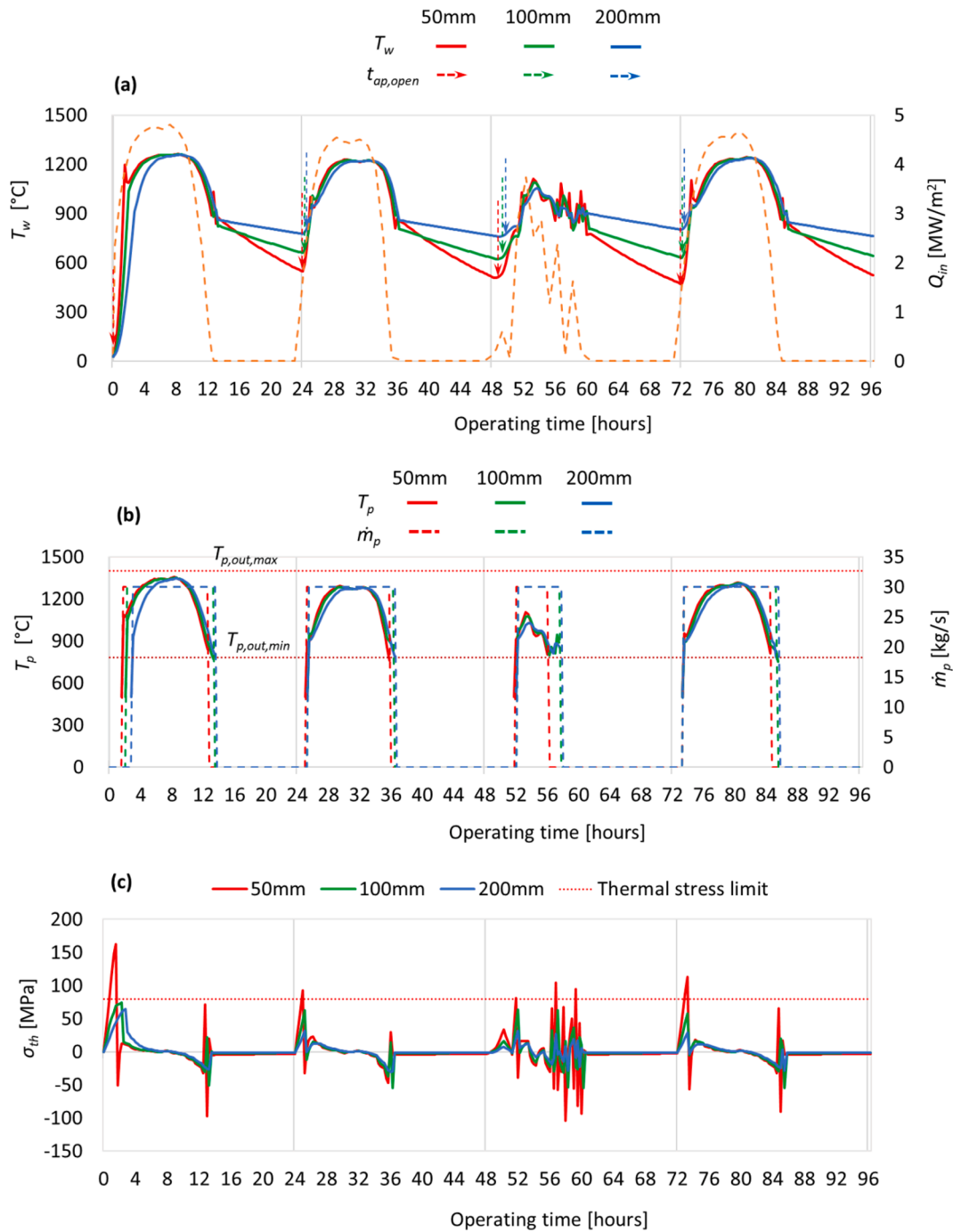
Fig. 6. The influence of the thickness of the inner refractory lining on the calculated time history of (a) the internal temperature of cavity wall, T_w, (b) the outlet temperature of the particles, T_p, and (c) thermal stress of the wall, σ_{th}, using the same solar time series. See Table 2 for other reference conditions.

instantaneous heliostat efficiency accounted for different losses, including cosine, reflection, attenuation, shading, blocking, and spillage. The cosine losses were calculated from the position of the sun for each DNI time-step using correlations reported previously (Duffie, 2013).

The control diagram for the strategy used to control particle temperature is shown in Fig. 3. The input solar radiation at the start of the solar day was firstly used to heat the receiver cavity walls to a set-point temperature, $T_{w,start} = 925\,°C$, without any flow of particles. For the next time-step at which $T_{w,start} \geq 925\,°C$, particles were fed into the receiver at the minimum flow-rate. A minimum acceptable outlet temperature of particles, $T_{p,out,min} = 800\,°C$, was set for them to be sent to the hot

storage unit. That is, particles were sent to the hot storage unit if $T_{p,out,min} \geq 800\,°C$, and to the cold storage unit if $T_{p,out,min} < 800\,°C$. The warm particles sent to the cold storage and returned hot air will increase the initial temperature of the particles. This temperature is expected to fall with time due to heat losses and a storage model is required to fully account for these losses. Here the focus is on the receiver only and the recirculated particles to the receiver were assumed to be preheated at $500\,°C$ for the present assessment.

The aperture cover was assumed to be made of the same insulating material as of the cavity walls and to be opened at the start of a receiver run when the solar flux to be sufficient for gains to overcome the losses, $Q_{in,min}$, that is, $Q_{in} > Q_{loss}$ causing a change in the slope of wall
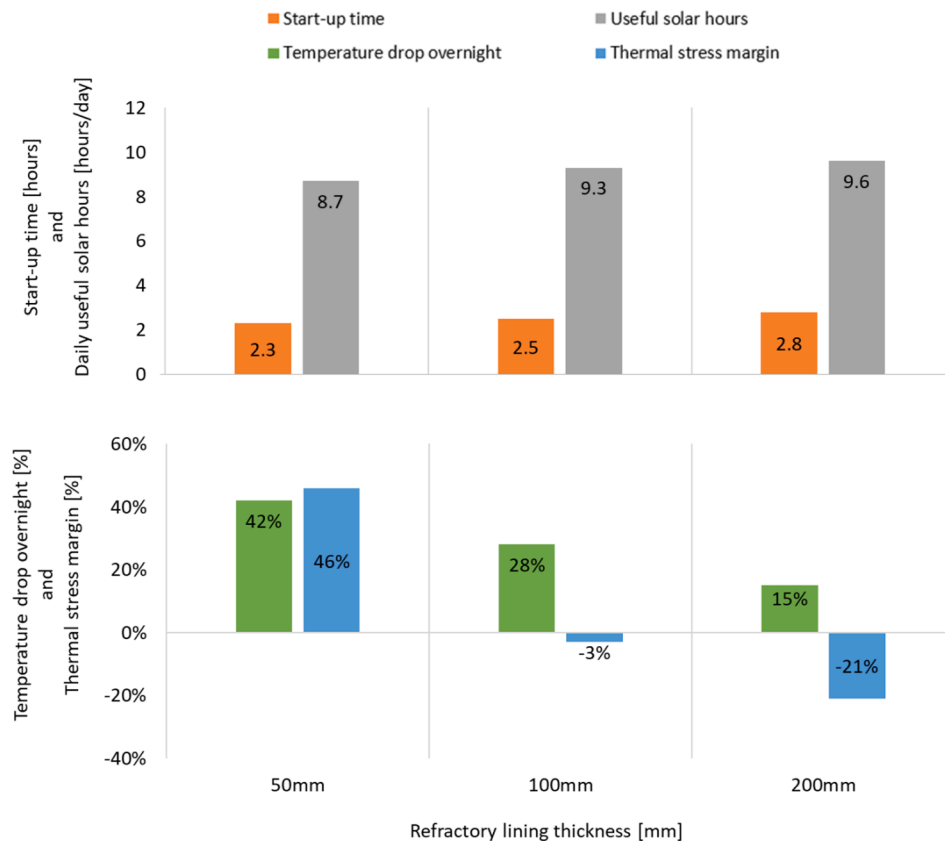
Fig. 7. The calculated average values of start-up time, useful daily solar hours, percentage drop in temperature overnight and thermal stress margin (where a negative indicates below the limit) for different inner refractory lining thicknesses. Other conditions are per Fig. 6.

temperature with time. Here the true start-up or pre-heat time, Δt_{start}, was defined as the difference between the time at which aperture opened, $t_{ap,open}$, and the start of particle feed, $t_{p,feed}$.

The heat loss mechanisms for the cases with an open and covered aperture are illustrated in Fig. 4. The receiver with an open aperture encounters conduction, convection, and re-radiation losses whereas, only conduction and convection from the wall to the surroundings occurs when the aperture is covered. A full description of each term and the heat transfer equations used to calculate them is presented previously (Rafique et al., 2021).

3. Results and discussion

3.1. Sensitivity to initial temperature of cavity internal wall

Fig. 5 presents the calculated results of the influence of the initial temperature of the cavity internal wall on the calculated transient temperatures and thermal stresses inside the receiver cavity for inner refractory lining thickness of 100 mm, for the clear summer day described in Section 2.1. Here the reference values of other geometric and operational parameters were employed, as shown in Table 2.

Fig. 5a presents the time history of the calculated inside wall temperature of the cavity, T_w, for a range of assumed initial temperatures, $T_{w,0}$, from 27 to 800 °C. It can be observed that the minimum threshold of concentrated solar flux needed for a positive change in the slope of wall temperature, T_w/t, is achieved at 0.1, 0.3, 0.4, 0.5, and 0.6 h for the cases with a value of $T_{w,0} = 27$, 200, 400, 600, and 800 °C, respectively. As expected, the calculated start-up time needed to heat the cavity internal wall to the set-point start-up temperature decreases with an increase in $T_{w,0}$. For example, 1.9 h are needed for the cavity wall to reach $T_{w,start} = 925$ °C, for a value of $T_{w,0} = 27$ °C, while this time is reduced by 26, 56, 74, and 84 % when the value of $T_{w,0}$ is increased to 200, 400,

600, and 800 °C, respectively. Furthermore, it can be observed from Fig. 5b that a minimum acceptable particle temperature, $T_{p,out,min}$, of 800 °C is achieved after 9 min from the start of particle feeding.

Fig. 5c presents the influence of $T_{w,0}$ on the calculated thermal stresses, σ_{th}. As expected, σ_{th} decreases with an increase in the value of $T_{w,0}$. The maximum σ_{th} is 106 MPa for $T_{w,0} = 27$ °C, which is above the allowable limit of 80 MPa for the refractory material. This reduces to $\sigma_{th} = 95$ MPa for $T_{w,0} = 200$ °C and to below the 80 MPa limit for $T_{w,0} \geq 400$ °C for the present conditions. This highlights the advantages of reducing heat losses overnight.

3.2. Influence of refractory lining thickness

Fig. 6 presents the calculated thermal response of the receiver during four successive days of operation for a range of inner refractory lining thicknesses varied from 50 to 200 mm. The reference values were employed for other parameters (Table 2). It can be observed that the magnitude of both the temperature drop overnight and the thermal stresses decrease with an increase in the refractory thickness, although the start-up time is also increased. For example, σ_{th} is calculated to range from −98 to 150 MPa and the overnight temperature drop $\Delta T_{w-n} = 340$ °C for a lining thickness of 50 mm. However, σ_{th} reduces by 48 % to only −51 to 78 MPa, while ΔT_{w-n} reduces by 35 % to 224 °C for a refractory thickness of 100 mm relative to the 50 mm case. Also, a refractory thickness of 100 mm only increases start-up time by 8 % and is calculated to give 6 % more useful daily solar hours than the 50 mm case. This is due to the compensating advantage offered by higher thermal mass refractory as the solar resource falls. These results show the value of optimizing refractory thickness.

Fig. 7 compares the calculated values of average start-up time, useful daily solar hours, the percentage drop in ΔT_{w-n} and thermal stress margin for different values of inner refractory lining thicknesses under the same
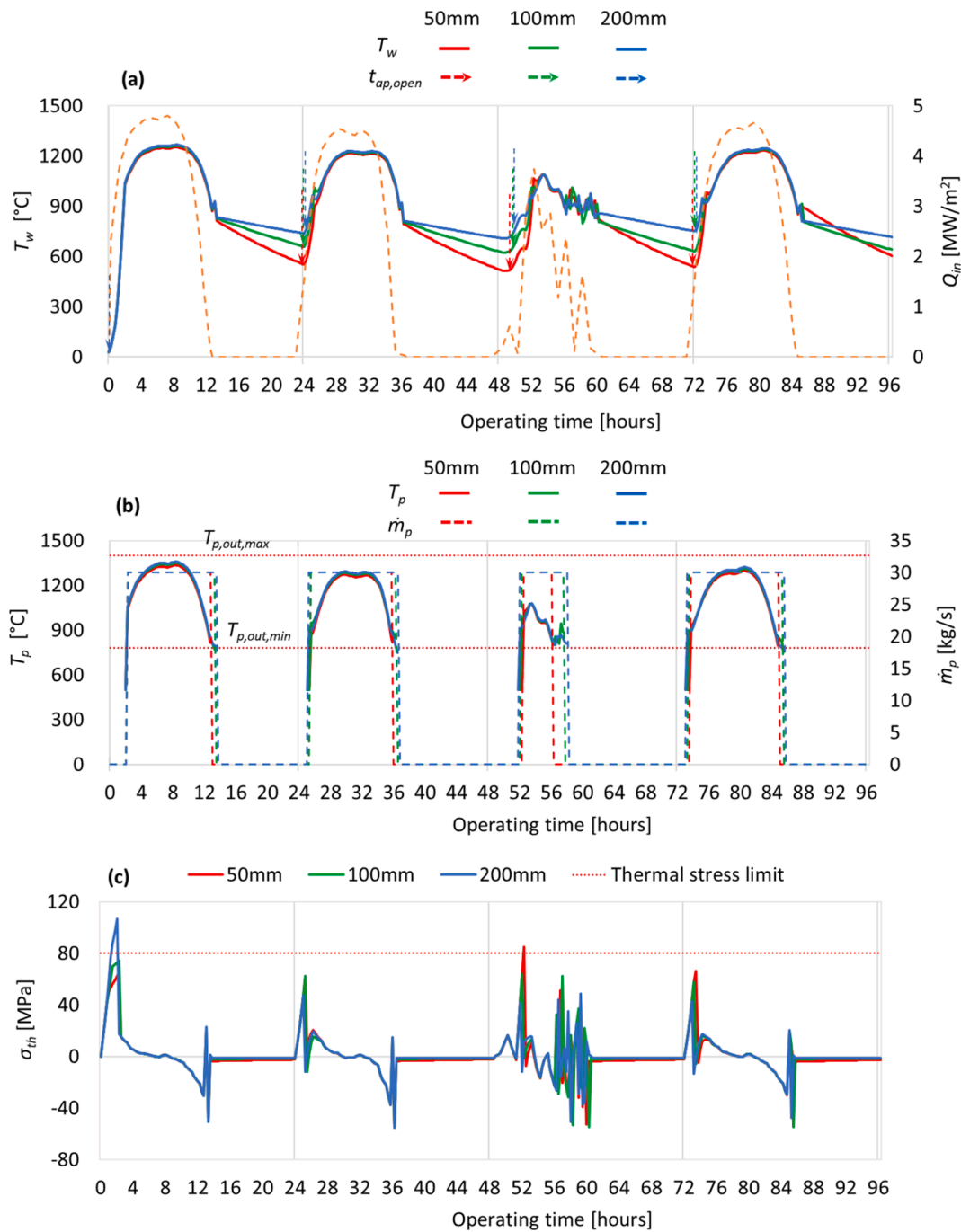
Fig. 8. The influence of the thickness of the insulation layer on the calculated time history of (a) the internal temperature of cavity wall, T_w, (b) the outlet temperature of the particles, T_p, and (c) thermal stress of the wall, σ_{th}, using the same solar time series. See Table 2 for other reference conditions.

conditions as of Fig. 6. Here a positive value of thermal stress margin corresponds to a value above the allowable limit whereas, a negative value corresponds to a value below the allowable limit, which is desirable.

It can be seen that a refractory lining thickness of 50 mm is estimated to lead to thermal stresses that are above the allowable limit by a margin of 46 %. However, an increase in the lining thickness to 100 and 200 mm is sufficient to reduce these to below the maximum allowable limit by a margin of 3 and 21 %, respectively. The overnight temperature is estimated to fall by 42 % for a receiver with a lining thickness of 50 mm. However, this reduces to 28 % and 15 %, respectively, for a lining thickness of 100 and 200 mm. For the conditions assessed here, the average start-up time for a refractory thickness of 50, 100, and 200 mm

is calculated to be 2.3, 2.5, and 2.8 h, while the corresponding useful daily solar hours are 8.7, 9.3, and 9.6 h/day, respectively.

3.3. Influence of insulation thickness

Fig. 8 presents the calculated time history of temperatures and thermal stresses during four successive days of operation for a range of thicknesses of the insulating layer from 50 to 200 mm using the same solar time series and using a refractory thickness of 100 mm. It can be seen that increasing the thickness of the insulation reduces the thermal losses overnight and the start-up time but increases the thermal stresses on the refractory inside. An insulation thickness of 200 mm is calculated to give lower temperature drops overnight and start-up time by a margin
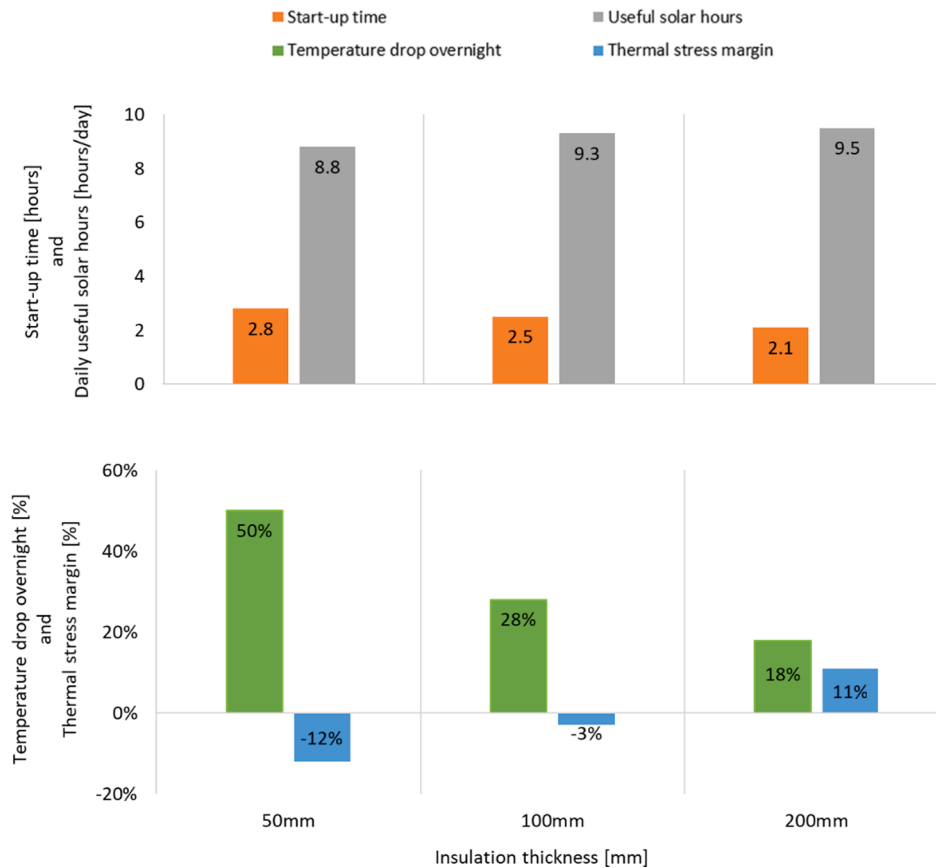
Fig. 9. The calculated average values of start-up time, useful daily solar hours, percentage drop in temperature overnight and thermal stress margin for different insulation thicknesses. Other conditions are per Fig. 8.

of 64 and 25 %, respectively relative to a receiver with an insulation thickness of 50 mm. However, this case causes the thermal stresses to exceed the allowable limit by 11 %.

Fig. 9 compares the calculated values of average start-up time, useful daily solar hours, the percentage drop in temperature overnight and thermal stress margin for different insulation thicknesses using the same conditions as of Fig. 8. The increase in insulation thickness helps to maintain the receiver cavity at a higher temperature with 50, 28, and 18 % drop in temperature overnight for 50, 100, and 200 mm, respectively. For an inner refractory thickness of 50 mm, start-up time of 2.8, 2.5, and 2.1 h are observed for insulation thicknesses of 50, 100, and 200 mm, respectively. The same thicknesses of insulation are calculated to give useful solar hours of 8.8, 9.3, and 9.5 h/day, respectively.

3.4. Influence of geometric scale

Fig. 10 presents the influence of geometric scale of the receiver on its thermal response. The calculated temperature of the cavity inside wall and thermal stresses are assessed for a range of values of inner diameter varied from 4 to 8 m, with the same radiation flux through the aperture. Here the ratios of other geometric parameters including aperture radius, receiver length, refractory, and insulation thickness were fixed and varied with the cavity's inner diameter. It can be observed that both the heat losses overnight and the thermal stresses reduce as the receiver is scaled up. For example, the predicted overnight temperature drop decreases by 36 and 57 % as the receiver is scaled up from 4 m to 6 and 8 m, respectively. The reduction in heat losses is due to the reduction of surface area to volume ratio with an increase in scale. However, this trend is non-linear, with an indication of a critical size needed to avoid significant temperature loss overnight. The impact on thermal stresses is also significant, with a decrease by 43 and 61 % with the same increase

in receiver diameter. These results highlight the advantages of upscaling the receiver on both stress and heat losses, although further assessment on the optical constraints of a heliostat field as a function of the scale of a receiver is required.

3.5. The case with no-refractory

Fig. 11 presents the thermal response of a receiver without a refractory for the same operating conditions as employed in Fig. 7. The material selected for this analysis was a metal alloy shell (Inconel (Shokrani et al., 2012)) of 15 mm thickness with no refractory layer. It can be seen that, the useful daily solar hours are only about 7.6 h, which correspond to a reduction by 16, 21 and 23 % relative to an inner refractory thickness of 50, 100, and 200 mm, respectively, given that the mass flow-rate of particles and minimum threshold temperature is the same for all cases. This is because of the greater heat losses that occur without the use of insulating and refractory layers. The use of refractory is expected to be more beneficial when annual solar variability is considered, due to it's potential to minimize the influence of solar transients and to reduce the overnight heat losses.

These calculated results indicate the advantage of refractory use in industrial-scale particle receivers which must be optimised for a range of competing influences. On the one hand, using a refractory lining allows the use of lower-cost materials (Rafique et al., 2021) along with more energy harvesting potential during the available solar day while, on the other hand it is more challenging to manage (Gregurek et al., 2020).

4. Conclusions

In conclusion, further evidence is provided of the potential to carefully size a refractory lining in high-temperature solar thermal receivers
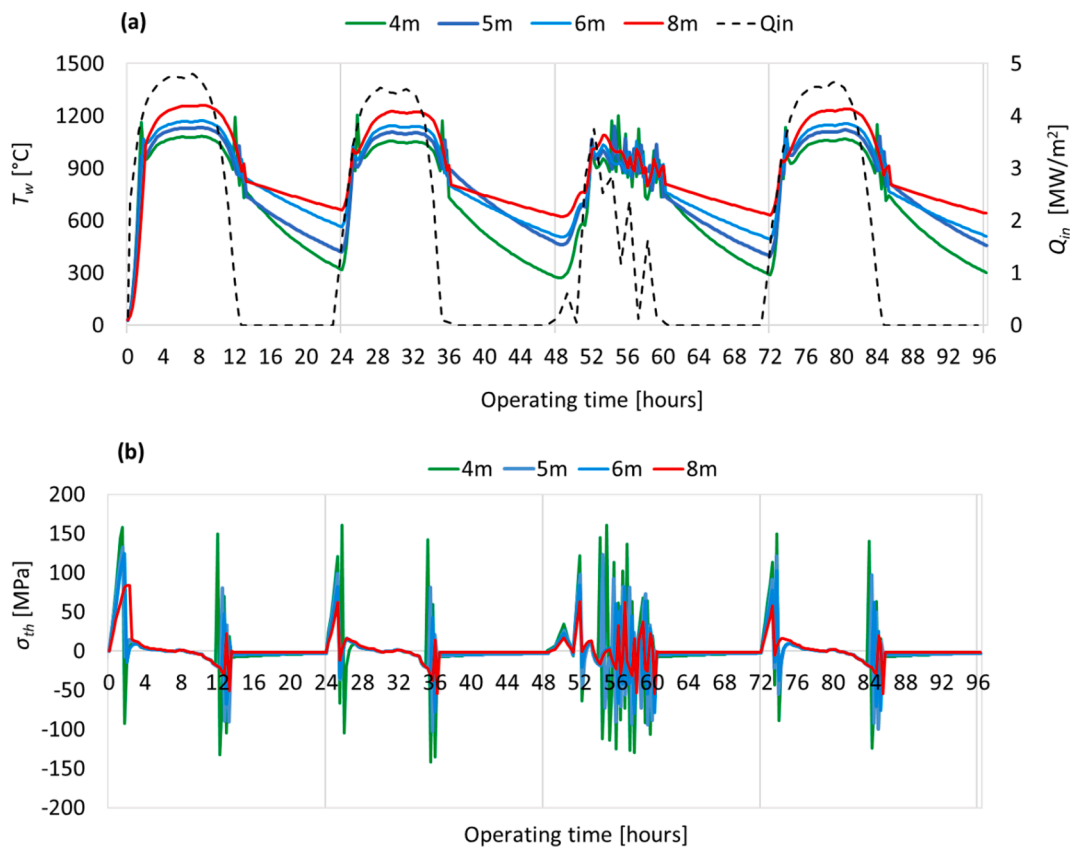
Fig. 10. The dependence of (a) the internal temperature of cavity wall, T_w, and (b) thermal stress of the wall, σ_{th}, on time for a series of receivers of various characteristic diameters. See Table 2 for other reference conditions.
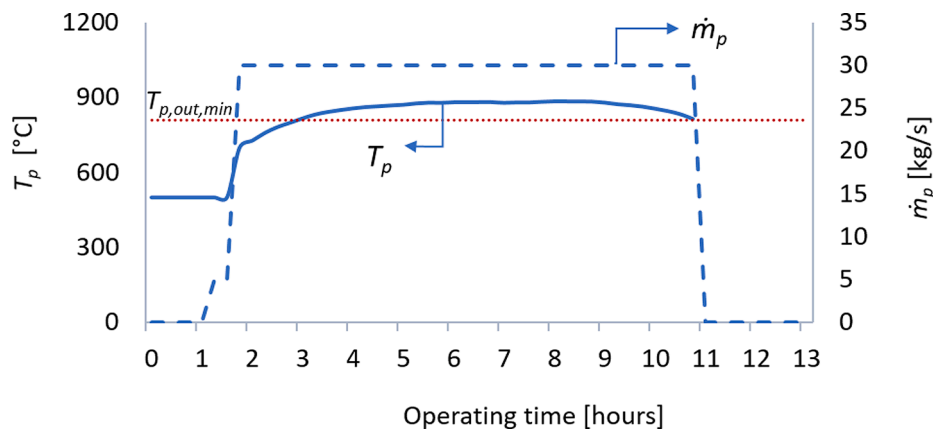

Fig. 11. The transient responses of a receiver cavity made of high-temperature Inconel shell with no refractory on a clear sky day, showing the outlet temperature of the particles, T_p. Other conditions are per Fig. 7.

to manage both heat losses and thermal stresses. In particular, it was found that it is possible to achieve a configuration for which the temperature drop overnight is only about 28 % of the operating temperature by both covering the aperture overnight and achieving sufficient geometric scale. In addition to the reduction in heat losses, this also reduces the thermal stresses and start-up time. For example, the combination of a cavity diameter of 8 m, a 100 mm thick refractory lining and a 100 mm thick insulation was found to achieve an operating solar day that is 21 % greater than that for the un-lined case, for the case with a minimum acceptable outlet particle temperature of 800 °C for this 4-day time series. The benefits of upscaling are significant, with the predicted overnight temperature drop and thermal stresses calculated to decrease by

57 and 61 %, respectively, as the receiver is scaled up from 4 to 8 m. The use of refractory also allows the use of lower-cost steels and extends the life of the receiver.

The thickness of the refractory lining should be optimized to be sufficiently thick to minimize temperature drop overnight and lower the thermal stresses, while being sufficiently thin to avoid excessive start-up time. However, some increase in thickness can also increase the useful solar hours by providing radiation even after the solar flux falls to below levels needed to maintain particle temperature alone. For example, the thermal stresses and overnight temperature drop for the reference case were calculated to decrease by 48 and 35 %, respectively, for a receiver with a lining thickness of 100 mm relative to a thickness of 50 mm. This

increase also caused an 6 % increase in useful daily solar hours despite a longer start-up time. Overall, for the cases assessed here, the optimum thickness was typically between 100 and 200 mm.

The thickness of the insulation should be optimized to reduce the thermal losses overnight and increase the useful operating hours, while preventing too much increase to the thermal stresses of the refractory layer. For the reference case with the inner refractory thickness of 100 mm and cavity diameter of 8 m, an insulation thickness of 200 mm was calculated to be reasonable, providing a lower temperature drop overnight by 64 % along with 8 % more useful daily solar hours relative to an insulation thickness of 50 mm.

Declaration of Competing Interest

The authors declare that they have no known competing financial interests or personal relationships that could have appeared to influence the work reported in this paper.

Acknowledgements

References

Abanades, S., Charvin, P., Flamant, G., 2007. Design and simulation of a solar chemical reactor for the thermal reduction of metal oxides: Case study of zinc oxide dissociation. Chem. Eng. Sci. 62 (22), 6323–6333.

Bureau of Meteorology *http://www.bom.gov.au/climate/glossary/seasons.shtml.* (accessed 04 October).

CET *https://www.adelaide.edu.au/cet/technologies/solar-expanding-vortex-particle-receiver-reactor-sevr.*

Callister, W., Rethwisch, D., 2018. Materials science and engineering: an introduction, 8th. Wiley, New York.

Charde, N., 2013. Microstructure and fatigue properties of dissimilar spot welded joints of AISI 304 and AISI 1008. International Journal of Automotive and Mechanical Engineering (7), 882.

Chinnici, A., Arjomandi, M., Tian, Z.F., Lu, Z., Nathan, G.J., 2015. A Novel Solar Expanding-Vortex Particle Reactor: Influence of Vortex Structure on Particle Residence Times and Trajectories. Sol. Energy 122, 58–75.

Dana, K., Sinhamahapatra, S., Tripathi, H.S., Ghosh, A., 2014. Refractories of alumina-silica system. Trans. Indian Ceram. Soc. 73 (1), 1–13.

Davis, D., Jafarian, M., Chinnici, A., Saw, W.L., Nathan, G.J., 2019. Thermal performance of vortex-based solar particle receivers for sensible heating,". Sol. Energy 177, 163–177.

Duffie JAa, 2013. Solar engineering of thermal processes. Wiley.

Ebert, M., Amsbeck, L., Rheinländer, J., et al., 2019. Operational experience of a centrifugal particle receiver prototype. AIP Conf. Proc. 2126 (1), 030018.

Flamant, G., 1982. Theoretical and experimental-study of radiant-heat transfer in a solar fluidized-bed receiver. AIChE J. 28, 529–535.

Gobereit, B., Amsbeck, L., Buck, R., Pitz-Paal, R., Röger, M., Müller-Steinhagen, H., 2015. Assessment of a falling solid particle receiver with numerical simulation. Sol. Energy 115, 505–517.

Gregurek, D., Reinharter, K., Schmidl, J., et al., 2020. Refractory Challenges in Lead and Zinc Furnaces. Springer International Publishing, Cham, pp. 19–30.

Heindl, R.A., Pendergast, W.L., 1937. Deformation and Young's Modulus of Fire-Clay Brick in Flexure at 1220° C. J. Res. Natl. Bur. Stand. (US) 19 (3), 353–366.

Ho, C.K., 2016. A review of high-temperature particle receivers for concentrating solar power. Appl. Therm. Eng. 109, 958–969.

Ho, C., Christian, J., Gill, D., Moya, A., Jeter, S., Abdel-Khalik, S., Sadowski, D., Siegel, N., Al-Ansary, H., Amsbeck, L., Gobereit, B., Buck, R., 2014. Technology Advancements for Next Generation Falling Particle Receivers. Energy Procedia 49, 398–407.

Ho, CK, J.M. Christian, J. Yellowhair, K. Armijo, S. Jeter, 2016. Performance Evaluation of a high-temperature falling particle receiver. ASME Power & Energy Conference, June 26–30, 2016, Charlotte, NC.

Ho, C.K., Iverson, B.D., 2014. Review of high-temperature central receiver designs for concentrating solar power. Renew. Sustain. Energy Rev. 29, 835–846.

Liu, X., Liu, W., 2003. Apparatus for growing monocrystalline group II-VI and III-V compounds. U.S. Patent Application No. 10/097,844.

Merchán, R.P., Santos, M.J., Medina, A., Calvo Hernández, A., 2022. High temperature central tower plants for concentrated solar power: 2021 overview. Renew. Sustain. Energy Rev. 155, 111828. https://doi.org/10.1016/j.rser.2021.111828.

Ortiz, O.A., Suárez, G.I., Nelson, A., 2005. Dynamic simulation of a pilot rotary kiln for charcoal activation. Comput. Chem. Eng. 29 (8), 1837–1848.

Rafique, M.M., Nathan, G., Saw, W., 2021. A mathematical model to assess the influence of transients on a refractory-lined solar receiver. Renewable Energy 167, 217–235.

Shokrani, Dhokia, V., Newman, S.T., Imani-Asrai, R., 2012. An Initial Study of the Effect of Using Liquid Nitrogen Coolant on the Surface Roughness of Inconel 718 Nickel-Based Alloy in CNC Milling. Procedia CIRP 3, 121–125.

Soo Too, Y.C., García, J., Padilla, R.V., Kim, J.-S., Sanjuan, M., 2019. A transient optical-thermal model with dynamic matrix controller for solar central receivers. Appl. Therm. Eng. 154, 686–698.

Sundén, B., Fu, J., 2016. Heat Transfer in Aerospace Applications. Academic Press.

Tan, T., Chen, Y., 2010. Review of study on solid particle solar receivers. Renew. Sustain. Energy Rev. 14 (1), 265–276.

Wu, W., Amsbeck, L., Buck, R., Uhlig, R., Ritz-Paal, R., 2014. Proof of Concept Test of a Centrifugal Particle Receiver. Energy Procedia 49, 560–568.

Zabolotsky, A.V., 2011. Thermal stress modeling for radiation heating of refractory ceramics. Proceedings of the 10th WSEAS International Conference on Heat Transfer.

Refractory ceramic fibre, 2022. https://thermo-fb.com/ceramic-fibre [accessed June 2021].

CHAPTER 5

MODELLED ANNUAL THERMAL PERFORMANCE OF A 50MW$_{th}$ REFRACTORY-LINED PARTICLE-LADEN SOLAR RECEIVER OPERATING ABOVE 1000°C

Statement of Authorship

Title of Paper	Modelled annual thermal performance of a 50MW$_{th}$ refractory-lined particle-laden solar receiver operating above 1000°C
Publication Status	☑ Published ☐ Accepted for Publication ☐ Submitted for Publication ☐ Unpublished and Unsubmitted work written in manuscript style
Publication Details	Rafique MM, Nathan G, Saw W. (2022) Modelled annual thermal performance of a 50MWth refractory-lined particle-laden solar receiver operating above 1000°C. Renewable Energy. 197: 1081-1093. https://doi.org/10.1016/j.renene.2022.07.111

Principal Author

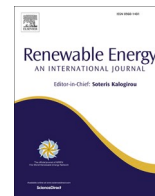| Name of Principal Author (Candidate)	Muhammad Mujahid RAFIQUE		
Contribution to the Paper	Performed the literature review and identified the potential gaps. Jointly defined the scope and aims of the paper. Jointly performed analysis, interpreted data, wrote the manuscript, and acted as corresponding author.		
Overall percentage (%)	60%		
Certification:	This paper reports on original research I conducted during the period of my Higher Degree by Research candidature and is not subject to any obligations or contractual agreements with a third party that would constrain its inclusion in this thesis. I am the primary author of this paper.		
Signature		Date	25/08/2022

Co-Author Contributions

By signing the Statement of Authorship, each author certifies that:

    i.   the candidate's stated contribution to the publication is accurate (as detailed above);

    ii.   permission is granted for the candidate in include the publication in the thesis; and

    iii.   the sum of all co-author contributions is equal to 100% less the candidate's stated contribution.

Name of Co-Author	Prof. Graham Nathan		
Contribution to the Paper	Supervised the work. Jointly defined the scope and aims of the paper. Jointly performed analysis and interpreted data. Critically reviewed the manuscript. Helped to improve the language, structure, and content of the manuscript.		
Signature		Date	15/9/2022

Name of Co-Author	Dr. Woei Saw		
Contribution to the Paper	Supervised the work. Jointly defined the scope and aims of the paper. Jointly performed analysis and interpreted data. Critically reviewed the manuscript. Helped to improve the language, structure, and content of the manuscript.		
Signature		Date	15/09/2022

Modelled annual thermal performance of a 50MW$_{\text{th}}$ refractory-lined particle-laden solar receiver operating above 1000°C

Muhammad M. Rafique [a,b,*], Graham Nathan [a,b], Woei Saw [a,c]

[a] Centre for Energy Technology, The University of Adelaide, SA, 5005, Australia
[b] School of Mechanical Engineering, The University of Adelaide, SA, 5005, Australia
[c] School of Chemical Engineering and Advanced Materials, The University of Adelaide, SA, 5005, Australia

ARTICLE INFO

ABSTRACT

The paper reports on the thermal performance of the sub-system for a solar thermal particle technology used to generate high temperature air, including refractory-lined particle-laden receiver, particle separator, particle storage and particle feeder. These assessments are made with a transient mathematical model developed to calculate the heat and mass transfer within the cavity of the receiver together with the thermal losses to the surroundings, incorporating the influence of solar transients during start-up, turndown or shutdown periods. New insights are provided of the influences of the variables of refractory configuration and of the potential operating controller parameters to manage the influence of solar variability on the annual thermal performance of the system, considering the useful thermal gain of hot air. The model is further used to advance the understanding of the sensitivity of the thermal performance to the mass flow rate of inlet air and mass loading of particles in the receiver on the sensible energy harnessed. The influence of the returned air temperature on the receiver thermal performance is also assessed, to provide insights on the suitability of the present configuration to re-heat already hot air in a CST system. Further to this, the thermal outputs are compared with available CFD data for this configuration, and with that reported for a cavity reactor, to provide information on the model validation.

1. Introduction

Concentrated solar thermal, CST, technologies are considered a potential alternative source of heat to fossil fuels for applications at a range of temperatures up to approximately 1000 °C [1,2]. However, further advancements are required to enable the deployment of CST technologies into energy-intensive industrial processes requiring high temperatures such as the calcination step in the alumina Bayer process, which requires a temperature of about 1000 °C [3,4]. Most commercially available CST technologies employ molten salts as heat transfer fluid, HTF [5]. Despite their advantages, this limits the use of CST to below 600 °C [6], preventing their practical integration into processes requiring temperatures above this. Particle based receivers are a promising class of technology for going to temperatures above 1000 °C [5,7–13]. However, the use of particles as the primary heat transfer medium, brings a range of technical challenges in particle handling and heat transfer, while also being a potential risk for occupational health and safety, together with environmental pollution [14], in the event of

particles egress from the receiver to the surroundings. The use of air as the HTF offers several potential benefits such as being safe, inexpensive and much easier to transport than particles, although this comes with the penalty of inferior heat transfer properties i.e., low heat capacity relative to other HTFs. New insights are therefore required about potential opportunities to enhance the useful thermal gain of air receivers. One of these potential opportunities is to transport particles in suspension within an air stream to increase the adsorption of radiation by the air. The temperatures above 1000 °C also require the use of refractory linings. Control strategies are also needed to manage transient operating conditions. This study aims to address these needs by modelling and investigating the thermal performance of a high temperature refractory-lined particle-laden solar receiver system to supply hot air to a downstream system.

While various configurations of high temperature central receiver have been studied [5,15–17], no efficient industrial scale air receiver operating above 1000 °C has been identified as being well suited to practical integration to heavy industrial processes. One class of air

---

receivers that have been widely reported previously in pursuit of high temperatures employs a cavity comprising a porous structure directly exposed to the concentrated solar radiations, termed a volumetric air receiver [1,18,19]. Some of the previous investigations of volumetric receivers, including Hoffschmidt et al. [20], Buck et al. [21], Patil et al. [1], and Pritzkow [22], have reported thermal efficiencies in the range of 69–71% with operating temperatures of 815–1133 °C. A summary of these receivers has been provided previously by Ho and Iverson [23], and Ávila-Marín [24]. The particle-driven solar receivers including particle-in-tube, rotary/centrifugal particle [8,9,25,26], falling particle [27–29], and fluidized bed [30–34] have also indicated their potential to achieve temperatures of >750 °C, which were summarized previously [16,35]. Table 1 provides a summary of their reported operating temperatures and thermal efficiency. Although these particle receivers have proven to achieve temperatures of around 1000 °C, there is a lack of available data of their industrial level system performance and suitability to re-heat returned warm air from a thermal storage system. The Solar Expanding Vortex Receiver, SEVR [36,37], is another configuration of cavity receiver that has the potential to provide high output temperature for different industrial applications offering the possibility of operating the device windowless, which would offer significant practical advantages [38]. However, there is a lack of knowledge of the performance of a system configured to provide hot air from the SEVR system, considering the influence of the time-constants of these various components in response to a long time-series of solar resource variability. This can be done experimentally, but this would be more expensive and time consuming. Therefore, simplified models with the potential of system integration are needed to provide further information of the thermal performance of new and existing designs of high-temperature receivers to supply hot air at temperatures of order 1000 °C or above to heavy industrial processes. The present work aims to fill this gap by reporting an approach which can be incorporated into a system model to assess different receiver types, and to assist in identifying which type of receiver is best suited to which application.

Although the literature indicates the advantage of refractory use in high temperature receivers to minimize the influence of solar transients and to reduce the heat losses from the receiver cavity [40,41]. No information is available of its relative significance when the interaction between multiple components in an industrial-scale solar thermal system is considered. This requires a comparative annual assessment of different inner refractory lining thicknesses relative to the case of no refractory using variable solar input for a whole year. Furthermore, previous assessments of a stand-alone refractory-lined SEVR found that controlling the mass inflow and aperture cover are sufficiently good to improve the receiver thermal response to short term solar transients [40]. However, little is known of the influences of these controls on the annual thermal performance of a directly irradiated refractory-lined high temperature receiver operating in a system to provide hot air, during transient operation over longer periods accounting for start-up, turndown, and shutdown periods. Therefore, another aim of the paper is to understand the relative significance of refractory use and of these operating controls on the thermal performance of SEVR, when operating in a solar thermal system to provide hot air during transient operation.

The use of solid particle suspensions within an air stream has the

potential to increase the effectiveness of the heat transfer mechanisms within the receiver cavity due to their high surface area per unit mass and capacity for direct absorption of concentrated solar radiations [42]. However, the quantitative benefit of the particle loading in the receiver is still unknown. This requires further investigation on the influence of particles' addition on the annual thermal gain of the primary HTF, for different values of particle mass loadings. Further to this, it is important to assess the sensitivity of the receiver's thermal performance to the temperature and mass flow rate of inlet air. This will help to find out whether there is a critical value of these parameters, for any given conditions. Hence this paper further aims to address these research gaps.

Considering the aforementioned needs, the overall objective of the present paper is to advance the understanding of the annual thermal performance of a multi-layered refractory-lined high temperature air receiver, with and without particles, in response to solar resource variability. More specifically, the first aim is to calculate and compare the trends in the output temperature of hot air, annual useful thermal gain and thermal efficiency of the receiver system operating with the mass flow and aperture cover controllers either on or off. The second aim is to calculate the impact of the thicknesses of the inner refractory lining on the annual thermal performance of a high temperature receiver. The third aim is to assess the trends in the annual thermal performance of the system as a function of the particle loading and inlet mass flow rate of the air. The fourth aim is to provide a quantitative understanding of the sensitivity of the receiver thermal performance to the temperature of the inlet air and particles.

2. Methodology

Fig. 1 presents a schematic diagram of the system that is well suited to deliver reheated air to temperatures of greater than 1000 °C in combination with a thermal storage system. The system is divided into five main parts: a heliostat field, a refractory-lined particle-laden cavity receiver, a cyclone separator, a sensible thermal storage device, and an industrial process. Here, we analyse only the receiver sub-system, which comprises a receiver, a cyclone and a particle feeder. The receiver chosen for this study is a cylindrical cavity, which is similar to many other cylindrical cavities (e.g. the DLR centrifugal receiver [43]), but has the specific details of the Solar Expanding Vortex Receiver (SEVR) patented by the University of Adelaide [36,37]. The details of SEVR fabrication and flow features are presented previously [37,44,45]. This novel configuration has a modified geometry, with the introduction of a conical section. The particle-laden flow exits in the direction which is radial to the axis of the receiver cavity. The SEVR operates at atmospheric pressure, which allows its windowless operation. To maintain the atmospheric pressure in the receiver when integrated with a thermal storage, the CST side and process sides are operated as two separate cycles – that is, charging and discharging as illustrated in Fig. 1. To keep the charging and discharging cycle separate, the warm air from the thermal storage is not directly sent back to the receiver rather it is used to preheat the ambient air in a heat exchanger. This allows the operation of a windowless receiver at atmospheric pressure. It also allows the system to operate with only low temperature, <300 °C, air blowers. A brief description of the receiver sub-systems is provided below:

- Central receiver: a multilayered refractory-lined SEVR as shown in Fig. 2. The receiver cavity comprises three layers, an inner ceramic refractory lining of fireclay, a middle layer of high-temperature insulation, and an outer protective steel shell.
- Cyclone separator: a centrifugal device that provides cleaned hot air by removing the majority of the particulate matter from the particle-laden flow leaving the receiver. Hot air at a lower temperature is returned from the thermal storage and mixed with hot particles from the cyclone to recover heat before being fed back to the receiver.
- Particle feeder: this mixes the hot particles from the cyclone with the return air from the thermal storage, and then feeds them to the

Table 1
An overview of different types of high temperature solar receivers.

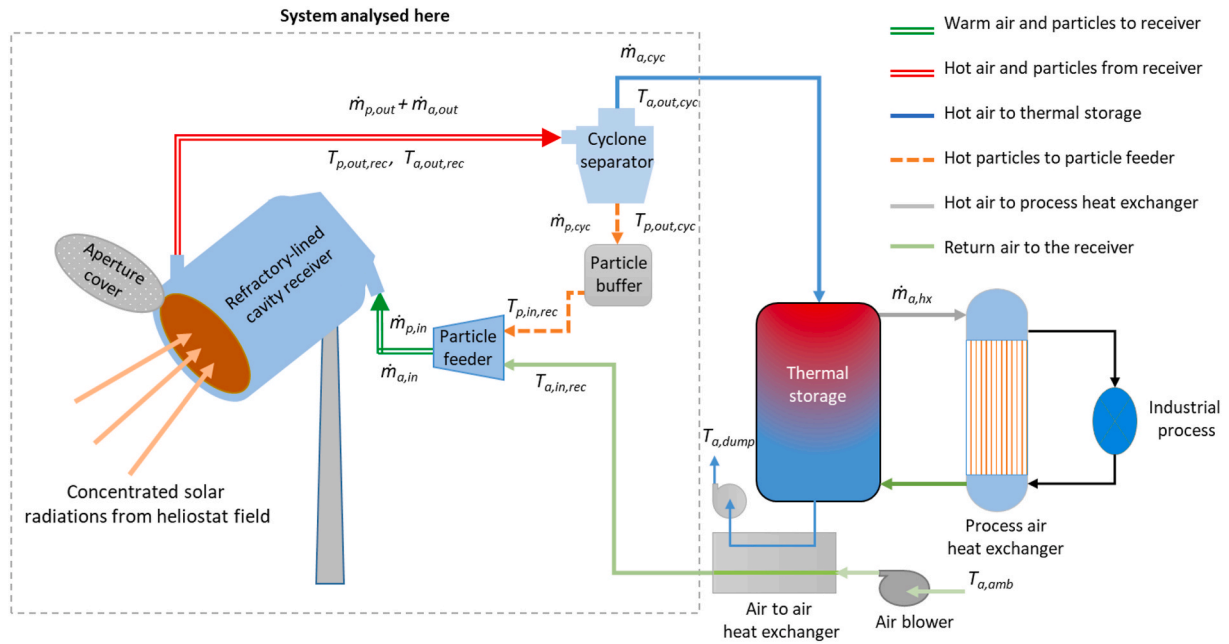| Receiver type	Operating temperature	Thermal efficiency	References
Volumetric air receiver	650–1133 °C	69–71%	[1,20–22,24, 39]
Rotary/centrifugal particle receiver	900 °C	75%	[8,9,25,26]
Falling particle receiver	>800 °C	up to 80%	[27–29]
Fluidized flow in tubes particle receiver	>750 °C	–	[30–32]

Fig. 1. Schematic diagram of the high temperature CST system components with the key terminology, with air as the heat transfer fluid and suspended particles in the receiver to augment heat transfer. The dashed line identifies the sub-system analysed here, comprising the receiver, cyclone and particle feeder.
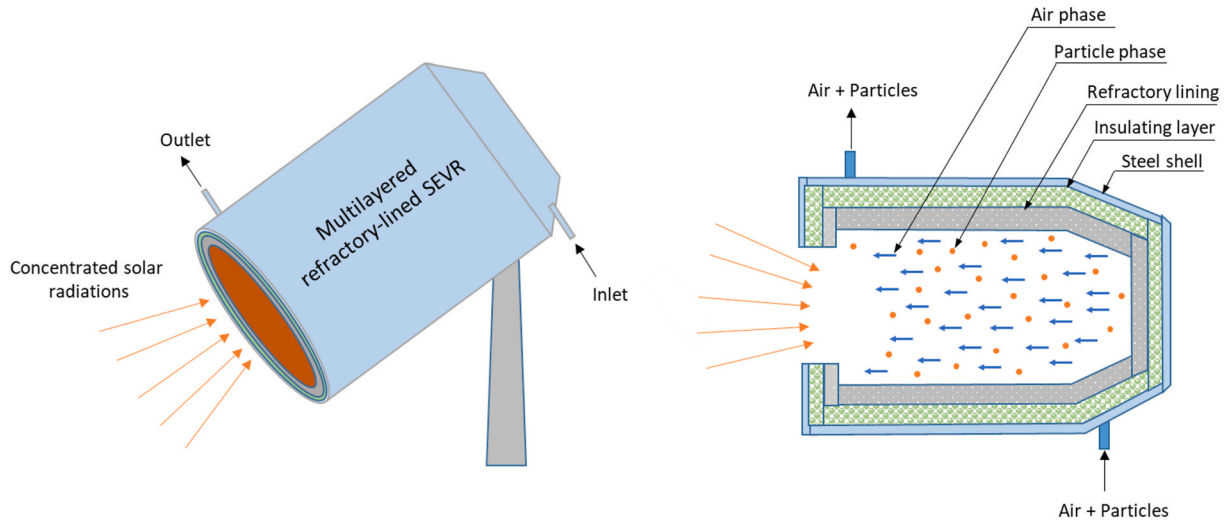

Fig. 2. A schematic diagram and the notation used to describe the multi-layered cavity Solar Expanding Vortex Receiver modelled here.

receiver. Here a range of inlet temperature of returned air was assessed to understand its impact on the performance of the receiver.

A transient mathematical model for the multilayered refractory-lined receiver described above was developed to calculate the thermal outputs from the receiver using solar resource data for a whole year. Fig. 3 illustrates the heat transfer mechanisms within a refractory-lined solar cavity receiver during start-up, normal operation, turndown, and shutdown. The transient model employs the governing mathematical equations for mass and energy flows through the receiver cavity, considering the particle and gas phases, thermal losses through conductive, convective and radiative heat transfer. The energy balance for each phase and the walls, during normal operation, can be written as follows:

The detailed formulation of each heat flow mechanism is presented previously [41]. The above energy balance equations for each phase and for the walls were arranged, variables and constants were separated, to calculate each of their temperatures for each iteration as follows:
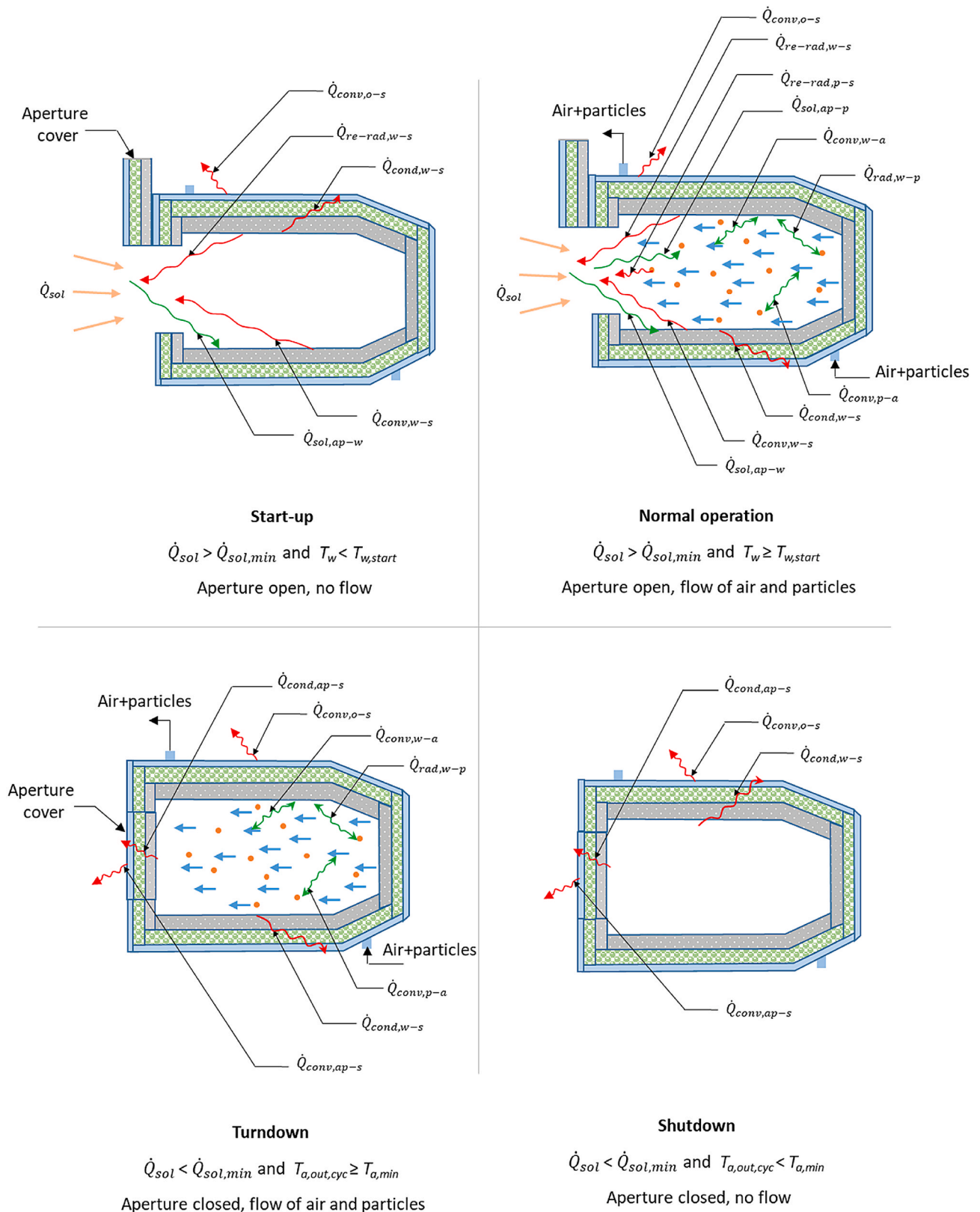
$$\dot{Q}_{sol,\,ap-w} = \dot{Q}_{tm} + \dot{Q}_{rad,\,w-p} + \dot{Q}_{conv,\,w-a} + \dot{Q}_{cond,\,w-s} + \dot{Q}_{conv,\,o-s} + \dot{Q}_{conv,\,w-s}$$
$$+ \dot{Q}_{re-rad,\,w-s} + \dot{Q}_{sol,ap-p} \tag{1}$$

$$\dot{m}_{p,out} \cdot c_{p,p,i} \cdot (T_{p,i} - T_{p,in}) = \dot{Q}_{rad,w-p} + \dot{Q}_{sol,ap-p} - \dot{Q}_{conv,\,p-a} - \dot{Q}_{re-rad,\,p-s} \tag{2}$$

$$\dot{m}_{a,out} \cdot c_{p,a,i} \cdot (T_{a,i} - T_{a,in}) = \dot{Q}_{conv,p-a} + \dot{Q}_{conv,w-a} \tag{3}$$

Fig. 3. An illustration of the heat transfer mechanisms within a refractory-lined solar cavity receiver during the four modes of operation, start-up, normal operation, turndown, and shutdown.

$$T_{w,i+1} = T_{w,i} + \frac{(t_{i+1} - t_i)}{\rho_w . c_{p,w} . V_w} \Big\{ \big[F_{ap-w} . A_{ap} . \dot{Q}_{sol,flux,i} \big] - \big[A_p . N_{p,i} . \varepsilon_p . \sigma . F_{w-p} . (T_{w,i}{}^4$$
$$- T_{p,i}{}^4) \big] - \big[\Upsilon_w . N_{p,i} . F_{w-p} . \alpha_p . A_{ap} . \dot{Q}_{sol,flux,i} \big] - \big[A_e . h_{w-a,i} . (T_{w,i} - T_{a,i}) \big]$$
$$- \big[U_{cond} . (T_{w,i} - T_s) \big] - \big[A_e . h_{w-s,i} . (T_{w,i} - T_s) \big]$$
$$- \big[A_e . \varepsilon_w . \sigma . F_{w-ap} . (T_{w,i}{}^4 - T_s{}^4) \big] - \big[\Upsilon_w . F_{w-ap} . A_{ap} . \dot{Q}_{sol,flux,i} \big]$$
$$- \big[A_{p,f} . \alpha_p . \dot{Q}_{sol,flux,i} . N_{p,i} . e^{at,ap-p} \big] \Big\}$$

(4)

$$T_{p,i+1} = T_{p,in} + \frac{N_{p,i}}{\dot{m}_{p,out} . c_{p,p,i}} \Big\{ \big[A_p . \varepsilon_p . \sigma . F_{w-p} . (T_{w,i}{}^4 - T_{p,i}{}^4) \big]$$
$$+ \big[\Upsilon_w . F_{w-p} . \alpha_p . A_{ap} . \dot{Q}_{sol,flux,i} \big] + \big[A_{p,f} . \alpha_p . \dot{Q}_{sol,flux,i} . e^{at,ap-p} \big]$$
$$- \big[A_p . h_{p-a,i} . (T_{p,i} - T_{a,i}) \big] - \big[A_p . \varepsilon_p . \sigma . F_{p-ap} . (T_{p,i}{}^4 - T_s{}^4) \big]$$
$$- \big[\Upsilon_p . F_{p-ap} . A_{ap} . \dot{Q}_{sol,flux,i} \big] \Big\}$$

(5)

$$T_{a,i+1} = T_{a,in} + \frac{1}{\dot{m}_{a,out} . c_{p,a,i}} \Big\{ \big[A_p . N_{p,i} . h_{p-a,i} . (T_{p,i} - T_{a,i}) \big] + \big[A_e . h_{w-a,i} . (T_{w,i}$$
$$- T_{a,i}) \big] \Big\}$$

(6)

here, T_w, T_p and T_a are the temperatures of the inside surface of the cavity enclosure, particles and air, respectively. Further details of the receiver model, with an explanation of each term, are provided in the Supplementary material.

3. Solution methodology and control algorithms

A MATLAB code was written to solve the coupled set of heat and mass transfer equations iteratively. The MATLAB code was linked with the Simulink environment for transient simulation of the receiver system using real-time input of solar resource data. Fig. 4 presents a flowchart for the solution methodology of the coupled heat transfer equations, which were solved iteratively for each time step. The energy into the receiver, thermal mass change of the receiver cavity, heat losses to the surroundings and energy exchange between three phases at each time step are used to calculate the new temperature fields. The controls for the aperture cover and mass flow rates are also illustrated in Fig. 4. Two feedback controllers, one for the aperture cover and the other for the mass flow rate, were evaluated here. The controllers compare the output values with the set point conditions within a feedback loop. Here, the
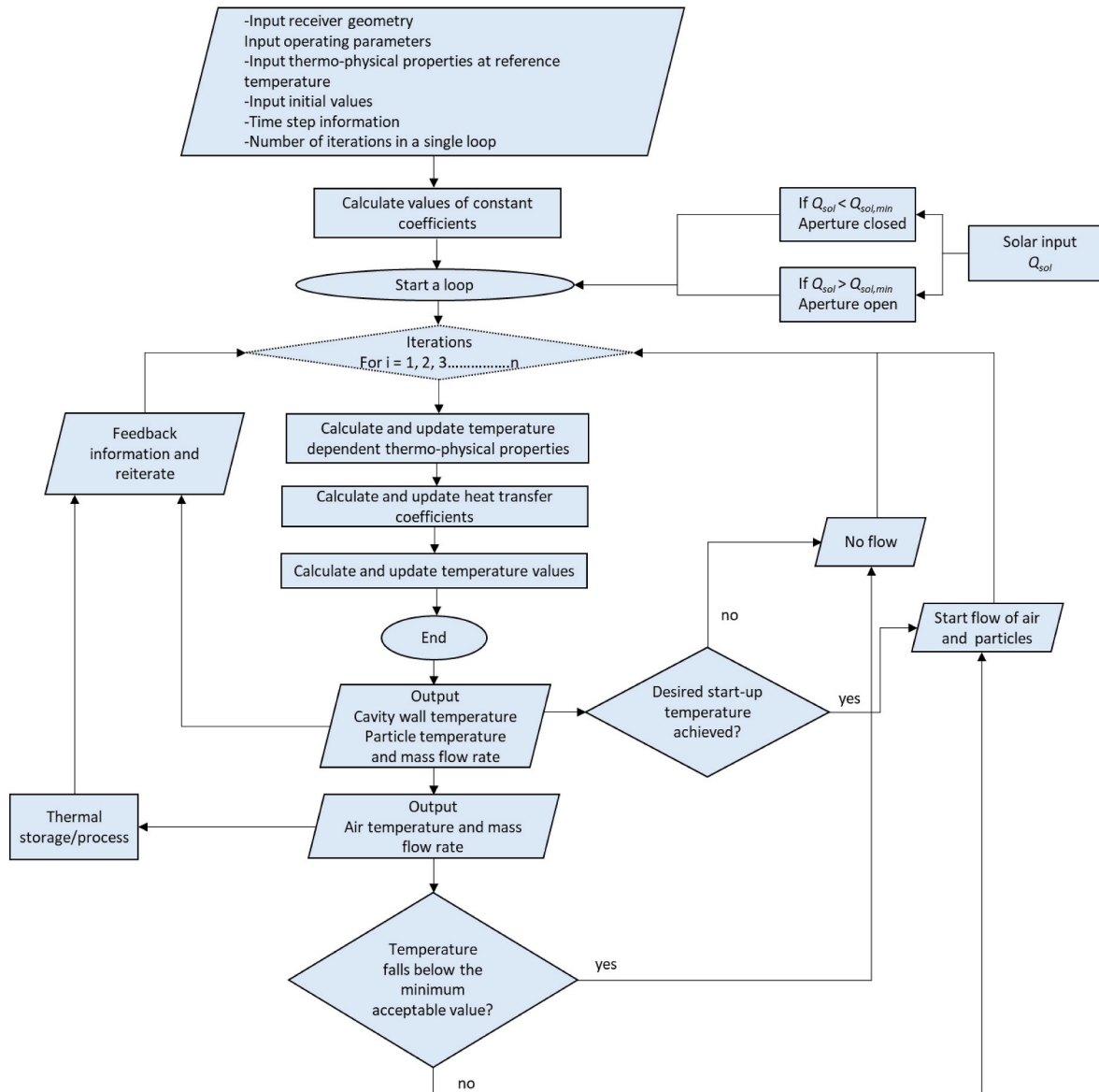

Fig. 4. The iterative procedure used to solve the heat transfer equations, together with the operating control strategy.

receiver aperture only opens when input solar flux is above a minimum threshold, $\dot{Q}_{sol} > \dot{Q}_{sol,min}$, to be sufficient for thermal gain to overcome the thermal losses. A flow of air or air and particles is introduced through the receiver cavity only when the inside wall temperature, $T_{w,start} \geq 900\,°C$. Further controls were implemented to stop the flow of air and particles when output temperature of the air from the cyclone separator falls below a minimum value, $T_{a,min} = 750\,°C$. The aperture was assumed to be closed during the shut-down period, when the flux is below the mininum threshold, to minimize the heat losses.

The annual useful thermal gain based on the hot air that leaves the cyclone, Q_u, and the annual thermal efficiency of the receiver sub-system based on the useful thermal gain of the air only, $\eta_{th,rec,sub}$, was determined as follows:

$$Q_u = \sum_{i=1}^{n} \left[\dot{m}_{a,cyc} . c_{p,a,i} . \left(T_{a,out,cyc,i} - T_{a,in,rec} \right) \right] \tag{7}$$

$$\eta_{th,rec,sub} = \frac{Q_u}{\sum_{i=1}^{n} A_{ap} . \dot{Q}_{sol,flux,i}} \times 100 \tag{8}$$

here $\dot{Q}_{sol,flux,i}$ is the variable solar flux input to the receiver aperture from the heliostat field which was computed in time steps of 15 min intervals.

4. Input conditions

Table 2 provides a summary of the conditions for the control of aperture cover and mass flow during start-up, turn down, normal operation, and shut down periods, whereas Table 3 presents the reference values and sensitivity variations of the input parameters. The thermal performance of the system was assessed with controller parameters listed in Table 2, to estimate the scale of their benefit, together with its sensitivity to the variations in the parameters listed in Table 3. The system was analysed for the real-time meteorological conditions with the direct normal irradiation recorded in Pinjarra, Australia [46]. The site has annual insolation of ~2285 kWh/m². The DNI data was used to obtain optical thermal input to the receiver aperture, with nominal thermal capacity of $P_{th,nom} = 50MW_{th}$, computed in time steps of 15 min over the period of 1 year using CSIRO's Heliosim software [47] and Monte Carlo ray tracing with radially staggered heliostat field layout optimized using COBYLA from the NLOpt library [48].

5. Model validation

The receiver model has been previously verified to show that the dynamic response of the system to various cases is consistent with available data in the literature and expectations [41]. Here, the accuracy of the receiver model was further verified by comparison with CFD simulations of an upscaled 50 MW$_{th}$ high temperature SEVR, for variations in the inlet temperatures and mass flow rates. Furthermore, the evolution of wall temperature and thermal losses from the receiver cavity were compared, at equivalent cavity wall temperature during the period when gradients are most significant i.e., start-up, with the data

Table 2
A summary of the controllers during start-up, turndown, normal operation, and shutdown periods.

Operating period	Conditions	Control parameter
Start-up	$\dot{Q}_{sol} > \dot{Q}_{sol,min}$	Aperture open
	$T_w < T_{w,start}$	No flow
Normal operation	$\dot{Q}_{sol} > \dot{Q}_{sol,min}$	Aperture open
	$T_w \geq T_{w,start}$	Flow of air and particles
Turndown	$\dot{Q}_{sol} < \dot{Q}_{sol,min}$	Aperture closed
	$T_{a,out,cyc} \geq T_{a,min}$	Flow of air and particles
Shutdown	$\dot{Q}_{sol} < \dot{Q}_{sol,min}$	Aperture closed
	$T_{a,out,cyc} < T_{a,min}$	No flow

Table 3
Geometric and input parameters.

	Input parameter	Unit	Reference value	Sensitivity variations
Geometric	D_{ap}/D_c	–	0.5	–
	D_c	m	8.0	–
	L_r/D_c	–	1.12	–
	L_b/D_c	–	0.5	–
	Δr_1	m	0.1	0.025–0.15
	Δr_2	m	0.1	–
	Δr_3	m	0.01	–
Operational	$P_{th,nom}$	MW$_{th}$	50	–
	$\dot{m}_{a,in}$	kg/s	50	30–170
	$\dot{m}_{p,in}/\dot{m}_{a,in}$	–	0.1	0–0.3
	$T_{a,in,rec}$	°C	600	27–800
	$T_{p,in,rec}$	°C	600	27–800
	$T_{a,min}$	°C	750	–
	$T_{a,amb}$	°C	27	–
	$k_{1,ref}$	W/m.K	6.5	–
	$k_{2,ref}$	W/m.K	0.05	–
	$k_{3,ref}$	W/m.K	45	–
	ε_w	–	0.93	–
	$C_{p,w,ref}$	J/kg.K	1050	–
	d_p	μm	120	–
	ρ_w	kg/m³	3150	–
	ε_p	–	0.90	–
	ρ_p	kg/m³	3270	–
	$C_{p,p,ref}$	J/kg.K	1150	–

available in the literature for a directly irradiated industrial scale cavity reactor.

5.1. Comparison with CFD simulations for receiver model

5.1.1. Comparison for a series of inlet temperatures

The accuracy of the receiver model for an upscaled 50 MW$_{th}$ SEVR using data obtained from CFD simulations performed with ANSYS/CFX 2019 R1 software. The CFD model has previously been verified against available experimental data from small-scale experiments [49,50]. The two models were compared with the same configuration of a high temperature cylindrical cavity receiver, SEVR, directly heated by a constant thermal input of 50 MW$_{th}$ with the same input conditions and other relevant parameters. The influence of inlet air temperatures on the outlet temperatures of air and particle phases were compared for different cases listed in Table 4a.

Fig. 5 compares the calculated results of the present model with that of CFD simulations, for a series of validation cases. Here the thermal efficiency of the receiver, η_{th}, is based on the useful thermal gain of both air and particles, to keep it consistent with the available CFD data. It can be observed that the output temperature of the air phase from the present model agrees with CFD simulations to within 0.9–8% and the output temperature of the particle phase to within 17–20%. Similarly, the present predictions of thermal efficiency agree within 4–12%. This is reasonable, given that the CFD model contains far more detail, but also

Table 4a
Operational input parameters used for CFD simulations which are employed for different validation cases from an upscaled SEVR, for a series of inlet temperatures.

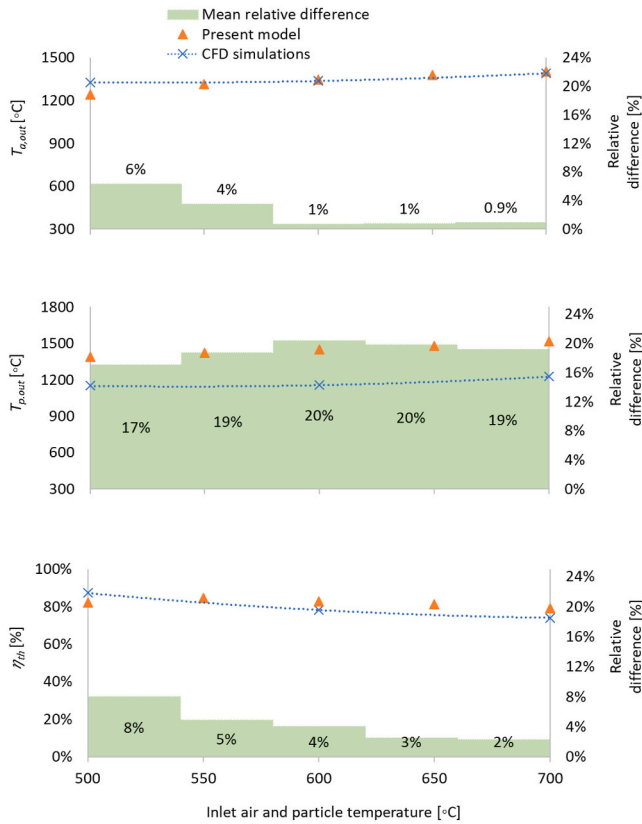| Case	$T_{a,in}$	$T_{p,in}$	$c_{p,a}$	Q_{in}	$\dot{m}_{a,in}$	$\dot{m}_{p,in}/\dot{m}_{a,in}$
	°C	°C	kJ/kg.°C	MW$_{th}$	kg/s	–
1	500	500	1.186	50	40	0.1
2	550	550	1.200	50	40	0.1
3	600	600	1.218	50	40	0.1
4	650	650	1.220	50	40	0.1
5	700	700	1.225	50	40	0.1

Fig. 5. Comparison of key output parameters obtained with the present model with those from the CFD simulations for a high temperature SEVR for the conditions shown in Table 4a.

note that the much lower computational expense of the present model makes it better suited for system-level transient models.

5.1.2. Comparison for a series of inlet mass flow rates

The present model was further verified by comparing the key thermal outputs with that of CFD simulations for variations in the inlet mass flow rates, with the conditions listed in Table 4b. The comparative results are presented in Fig. 6. These results indicate that the present model is sufficiently reliable, with the output temperature of the air, particles and cavity wall agreeing with CFD simulations to within 2–5%, 16–23% and 0.4–9%, respectively, for variations in the inlet mass flow rate with a particle mass loading of 0.1.

5.2. Comparison of thermal losses and wall temperature with an upscaled reactor

The accuracy of the present model was further verified by comparing the thermal losses from the receiver cavity during start-up, for different inner cavity wall temperatures, with the numerical data available for an industrial scale directly-irradiated reactor reported by Charvin et al.

Table 4b
Operational input parameters used for CFD simulations which are employed for different validation cases from an upscaled SEVR, for a series of inlet mass flow rates.

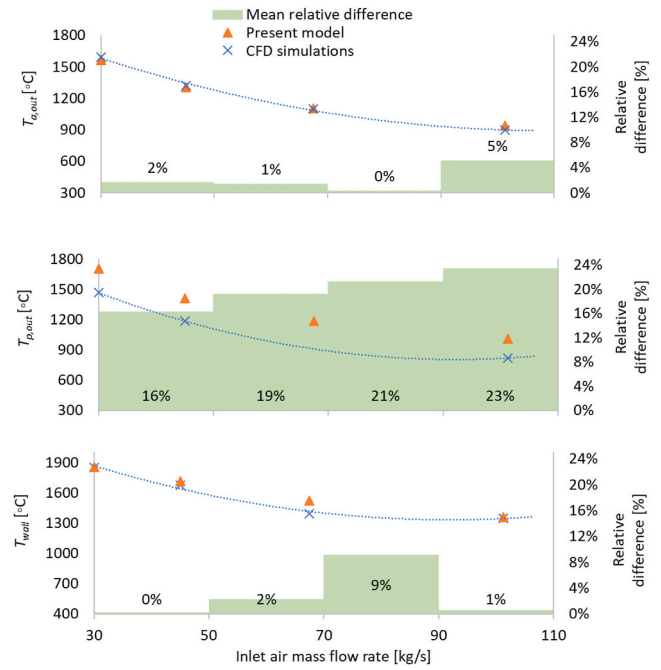| Case	$\dot{m}_{a,in}$	$\dot{m}_{p,in}$	Q_{in}	$T_{a,in}$	$T_{p,in}$
	kg/s	kg/s	MW$_{th}$	°C	°C
1	30	3	52.5	600	600
2	45	4.5	52.5	600	600
3	67	6.7	52.5	600	600
4	101	10.1	52.5	600	600

Fig. 6. Comparison of the calculated values of the output temperatures with those obtained from the CFD simulations, for a series of inlet mass flow rates. The other input parameters were matched for both models (Table 4b).

[51]. The reactor features a cylindrical cavity enclosure with inner refractory of alumina surrounded by two different insulating layers, with a small amount of inert gas at the beginning of operation. Table 5 presents the parameters used for the simulations of the cavity reactor with the Fortran numerical tool [51]. The same input parameters were employed in the present model and the values of thermal losses were compared at equivalent wall temperatures.

Fig. 7 presents a comparison of conductive, convective and re-radiation heat losses obtained with the present and previous [51] models as a fraction of input power, for variations in cavity wall temperature. The thermal losses for the present model are calculated using two methods. The first approach employs the same approximation of a fixed global value of the heat transfer resistance for conduction losses, $R = 2.6 \times 10^{-4}$ K/W as employed previously [51], while the second considers the thicknesses and properties of each component of the three cavity layers. It can be seen that the aperture losses due to convection and re-radiation agree to within 7%, for both methods. The wall losses calculated using the two methods differ significantly. This shows that the two models agree well when employing the same heat transfer resistance for wall losses, but the value predicted by the present model is lower, by a margin of up to 85%, when using the detailed model. This both gives confidence in the present model and highlights the

Table 5
The input parameters used for both models for validation of heat transfer, based on the conditions used by Charvin et al. [51].

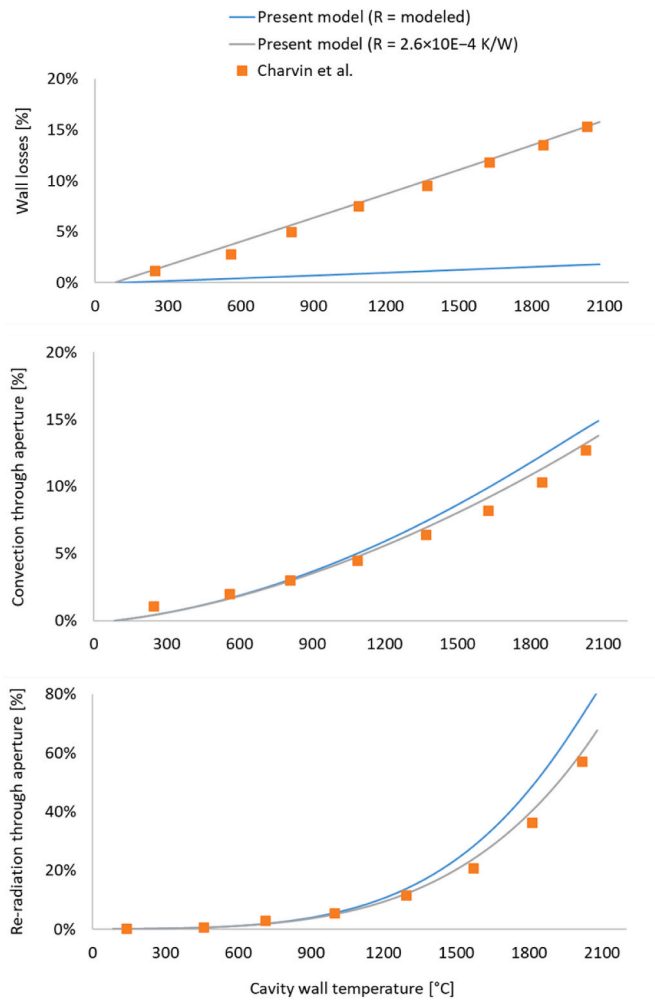| Parameter	Unit	Value
$Q_{sol,in}$	MW$_{th}$	50
D_{ap}	m	5
$D_{reactor}$	m	8
$L_{reactor}$	m	8
n_1	moles	3.5x10^5
Δr_2	m	0.025
Δr_3	m	0.025
ρ_w	kg/m^3	3800
K_1	W/m.K	8
K_2	W/m.K	0.5
K_3	W/m.K	0.05

Fig. 7. Comparison of the thermal losses, as a fraction of input power, from a cavity receiver calculated using the present model with the data presented by Charvin et al. [51] for the start-up of an industrial scale cavity reactor.

importance of accounting for the details of the conduction losses.

Fig. 8 compares the calculated results for the evolution of the cavity wall temperature during start-up obtained from the present model and that of ref [51] for three different cases. It can be seen that the present model agrees with the literature to within 4–5%, for different cases. This further suggests that the present model is sufficiently reliable to assess the influence of transients on the refractory-lined solar receivers.

6. Results and discussions

6.1. Influence of control parameters

Figs. 9 and 10 present the calculated thermal outputs from the receiver system operating with controllers for mass flow and aperture cover listed in Table 2 which are either on or off, for a transient DNI input on a cloudy summer day (2nd January 2017) in Pinjarra. The reference values of other parameters were used (Table 3).

Fig. 9 shows that the system operating with the controllers turned off during start-up, turn-down and shut-down periods is calculated to give 5.1h of daily useful solar hours, when $T_{a,out,cyc} \geq T_{a,min}$, whereas these hours are increased by 41% to a value of 8.6h when the mass flow and aperture cover controllers are on (Fig. 10). This trend is expected because the start-up time is reduced by introducing a time delay between the onset of the solar resource and the introduction of particle-laden air and because covering the aperture during periods of low
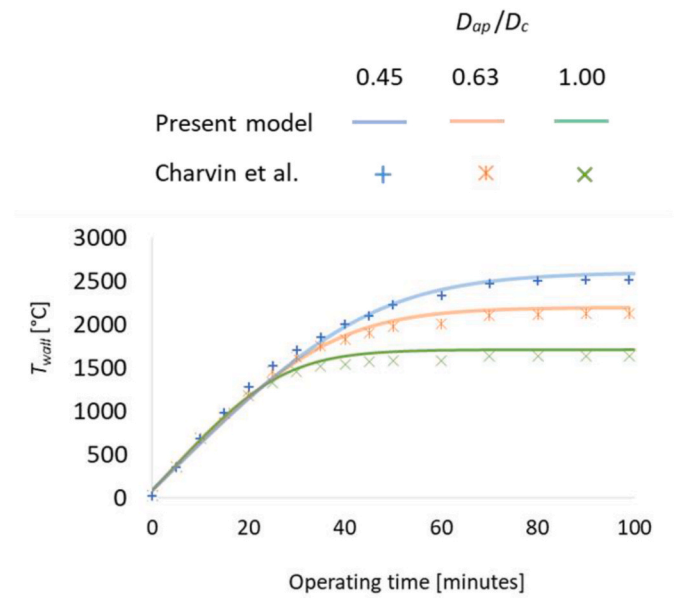

Fig. 8. Comparison of the cavity wall temperature evolution calculated using the present model with the simulations of Charvin et al. [51] for an industrial-scale cavity reactor, for similar geometric parameters and operating conditions.
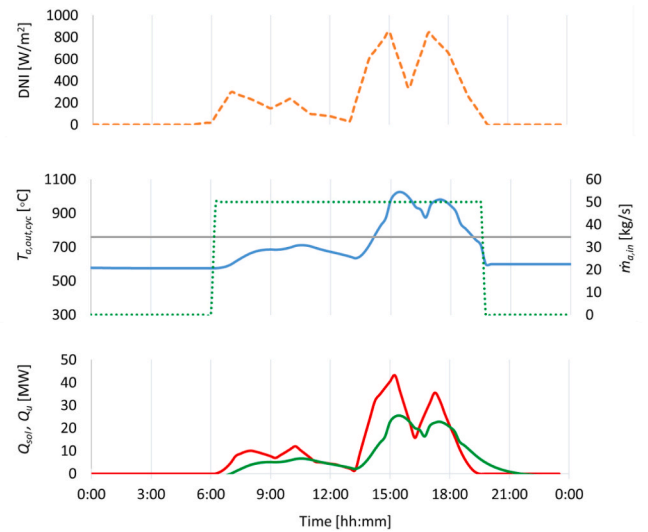

Fig. 9. The calculated thermal outputs from the receiver system when controllers, listed in Table 2, are off, for a transient DNI input on a cloudy summer day in Pinjarra, Australia (2nd January, 2017). See Table 3 for other reference conditions.

solar resource reduces the thermal losses to the surroundings. Similarly, Fig. 11 presents the calculated thermal outputs with controllers either on or off, for a clear sky DNI input. It can be observed that, even on a clear sky day with no significant solar transients, the use of the start-up controller reduces the heating time of HTF after its introduced into the receiver. For example, the heating time to achieve $T_{a,out,cyc} \geq T_{a,min}$ is reduced by 7% when the controllers are on relative to the case when these are off.

Fig. 12 compares the calculated annual useful thermal gain, Q_u, and thermal efficiency, $\eta_{th,rec,sub}$, of a receiver system operating with and without controls listed in Table 2, employing variable solar data for a whole year in Pinjarra, Australia. It can be observed that the implementation of controls for the mass flow rate and aperture cover increases
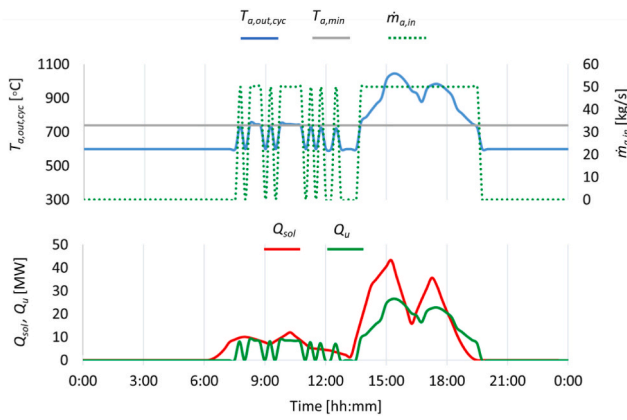
Fig. 10. The calculated thermal outputs of the receiver system operating with controllers on during each mode of operation, for the same conditions as of Fig. 9. Refer to Table 2 for a summary of the controls during start-up, normal operation, turn-down, and shut-down periods.
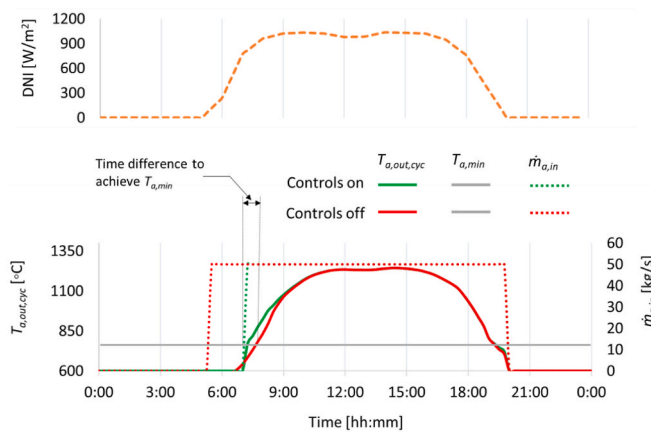

Fig. 11. The calculated output temperature of the receiver system operating with operating controls either on or off, for a clear sky DNI input in Pinjarra, Australia (3rd January, 2017). See Table 2 for control variables.
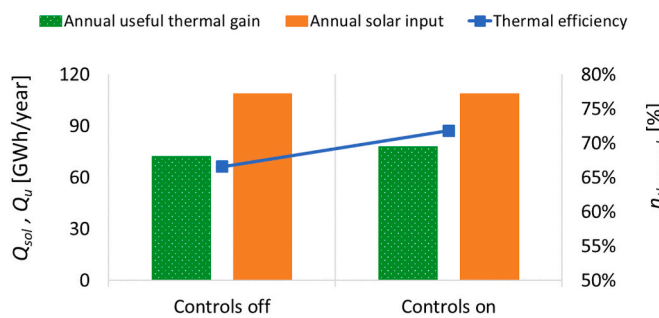

Fig. 12. Comparison of the calculated annual useful thermal gain, Q_u, and annual thermal efficiency, $\eta_{th,rec,sub}$, of a receiver system operating with operating controls either on or off, employing variable solar data for a whole year. See Table 2 for control variables and Table 3 for other reference conditions.

the useful thermal gain relative to the case when these are off. The value of Q_u and $\eta_{th,rec,sub}$ are calculated to increase by 8% for a receiver operating with these controllers on in comparison with their off state, when any thermal gain during the periods of $T_{a,out,cyc} < T_{a,min}$ is ignored as it is not useful for a high temperature industrial application.

These results further indicate that the implementation of required controls during start-up, turndown and shutdown provides the benefit of

enhancing the thermal performance of a refractory lined solar receiver system, by improving its transient thermal response.

6.2. Influence of inner refractory thickness

Fig. 13 presents the calculated values of annual thermal performance of the receiver system for a range of inner refractory lining thicknesses varied from 25 to 150 mm using annual variable solar input data. The significance of each value of refractory thickness is evaluated relative to the case of no-refractory, a receiver with only a high temperature metal alloy shell without any refractory. Here, the other reference conditions are the same for all the cases (Table 3). The calculated results show that both Q_u and $\eta_{th,rec,sub}$ are increased by 30, 34 and 37% for an inner refractory thickness of 25, 50, and 150 mm, respectively, relative to the case of no refractory. This is because of the greater heat losses that occur without the use of insulating and refractory layers.

The calculated results are an indication of the potential benefits of refractory use in high temperature receivers, when optimized for a range of competing influences and operated with proper controls to manage the influence of solar transients during start-up, turndown and shutdown. Also, the refractory lining potentially allows the use of lower-cost materials [41] along with more energy harvesting potential during a whole year.

6.3. Influence of particle loading

Fig. 14 presents the influence of the particle loading, $\dot{m}_{p,in}/\dot{m}_{a,in}$, varied from 0 to 0.3, on the calculated annual useful thermal gain, Q_u, and thermal efficiency, $\eta_{th,rec,sub}$. The other reference conditions are listed in Table 3. It can be observed that each value of $\dot{m}_{p,in}/\dot{m}_{a,in}$ is calculated to give a better Q_u relative to the case of no particles. For the conditions assessed here, Q_u and $\eta_{th,rec,sub}$ are calculated to increase by 11, 15 and 17% when $\dot{m}_{p,in}/\dot{m}_{a,in}$ is increased from 0 to 0.1, 0.2 and 0.3, respectively. These results indicate that the addition of particles has a positive impact on the annual thermal performance of the present configuration of air receiver system. This is attributed to the increased radiation adsorption by the particle suspensions within the air stream and increase in the effectiveness of the heat transfer mechanisms within the receiver cavity due to their high surface area per unit mass.
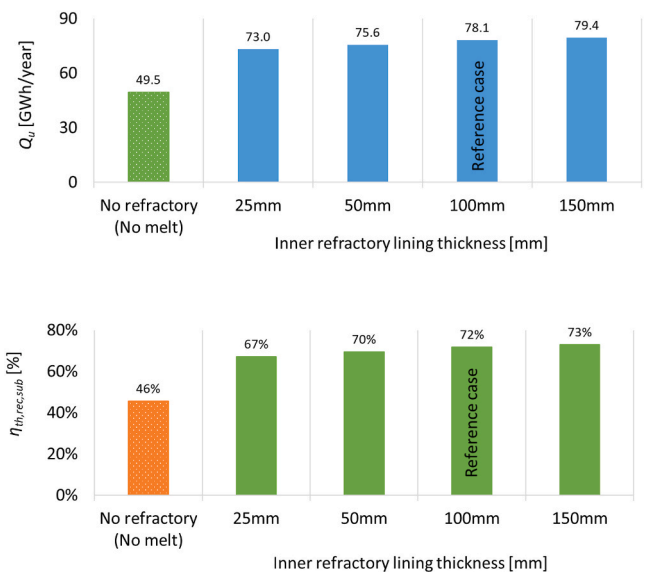

Fig. 13. Calculated annual useful thermal gain, Q_u, and annual thermal efficiency, $\eta_{th,rec,sub}$, as a function of the inner refractory lining thickness, employing variable solar input data for a whole year. Here no melt condition is assumed for no-refractory case. The other reference conditions are listed in Table 3.
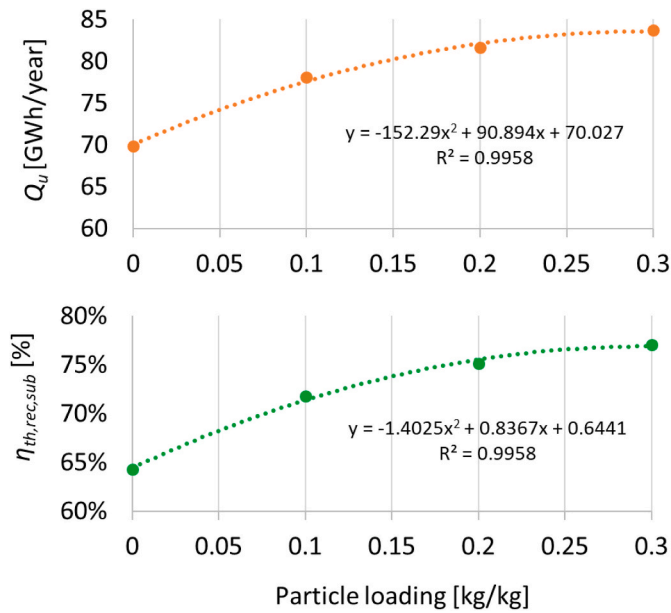
y = -152.29x² + 90.894x + 70.027
R² = 0.9958

y = -1.4025x² + 0.8367x + 0.6441
R² = 0.9958

Fig. 14. Calculated annual values of useful thermal heat gain, Q_u, and thermal efficiency, $\eta_{th,rec,sub}$, for various values of particle loading, $\dot{m}_{p,in}/\dot{m}_{a,in}$. See Table 3 for other reference input conditions.

6.4. Influence of inlet mass flow rates

Fig. 15 presents the influence of the inlet mass flow rate of air, $\dot{m}_{a,in}$, on the calculated annual useful thermal gain of the receiver system, Q_u, and annual thermal efficiency, $\eta_{th,rec,sub}$. Here the minimum acceptable value of output air temperature, $T_{a,min}$, is same for all cases. It can be observed that the calculated thermal performance of the receiver system increases with an increase in $\dot{m}_{a,in}$. For the conditions assessed here, $\eta_{th,rec,sub}$ is calculated to increase by 5, 8, 11, and 14% when $\dot{m}_{a,in}$ increases from 30 kg/s to 40, 50, 70 and 100 kg/s, respectively. This is consistent with the expectation because increasing the mass flow rate will decrease the temperature rise of the two-phase flow by an energy balance. This in
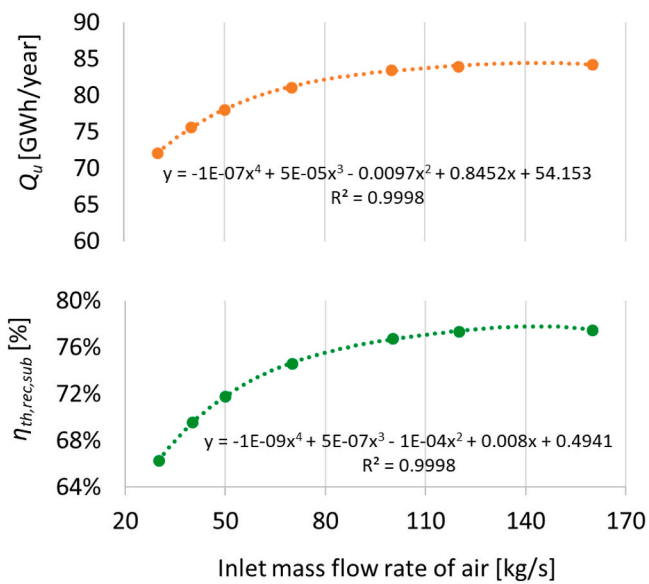
turn results in lower thermal losses and higher useful thermal gain.

It can also be observed that for the conditions assessed here, there is no significant increase in the receiver thermal performance for $\dot{m}_{a,in} > 100$ kg/s. This shows that there is a critical value of $\dot{m}_{a,in}$ above which thermal losses dominate the improvements in the useful thermal gain.

6.5. Influence of inlet temperatures

Fig. 16 presents the calculated values of the annual useful thermal gain, Q_u, and thermal efficiency, $\eta_{th,rec,sub}$, for a range of inlet air and particle temperatures, with a fixed value of $T_{a,min}$ for all cases. As expected, an increase in the inlet temperatures to the receiver causes a decrease in Q_u and $\eta_{th,rec,sub}$. This is due to an increase in the thermal losses to the surroundings resulting in a decrease in the difference between inlet and outlet temperature i.e., $T_{a,out}$ doesn't increase in the same value as $T_{a,in}$. For the conditions assessed here, the calculated $\eta_{th,rec,sub}$ is decreased by 4%, 10% and 17% when inlet temperature of both air and particles is increased from 27 °C (ambient) to 400, 600 and 800 °C, respectively. These calculated results further suggest that the annual thermal performance of the present system is calculated to be $\eta_{th,rec,sub} = 80\%$ when heating cold HTF entering at ambient temperature, which is comparable to other high temperature receiver systems listed in Table 1. These results also indicate that the present configuration of the receiver system achieves $\eta_{th,rec,sub} = 72–76\%$, when reheating already hot air returning at 600 to 400 °C.

This is an indication of the potential advantage offered by the use of particles in suspension within an air stream and refractory-lining in high temperature solar receivers, which offers the opportunity of practical implementation of an industrial scale high temperature air receiver.

The results presented in this paper highlight the further scope and significance of the present transient approach, which is to integrate and simulate a complete CST plant with real-time interaction between the receiver, coupled storage and other system components to assess different system types, and to assist in identifying which type of system is best suited to which application.
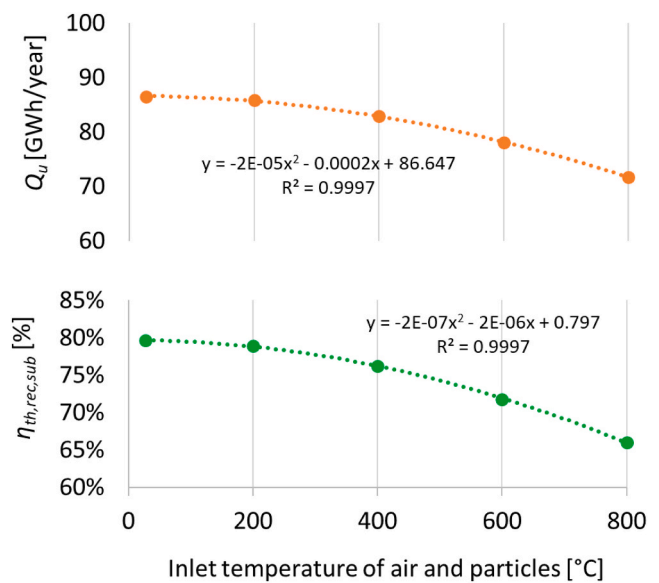

y = -1E-07x⁴ + 5E-05x³ - 0.0097x² + 0.8452x + 54.153
R² = 0.9998

y = -1E-09x⁴ + 5E-07x³ - 1E-04x² + 0.008x + 0.4941
R² = 0.9998

Fig. 15. Influence of the mass flow rate of inlet air on the calculated thermal performance of refractory-lined SEVR. The other reference conditions are listed in Table 3.

y = -2E-05x² - 0.0002x + 86.647
R² = 0.9997

y = -2E-07x² - 2E-06x + 0.797
R² = 0.9997

Fig. 16. Influence of the temperature of inlet air and particles on the calculated useful thermal gain, Q_u, and thermal efficiency, $\eta_{th,rec,sub}$, when accounting for transient losses through a year of operation. The other reference conditions are listed in Table 3.

7. Conclusions

In conclusion, the net thermal performance of receiver sub-system has been estimated to span between 80 to 72% when heating air to temperatures of order of 1000°C with inlet temperatures of ambient to 600°C, respectively, when accounting for start-up, turndown and shut-down losses through a year of transient operation. This differs from previous assessments which have typically only reported instantaneous efficiencies for the receiver. The main findings of the present analysis are as follows:

- The transient mathematical model developed for a high temperature particle-laden solar receiver was found to yield a reasonable agreement with the available CFD data from an up-scaled SEVR under solar simulated conditions for variations in the inlet mass flow rates, with a relative difference of up to 5% in air temperature at the receiver outlet. Furthermore, the output air temperature calculated with the present model agreed with the CFD simulations to within 6% for variations in the inlet temperatures.
- The model confirms the technical feasibility of the proposed system to re-heat air that is returned from a process at an already elevated temperature. This point distinguishes the present air heater from those reported previously, such as for volumetric receivers.
- A refractory-lined solar receiver operating with mass flow rate and aperture cover controllers is calculated to give 8% more annual useful thermal gain relative to the case when these controllers are off.
- For the conditions assessed here, the results highlight the relative advantage of refractory use in high temperature particle-laden re-ceivers, when optimized for a range of competing influences. A refractory-lined solar receiver with inner refractory and insulating layer thickness of 100 mm was calculated to provide 36% more annual useful thermal gain relative to the case of no refractory under the same operating conditions.
- For the conditions assessed here, the receiver annual thermal per-formance is calculated to enhance by 5, 11 and 14% when $\dot{m}_{a,in}$ increases from 30 kg/s to 50, 70 and 100 kg/s, respectively. However,

there is no significant increase in the receiver thermal performance for $\dot{m}_{a,in} > 100$ kg/s.
- The use of particles in suspension within an air stream has a positive impact on the annual thermal performance of a refractory-lined air receiver system. For the reference case assessed here, the addition of 10% particle to the air is calculated to give 11% more annual useful thermal gain relative to the case of no particle.

CRediT authorship contribution statement

Muhammad M. Rafique: Conceptualization, Methodology, Soft-ware, Validation, Formal analysis, Visualization, Project administration, Data curation, Resources, Writing – original draft, Writing – review & editing. **Graham Nathan:** Supervision, Methodology, Resources, Project administration, Funding acquisition, Writing – review & editing. **Woei Saw:** Supervision, Methodology, Resources, Project administration, Funding acquisition, Writing – review & editing.

Declaration of competing interest

The authors declare that they have no known competing financial interests or personal relationships that could have appeared to influence the work reported in this paper.

Acknowledgments

Nomenclature

A	area [m^2]
c_p	specific heat capacity [J/kg.K]
D	cavity diameter [m]
d_p	mean particle diameter [m]
e^{at}	geometric attenuation factor [$-$]
F	radiation shape factor [$-$]
$\dot{Q}$	energy flow rate [W]
h	heat transfer coefficient [W/m^2.K]
k	thermal conductivity [W/m.K]
L_r	length of cylindrical section [m]
L_b	horizontal length of conical back section [m]
$\dot{m}$	mass flow rate [kg/s]
N_p	number density of particles [$-$]
Q	annual thermal energy [Wh/year]
R	resistance to heat flow [K/W]
T	temperature [K]
t	time [s]
u	velocity [m/s]
U	Overall conductive heat transfer resistance [W/K]
V	volume [m^3]
Δr	thickness of cavity layer [m]

Greek letters

α	absorptivity [$-$]

Υ	reflectivity (1- α) [−]
ε	emissivity [−]
σ	Stefan-Boltzmann constant [W/m^2.K^4]
η	efficiency [%]
ρ	density [kg/m^3]

Subscripts

1, 2, 3	cavity layer 1, 2, and 3
a	air
ap	aperture
c	cavity
cond	conduction
conv	convection
cyc	cyclone separator
e	effective
f	frontal
i	iteration number
eq	equivalent
o	outer surface
p	particle
ref	ref value at ambient temperature
re-rad	re-radiation
s	surroundings
sol	solar
tm	thermal mass
th	thermal
u	useful
w	cavity wall lining

Appendix A. Supplementary data

Supplementary data to this article can be found online at https://doi.org/10.1016/j.renene.2022.07.111.

References

[1] V.R. Patil, F. Kiener, A. Grylka, A. Steinfeld, Experimental testing of a solar air cavity-receiver with reticulated porous ceramic absorbers for thermal processing at above 1000 °C, Sol. Energy 214 (2021) 72–85.

[2] E. Casati, A. Lankhorst, U. Desideri, A. Steinfeld, A co-located solar receiver and thermal storage concept using silicate glass at 1000°C and above: experiments and modeling in the optically-thick regime, Sol. Energy 177 (2019) 553–560.

[3] D. Davis, F. Müller, W. Saw, A. Steinfeld, G. Nathan, Solar-driven alumina calcination for CO2 mitigation and improved product quality, Green Chem. 19 (13) (2017) 2992–3005.

[4] M.M. Rafique, G. Nathan, W. Saw, Uncertainty in predicting the start-up time and losses for a high temperature particle receiver due to solar resource variability, in: ASME 2020 14th International Conference on Energy Sustainability, 2020.

[5] C.K. Ho, Advances in central receivers for concentrating solar applications, Sol. Energy 152 (2017) 38–56.

[6] G. Nathan, M. Jafarian, B. Dally, W. Saw, P. Ashman, E. Hu, A. Steinfeld, Solar thermal hybrids for combustion power plant: a growing opportunity, Prog. Energy Combust. Sci. 64 (2018) 4–28.

[7] T. Tan, Y. Chen, Review of study on solid particle solar receivers, Renew. Sustain. Energy Rev. 14 (1) (2010) 265–276.

[8] W. Wu, D. Trebing, L. Amsbeck, R. Buck, R. Pitz-Paal, Prototype testing of a centrifugal particle receiver for high-temperature concentrating solar applications, J. Sol. Energy Eng. 137 (4) (2015).

[9] W. Wu, R. Uhlig, R. Buck, R. Pitz-Paal, Numerical simulation of a centrifugal particle receiver for high-temperature concentrating solar applications, Numer. Heat Tran., Part A: Applications 68 (2) (2015) 133–149.

[10] B.H. Mills, C.K. Ho, N.R. Schroeder, R. Shaeffer, H.F. Laubscher, K.J. Albrecht, Design evaluation of a next-generation high-temperature particle receiver for concentrating solar thermal applications, Energies 15 (5) (2022) 1657.

[11] X. Xie, H. Xu, D. Gan, M. Ni, J. Yan, K. Cen, G. Xiao, A sliding-bed particle solar receiver with controlling particle flow velocity for high-temperature thermal power generation, Renew. Energy 183 (2022) 41–50.

[12] Q. Kang, R. Dewil, J. Degrève, J. Baeyens, H Zhang, Energy analysis of a particle suspension solar combined cycle power plant, Energy Convers. Manag. 163 (2018) 292–303.

[13] H. Zhang, H. Benoit, I. Perez-Lopèz, G. Flamant, T. Tan, J. Baeyens, High-efficiency solar power towers using particle suspensions as heat carrier in the receiver and in the thermal energy storage, Renew. Energy 111 (2017) 438–446.

[14] Q. Kang, G. Flamant, R. Dewil, J. Baeyens, H.L. Zhang, Y.M. Deng, Particles in a circulation loop for solar energy capture and storage, Particuology 43 (2019) 149–156.

[15] M.S. Mahdi, A.F. Khudheyer, Central receivers design in concentrated solar thermal power plants: a review, IOP Conf. Ser. Mater. Sci. Eng. 1094 (1) (2021), 012018.

[16] R.P. Merchán, M.J. Santos, A. Medina, A.C. Hernández, High temperature central tower plants for concentrated solar power: 2021 overview, Renew. Sustain. Energy Rev. 155 (2022), 111828.

[17] A. Godini, S. Kheradmand, Optimization of volumetric solar receiver geometry and porous media specifications, Renew. Energy 172 (2021) 574–581.

[18] S. Luque, G. Menéndez, M. Roccabruna, J. González-Aguilar, L. Crema, M. Romero, Exploiting volumetric effects in novel additively manufactured open solar receivers, Sol. Energy 174 (2018) 342–351.

[19] M. Nakakura, K. Matsubara, S. Bellan, T. Kodama, Direct simulation of a volumetric solar receiver with different cell sizes at high outlet temperatures (1,000–1,500 °C), Renew. Energy 146 (2020) 1143–1152.

[20] B. Hoffschmidt, R. Pitz-Paal, M. Böhmer, T. Fend, P. Rietbrock, 200 kW{sub th} open volumetric air receiver (HiTRec) of DLR reached 1000 deg C average outlet temperature at PSA, J. Phys. 4 (1999) 551–556. Medium: X; Size: page(s).

[21] R. Buck, T. Brauning, T. Denk, M. Pfander, P. Schwarzbozl, F. Tellez, Solar-hybrid gas turbine-based power tower systems (REFOS)*, J. Sol. Energy Eng. 124 (1) (2001) 2–9.

[22] W.E.C. Pritzkow, Pressure loaded volumetric ceramic receiver, Sol. Energy Mater. 24 (1) (1991) 498–507.

[23] C.K. Ho, B.D. Iverson, Review of high-temperature central receiver designs for concentrating solar power, Renew. Sustain. Energy Rev. 29 (2014) 835–846.

[24] A.L. Ávila-Marín, Volumetric receivers in solar thermal power plants with central receiver system technology: a review, Sol. Energy 85 (5) (2011) 891–910.

[25] W. Wu, L. Amsbeck, R. Buck, R. Uhlig, R. Ritz-Paal, Proof of concept test of a centrifugal particle receiver, Energy Proc. 49 (2014) 560–568.

[26] W. Wu, L. Amsbeck, R. Buck, N. Waibel, P. Langner, R. Pitz-Paal, On the influence of rotation on thermal convection in a rotating cavity for solar receiver applications, Appl. Therm. Eng. 70 (1) (2014) 694–704.

[27] N.P. Siegel, C.K. Ho, S.S. Khalsa, G.J. Kolb, Development and evaluation of a prototype solid particle receiver: on-sun testing and model validation, J. Sol. Energy Eng. 132 (2) (2010).

[28] M. Röger, L. Amsbeck, B. Gobereit, R. Buck, Face-down solid particle receiver using recirculation, J. Sol. Energy Eng. 133 (3) (2011).

[29] T. Tan, Y. Chen, Z. Chen, N. Siegel, G.J. Kolb, Wind effect on the performance of solid particle solar receivers with and without the protection of an aerowindow, Sol. Energy 83 (10) (2009) 1815–1827.

[30] G. Flamant, D. Gauthier, H. Benoit, J.L. Sans, B. Boissière, R. Ansart, M. Hemati, A new heat transfer fluid for concentrating solar systems: particle flow in tubes, Energy Proc. 49 (2014) 617–626.

[31] G. Flamant, D. Gauthier, H. Benoit, J.L. Sans, R. Garcia, B. Boissière, R. Ansart, M. Hemati, Dense suspension of solid particles as a new heat transfer fluid for concentrated solar thermal plants: on-sun proof of concept, Chem. Eng. Sci. 102 (2013) 567–576.

[32] H. Benoit, I.P. López, D. Gauthier, J.L. Sans, G. Flamant, On-sun demonstration of a 750 C heat transfer fluid for concentrating solar systems: dense particle suspension in tube, Sol. Energy 118 (2015) 622–633.

[33] T. Kodama, S. Enomot, T. Hatamachi, N. Gokon, Application of an internally circulating fluidized bed for windowed solar chemical reactor with direct irradiation of reacting particles, J. Sol. Energy Eng. 130 (1) (2008).

[34] S. Bellan, T. Kodama, K. Matsubara, N. Gokon, H.S. Cho, K. Inoue, Thermal performance of a 30 kW fluidized bed reactor for solar gasification: a CFD-DEM study, Chem. Eng. J. 360 (2019) 1287–1300.

[35] C.K. Ho, A review of high-temperature particle receivers for concentrating solar power, Appl. Therm. Eng. 109 (2016) 958–969.

[36] CET.*https://www.adelaide.edu.au/cet/technologies/solar-expanding-vortex-particle-receiver-reactor-sevr*.

[37] A. Chinnici, M. Arjomandi, Z.F. Tian, Z. Lu, G. Nathan, A novel solar expanding-vortex particle reactor: influence of vortex structure on particle residence times and trajectories, Sol. Energy 122 (2015) 58–75.

[38] S. Long, T.C. Lau, A. Chinnici, G. Nathan, The flow-field within a vortex-based solar cavity receiver with an open aperture, Exp. Therm. Fluid Sci. 123 (2021) 110314.

[39] H. Stadler, D. Maldonado, M. Offergeld, P. Schwarzbözl, J. Trautner, CFD model for the performance estimation of open volumetric receivers and comparison with experimental data, Sol. Energy 177 (2019) 634–641.

[40] M.M. Rafique, G. Nathan, W. Saw, Thermal response of multilayered refractory-lined solar receivers to transient operation, Sol. Energy 243 (2022) 70–80, https://doi.org/10.1016/j.solener.2022.07.037.

[41] M.M. Rafique, G. Nathan, W. Saw, A mathematical model to assess the influence of transients on a refractory-lined solar receiver, Renew. Energy 167 (2021) 217–235.

[42] D. Davis, M. Jafarian, A. Chinnici, W. Saw, G. Nathan, Thermal performance of vortex-based solar particle receivers for sensible heating, Sol. Energy 177 (2019) 163–177.

[43] M. Ebert, L. Amsbeck, J. Rheinländer, B. Schlögl-Knothe, S. Schmitz, M. Sibum, R. Uhlig, R. Buck, Operational experience of a centrifugal particle receiver prototype, AIP Conf. Proc. 2126 (1) (2019), 030018.

[44] A. Chinnici, M. Arjomandi, Z. Tian, G. Nathan, A novel solar expanding-vortex particle reactor: experimental and numerical investigation of the iso-thermal flow field and particle deposition, Sol. Energy 133 (2016) 451–464.

[45] A. Chinnici, Y. Xue, T.C. Lau, M. Arjomandi, G. Nathan, Experimental and numerical investigation of the flow characteristics within a solar expanding-vortex particle receiver-reactor, Sol. Energy 141 (2017) 25–37.

[46] Bureau of Meteorology. *http://www.bom.gov.au/climate/glossary/seasons.shtml*. [cited 2019 04 October].

[47] D.F. Potter, J. Kim, A. Khassapov, R. Pascual, L. Hetherton, Z. Zhang, Heliosim: an integrated model for the optimisation and simulation of central receiver CSP facilities, AIP Conf. Proc. 2033 (1) (2018), 210011.

[48] Steven G. Johnson. The NLopt nonlinear-optimization package, *http://github.com/stevengj/nlopt*.

[49] D. Ang, A. Chinnici, Z. Tian, W. Saw, G. Nathan, Influence of Particle Loading, Froude and Stokes Number on the Global Thermal Performance of a Vortex-Based Solar Particle Receiver 184, Renewable Energy, 2021, pp. 201–214.

[50] D. Ang, Y. Tang, A. Chinnici, Z. Tian, W. Saw, T. Lau, I. Ingenhoven, Z. Sun, G. Nathan, Thermal Performance Analysis of a Scaled-Up Suspension Flow Receiver for Generation of Industrial Process Heat: A Computational Study, SolarPACES, 2021. Virtual.

[51] P. Charvin, S. Abanades, P. Neveu, F. Lemont, G. Flamant, Dynamic modeling of a volumetric solar reactor for volatile metal oxide reduction, Chem. Eng. Res. Des. 86 (11) (2008) 1216–1222.

CHAPTER 6

PERFORMANCE ASSESSMENT OF A SYSTEM TO PROVIDE STEADY HIGH TEMPERATURE AIR VIA SOLAR THERMAL PARTICLE TECHNOLOGY WITH STORAGE AND COMBUSTION BACK-UP

This chapter is written in manuscript form for submission to a peer reviewed journal.

Statement of Authorship

Title of Paper	Performance assessment of a system to provide steady high temperature air via solar thermal suspension flow technology with storage and combustion back-up
Publication Status	☐ Published ☐ Accepted for Publication ☐ Submitted for Publication ☑ Unpublished and Unsubmitted work written in manuscript style
Publication Details	Rafique MM, Saw W, Lee L, Ingenhoven P, Nathan G (2022). Performance assessment of a system to provide steady high temperature air via solar thermal suspension flow technology with storage and combustion back-up. To be submitted.

Principal Author

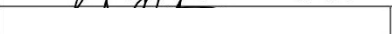| Name of Principal Author (Candidate)	Muhammad Mujahid RAFIQUE		
Contribution to the Paper	Performed the literature review and identified the potential gaps. Jointly defined the scope and aims of the paper. Jointly performed analysis, interpreted data, wrote the manuscript, and acted as corresponding author.		
Overall percentage (%)	60%		
Certification:	This paper reports on original research I conducted during the period of my Higher Degree by Research candidature and is not subject to any obligations or contractual agreements with a third party that would constrain its inclusion in this thesis. I am the primary author of this paper.		
Signature		Date	21/11/2022

Co-Author Contributions

By signing the Statement of Authorship, each author certifies that:

i. the candidate's stated contribution to the publication is accurate (as detailed above);

ii. permission is granted for the candidate in include the publication in the thesis; and

iii. the sum of all co-author contributions is equal to 100% less the candidate's stated contribution.

Name of Co-Author	Dr. Woei Saw		
Contribution to the Paper	Supervised the work. Critically reviewed the manuscript. Jointly defined the scope and aims of the paper. Helped to improve the language, structure, and content of the manuscript.		
Signature		Date	7/12/2022

Name of Co-Author	Dr. Leok Lee		
Contribution to the Paper	Provided system modelling support. Helped to improve the content of the manuscript.		
Signature		Date	07/12/2022

Name of Co-Author	Dr. Philip Ingenhoven		
Contribution to the Paper	Provided system modelling support. Helped to improve the content of the manuscript.		
Signature		Date	7/12/2022

Name of Co-Author	Prof. Graham Nathan		
Contribution to the Paper	Supervised the work. Jointly defined the scope and aims of the paper. Critically reviewed the manuscript. Helped to improve the language, structure, and content of the manuscript.		
Signature		Date	7/12/2022

Performance assessment of a system to provide steady high temperature air via solar thermal suspension flow technology with storage and combustion back-up

Muhammad M. Rafique[1, 2*], Woei Saw[1, 3], Leok Lee[1, 2], Philip Ingenhoven[1,3], Graham Nathan[1, 2]

[1]Centre for Energy Technology, The University of Adelaide, SA 5005, Australia

[2]School of Mechanical Engineering, The University of Adelaide, SA 5005, Australia

[3]School of Chemical Engineering and Advanced Materials, The University of Adelaide, SA 5005, Australia

Abstract

The performance of a high-temperature concentrated solar thermal plant based on a 50MW$_{th}$ suspension flow solar particle receiver sub-system integrated with sensible thermal storage and combustion backup is analyzed, to supply steady output of reheated air to a downstream thermochemical process. The analysis is performed with transient mathematical models of the receiver and packed bed thermal storage sub-systems considering solar resource variability, written in a Simulink environment, to estimate useful annual thermal gain, thermal efficiency, solar share and levelized cost of solar heat, for a range of parameters including particle mass loading, air mass flow rate, thermal storage capacity and solar multiple. The time-dependent temperature fields of the receiver and thermal losses, together with their influence on the performance of the combined system are reported for each condition with a transient input solar resource spanning over a whole year. New insights are provided of the relative tradeoffs between these parameters on the overall system performance, solar share and levelized cost of solar energy. Also reported is the sensitivity of the levelized cost to different system combinations sized to provide a solar share of up to 75% of the yearly process thermal demand, along with the influence of the specific costs of the system components varied in the range of ±60%.

Keywords: Concentrating solar thermal; suspension flow solar particle receiver; solar transients; techno-economics; LCOH; annual energy yield; solar share.

---

*Corresponding author

Email address: muhammad.rafique@adelaide.edu.au

1. Introduction

The application of concentrated solar thermal, CST, technologies to supply heat to thermochemical processes is receiving growing attention due to its potential to lower greenhouse gas emissions from hard-to-abate industrial applications [1]. However, present commercially available CST technologies are both relatively expensive and have an operating temperature limited to below 600°C [2], due to the flux limitations of thin metal conducting tubes and the use of commercially-available molten salts, which become chemically unstable above 580°C and also require trace heating to avoid solidification. This is well below the temperature of typical thermochemical processes, such as that for the calcination in the alumina Bayer process of about 1000°C [3]. In this regard, the use of particles in suspension within an air flow, inside a directly irradiated refractor-lined cavity receiver, is a promising class of technology for operating at temperatures well above 1000°C and is one of the potential pathways for the next-generation CST plants [4, 5]. While the literature provides evidence that suspension flow solar particle receivers have the potential to supply reheated air to high temperature industrial processes at temperatures of 1000°C, little is known on the system-level performance of these receivers, either alone or when operating in combination with a sensible thermal storage system and combustion backup to provide steady high temperature air to a downstream process. Further to this, most of the techno-economic studies for solar receiver technologies have been undertaken with a selected value of DNI, so that the combined effects of key parameters to real-time seasonal variability accounting for transient losses through a year of operation at a potential plant site, are still unclear. Hence, there is a need for assessments that provide new understanding of the system level performance of these CST systems with full consideration of transients and of the levelized cost of the energy. This paper aims to fill these gaps.

A range of particle-based receiver and storage technologies are under development, notably the falling particle receivers led by Sandia Laboratory [6-8], a centrifugal receiver led by DLR [9-12] and tubular fluidized beds led by CNRS [13]. The thermal performance of these receivers when operating alone has been reported to be in the range of 75 to 80% when operating at temperatures of 750 to 900°C. However, their performance when integrated into complete systems has only been reported for the generation of electricity using steam and gas turbine cycles [14-20]. These are typically designed to provide schedulable power, which

is different from industrial processes, which typically operate at steady-state for the majority of the year. Limited information is therefore available of their performance when integrated into systems that produce continuous high temperature heat, above 1000°C, for heavy industrial applications such as the production of alumina. There is also a lack of available data of the performance of solar systems when used to reheat warm air that has been returned from a process or thermal storage system, at temperatures >300°C. The present work also aims to meet these needs.

A class of particle technology that is well suited to heating of air to high temperatures is the suspension flow solar expanding vortex receiver (SEVR), which employs direct irradiation to heat a vortex flow of air and suspended particles in a cylindrical cavity. The vortex receiver was chosen for the present analysis because it has been demonstrated in the laboratory to deliver temperatures of >1300°C [21-23]. In addition, the net thermal efficiency of a SEVR receiver sub-system has been estimated to span between 72 and 80%, with further improvements possible, when heating air to temperatures of the order of 1000°C with steady inlet temperatures of ambient to 600°C, respectively [24]. Nevertheless, limited information has been reported of the system level performance of a complete CST plant with relative tradeoffs between these components, considering the real-time interaction between receiver and thermal storage, or of the levelized cost of the heat, *LCOH*. Hence, there is a need to estimate the performance of these receivers in combination with thermal storage and other components of a CST system, together with their estimated *LCOH* for the solar energy component. This paper aims to meet this need. A further aim is to establish a baseline of performance and cost which can be used to develop further improvements by comparison with alternative systems and technologies such as volumetric air receivers [5, 25, 26] and falling particle curtain receivers [6-8], although that is beyond the scope of the present investigation.

Previous studies have reported that the use of solid particle suspensions within an air stream has the potential to increase the thermal performance of the SEVR [27], which results in a better overall performance of the CST system and a lower cost of energy. For example, the recent work by Ingenhoven et al. [28] for a packed bed thermal storage operating in combination with a SEVR, to supply hot air at temperatures of >1000°C, highlighted that the addition of only 10% particle mass loading can lower *LCOH* by 20% relative to the air-only

case. However, no information has been reported of the sensitivity of the system level performance to the progressive increase of the particle mass loading. Furthermore, there is no data available about the effect of this parameter varied in combination with a range of other parameters including mass flow rate of air, thermal storage capacity and solar multiple, for the relative tradeoffs between the performance of the receiver and thermal storage sub-systems while operating in a combined CST system. Hence, there is a need to understand the performance of a complete CST plant to a range of these parameters considering the real-time interaction between the receiver and coupled storage. This will help to find out whether there is a critical value of these parameters, for any given conditions. The present assessments aim to meet these needs by quantifying the thermal outputs and *LCOH* for combined variations in these parameters.

Considering the needs identified above, the overall objective of this paper is to advance the understanding on the system level performance of a windowless vortex-based high-temperature refractory-lined suspension flow solar particle receiver operating in combination with a packed bed sensible thermal storage and combustion backup, to supply reheated air to thermochemical processes at 1100°C. More specifically, the first aim is to provide new understanding of the coupled influences between the performance of the receiver and storage sub-systems on that of the combined CST system for variations in the particle mass loading, air mass flow rate, solar multiple and thermal storage capacity. That is, it aims to understand the influence of these parameters on the thermal response of the receiver and storage considering real-time interaction between them, and on the solar share. The second aim is to provide new knowledge about the levelized cost of the solar component of the energy supplied to the downstream process, by employing a consistent set of cost correlations for both capital and operating costs, for different combinations of the system parameters. It specifically aims to investigate of the dependence of particle mass loading on the cost of energy. The third aim is to understand the sensitivity of *LCOH* to variations in the costs of the heliostats, central receiver, thermal storage, and transmission line varied in the range of ±60%. This assesses the economic viability of the present CST system by comparing the cost of this option with other renewable options, especially with the reported costs of green hydrogen.

2. Materials and methods

2.1. System description

Figure 1 presents schematic diagrams of the combined CST system and two different configurations of the receiver sub-system analyzed here. These configurations of the receiver sub-system are described in section 2.3. In the combined CST system, the hot air from the receiver sub-system is used to charge one of the thermal energy storage (TES) devices with the lowest state of charge. Here the state of charge means the available charged energy in the storage device. That is, a fully charged storage has the highest state of charge. Once a TES device is fully charged, it is discharged to the process while hot air from the receiver is used to charge another device. To keep the charging and discharging cycles separate, the warm air from the thermal storage is used to preheat the ambient air in a heat exchanger, rather than being returned to the receiver. This allows the operation of the windowless receiver at atmospheric pressure, to mitigate particle egress through the open aperture. It also allows the system to operate with only low-temperature fans. The need to direct the hot air to the storage system, rather than directly to the plant, is driven by the need to avoid sending carry-over particles from the receiver to the industrial process since sending it through the packed bed storage system also serves as the second stage of the particle filter, along with energy storage. The system under evaluation also employs a backup burner to allow the continuous supply of thermal energy to the process at a desired steady temperature – chosen here to be $1100^{\circ}C$.

The Simulink environment was used to develop a complete system model using transient heat and mass transfer sub-models written in MATLAB [29], except for that of the heliostat field subsystem for the collection of the solar resource. The heliostat field sub-system was designed and modeled separately to compute the optical input to the solar receiver with the present geometric dimensions of a 50MW$_{th}$ system, as described below. This relatively small thermal scale was chosen because of the limitations of the scales at which high temperature CST systems have been demonstrated, and operation at these smaller scales is a necessary first step before going to larger scales in future work.

The integrated Simulink model is comprised of different blocks with model equations for each component, which interact with each other during the operation. An illustration of the Simulink model is provided in the supplementary data file. A detailed description of the

receiver subsystem and integrated system has been provided previously [24, 28]. Here individual sub-systems of the integrated CST system are described briefly.

2.2. Heliostat field sub-system

The heliostat field system was modeled separately to calculate the concentrated solar radiation at the present design of SEVR cavity aperture. The radially staggered heliostat field was optimized using COBYLA from the NLOpt library [30]. The solar thermal input, $\dot{Q}_{sol,helio}$, to the receiver aperture was calculated using CSIRO's Heliosim software [31] and Monte Carlo ray tracing with optimized radially staggered heliostat field layout. Solar Direct Normal Irradiance (DNI) data from Learmonth, Australia [32] was used to compute the optical thermal input directed into an open aperture cavity, located at the top of a tower, for 15-minute time steps over a year.

2.3. Receiver sub-system

A refractory-lined cylindrical cavity receiver termed as Solar Expanding Vortex Receiver (SEVR) [33, 34] (Fig. 2) was considered here. The receiver cavity walls were assumed to be made with three layers comprising the inner ceramic refractory lining of fireclay, middle high-temperature insulation, and outer protective steel shell. The geometric parameters of the receiver are given in Table 1. The transient mathematical model of Rafique et al. [24, 35] was extended to calculate the thermal outputs of the receiver at every time step. This model has been previously verified to show that the response of the system to various parameters is consistent with available data and expectations [24, 35]. A summary of different validation cases, reported previously, is listed in Table 2.

The inlet temperature to the receiver was calculated for each time step, accounting for the variations in the returned temperature from the integrated thermal storage. This return air is used to pre-heat cold-ambient air with an air-to-air heat exchanger. This indirect heating process is required, even though the heat exchanger constitutes an exergy loss, in part because it is the most appropriate place in the circuit to position the fan and, in part, because it provides a way to maintain the device, which is open to the atmosphere, at atmospheric pressure.

2.3.1. Configurations of the receiver sub-system

Two different configurations of the receiver sub-system analyzed are as follows:

- **M1**: This configuration comprises of a suspension flow particle receiver, cyclone separator, heat exchanger, particle feeder, and fans. Air, together with the suspended particles that are used to enhance radiation adsorption, is used as the heat transfer medium in the receiver, with a range of mass flow rates varied to achieve output temperatures between $800 - 1500^oC$. Where used, the hot particles are then separated from the hot air and used to further preheat the incoming air that is already warm before it enters the receiver. The hot air is then directed to the storage sub-system.

- **M2**: This configuration comprises of an air-only receiver, with a heat exchanger and fans but without any of the particle-feeding or handling components. A range of air mass flow rate values are used, corresponding to variations in the output temperature between $800 - 1200^oC$.

2.4. Thermal storage sub-system

The thermal sub-storage system consists of a set of thermocline packed-bed storage devices filled with alumina balls, placed inside a cylinder insulated using fire bricks and ceramic fibers (Fig. 3). The simplified one-dimensional model of Ingenhoven et al. [36] was used to estimate the thermal performance of the storage device, in a way that accounts for the dominant source of losses whilst still being computationally tractable for a system model. This model has been previously validated with the available data [36], summarized in Table 2. A detailed analysis of the storage system was presented previously [28]. From the storage system, hot air is fed via refractory-lined pipes to the process.

Table 1. Geometric parameters and operating conditions.

|	Input parameter	Symbol	Units	Reference value	Sensitivity variations
Solar receiver	Cavity diameter	D_c	m	8	-
	Diameter ratio of aperture to cavity	D_{ap}/D_c	-	0.55	-
	Ratio of length to cavity diameter	L/D_c	-	1.6	-
	Inner refractory thickness	Δr_1	mm	100	-
	Insulation thickness	Δr_2	mm	100	-
	Receiver mass flow rate of air	$\dot{m}_{a,rec}$	kg/s	50	$30 - 100$
	Particle loading ratio	$R_p = \dot{m}_{p,rec}/\dot{m}_{a,rec}$	%	10%	$0 - 40\%$
	Particle diameter	d_p	μm	120	-
Thermal storage	Number of regenerators	N_s	-	2	-
	Minimum charging temperature	$T_{ch,min}$	°C	850	-
	Minimum discharging temperature	$T_{dis,min}$	°C	600	-
	Total storage capacity	H	hours	8	$4 - 16$
Process	Process input temperature	$T_{a,pro,in}$	°C	1100	-
	Process return temperature	$T_{a,pro,out}$	°C	600	-
	Solar multiple	SM	-	2.5	$2.5 - 5$
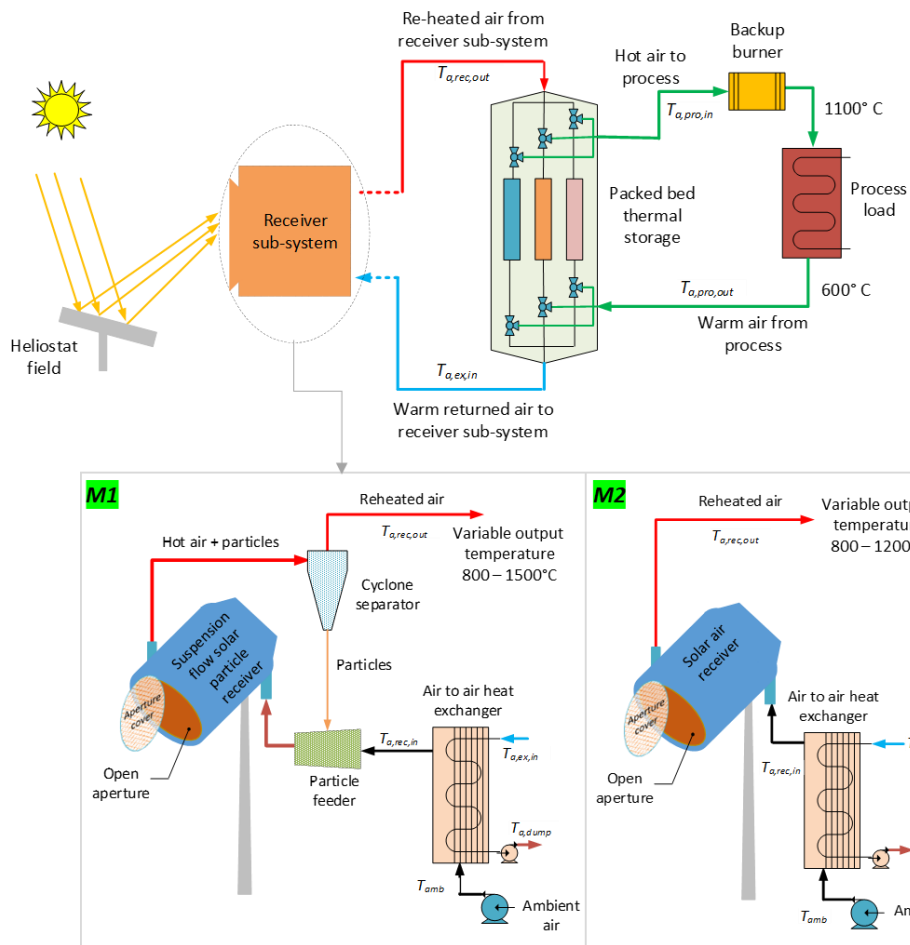
Figure 1. Schematic diagram of the system to deliver a steady supply of hot air from a suspension flow solar particle receiver and packed-bed sensible thermal storage with combustion back-up. Here two different configurations of the receiver sub-systems are shown, **M1)** air receiver with suspended particles and with a fixed mass flow rate allowing variations in the output air temperature between 800 – 1500°C; and **M2)** air-only receiver, here operated with a range of mass flow rates allowing variations in the output temperature between 800 – 1200°C.
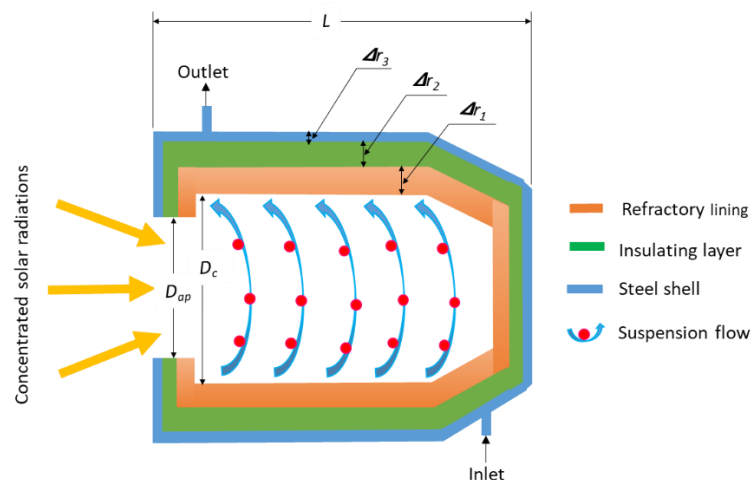
Figure 2. The notation used to describe the multi-layered refractory-lined solar suspension-flow particle receiver.
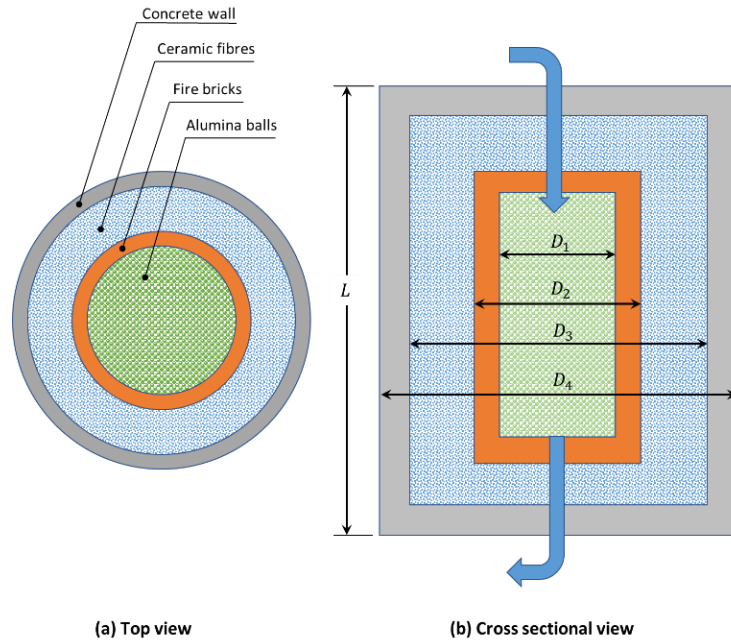
(a) Top view **(b) Cross sectional view**

Figure 3. An illustration of the packed bed thermal energy storage system modelled here.

Table 2. The details of different cases assessed for the validation of the present sub-models of suspension flow solar particle receiver and packed bed thermal storage. Further descriptions of each case were reported previously [24, 36].

Sub-system models	Inputs		Outputs compared (X_{mod})	Data available for comparison (X_{ref})	Discrepancy $\lvert X_{ref} - X_{mod}\rvert / X_{ref}$	
	Parameters	Sensitivity variations			Min (%)	Max (%)
Suspension flow solar particle receiver	Inlet air mass flow rate	30 – 101 kg/s	Air temperature	CFD simulations (50 MW$_{th}$ SEVR) [37, 38]	2	5
			Particle temperature		16	23
			Wall temperature		0.4	9
	Inlet temperatures	500 – 700°C	Air temperature		1	6
			Particle temperature		17	19
			Thermal efficiency		2	8
	Cavity wall temperature	300 – 2100°C	Wall losses	50 MW$_{th}$ cylindrical cavity reactor [39]	1	5
			Convection losses		2	7
			Re-radiation losses		1	7
	Aperture to cavity diameter	0.45 – 1	Heating time		3	5
			Wall temperature		4	12
Packed bed thermal storage	Storage height	0 – 1.2m	Storage temperature	Lab scale high temperature rock bed thermal storage system [40]	2	7
	Charging time	0 – 3h			3	12

3. Solution methodology

Figure 4 presents a logic diagram of the control system described above (Fig. 1). The receiver aperture is considered to be open only when solar resource is above a minimum threshold. The flow of air and particles is continued after the aperture is closed until the output temperature of the air falls below a minimum acceptable value allowing the receiver to operate after sunset due to the thermal mass of refractory. The hot air from the receiver sub-system is used to charge the thermal energy storage device, which is discharged to the process via refractory-lined pipes. Additional heat is provided using a backup burner to maintain a steady supply of hot air at 1100°C, as required for the process, for periods where the energy supplied by the CST system is insufficient. A detailed description of the receiver operating strategy during start-up, turndown and shutdown was reported previously [24], whereas the charging and discharging strategy of the sensible thermal storage was described elsewhere [36].

Figure 5 presents a schematic diagram with the terminologies used to describe the heat flows through the CST system. The output temperature of hot air from the receiver sub-system, $T_{a,rec,out}$, was calculated at each time step i, together with the mass flow rate into the receiver, $\dot{m}_{a,rec}$, and specific heat capacity, c_{pa}, to obtain the useful thermal energy output from the receiver, $\dot{Q}_{a,rec,out}$, as follows:

$$\dot{Q}_{a,rec,out} = \dot{m}_{a,rec} C_{pa}(T_{a,rec,out} - T_{a,rec,in}) \qquad . \tag{1}$$

The hot air from the receiver sub-system was transported to the thermal storage where it charges a discharged (fully or partially) packed bed. The fully charged bed was connected to the process side via insulated pipes. The thermal power in the air from the storage to the transmission pipes, $\dot{Q}_{a,st,out}$, and from the transmission pipes to the process, $\dot{Q}_{a,pro,in}$, was calculated as follows:

$$\dot{Q}_{a,st,out} = \dot{Q}_{a.st,in} - \dot{Q}_{st,loss} \qquad , \tag{2}$$

$$\dot{Q}_{a,pro,in} = \dot{Q}_{a,st,out} - \dot{Q}_{pipe,loss} \qquad , \tag{3}$$

where, $\dot{Q}_{st,loss}$ and $\dot{Q}_{pipe,loss}$ are the storage and pipe losses, respectively. The diameter of the transmission pipe and insulation thickness, with an assumed distance of 1000m between

thermal storage and process, were optimized to achieve the transmission pipeline effectiveness of 95% as described the previous work [28, 41].

The efficiency of the receiver, η_{rec}, and of the thermal storage, η_{st}, was estimated using equations 4 and 5, respectively.

$$\eta_{rec} = \frac{\dot{Q}_{a,rec,out}}{\dot{Q}_{sol,helio}} \qquad , \qquad (4)$$

$$\eta_{st} = \frac{\dot{Q}_{a,st,out}}{\dot{Q}_{a,rec,out}} \qquad , \qquad (5)$$

Here $\dot{Q}_{a,rec,out}$ is the useful thermal gain of the receiver, $\dot{Q}_{sol,helio}$ is the optical thermal input introduced into the receiver aperture from the heliostat field, after accounting for the optical losses associated with the solar collection system, and $\dot{Q}_{a,st,out}$ is the thermal output from the thermal storage to the transmission pipeline.

The thermal energy supplied by the CST system, $\dot{Q}_{a,pro,in}$, relative to the process load demand, $\dot{Q}_{demand}$, was used to calculate the solar share, SS, of the plant as follows:

$$SS = \frac{\dot{Q}_{a,pro,in}}{\dot{Q}_{demand}} \qquad . \qquad (6)$$

The solar multiple, SM, taken from the previous study [28], is defined as follows:

$$SM = \frac{\dot{Q}_{des,th}}{\dot{Q}_{demand}} \qquad . \qquad (7)$$

Here, the dimensions of the SEVR were chosen for a designed thermal capacity of $\dot{Q}_{des,th}$ = 50MW$_{th}$ at peak conditions and the process side heat demand was varied to simulate different values of solar multiple. Note that, this does not correspond to a true assessment of the effects of thermal scale, since the SM was defined for different process demands with a fixed size of the solar plant. This is because of the requirement of different upscaled receiver sub-system designs to be used with a range of heliostat field sizes, as also explained previously [28, 36]. Further work is needed to address the concept of upscaling the SEVR by considering the wider range of issues.

The economic evaluation of the CST system described above was performed by employing a consistent set of cost correlations for both capital and operating costs. Table 3 presents the

estimated costs of each component. The detailed calculations of these costs have been reported previously [28]. The economic evaluation was performed in terms of levelized cost of solar heat (*LCOH*) which is determined as follows:

$$LCOH = \frac{\alpha_f C + OM}{\dot{Q}_{a,pro,in}} \qquad .$$
(8)

Here *C* is the total capital investments, *OM* is the annual operating and management costs, and $\dot{Q}_{a,pro,in}$ is the annual thermal energy supplied to the process by the CST system. The annuity factor, α_f, is given as a function of the discount rate, *d*, and project lifetime in years, *n*.

$$\alpha_f = \frac{d.(1+d)^n}{(1+d)^n - 1} \qquad .$$
(9)

Here the estimated *LCOH* is only for the solar component of the energy and the cost of combustion backup is explicitly excluded from the calculations, to avoid confusing the cost of solar with that of the backup source of fuel (fossil or renewable).
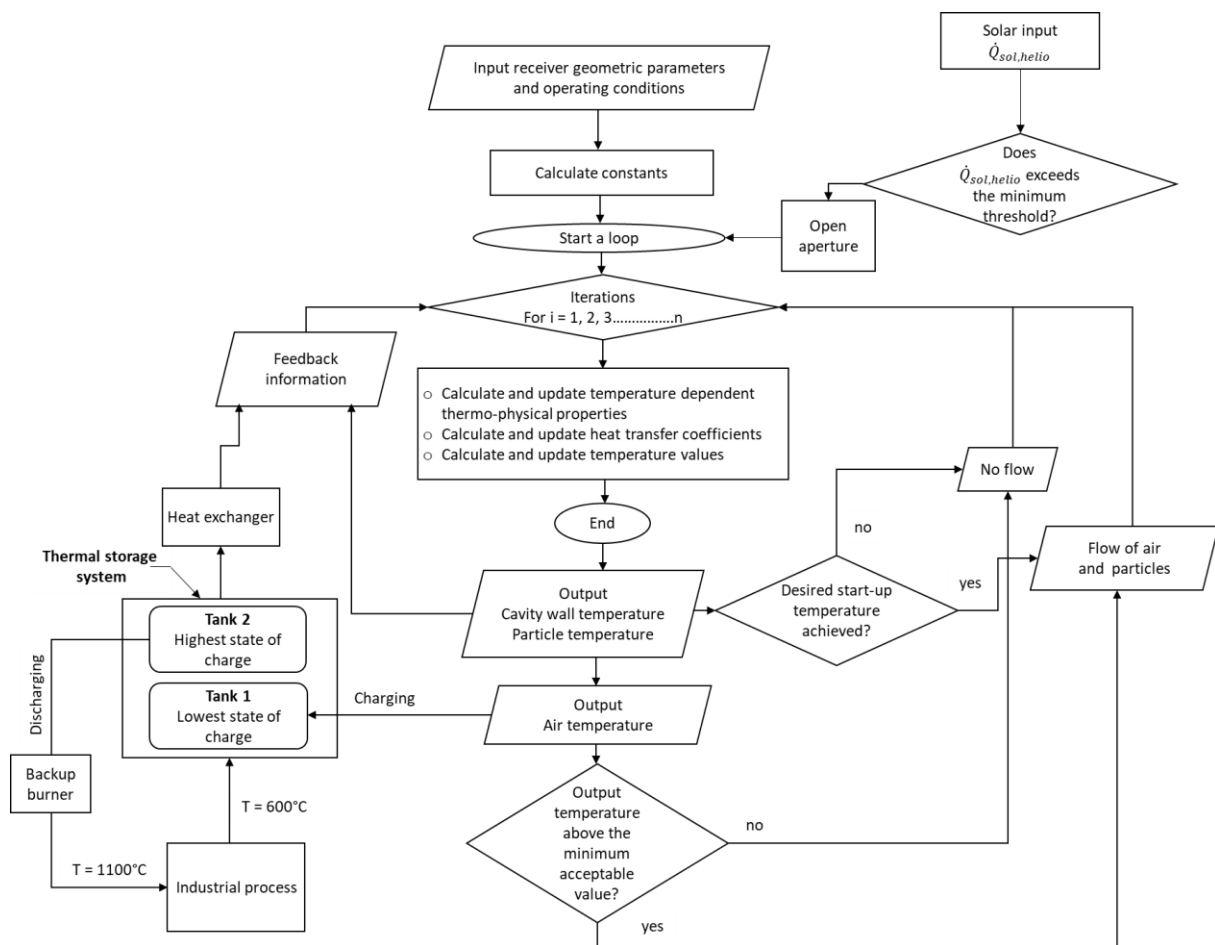

Figure 4. Logic diagram of the control system used to achieve a steady outflow at constant air temperature from a transient solar thermal input.
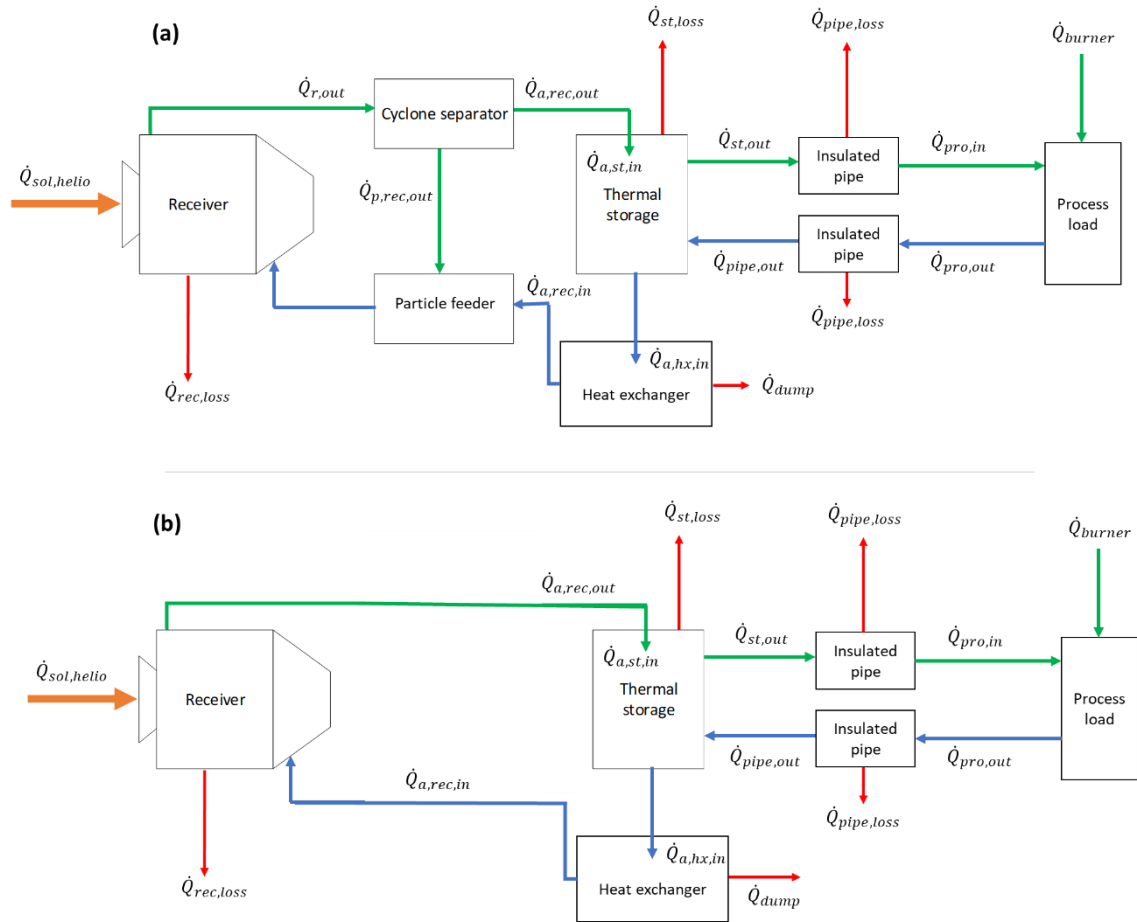
Figure 5. Schematic diagrams of the heat flow through the hybrid solar thermal-combustion system, with **(a)** suspension flow particle receiver sub-system and **(b)** air-only receiver sub-system.

Table 3. Estimated costs for the present configuration of the CST system. The detailed calculations for each component were presented previously [28].

Cost component	Reference value	Units
Solar field and tower	24.96 million	US$
Receiver sub-system (no particle)	8.65 million	US$
Receiver sub-system (with particles)	9.26 million	US$
Thermal storage sub-system	0.04 million	US$/MWh
Transmission pipeline	17.25 million	US$
O&M	2% of total capital cost	US$/year
EPC and owner cost	30% of total capital cost	US$
Lifetime	30	years
Discount rate	7	%

4. Results and discussion
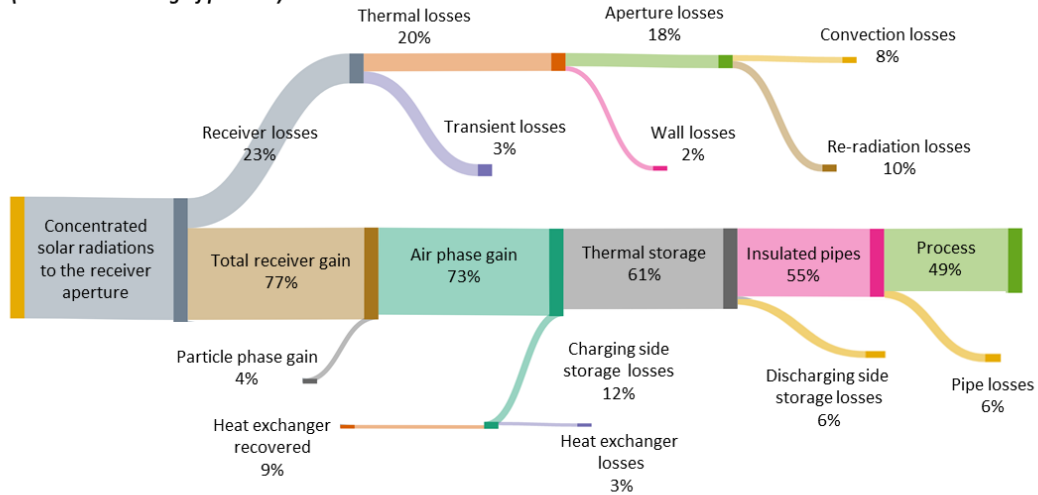
4.1. Sankey diagram of CST system

Figure 6 presents Sankey diagrams illustrating the energy flows within the two configurations of integrated CST system shown in Fig. 5, namely that with (*M1*) and without (*M2*) a suspension of particles in the receiver, for the reference conditions listed in Table 1. The data shown is for the combined system from the concentrated solar energy to the receiver aperture to the downstream process. The heliostat field system, which is not shown here, was modeled separately giving an annual solar field efficiency of ~59% [28].

For configuration *M1*, with a 10% mass loading of suspended particles, 77% of the incident energy through the aperture of the receiver cavity is captured by the particle-laden flow with 4% carried by the particle phase. This configuration is calculated to provide 49% of the thermal input to the downstream process, with losses of 23 and 18% associated with the receiver and thermal storage sub-systems, respectively. Of the 23% annual receiver losses, 20% are in the form of thermal losses including aperture losses (18%) and wall losses (2%).

In contrast, the system with receiver configuration *M2* (without particles) converts only 38% of incident thermal energy to useful energy, with annual losses of 36 and 21% associated with the receiver and thermal storage sub-systems, respectively. This shows that the addition of particles to adsorb the radiation delivers a substantial net benefit, despite the added complexity and additional components needed to introduce them to the system. In the following, a parametric study is also used to address the sensitivity of system performance to a progressive increase in particle mass loading.

Overall, these results highlight the benefit of suspended particles for a better trade-off between the performance of individual sub-systems. That is, the addition of suspended particles not only improves the thermal performance of the receiver, due to enhanced energy adsorption in the receiver cavity, it also results in a higher thermal storage charging temperature which is required for the better performance of the present configuration of the storage system, as also highlighted previously [28].
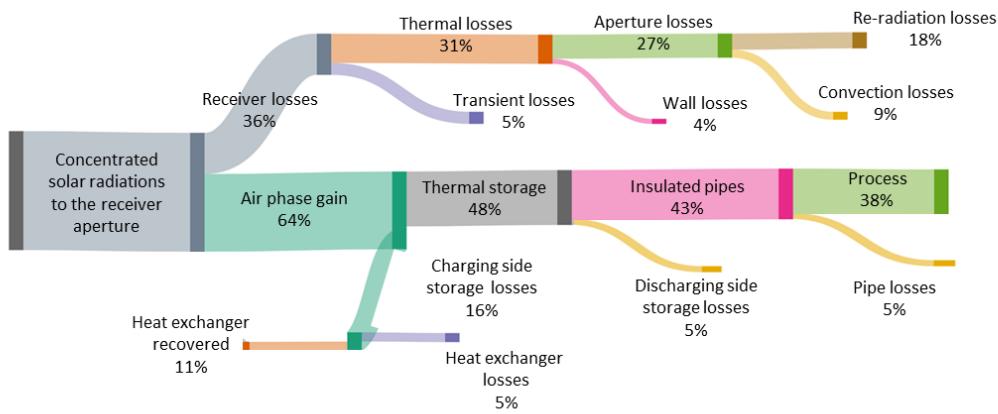
Figure 6. Sankey diagrams of the annual energy flows relative to the thermal input into the receiver for the reference cases of operation for two configurations of integrated CST system with suspension flow solar particle receiver (*M1*) and air-only receiver without suspended particles (*M2*), together with the packed bed thermal storage, to supply reheated air to a downstream thermochemical process. The other reference conditions are listed in Table 1.

4.2. Time history of the interaction between sub-systems

Figure 7 presents the calculated values of air temperatures and thermal energy flows across different components of the integrated CST system, and receiver thermal losses, for different values of inlet air mass flow rate to the receiver, $\dot{m}_{a,rec}$, with and without the addition of particles for a short-term time series of solar input at the site of Learmonth (1st January 2017). The other reference conditions are listed in Table 1.

It can be observed that an increase in the value of $\dot{m}_{a,rec}$ has the effect of decreasing the air temperature at the receiver outlet, $T_{a,rec,out}$, by an energy balance. This, in turn, results in lower thermal losses and higher thermal gain by the receiver, $\dot{Q}_{a,rec,out}$, which is consistent with the expectation. For example, the calculated instantaneous peak value of $T_{a,rec,out}$ is decreased by 26 and 33% when $\dot{m}_{a,rec}$ is increased from 30kg/s to 50 and 70kg/s, respectively. However, the resulting instantaneous peak value of $\dot{Q}_{a,rec,out}$ is increased by 9 and 15% for the same increase in $\dot{m}_{a,rec}$. However, it should be noted that, despite a higher $\dot{Q}_{a,rec,out}$, with an increase in $\dot{m}_{a,rec}$, the receiver sub-system does not typically achieve $T_{a,rec,out}$ above the demand value with a higher value of $\dot{m}_{a,rec}$, due to poor solar irradiation during the winter season or cloudy days. Hence, there is always a trade-off between the thermal performance and required output temperature from the system.

It can also be seen that the addition of particles increases the value of $T_{a,rec,out}$ by lowering the re-radiation losses. This is attributed to the increased radiation adsorption by the particles due to the increase of surface area and improved heat transfer within the receiver cavity, and then to the storage system. It should be noted that the increase of $\dot{m}_{a,rec}$ decreases the residence time within the receiver cavity, thereby reducing the corresponding thermal energy transferred to the air phase. This results in a relative decrease in the benefits of particle addition with an increase in the value of $\dot{m}_{a,rec.}$ For example, $T_{a,rec,out}$ is calculated to increase by 23, 12 and 8% with the addition of only 10% mass of particles to the air stream for $\dot{m}_{a,rec}$ = 30, 50 and 70kg/s, respectively. This effect provides further motivation for the assessment of the quantitative benefits offered by the progressive increase in the particle mass loadings, varied in combination with other key parameters (Section 4.3).

Figure 8 presents the influence of the thermal storage capacity, for different values of the inlet mass flow rates, on the calculated time history of the returned air temperature to the

receiver sub-system from the thermal storage, $T_{a,rec,in}$. It can be observed that a higher value of $\dot{m}_{a,rec}$ requires a larger storage size for the effective utilization of the receiver useful thermal gain. For example, a smaller storage size at a higher value of $\dot{m}_{a,rec}$ results in hot air being returned to the receiver sub-system. For $\dot{m}_{a,rec}$ =70kg/s, the peak value of the returned temperature from the coupled storage, $T_{a,rec,in}$, is increased by 38% from 478 to 770°C, as the storage size is decreased from 16 to 4h.

In summary, these findings show a strong dependence of the overall system performance and its optimization, to the variation in different parameters, on the interaction between the individual sub-systems. This further highlights the importance of considering real-time interaction and the trade-off between the sub-systems, rather than assuming a steady thermal input for individual components operating in isolation, while optimizing these systems for a specific application.
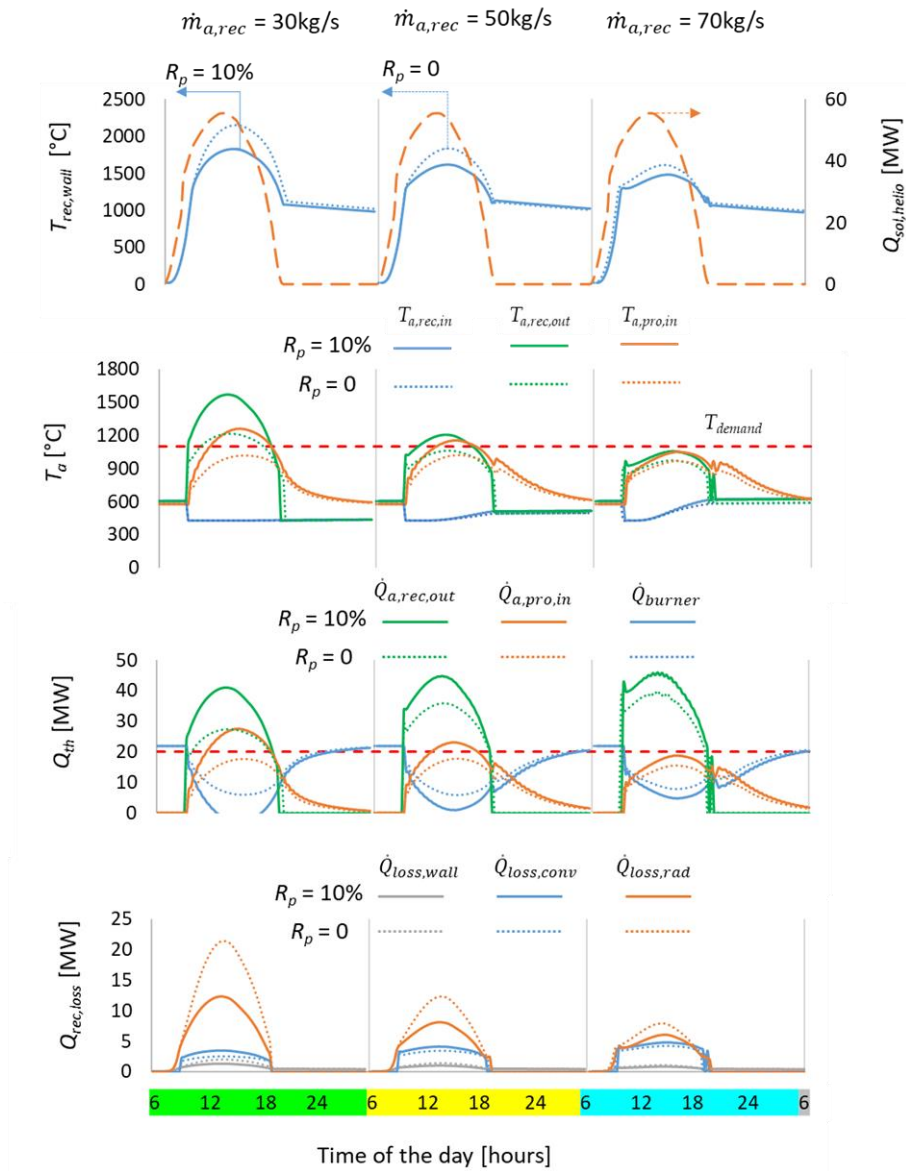
Figure 7. Influence of the mass flow rate of inlet air, $\dot{m}_{a,rec}$, with and without the addition of particles on the calculated time history of the air temperatures, energy flows through the CST system and receiver thermal losses, during the summer season (1st January 2017) at the site of Learmonth. The other reference conditions are listed in Table 1.
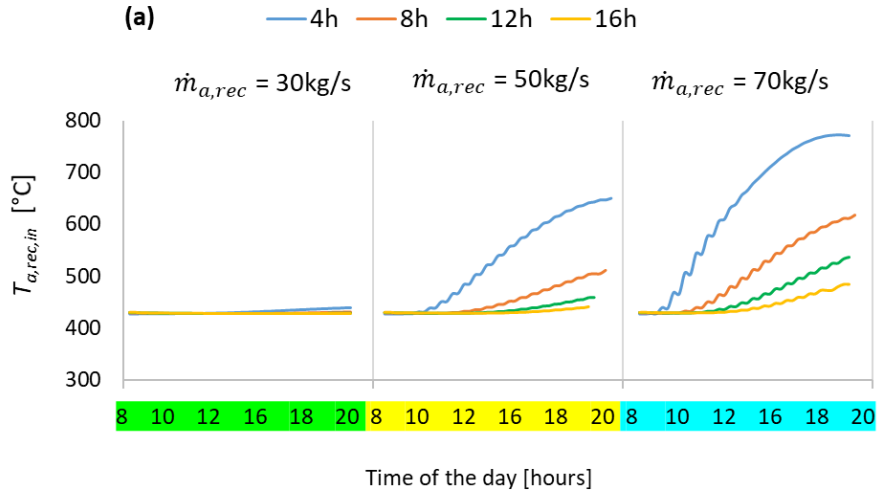
Figure 8. Influence of the thermal storage capacity for different values of the inlet mass flow rates on the calculated time history of the returned air temperature to the receiver sub-system from the thermal storage, $T_{a,rec,in}$, during the summer season (1st January 2017) at the site of Learmonth. The other reference conditions are listed in Table 1.

4.3. Annual performance

Figure 9 presents the calculated annual averaged values of receiver efficiency, η_{rec}, thermal storage efficiency, η_{st}, solar share, *SS*, and levelized cost of solar heat, *LCOH*, for a range of particle mass loadings, R_p, with a range of air mass flow rates into the receiver, $\dot{m}_{a,rec}$. The other reference conditions are listed in Table 1.

It can be observed that the system performance increases with the increase in the value of particle mass loading, which is expected. However, it can be noted that the quantitative benefits of the particle suspensions within the air stream are different for each value of $\dot{m}_{a,rec}$. For example, a system with $\dot{m}_{a,rec}$ = 30kg/s is calculated to have the thermal performance of the receiver sub-system increased by 22%, 30% and 36% as the R_p is increased from 0 to 10%, 20% and 40%, respectively. Whereas, the thermal performance of the receiver sub-system with $\dot{m}_{a,rec}$ = 100kg/s is calculated to increase by only 7%, 11% and 15% for the same increase in R_p.

The increase in the particle mass loadings also increases the efficiency of the thermal storage system. This is due to enhanced radiation adsorption by introducing particles into the air stream resulting in higher charging temperature which increases the efficiency of the present storage system. For example, η_{st} is calculated to increase by 10, 15, 17 and 23% with the

addition of 40% mass of particles to the air stream for $\dot{m}_{a,rec}$ = 30, 50, 70 and 100kg/s, respectively.

It can also be seen that there is an optimum value of $\dot{m}_{a,rec}$ for the present receiver geometry at which progressive increase in the mass loading of suspended particles continues to bring a better performance of the overall CST system, and increases its economic feasibility. However, the relative magnitude of these benefits is lower as the value of R_p is increased. Here a system with $\dot{m}_{a,rec}$ = 50kg/s, R_p = 40%, SM = 2.5 and H = 8h is calculated to give an overall solar share which is 43% higher than for the air-only configuration (*M2*). The *LCOH* for this configuration is also about 38% lower than that for the configuration *M2*, despite a ~7% additional cost of the particle management system.

In summary, the overall results indicate that the addition of particles has a positive impact on the annual performance of the combined CST system to reach a higher solar share at a lower overall *LCOH*. This is attributed to the increased radiation adsorption by the particle suspensions within the air stream and the increase in the effectiveness of the heat transfer mechanisms within the receiver cavity due to their high surface area per unit mass. Note that it is also important to address the challenges associated with the egress of particles for the studied range of particle mass loading. This is beyond the scope of the present investigation, which only aims to assess the sensitivity of system performance to particle mass loading.
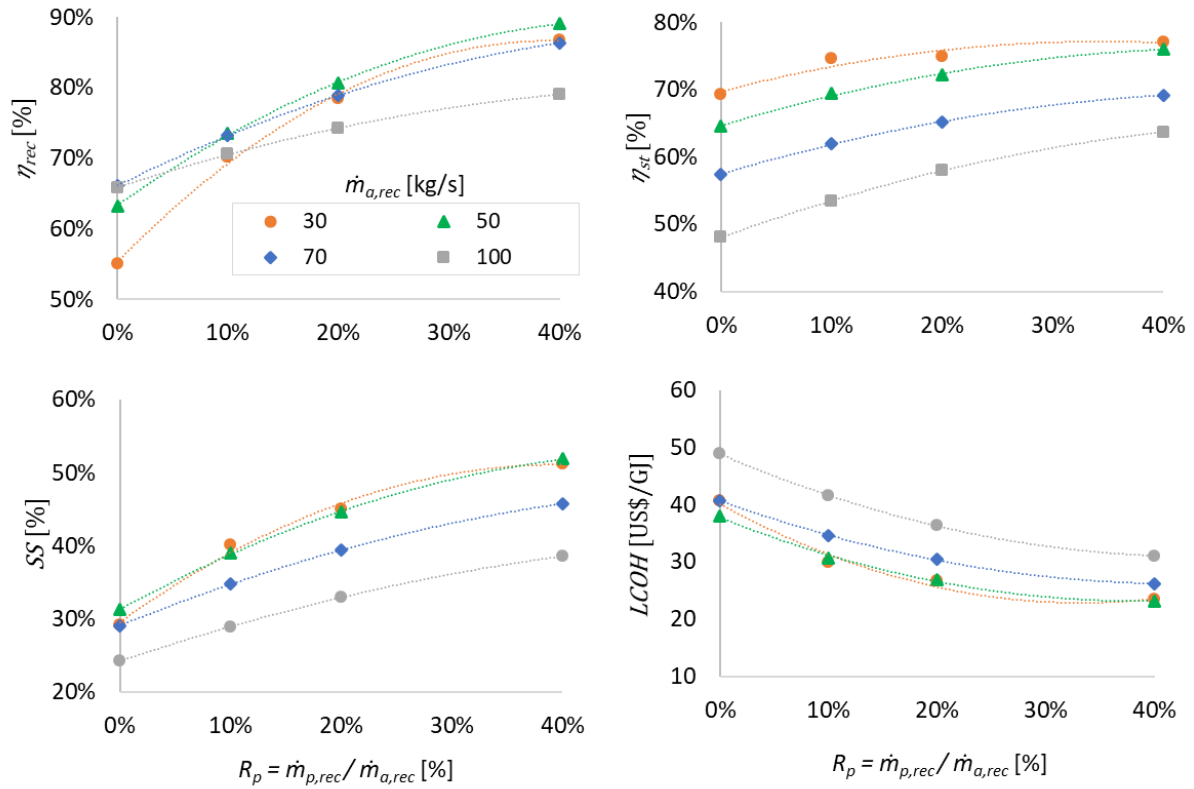
Figure 9. Calculated annual averaged values of receiver efficiency, η_{rec}, thermal storage efficiency, η_{st}, solar share, *SS*, and levelized cost of solar heat, *LCOH*, for a range of a particle mass loading, R_p, and air mass flow rate into the receiver, $\dot{m}_{a,rec}$. The other reference conditions are listed in Table 1.

Figure 10 presents the calculated annual averaged values of receiver efficiency, η_{rec}, thermal storage efficiency, η_{st}, solar share, *SS*, and levelized cost of solar heat, *LCOH*, for a range of thermal storage sizes, *H*, and solar multiples, *SM,* with R_p = 0, 10% and 40*%*. In general, it can be seen that the increase in storage capacity, for each value of *SM*, causes an increase in η_{rec} and a reduction in η_{st}. These changes are more significant for R_p = 40% when *SM* ≥ 3.5. For example, η_{rec} is calculated to increase by 3%, 18% and 38% when thermal storage capacity is increased from 4 to 16h for the case of *SM* = 2.5, 3.5 and 5, respectively. This improvement in the receiver thermal performance also results in up to 16% decrease in *LCOH* for the same increase in the thermal storage capacity, despite added cost of additional storage devices. The increase in η_{rec} with storage capacity is attributed to the dependence of $T_{a,rec,in}$ on storage capacity for each value of *SM*. These results indicate that it is important to carefully size a thermal storage system, for each value of *SM*, to better utilize the thermal gain of the receiver.

It can also be seen that the improvement in the receiver thermal performance due to suspended particles offers significant economic benefits, along with a higher solar share. For example, a system with 40% mass of suspended particles in the air stream is calculated to give a solar share of 75% which is 44% higher, at a 40% lower $LCOH$, relative to the air-only case. However, it is important to note that these trends are highly non-linear and an increase in particle mass loading only offers some significant benefit when used in combination with the correct storage capacity for each condition. For the case with only 10% mass of suspended particles, the increase in thermal storage capacity does not have a significant impact on SS (only by less than 2%). While for the case with R_p = 40%, SS is calculated to increase by some 16% points, with 14% lower $LCOH$, when thermal storage capacity is increased from 4h to 16h. This further highlights the importance of effective utilization of available resources and optimizing the system as a whole with combined variations in key parameters, rather than of the individual components.

Overall, these results further indicate the potential of this solar thermal suspension flow technology to configure for higher solar shares, required to meet the carbon reduction targets, at a relatively lower increase in the cost of solar energy. This is significant to decarbonize high-temperature thermal processes.
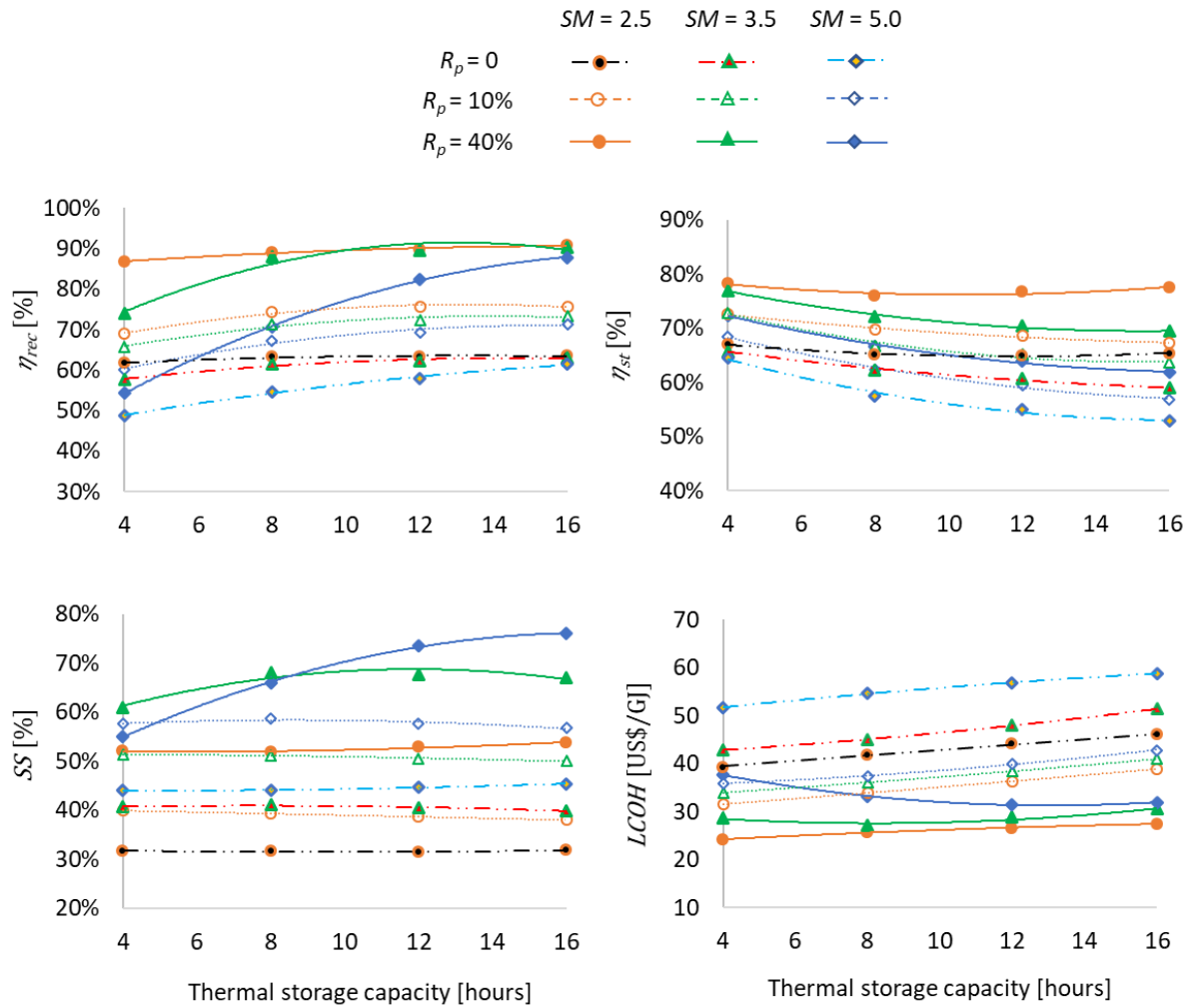
Figure 10. Calculated annual averaged values of receiver efficiency, η_{rec}, thermal storage efficiency, η_{st}, solar share, *SS*, and levelized cost of solar heat, *LCOH*, for a range of thermal storage capacity, *H,* and solar multiples, *SM*, with R_p = 0, 10% and 40%. The other reference conditions are listed in Table 1.

4.3.1. Sensitivity to the component's costs

Figures 11 and 12 show the sensitivity of *LCOH* for the system with R_p = 40%, configured to achieve *SS* = 50% and 75%, to ±60% variations in the CAPEX of the system components including solar field, central receiver, thermal storage, and transmission pipeline.

Figure 11 shows the influence of the variations in the component's costs varied individually, on *LCOH*. It can be observed that the effects of the solar field cost on *LCOH* are most obvious followed by the transmission pipeline, while other parameters have comparatively less important influences. For example, the calculated influence of the cost of the transmission pipeline, receiver and thermal storage on the overall *LCOH* is 31%, 62% and 76% lower than that of the cost of the solar field, respectively, as shown using best-fit equations in Fig. 11a.

Figure 12 shows the influence of the combined variations in the CAPEX of all system components, on *LCOH*. Overall, the present system demonstrates an encouraging future potential with an expected drop in the components costs with allowance for technology development and mass production, considering the SunShot [42] initiative targets to reduce the solar energy cost by 50% until 2030. For the conditions assessed here, when the cost of heliostats, central receiver, thermal storage, and transmission pipeline is reduced by 20%, the *LCOH* is reduced to 18 and 26 US$/GJ with *SS* = 50% and 75%, respectively. This is comparable to the current cost of green hydrogen production, which is around 2.5 – 6 USD/kg (21 – 51 USD/GJ) [28, 43]. It should be noted that there is a strong potential for further cost reductions, with the technological improvements and a decrease in the discount rate. For example, it can be observed (from Fig. 12) that the cost of solar energy is calculated to drop further by ~17% with an expected drop in the discount rate from 7 to 5%.
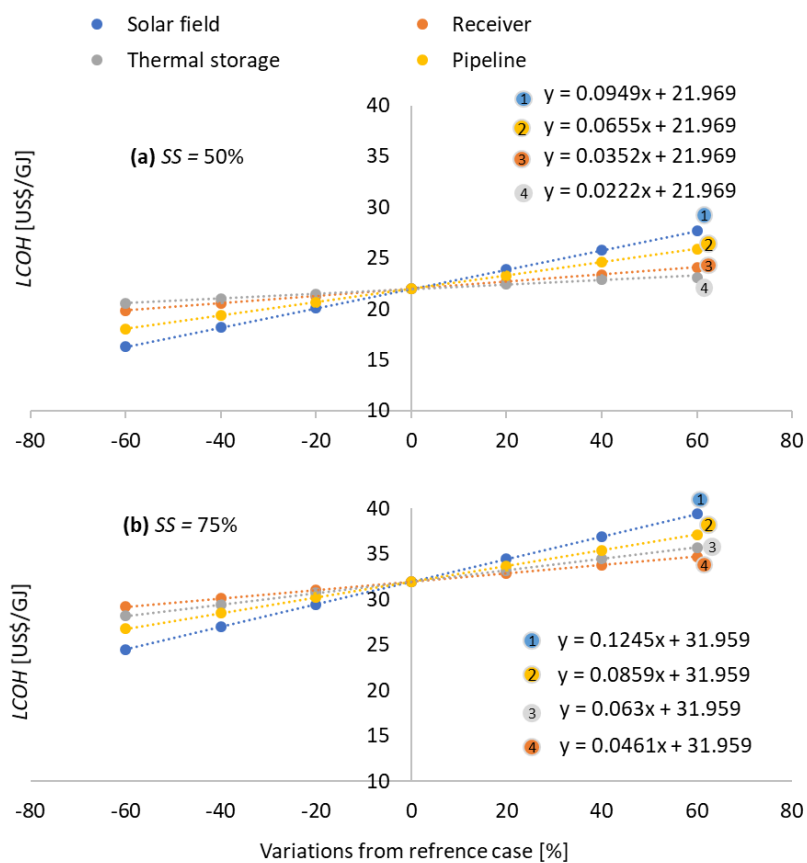

Figure 11. Sensitivity analysis of the influence of the specific costs of the solar field, central receiver, thermal storage, and transmission line varied in the range of ±60%, on the overall *LCOH* for two combinations of the present system to achieve *SS* = 50 and 75% with R_p = 40%.
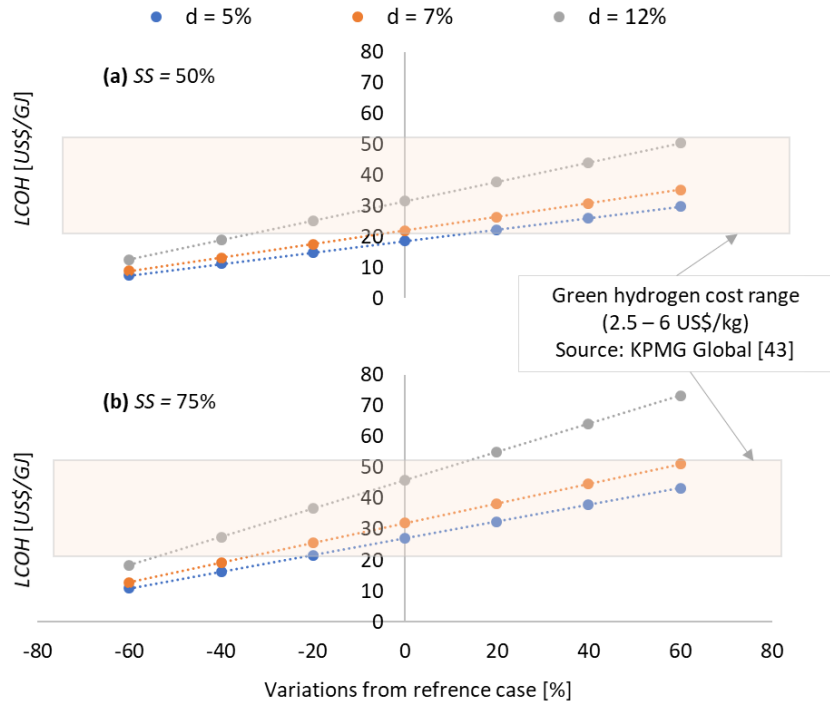
Figure 12. Sensitivity analysis of the combined influence of the components costs varied in the range of ±60%, on the overall *LCOH* for the present system configured to achieve *SS* = 50% and 75% with R_p = 40%, and discount rate (d) of 5%, 7% and 12%.

5. Conclusions

The key outcomes of the current study are as follows:

- The particle mass loading has a strong influence on the thermal performance of the CST system, and its economic feasibility. For the reference case assessed here, the thermal performance of the combined system is calculated to improve by 43% with the addition of 40% mass loading of particles into the air stream relative to the air-only case. This improvement in thermal performance translates into 38% drop in the *LCOH* and 43% increase in solar share.

- There is an optimum value of air mass flow rate which offers the highest benefits of particle addition, for a given geometry of the receiver. For the present configuration of the particle-laden air re-heating system, the addition of only 10% mass of particles results in 22% increase in η_{rec} when $\dot{m}_{a,rec}$ = 30kg/s. However, η_{rec} is calculated to increase by only 7% for $\dot{m}_{a,rec}$ = 100kg/s.

- A smaller storage results in a higher returned temperature to the receiver causing a decrease in the performance of receiver and combined system. For $\dot{m}_{a,rec}$ =70kg/s, the

peak value of the returned temperature from the coupled storage is calculated to increase by 38% when the thermal storage capacity is decreased from 16 to 4h.

- There is a strong dependence of the overall system performance and its economic feasibility on the interaction between the individual sub-systems, indicating the importance of carefully sizing the sub-systems in combination. For the case with R_p = 40% and *SM* = 5, the performance of the combined system is calculated to increase by 28% when the thermal capacity of integrated storage is increased from 4 to 16h. The value of *LCOH* is decreased by ~16% for the same change, despite the added cost of thermal storage.

- The trends in the optimization process are highly dependent on the particle mass loading used in combination with the correct storage capacity for each value of solar multiple, and are non-linear. For the case with only 10% mass of suspended particles, the annual solar share is increased by 40%, with only 6% increase in *LCOH*. More importantly, the solar share is further increased by some 16% points (from 59% to 75%) along with 14% drop in *LCOH*, when mass loading of suspended particles is increased from 10% to 40%. However, this solar share is increased by only 5% points when a thermal storage capacity of 8h is used, instead of 16h.

- There is a strong potential of a decrease in the cost of energy from CST systems with some allowance for technology development and with a drop in component costs due to mass production. For example, the value of *LCOH* is calculated to drop by 35% with an expected drop of 20% in the cost of system components and with discount rate dropping from 7% to 5%.

Overall, the modelled performance of the present system indicates an encouraging techno-economic potential of CST technology to supply high temperature heat to industrial processes and provide a driving force to investigate larger thermal scales, to estimate the likely benefit from economies of scale. It should also be noted that this technology also offers the benefits of reducing CO_2 emissions adding a premium to the product value as well as offering the potential of further cost reduction, should CO_2 reduction credits be implemented in the future.

References

[1] Chinnici, A., Tian, Z. F., Lim, J. H., Nathan, G. J., and Dally, B. B., 2017, "Comparison of system performance in a hybrid solar receiver combustor operating with MILD and conventional combustion. Part I: Solar-only and combustion-only employing conventional combustion," Solar Energy, 147, pp. 489-503.

[2] Nathan, G. J., Jafarian, M., Dally, B. B., Saw, W. L., Ashman, P. J., Hu, E., and Steinfeld, A., 2018, "Solar thermal hybrids for combustion power plant: A growing opportunity," Progress in Energy and Combustion Science, 64, pp. 4-28.

[3] Davis, D., Müller, F., Saw, W. L., Steinfeld, A., and Nathan, G. J., 2017, "Solar-driven alumina calcination for CO_2 mitigation and improved product quality," Green Chemistry, 19(13), pp. 2992-3005.

[4] Fernández-Torrijos, M., Albrecht, K. J., and Ho, C. K., 2018, "Dynamic modeling of a particle/supercritical CO_2 heat exchanger for transient analysis and control," Applied Energy, 226, pp. 595-606.

[5] Ho, C. K., and Iverson, B. D., 2014, "Review of high-temperature central receiver designs for concentrating solar power," Renewable and Sustainable Energy Reviews, 29, pp. 835-846.

[6] Siegel, N. P., Ho, C. K., Khalsa, S. S., and Kolb, G. J., 2010, "Development and Evaluation of a Prototype Solid Particle Receiver: On-Sun Testing and Model Validation," Journal of Solar Energy Engineering, 132(2).

[7] Röger, M., Amsbeck, L., Gobereit, B., and Buck, R., 2011, "Face-Down Solid Particle Receiver Using Recirculation," Journal of Solar Energy Engineering, 133(3).

[8] Tan, T., Chen, Y., Chen, Z., Siegel, N., and Kolb, G. J., 2009, "Wind effect on the performance of solid particle solar receivers with and without the protection of an aerowindow," Solar Energy, 83(10), pp. 1815-1827.

[9] Wu, W., Uhlig, R., Buck, R., and Pitz-Paal, R., 2015, "Numerical Simulation of a Centrifugal Particle Receiver for High-Temperature Concentrating Solar Applications," Numerical Heat Transfer, Part A: Applications, 68(2), pp. 133-149.

[10] Wu, W., Trebing, D., Amsbeck, L., Buck, R., and Pitz-Paal, R., 2015, "Prototype Testing of a Centrifugal Particle Receiver for High-Temperature Concentrating Solar Applications," Journal of Solar Energy Engineering, 137(4).

[11] Wu, W., Amsbeck, L., Buck, R., Uhlig, R., and Ritz-Paal, R., 2014, "Proof of Concept Test of a Centrifugal Particle Receiver," Energy Procedia, 49, pp. 560-568.

[12] Wu, W., Amsbeck, L., Buck, R., Waibel, N., Langner, P., and Pitz-Paal, R., 2014, "On the influence of rotation on thermal convection in a rotating cavity for solar receiver applications," Applied Thermal Engineering, 70(1), pp. 694-704.

[13] Flamant, G., Gauthier, D., Benoit, H., Sans, J.-L., Garcia, R., Boissière, B., Ansart, R., and Hemati, M., 2013, "Dense suspension of solid particles as a new heat transfer fluid for concentrated solar thermal plants: On-sun proof of concept," Chemical Engineering Science, 102, pp. 567-576.

[14] Rovense, F., Reyes-Belmonte, M. Á., Romero, M., and González-Aguilar, J., 2022, "Thermo-economic analysis of a particle-based multi-tower solar power plant using unfired combined cycle for evening peak power generation," Energy, 240, p. 122798.

[15] Behar, O., Grange, B., and Flamant, G., 2020, "Design and performance of a modular combined cycle solar power plant using the fluidized particle solar receiver technology," Energy Conversion and Management, 220, p. 113108.

[16] Reyes-Belmonte, M. A., Sebastián, A., Spelling, J., Romero, M., and González-Aguilar, J., 2019, "Annual performance of subcritical Rankine cycle coupled to an innovative particle receiver solar power plant," Renewable Energy, 130, pp. 786-795.

[17] González-Portillo, L. F., Albrecht, K., and Ho, C. K., 2021, "Techno-Economic Optimization of CSP Plants with Free-Falling Particle Receivers," Entropy, 23(1), p. 76.

[18] Albrecht, K. J., Bauer, M. L., and Ho, C. K., "Parametric Analysis of Particle CSP System Performance and Cost to Intrinsic Particle Properties and Operating Conditions," Proc. ASME 2019 13th International Conference on Energy Sustainability collocated with the ASME 2019 Heat Transfer Summer ConferenceV001T03A006.

[19] Buck, R., and Giuliano, S., 2018, "Impact of Solar Tower Design Parameters on xCO2-based Solar Tower Plants."

[20] Merchán, R. P., Santos, M. J., Medina, A., and Calvo Hernández, A., 2022, "High temperature central tower plants for concentrated solar power: 2021 overview," Renewable and Sustainable Energy Reviews, 155, p. 111828.

[21] Z'Graggen, A., Haueter, P., Maag, G., Romero, M., and Steinfeld, A., 2008, "Hydrogen production by steam-gasification of carbonaceous materials using concentrated solar energy—IV. Reactor experimentation with vacuum residue," International Journal of Hydrogen Energy, 33(2), pp. 679-684.

[22] Z'Graggen, A., Haueter, P., Maag, G., Vidal, A., Romero, M., and Steinfeld, A., 2007, "Hydrogen production by steam-gasification of petroleum coke using concentrated solar power—III. Reactor experimentation with slurry feeding," International Journal of Hydrogen Energy, 32(8), pp. 992-996.

[23] Z'Graggen, A., Haueter, P., Trommer, D., Romero, M., de Jesus, J. C., and Steinfeld, A., 2006, "Hydrogen production by steam-gasification of petroleum coke using concentrated solar power—II Reactor design, testing, and modeling," International Journal of Hydrogen Energy, 31(6), pp. 797-811.

[24] Rafique, M. M., Nathan, G., and Saw, W., 2022, "Modelled annual thermal performance of a 50MWth refractory-lined particle-laden solar receiver operating above 1000°C," Renewable Energy, 197, pp. 1081-1093.

[25] Ávila-Marín, A. L., 2011, "Volumetric receivers in Solar Thermal Power Plants with Central Receiver System technology: A review," Solar Energy, 85(5), pp. 891-910.

[26] Stadler, H., Schwarzbözl, P., Maldonado, D., Broeske, R., Andlauer, F., Trautner, J., and Schrüfer, J., 2019, "Performance assessment of an improved open volumetric receiver design with 240 MWth," AIP Conference Proceedings, 2126(1), p. 030057.

[27] Davis, D., Jafarian, M., Chinnici, A., Saw, W. L., and Nathan, G. J., 2019, "Thermal performance of vortex-based solar particle receivers for sensible heating," Solar Energy, 177, pp. 163-177.

[28] Ingenhoven et. al, 2022, "Techno-economic assessment from a transient simulation of a concentrated solar thermal plant for deliver high temperature industrial process heat," To be submitted.

[29] (2022a), M., "Natick, Massachusetts: The MathWorks In."

[30] Steven G. Johnson, "The NLopt nonlinear-optimization package, http://github.com/stevengj/nlopt."

[31] Potter, D. F., Kim, J.-S., Khassapov, A., Pascual, R., Hetherton, L., and Zhang, Z., 2018, "Heliosim: An integrated model for the optimisation and simulation of central receiver CSP facilities," AIP Conference Proceedings, 2033(1), p. 210011.

[32] Bureau of Meteorology, "http://www.bom.gov.au/climate/glossary/seasons.shtml."

[33] CET, "https://www.adelaide.edu.au/cet/technologies/solar-expanding-vortex-particle-receiver-reactor-sevr."

[34] Chinnici, A., Arjomandi, M., Tian, Z. F., Lu, Z., and Nathan, G. J., 2015, "A Novel Solar Expanding-Vortex Particle Reactor: Influence of Vortex Structure on Particle Residence Times and Trajectories," Solar Energy, 122, pp. 58-75.

[35] Rafique, M. M., Nathan, G., and Saw, W., 2021, "A mathematical model to assess the influence of transients on a refractory-lined solar receiver," Renewable Energy, 167, pp. 217-235.

[36] Ingenhoven, P., Saw, W., Rafique, M., Potter, D., Chinnici, A., and Nathan, G., 2021, "Energetic assessment of a high temperature packed bed storage system in combination with a solar expanding vortex receiver," Solar World Congress, Solar Energy Society, Virtual.

[37] Ang, D., Chinnici, A., Tian, Z. F., Saw, W. L., and Nathan, G. J., 2021, "Influence of particle loading, Froude and Stokes number on the global thermal performance of a vortex-based solar particle receiver," Renewable Energy.

[38] Ang et al., 2021, "Thermal performance analysis of a scaled-up suspension flow receiver for generation of industrial process heat: A computational study," SolarPACESVirtual.

[39] Charvin, P., Abanades, S., Neveu, P., Lemont, F., and Flamant, G., 2008, "Dynamic modeling of a volumetric solar reactor for volatile metal oxide reduction," Chemical Engineering Research and Design, 86(11), pp. 1216-1222.

[40] Meier, A., Winkler, C., and Wuillemin, D., 1991, "Experiment for modelling high temperature rock bed storage," Solar Energy Materials, 24(1), pp. 255-264.

[41] Leok et al., 2022, "Transmission system for high temperature CST, to be submitted.."

[42] SunShot 2030, "https://www.energy.gov/eere/solar/sunshot-2030."

[43] KPMG Global, "The Hydrogen Trajectory - KPMG Global Available online: https://home.kpmg/xx/en/home/insights/2020/11/the-hydrogen-trajectory.html."

CHAPTER 7

CONCLUSIONS AND FUTURE WORK

This page is intentionally left blank

7.1. Conclusions

The present thesis provides new understandings about the potential benefits of optimized multilayered refractory use in high temperature particle-laden receivers, to supply process heat at temperatures at or above 1000°C, with a better trade-off between operating temperature, start-up time, overnight temperature drops and useful thermal outputs under transient operating conditions. The thermal performance of the system was evaluated using a transient mathematical model developed for a multilayered refractory-lined particle-laden receiver system, which calculates the time dependent thermal outputs and energy balance in the receiver considering the real-time solar resource variability. The study considered and analysed the performance of the receiver as a standalone system as well as an integrated complete CST system with sensible thermal storage. The main conclusions from this research are as follows:

I.   The operation of a high temperature particle-laden receiver to transient solar input, for the conditions assessed here, highlighted the role of refractory thickness in damping the solar fluctuations.

   o   For example, even the thinnest refractory of 50mm was calculated to have a significant compensating advantage of damping out the fluctuations in the output temperature due to intermittent cloud. The temperature of wall and particles only drops by few degrees following the total slump in solar power to nearly zero.

II. There is a potential to achieve an optimized configuration of the refractory-lined solar receiver for a better trade-off between the conditions of relevance including operating temperature, thermal losses, start-up time, and overall thermal performance.

   o   The refractory lining should be sufficiently thick to minimize the temperature drop overnight and thermal losses, while being sufficiently thin to avoid

excessive start-up time. However, the optimal thickness of the refractory also offers a compensating advantage by providing useful thermal output even after the solar flux falls.

- For example, a refractory thickness of 100mm was calculated to give 6% more useful daily solar hours in comparison with a thickness of 50mm despite 8% longer start-up time.

III. Maintaining the inside of the refractory-lined cavity receiver at a higher temperature overnight with insulation is beneficial in terms of reduced start-up time.

- For example, the start-up time was reduced by 26 to 84% when the cavity was maintained at 200 to 600°C overnight instead of cooling down to ambient.
    - This is quite significant for the long-term operation of the receiver as the overnight temperature drop can be minimized by managing its transient operation during the shutdown.
        - For 8m diameter cavity with 100mm thickness of both the inner refractory and insulating layer, the temperature drop overnight was only about 28% of the operating temperature when the aperture was covered during the shutdown period.

IV. The annual assessments of the sensitivity of the thermal performance of a high temperature multilayered refractory lined particle-laden receiver system, operating under the influence of solar resource variability, revealed that the use of refractory lining in high temperature receivers has the potential to increase the annual thermal performance.

- For example, a refractory-lined solar receiver with inner refractory and insulating layer thickness of 100 mm was calculated to provide 36% more annual useful thermal gain relative to the case of no refractory under the same

operating conditions, when operated with the required controllers to manage the influence of solar transients during start-up, turn down, and shutdown periods.

V.   The annual assessments of the receiver subsystem confirmed the technical feasibility of the multilayered refractory-lined Solar Expanding Vortex Receiver to reheat air at an already elevated temperature, which is returned from the process or coupled thermal storage.

   o   The net thermal performance of the receiver sub-system was estimated to span between 80 to 72% when heating air to temperatures of the order of $1000^{\circ}C$ with inlet temperatures of ambient to $600^{\circ}C$, respectively, when accounting for start-up, turndown and shutdown losses through a year of transient operation.

VI.   The assessments of the integrated CST system revealed that there is a strong trade-off between the thermal performance of the receiver subsystem and thermal storage system, for the variations in different parameters.

   o   For a system with 8h of thermal storage, the thermal performance of receiver sub-system was calculated to increase by 7.3% when the mass flow rate of air was increased from 30 to 70kg/s. However, the thermal performance of storage sub-system decreased by 15.2% for the same increase in mass flow rate.

VII.   The particle mass loading has a strong influence on the thermal performance of the integrated CST system, and on its economic feasibility, when supplying reheated air at temperatures of above $1000^{\circ}C$ with real-time variations in the returned temperature from the coupled thermal storage.

- For example, the thermal performance of the combined system is calculated to improve by 21 to 43% with the addition of 10 to 40% mass loading of particles into the air stream relative to the air-only case.
  - This improvement in thermal performance results in up to 38% drop in the cost of energy.

VIII. There is a strong dependence of the overall system performance and its economic feasibility on the interaction between the individual sub-systems, indicating the importance of carefully sizing the sub-systems in combination rather than in isolation.
- For the case with particle mass loading of 40%, the performance of the combined system is calculated to increase by 28% when the thermal capacity of integrated storage is increased from 4 to 16h.
  - The levelized cost of solar energy is decreased by ~16% for the same change, despite of the additional cost of thermal storage.

7.2. Recommendations for future work

The limitations of the present transient approach can be addressed in future by incorporating the non-uniform distribution of the solar flux and considering the internal temperature gradients, of both cavity walls and particles. Furthermore, the influence of recirculation of the particle-laden flow inside the receiver cavity can be included in the future model by the inclusion of a recirculation model term, which requires further experimental data. This will also help to determine the uneven distribution of particles inside the receiver cavity and the blocking of radiations by the individual particles. Another possible improvement in the model is the dependence of the particle's residence time on the Stokes number and receiver geometry, which also requires a recirculation model term.

This thesis establishes a baseline of performance and cost for refractory lined SEVR system, to deliver high temperature industrial heat, which can be used to develop further improvements by comparison with alternative systems and technologies, such as volumetric air receivers and falling particle curtain receivers. Further work is also needed to prove the concept of upscaling the SEVR by determining the receiver dimensions and flow features, to estimate the likely benefit from economies of scale, along with some experimental work on the multilayered refractory lined SEVR.

Furthermore, there is a need to investigate the use of alternative gases such as helium, carbon dioxide, argon or a mixture of two or more, as a replacement of air. This should be studied based on their thermo-physical properties, availability, corrosivity, and associated costs relative to air. Furthermore, other heat transfer fluids such as steam can also be investigated as an alternative to particle-laden flow. The use of steam will help to operate the receiver under pressurized conditions with an aperture window cover and is reported to offer the potential of achieving temperatures of above 1000°C without any suspended particles.

The use of solar thermal technology for decarbonization of high temperature industrial processes is calculated to increase the cost relative to high carbon-emitting fossil fuels. This arises the need of plant optimization for comparison with other low carbon streams, alongside further investigations of the options of hybrid systems to trade-off between cost and emissions. Furthermore, it is important to evaluate the options from a lifecycle perspective to consider the emissions in the fuel chain and the manufacturing of the energy conversion technology.